ACS SYMPOSIUM SERIES 1053

Polymeric Delivery of Therapeutics

EDITED BY

Sarah E. Morgan and Robert Y. Lochhead

Downloaded by 89.163.34.136 on June 23, 2012 | http://pubs.acs.org
Publication Date (Web): November 17, 2010 | doi: 10.1021/bk-2010-1053.fw001

Polymeric Delivery of Therapeutics

Downloaded by 89.163.34.136 on June 23, 2012 | http://pubs.acs.org
Publication Date (Web): November 17, 2010 | doi: 10.1021/bk-2010-1053.fw001

Downloaded by 89.163.34.136 on June 23, 2012 | http://pubs.acs.org
Publication Date (Web): November 17, 2010 | doi: 10.1021/bk-2010-1053.fw001

ACS SYMPOSIUM SERIES **1053**

Polymeric Delivery of Therapeutics

Sarah E. Morgan, Editor
School of Polymers and High Performance Materials
University of Southern Mississippi

Robert Y. Lochhead, Editor
School of Polymers and High Performance Materials
University of Southern Mississippi

Sponsored by the
ACS Division of Polymer Chemistry

American Chemical Society, Washington, DC

Downloaded by 89.163.34.136 on June 23, 2012 | http://pubs.acs.org
Publication Date (Web): November 17, 2010 | doi: 10.1021/bk-2010-1053.fw001

Library of Congress Cataloging-in-Publication Data

Polymeric delivery of therapeutics / Sarah E. Morgan, editor, School of Polymers and High Performance Materials University of Southern Mississippi, Robert Y. Lochhead, editor, School of Polymers and High Performance Materials, University of Southern Mississippi ; sponsored by the ACS Division of Polymer Chemistry.
p. ; cm. -- (ACS symposium series ; 1053)
Includes bibliographical references and index.
ISBN 978-0-8412-2583-1 (alkaline paper) 1. Polymeric drug delivery systems. I. Morgan, Sarah E., 1958- II. Lochhead, Robert Y., 1943- III. American Chemical Society. Division of Polymer Chemistry. IV. Series: ACS symposium series ; 1053.
[DNLM: 1. Drug Delivery Systems--methods. 2. Polymers--therapeutic use. 3. Drug Carriers--methods. 4. Polymers--chemistry. QV 785]
RS201.P65P638 2010
615’.19--dc22
2010044833

The paper used in this publication meets the minimum requirements of American National Standard for Information Sciences—Permanence of Paper for Printed Library Materials, ANSI Z39.48n1984.

Copyright © 2010 American Chemical Society

Distributed by Oxford University Press

All Rights Reserved. Reprographic copying beyond that permitted by Sections 107 or 108 of the U.S. Copyright Act is allowed for internal use only, provided that a per-chapter fee of $40.25 plus $0.75 per page is paid to the Copyright Clearance Center, Inc., 222 Rosewood Drive, Danvers, MA 01923, USA. Republication or reproduction for sale of pages in this book is permitted only under license from ACS. Direct these and other permission requests to ACS Copyright Office, Publications Division, 1155 16th Street, N.W., Washington, DC 20036.

The citation of trade names and/or names of manufacturers in this publication is not to be construed as an endorsement or as approval by ACS of the commercial products or services referenced herein; nor should the mere reference herein to any drawing, specification, chemical process, or other data be regarded as a license or as a conveyance of any right or permission to the holder, reader, or any other person or corporation, to manufacture, reproduce, use, or sell any patented invention or copyrighted work that may in any way be related thereto. Registered names, trademarks, etc., used in this publication, even without specific indication thereof, are not to be considered unprotected by law.

PRINTED IN THE UNITED STATES OF AMERICA

Downloaded by 89.163.34.136 on June 23, 2012 | http://pubs.acs.org
Publication Date (Web): November 17, 2010 | doi: 10.1021/bk-2010-1053.fw001

Foreword

The ACS Symposium Series was first published in 1974 to provide a mechanism for publishing symposia quickly in book form. The purpose of the series is to publish timely, comprehensive books developed from the ACS sponsored symposia based on current scientific research. Occasionally, books are developed from symposia sponsored by other organizations when the topic is of keen interest to the chemistry audience.

Before agreeing to publish a book, the proposed table of contents is reviewed for appropriate and comprehensive coverage and for interest to the audience. Some papers may be excluded to better focus the book; others may be added to provide comprehensiveness. When appropriate, overview or introductory chapters are added. Drafts of chapters are peer-reviewed prior to final acceptance or rejection, and manuscripts are prepared in camera-ready format.

As a rule, only original research papers and original review papers are included in the volumes. Verbatim reproductions of previous published papers are not accepted.

ACS Books Department

Downloaded by 89.163.34.136 on June 23, 2012 | http://pubs.acs.org
Publication Date (Web): November 17, 2010 | doi: 10.1021/bk-2010-1053.pr001

Preface

Polymeric delivery of therapeutics applies to a wide range of applications, including medical, pharmaceutical, cosmetics, personal care and nutrition markets. Recent advances in polymer synthesis and characterization techniques, most notably new controlled living polymerization routes for synthesis of targeted molecular architectures and advanced techniques for manipulation and characterization of nanostructures in polymer matrices, enable advances in therapeutic delivery that were unimaginable a few years ago. Health, medical and personal care markets represent the fastest growing markets in the chemical industry in the US and world wide. This symposium series book includes contributions from academic and industrial researchers developing controlled polymer structures for delivery of therapeutics in biomedical, pharmaceutical, personal care and cosmetic applications, and includes a summary of intellectual property considerations in the field. It is intended to provide relevant and timely information for those involved in research and development in this rapidly growing field.

The book is organized in four sections. The first section includes two comprehensive overview chapters, one devoted to advances in polymeric delivery for the cosmetic and personal care market and the other devoted to polymers in nano pharmaceuticals. The next section includes contributions on synthesis and analysis of polymers with controlled architectures for biomedical applications. The third section is devoted to industrial contributions with state-of-the-art developments in personal care applications. The final section provides information on recent trends in U.S. patent law for polymeric delivery of therapeutics.

Sarah E. Morgan

School of Polymers and High Performance Materials
The University of Southern Mississippi
Hattiesburg, MS 39406

Robert Y. Lochhead

School of Polymers and High Performance Materials
The University of Southern Mississippi
Hattiesburg, MS 39406

Downloaded by 89.163.34.136 on June 23, 2012 | http://pubs.acs.org
Publication Date (Web): November 17, 2010 | doi: 10.1021/bk-2010-1053.ch001

Chapter 1

A Review of Recent Advances in the Polymeric Delivery of Attributes in Cosmetics and Personal Care Products

Robert Y. Lochhead[*]

School of Polymers and High Performance Materials, The University of Southern Mississippi, Hattiesburg, MS 39406-0001, USA.
[*]Robert.Lochhead@usm.edu

A multitude of polymers are used to deliver desired attributes to skin and hair in personal care products. This article reviews recent trends in the use of polymers to deliver personal care attributes. Precisely constructed block and graft copolymers widen the range of available mechanical properties and compatibilities. Hydrophobic stimuli responsive polymers can be triggered to become hydrophilic by changes in their environment and this can confer waterproof properties at low temperature and easy water removal at higher temperatures. Transfer-resistant cosmetics are derived from silicone resins. The structure/property relationships for rheology modifiers continue to be probed with surprising observations. Delivery systems for rinse-off products from complex coacervates have been extended to the delivery of colors and fragrances. Polymeric antimicrobials promise product preservation while minimizing the concern of skin permeation.

Precise Molecular Tailoring for Simultaneous Enablement of Contrasting Qualities

Since the 1970's it has been understood that conflicting properties can be achieved by incorporating copolymer blocks within the same polymer molecule. Thus, glassy blocks combined with elastomeric blocks enable thermoplastic elastomers and amphipathic block copolymers offer the similar surface active and aggregation properties as surfactants at a larger scale and with slower

In Polymeric Delivery of Therapeutics; Morgan, S., et al.;
ACS Symposium Series; American Chemical Society: Washington, DC, 2010.

Downloaded by 89.163.34.136 on June 23, 2012 | http://pubs.acs.org
Publication Date (Web): November 17, 2010 | doi: 10.1021/bk-2010-1053.ch001

kinetics. Precise molecular block structures were first realized by anionic living polymerization but such anionic synthesis could only be conducted in aprotic media and this severely limited the choice of monomers and solvents. The introduction of free radical living polymerization greatly diversified the range of block and graft copolymers that could be precisely synthesized (*1*). Living free radical polymerizations are now possible by several different mechanisms such as atom transfer radical polymerization (ATRP), nitroxide mediated polymerization (NMP), and radical addition fragmentation transfer (RAFT), boron-medited polymerization, and catalytic chain transfer polymerization (CCP). The advent of these new polymers is allowing formulators to overcome the frustrating challenge of blending dissimilar polymers to try to achieve conflicting properties within the same formulation. In this context it is well-known that the low entropy of mixing disfavors compatibility between different polymers and mixing at the molecular level can be achieved by covalently bonding dissimilar polymer segments as blocks in tailored copolymers. Living polymerization enables the construction of copolymers consisting of blocks of precise molecular weights. This was first achieved by anionic living polymerization, in which the rate of initiation is much faster than the rate of chain propagation, and the rate of termination is essentially negligible. These characteristics allow all of the chains to be initiated almost simultaneously and then to grow at the same rate. Well-behaved living polymerizations produce polymers having a polydispersity index close to unity. Once the available monomer is depleted, the chain ends remain active and a second monomer can be added to propagate a chemically-different block on the end of the first chain to create a block copolymer. The main drawback of anionic living polymerization is that it is easily terminated by the presence of protic substances that are almost ubiquitous in polymerization solvent and monomers. Moreover, the crossover reaction from one block to another is also frequently disfavored. These drawbacks severly limit the versatility and utility of living anionic polymerization. On the other hand, a wide variety of monomers can be polymerized by radical polymerization. However, in traditional radical initiation, propagation and termination occur throughout the duration of the polymerization process and the lifetime of a propagating chain is less than one second. Therefore, during a traditional free radical polymerization, the reaction comprises mainly ‘dead’ chains with a relatively small number of initiations and propagating chains. On the other hand, in living radical polymerization the initiation step is rapid compared to the propagation step and, as a consequence the chains are all initiated simultaneously. The important feature of living free radical polymerization is the propagation step in which there is a repeating exchange between active propagation and dormancy. The dormant chains can be reactivated and the rate of polymerization is essentially controlled by balancing the rates of activation and deactivation. At any given time the number of dormant chains greatly predominate over the number of propagating chains and this allows precise control of molecular weight and also transfer to additional monomer(s) to create precise block copolymers. In living free radical polymerization, the lifetime of a propagating chain is greater than an hour but all of the other characteristics of radical polymerization, such as the reactivity ratio between monomers, are essentially maintained. Examples of conflicting properties in skin makeup properties are gloss or matteness, good adhesion to the support and resistance to mechanical transfer or removal by secreted sweat or sebum but easy removability after use. Block, graft and gradient copolymers serve to compatibilize such compositions and gradient polymers have been proposed for this purpose (*2*). Block copolymers of styrene and butadiene or isoprene, can thicken oils to give clear gels.

Amphipathic block copolymers are a subset of polymers that can be synthesized by living polymerization. These polymers self-assemble to form complex, well-defined mesomorphic structures and this allows these polymers to thicken aqueous solutions to form viscoelastic gels (*3*, *4*). Hydrogels can be formed without covalent cross links from such amphipathic block copolymers because the aggregated hydrophobic blocks can act as junction zones within the structure. Such hydrogels can offer advantages in processing and in 'self-healing' properties whereby junction zones that are disrupted by shear or extension may re-form in the quiescent state. Moreover, these amphipathic block copolymers can allow tailoring of physical and mechanical properties, and also control of water adsorption and transmission. This is done by adjusting the size and number of blocks. Copolymers consisting of hydrophobic blocks (such as long-chain alkyl methacrylates), hydrophilic blocks (such as acrylic acid), and middle blocks, (such as short alkyl chain methacrylate such as butyl methacrylate) (*5*) are stimuli-responsive insofar as the water content of their hydrogels can be adjusted by changing the pH.

One particularly interesting class of amphipathic polymers are the so-called side-chain crystalline polymers (SCCP), which have hydrophilic backbones and a plethora of closely-spaced hydrophobic linear alkyl side-chains. These are usually copolymers of short and long-chain alkyl (meth)acrylates. They exhibit the interesting property of being hydrophobic below the melting point of the side chains but they become hydrophilic when the side-chains melt. The triggered transition from hydrophobic to hydrophilic can be tightly controlled to within a degree or two and that property has made them useful as stimuli-responsive seed-protective polymers (*6*). Thus seeds can be safely planted in winter with their SCCP waterproof coats which become hydrophilic at Springtime temperatures to allow water into the seed and initiate germination. These copolymers have now been shown to be useful oil thickeners for cosmetic compositions that have continuous oil phases. (*7*, *8*)· The mechanism of thickening depends upon the crystalline chains forming a gel network in non-polar oils when cooled below their melting point. The melting point of the side chains is adjusted to confer good flow and deposition at skin temperature when the gel is applied to the skin.

Ethylenediamine/Stearyl Dimer Dilinoleate and Tallate Copolymers are telechelic polymers that self-assemble to form clear-gel oil-phases. Traditionally, waxes have been used for this purpose but the wax-gelled systems tend to be translucent or hazy. The clear gels convey more intense and brighter colors than the traditional wax gellants. Variants of this chemistry have been introduced by linking internal polyether blocks and internal fatty blocks into the polyamides (*9*). The new polymers have higher molecular weights and they are effective as gellants at low concentrations. They are viscoelastic thickeners in some solvents and soft or hard gels can be tailored by judicious selection of solvents. The higher

Downloaded by 89.163.34.136 on June 23, 2012 | http://pubs.acs.org
Publication Date (Web): November 17, 2010 | doi: 10.1021/bk-2010-1053.ch001

molecular weights favor the formation of tough flexible films upon evaporation of the solvents.

Transfer-Resistant Color Cosmetics

Many wearers of lipstick desire a product that is delivered easily and uniformly to the lips but, once applied, it should not transfer to other surfaces. This paradox was addressed by the introduction of 'transfer-resistant' lipstick by Revlon in the 1990's (*10*), and since that time silicone resins have been a preferred ingredient to achieve transfer resistance in color cosmetics. These silicone resins are known as " MQ" or "MT "resins to signify that they consist of polymers constructed from monofunctional (M), trifunctional (T), and/or quatrifunctional (Q) silane functional groups. A wide range of cosmetic compositions containing high molecular weight, particulate MQ resin have been claimed (*11*). It has been found that the finish of cosmetic compositions can be improved by tailoring the properties of MQ and MT resins by adjusting the ratio of M:Q or M: T units in the resin. In particular, improved finish is achieved when the number of M units is up to three times greater than the number of Q units (*12*). However, one drawback of the MQ and MT resins is that they are not compatible with polar media and this poses difficulties for formulation in aqueous compositions. Compatibility and desirable silky feel is achieved by incorporating low molecular weight cyclosiloxanes..

More recently attempts have been made to achieve transfer resistance by including film-forming polymers in color cosmetics. In this application the physical demands on the polymer are considerable when it is considered that a smile represents a 500% extension and a 'pucker' is a 200% compression of the applied film. Moreover, the polymers must also resist food oils and liquids ranging from water to alcohol to hot beverages, to sweat and sebum. These extreme properties are achieved by applying a film of a silicone resin and a polyamide-silicone copolymer over the lipstick color layer on the keratin (*13*). These films are even claimed to be capable of resisting several washing cycles.

Downloaded by 89.163.34.136 on June 23, 2012 | http://pubs.acs.org
Publication Date (Web): November 17, 2010 | doi: 10.1021/bk-2010-1053.ch001

Rheology Modifiers

Thickeners, or rheology modifiers, are used by the personal care formulator to achieve stability against settling during storage and also to confer the desired delivery characteristics when consumer products are applied to the human substrate. For example the rheology modifier should improve body, smoothness and silkiness, making the product more aesthetically pleasing (*14*).

Rheology modifiers may be natural, semi-synthetic or synthetic. For example, natural rheology modifiers include casein, alginates, guar gum, xanthan gum and gum tragacanth, semi-synthetic thickeners include modified celluloses such as carboxymethylcellulose, methyl cellulose, hydroxyethyl cellulose, hydroxypropyl cellulose. Synthetic rheology modifiers include polyelectrolytic acrylic polymers and maleic anhydride copolymers.

The term “associative” thickener is defined as water-soluble or water-swellable polymer that has chemically attached hydrophobic groups that are capable of hydrophobic associations similar to those of conventional surfactants. The most usually encountered attached “hydrophobes” are alkyl or aralkyl groups containing from about 4 to about 30 carbon atoms. It is common for thee hydrophobes to be linked to the chain by means of polyoxyethylene spacer groups. Commercially available associative are usually classified as one of three types, namely:

- naturally derived nonionic thickeners such as hydrophobically-modified hydroxyethyl cellulose (HMHEC),
- synthetically derived nonionic thickeners such as hydrophobically-modified ethoxylated urethanes (HEUR) and Hydrophobically-modified aminoplast technology (HEAT) copolymers,
- synthetically derived anionic thickeners such as hydrophobically-modified alkali-swellable emulsion polymers (HASE).

Hydrophobically-Modified Hydroxyethyl Cellulose (HMHEC)

Water-soluble cellulose derivatives are modified with hydrophobic groups usually by functionalizing some portion of the free hydroxyl groups in the cellulose polymer. An example of a HMHEC is cetyl hydroxyethylcellulose.

Hydrophobically-Modified Ethoxylated Urethanes (HEUR) and Hydrophobically-Modified Aminoplast Technology (HEAT) Copolymers (*15*)

Generally, these compounds are prepared by joining *bis*-hydroxyl polyethers with isocyanates or aminoplast couplers. Commonly, the hydrophilic polyether polyol adduct is a polyalkylene glycol such as polyethylene glycol, polypropylene glycol, or polybutylene glycol, having a molecular weight in the range of 200 to about 20,000. Alkyl isocyanates or aminoplasts are used to attach hydrophobic moieties the hydrophilic chains. The polymer may be blocky (*16*), comb-like (*17*) or star-like in configuration.

Hydrophobically-Modified Alkali-Soluble Emulsion Polymers (HASE)

HASE polymers are prepared as emulsion copolymers (*18*) The acrylic carboxylate emulsion polymers are water-insoluble colloidal dispersions that become soluble or swellable in water and confer thickening when the pH is adjusted above about 5.5, with an upper limit of to about 12. A typical HASE thickener would be a *ter*polymer of methacrylic acid, an acrylate such as ethyl acrylate, and a (meth)acrylic ester of an alkoxylated long chain (C8-C30) alcohol, and sometimes a small quantity of a crosslinking agent.

These are high molecular weight polymers, having molecular weights in the range 50,000 to 500,000 Daltons. Typical HASE thickeners are those described by the INCI names Acrylates Copolymer, Acrylates/Steareth-20-Methacrylate copolymer or Acrylates/ Beheneth-25 – Methacrylate copolymer, Polyacrylate-X

Downloaded by 89.163.34.136 on June 23, 2012 | http://pubs.acs.org
Publication Date (Web): November 17, 2010 | doi: 10.1021/bk-2010-1053.ch001

or Acrylates Crosspolymer-X, where X is a definite number (*19*). For example, the Acrylates/ Beheneth – Methacrylate copolymer is a random copolymer of alkyl (probably ethyl) acrylate, acrylic acid, methacrylic acid and the methacrylate ester of behenyl polyethoxylate, with an average ethylene oxide degree of polymerization of 25. HASE thickeners are provided in the form of emulsion polymers at low pH. When the pH is raised above a pH of about 5.5, the latex particles swell and 'dissolve' as the polyacrylate chains are neutralized to become polyelectrolytes. Hydrophobic association between the polyelectrolyte chains results in the formation of an intermolecular network that significantly enhances the viscosity of the system.

These HASE thickeners do display a number of attributes that make them favorable for rheology modification of personal care products:

- They are available in a liquid form, at about 20% solids. They are easily cold-processed in comparison with powder products that require special dispersion techniques to avoid clumping or the formation of 'fisheyes' in the finished formulation.
- The associative thickeners show a degree of electrolyte tolerance that is superior to the straightforward polyelectrolyte thickeners.
- The associative thickeners can interact synergistically with surfactants and with hydrophobic particles to enhance the viscosity of final formulations.
- They show Ellis-type rheology, with a definite yield stress. As a result, they can stably suspend particles within formulations, but they also display shear-thinning characteristics that ease flow and application to the desired substrate(s).
- They are usually effective in the pH range 5.5–12. The pH of the associative thickener product as received is about 2.5 to 3.5.
- Acrylates/Beneneth-25-Methacrylate copolymer is capable of adequately thickening peroxide formulations for application in consumer products.
- Unlike the natural thickeners, these associative thickeners are resistant to enzyme-mediated and microbiological degradation.

Judicious formulation of surfactants with associative thickeners can lead to improvements in viscosity and adjustments in the rheology of the system (*20–23*). For nonionic surfactants, enhanced thickening is usually observed when the HLB of the surfactant system is below 12. However, care must be taken when using surfactant as co-micellization with an excess number of surfactant micelles can destroy the hydrophobic association between the polymer chains and cause a catastrophic drop in viscosity.

Typical cosmetic and personal care formulations containing the mixed surfactant/associative thickeners include (a) dandruff shampoos, astringents and sunscreens containing zinc compounds (such as zinc pyrithione, zinc phenol and zinc oxide, respectively) as active ingredient and mixed surfactant/associative thickener (2%) to maintain the zinc salts in suspension; (b) depilatories containing calcium salts of thioglycolic acid as the active ingredient and mixed surfactant/associative thickener (2%) to prevent the calcium salt

Downloaded by 89.163.34.136 on June 23, 2012 | http://pubs.acs.org
Publication Date (Web): November 17, 2010 | doi: 10.1021/bk-2010-1053.ch001

Downloaded by 89.163.34.136 on June 23, 2012 | http://pubs.acs.org
Publication Date (Web): November 17, 2010 | doi: 10.1021/bk-2010-1053.ch001

from settling out; (c) shampoos containing sodium salts/surfactants (such as cocamidopropyl betaine, sodium lauryl sulfate and polyquaterium-10 (cellulose-2-hydroxyethyl-2-hydroxy-3-›trimethylammoniopropyl ether, chloride)) and mixed surfactant/associative thickener (5-10%) to maintain desired viscosity; (d) facial make-ups (such as eye shadow and face powder) and sunscreens containing pigments (such as clay, silica, calcium carbonate, titanium dioxide and zinc oxide) and mixed surfactant/associative thickener (1%) to provide desirable consistency when applied to the skin; (e) hand creams and hand lotions containing various oils and mixed surfactant/associative thickener (2%) to prevent mineral oil/water separation and to provide desired consistency and feel upon application; and (f) acidic personal care products such as .alpha.-hydroxy acids containing cationic surfactants, mild organic acids (such as lactic acid, citric acid, glycolic acid and fruit acids) and mixed surfactant/associative thickener (1-2%).

For HASE thickeners it has been taught that the particular structure of the polymeric backbone which generates the water-solubility is not critical to the performance of the polymer in the thickening operation other than providing hydrophilic quality to the molecule. What is critical is the placement of the complex hydrophobic groups in the polymer chain which confer enhanced thickening by hydrophobic association in the aqueous system (*24*). these hydrophobic group associations are dynamic molecular interactions that occur in aqueous solution. The duration of time that an individual hydrophobic association exists is related to the (1) chemical potential of the hydrophobe in its associated state compared to its molecular isolation in the aqueous environment and (2) steric factors. The chemical potential of the hydrophobe, Δμ, can be roughly estimated by the equation (*25*):

$$\Delta\mu = 2\mathrm{RT} - \frac{\mathrm{V_s} + \mathrm{V_p}}{2}\left(\delta_\sigma - d_p\right)^2 x^2$$

wherein R is the universal gas constant; T is the temperature in degrees Kelvin; Vs and Vp are the molar volumes of the solvent (water) and hydrophobe respectively; δs and δp are the solubility parameters of the solvent (water) and hydrophobe respectively; and x is the volume fraction concentration of hydrophobe present. The more negative the value of Δμ, the stronger the propensity to form and maintain hydrophobic associations. The molar volumes are a linear function of alkyl chain length. Thus, strong hydrophobic associations are possible where there is a large disparity between the molar volumes of the solvent (water) and the hydrophobe as well as a large difference between the solubility parameters. When the chemical potential is zero or positive, aggregation by hydrophobic association is not expected. The number of hydrophobic groups required to provide optimum thickening efficiency can be decreased by either increasing the molar volume of the hydrophobe or by reducing its contribution to the solubility parameter (*24*). For the steady shear responses of the various n-alkyl HASE polymers at a polymer concentration of 10 $\mathrm{gl^{-1}}$ it is found that that there is a progressive increase in viscosity building as the size of the hydrophobe is increased (*24*). There are no major qualitative differences with varying hydrophobe size, except that with longer n-alkyl chains, the magnitude of the storage modulus G' begins to exceed that of the loss modulus G". Each of the polymers shows a power law relationship of the form $G' \sim c^n$, with the power law exponent n increasing with hydrophobe size (*26*).

Dynamic Light Scattering studies revealed that the hydrophobicity of the macromonomer strongly influences the diffusion coefficient of the network cluster. With increasing carbon number on the hydrophobic macromonomer, the diffusion coefficient of the cluster decreases and the hydrodynamic correlation length increases due to the reduction in the number of hydrophobic junctions inside the cluster (*27*). Based upon these measurements and deductions it is reasoned that large, complex hydrophobic groups are recommended to achieve the highest performance in associative thickening (*28*, *29*). There is also an optimum length for the hydrophilic spacing group (*30*), which is commonly polyoxyethylene.

There are three concentration regimes that can be explained by different modes of hydrophobic association (*31*). In the most dilute regime, the polymer chains are isolated and the hydrophobes interact intramolecularly. There is an intermediate regime, in which the steady shear viscosity and the elastic modulus increase dramatically with polymer concentration. This increase is attributed to the polymer chains becoming overlapped and the intramolecular interactions becoming substituted by intermolecular interactions with increasing polymer concentration. In the third regime the hydrophobes are engaged in intermolecular interaction and a weaker dependence of viscosity with polymer concentration is observed. It is also noted that there is an optimum level of macromonomer substitution for the highest viscosity. In this case that level is about 1 mol percent of macromonomers.

HASE polymers have limited use as rheological modifiers in aqueous formulations because they have little thickening ability at less than 1%; high concentrations are not economically desirable, and high viscous HASE polymers are difficult to handle during manufacturing. Consequently additional rheological modifiers are sometimes used to offset these disadvantages of HASE copolymers. For example, HASE properties have been enhanced by adding surfactants to the composition; using macromonomer-derived associative polymers as co-thickeners; adding a mixture of multiphobe and monophobe compounds; or suppressing the viscosity of HASE polymers by complexation of the hydrophobic moieties of the polymer with cyclodextrin. However, a new Acrylates Copolymer that contains semi-hydrophobic monomers such as hydroxypropylacrylate, shows a reverse behavior in surfactant systems. Upon initial neutralization with base the viscosity increases only when the pH value reaches 6 to 6.5. Some crosslinked HASE polymers, (Acrylates Crosspolymer) exhibit so-called 'back-acid' thickening when the pH of the neutral system is reduced. The viscosity increases once more even down to a pH of 5 which is desirable for pH-balanced shampoos (*32*, *33*).

Thickening at neutral pH is well understood and achievable by the use of carboxylate-type thickeners. However, thickening of acid systems is desired. Copolymers obtained from 2-acrylamido-2-methylpropanesulfonic acid or its salt, dialkylacrylamide and cross-linking monomers provide thickening

Downloaded by 89.163.34.136 on June 23, 2012 | http://pubs.acs.org
Publication Date (Web): November 17, 2010 | doi: 10.1021/bk-2010-1053.ch001

at acid pH ranges with limited or no stickiness. Similarly copolymers of 2-acrylamido-2-methylpropanesulphonic acid (also known as N-acryloyl taurate) and acrylic acid are useful because, unlike conventional acrylic acid thickeners, they can increase the viscosity of low pH compositions and they resist significant viscosity loss in the presence of interfering ions. For example, they can thicken compositions containing the UV-A sunscreen 1,4-benzene[di(3-methylidene-10-camphorsulfonic)]acid. Ammonium Acryloyl Taurate/Vinyl Pyrrolidone Copolymer is an efficient thickener and stabilizer for emulsion compositions containing alpha- and beta-hydroxyacids (*34*, *35*). A measurable yield stress with desirable shear-thinning characteristics can be achieved with such polymers if the molecular weight is higher than 6,000,000 and if the polymers contains greater than 20 percent 2-acrylamido-2-methylpropanesulphonate.

Comb copolymers of N-acryloyl taurate with commercially available macromonomers also exhibit good thickening, emulsifying properties and clarity (*36–38*).

Microgel-like water swelling polymers can be manufactured by reverse phase emulsion polymerization by choosing the temperature and surfactant in such a ways that a water/oil microemulsion or fine emulsion can be prepared so that a nanometer order particle sized can be controlled. These polymers are exemplified by copolymers of dimethylacrylamide and 2-acrylamido-2-methylpropanesulfonic acid.

Another advance in associative thickeners is the development of hydrophobically modified cationic or amphoteric thickeners which have been announced in a patent application, which is a continuation of US patent 7288476. The copolymers contain cationic monomers selected from diallyldimethyl-ammonium chloride and methacrylamidopropyltrimethylammonium chloride. The cationic copolymer is either acrylamide/diallyldimethylammonium chloride copolymer or acrylamide/diallyldimethylammonium chloride/acrylic acid terpolymer. These polymers offer improved compatibility with cationic and low pH formulations.

Hair Fixatives

Synthetic film forming polymers have been used to deliver hairstyling since the 1950s. These polymers should be designed to exhibit a duality of purpose: they must hold the hair in its desired shape, even under conditions of high humidity, but after use they should be completely removed by shampoo. In conventional random copolymers there is usually a compromise between these paradoxical properties and many conventional fixative polymers are sensitive to moisture from humidity, rain or sweat and this reduces the durability of the hairstyle. The technological hurdle is raised by regulations that limit the amount of volatile organic compounds in hair fixatives making it desirable to use aqueous-based formulations to deliver humidity-resisting polymers that can instantly be removed by shampoo. Good fixation with less susceptibility to moisture can be achieved from compositions containing a fixative polymer having

Downloaded by 89.163.34.136 on June 23, 2012 | http://pubs.acs.org
Publication Date (Web): November 17, 2010 | doi: 10.1021/bk-2010-1053.ch001

an acidic vinyl monomer, a hydrophobic nonionic vinyl monomer, two associative monomers, and a semihydrophobic monomer; and another copolymer comprising a C3-C8 ethylenically unsaturated monocarboxylic acid monomer , a nonionic vinyl monomer, and a hydroxy-substituted nonionic vinyl monomer (*39*). For example, compositions containing Polyacrylate-14 and Acrylates/ Hydroxyesters Acrylates Copolymer provides the desired properties. Polyacrylate-14 is a polymer that contains hydrophilic, semihydrophobic and hydrophobic monomers. It exhibits the dual advantages of being a hair-gel thickener and a film-forming hair fixative (*40*).

The crosslinked derivative, Polyacrylate-2 Crosspolymer (*41*) is a branched acrylate copolymer of C1-C4 alkyl(meth)acrylate, (meth)acrylic acid and an amphipathic moiety that contains silicone side chains and associative hydrophobic chains (*42*). Soft, hydrophobic domains are randomly combined with hard, hydrophilic domains to form the backbone of this polymer, and this results in the simultaneous achievement of the paradoxical properties of stiffness and humidity resistance, with resistance to flaking, combined with the sensory attributes of shine enhancement and ease of distribution through hair. Another rheology modifier/hair styling resin for delivery from aqueous systems (*43*) is a crosslinked linear poly(vinyl amide/ polymerizable carboxylic acid copolymer, in which the vinyl amide is selected from vinylpyrrolidone, vinylcaprolactam, N-vinylformamide, or N-vinylacetamide. The polymerizable carboxylic acid can be (meth)acrylic acid.

Restylable hair fixatives and mascaras are possible with elastomeric particulate microspheres (*44*). The microspheres are particles of diameter between 10 and 250 microns and they contain crosslinked silicone elastomer (preferably dimethicone/vinyl dimethicone crosspolymer) (*45*), poly(2- ethylhexyl acrylate) or poly (butyl acrylate), having a low glass transition temperatures of less than -20°C. The relatively large particle size limits the extent of adhesion and allows the hairs to be easily peeled and re-adhered (*46*).

Downloaded by 89.163.34.136 on June 23, 2012 | http://pubs.acs.org
Publication Date (Web): November 17, 2010 | doi: 10.1021/bk-2010-1053.ch001

Polymers for the Delivery of Long-Lasting, Quick Change Styles

Temporary hair styling is achieved by combining hair fixative polymers with heating devices. However, these styles rarely last for more than one day and the styles tend to be unchangeable once set in place In this respect, an interesting advance has been disclosed for the long-term styling of hair with the option of changing the shape anytime at will (*47*). This is achieved by placing a polysiloxane/urea block copolymer to the hair and applying heat. The block copolymer is substantive to the hair and the treatment is durable. Moreover, because the polymer is thermoplastic, the style can be changed at any time by the reapplication of heat sufficient to melt the polymer. The polymers are synthesized by chain extending polyether and polyester polyols or *bis*-hydroxyalkylsilicones and /or and alpha, omega aminosilicone with an appropriate di-isocyanate coupler. The polymer formulation is applied to the hair, and heated with a curling iron to 200°C to produce a ringlet that can be easily straightened with a flat iron and then re-curled with a curling iron as desired.

Polymers To Strengthen Permed Hair

Permanent waving of hair is achieved by reducing of the disulfide bonds of the hair, confining the hair to a desired configuration, then oxidizing the SH groups back to S-S to hold the hair in its new style. This process inevitably weakens the hair fibers. Reduction of the hair in the presence of a fixing polymer that is precipitated by the reducing agent re-strengthens the hair (*48*). The precipitated polymer holds the hair in shape during the reduction and fixing steps and this alleviates the need for mechanical tensioning. Moreover, the set lasts twice as long as the conventional treatment. Crotonic acid/ vinyl acetate/ vinyl t-butyl benzoate terpolymer is preferred for this treatment.

Hair Conditioning Polymers

In its pristine state hair has a hydrophobic surface but oxidation and/or treatment with surfactants causes the hair surface to become hydrophilic. As a consequence the hair loses its natural conditioning. Conditioning of damaged hair is commonly achieved by treatment with aqueous formulations that contain fatty alcohols, cationic surfactants and optionally silicones. These components are considered to adsorb in a hydrophilic head-down- hydrophobic tail up conformation that confers hydrophobicity on the damaged hydrophilic hair surface. Cationic conditioning polymers are used to enhance the conditioning properties, especially to mitigate the effects of extreme processing that are experienced during hair-straightening. However, the addition of polymers to these already viscous compositions can render them unspreadable. In this context, compositions that readily spread on hair to confer disentangling and feel benefits, can be formulated using a polyol and/or an aminosilicone with a cationic polyvinyllactam (*49*, *50*). The preferred polymer for this purpose is Polyquaternium-55, which is the polymeric quaternary ammonium chloride formed from vinylpyrrolidone, dimethylaminopropyl methacrylate and methacryloyl-aminopropyl-lauryldimonium chloride.

Polyampholytes have been commercially available as conditioning polymers for a considerable time. A prominent example is Polyquaternium-39, which is a copolymer of diallyldimethylammonium chloride, acrylamide, and acrylic acid. When this is polymerized in a single batch process, the mismatch in reactivity ratios between these monomers results in lack of compositional uniformity. An improved version of this type of terpolymer of diallyldimethylammonium chloride, acrylamide, and acrylic acid has been made by a monomer feed method for better control of molecular weight and composition (*51*).

Copolymers comprising a diallylamine (typically diallyldimethyl ammonium chloride) and vinyllactam monomers (typically polyvinylpyrrolidone) are useful film-formers that confer conditioning properties such as good wet and dry combability feel, volume, and handle-ability (*52*).

An interesting stimuli-responsive system is formed from responsive particles with two contrasting polymers adsorbed to the particle core (*53*). These moieties adsorb to the hydrophilic hair surface and render it hydrophobic, thereby conferring conditioning attributes to the hair. For example, grafting of

Downloaded by 89.163.34.136 on June 23, 2012 | http://pubs.acs.org
Publication Date (Web): November 17, 2010 | doi: 10.1021/bk-2010-1053.ch001

aminopropyl-terminated dimethicone and polyethylenimine on titanium dioxide particles produces responsive particles. These particles form stable dispersions in water and aqueous solutions because they are sterically-stabilized by expansion of the polyethylenimine into the aqueous medium. However, when they are deposited on hair and dried, the polyethylenimine layer collapses and the dimethicone layer expands to render the surface hydrophobic.

Complex Coacervation and Encapsulation for Delivery

Two-in-one shampoos based upon complex coacervation were introduced in the 1970's and this mode of deposition continues to be improved. The first two-in-one shampoos depended on a complex coacervate being formed between anionic surfactant and the cationic hydroxyethylcellulose, Polyquaternium-10. This complex was solubilized in excess surfactant and it phase-separated as a coacervate liquid phase upon dilution during the rinsing cycle. Subsequently this triggered phase separation has been used to deposit conditioning agents such as silicones and therapeutics such as the anti-dandruff agent Zinc Pyrithione.

Hydrophobic modification of cationic hydroxyethylcellulose is claimed to endow better efficacy. Thus, Polyquaternium-67 is a hydrophobically-modified cationic hydroxyethylcellulose. This type of polymer having a degree of polymerization of 4,000 to 10,000 anhydroglucose units and a degree of hydrophobic substitution of 0.0008 to 0.08 moles per anhydroglucose ring provides enhanced depositions of cosmetic oil from a body wash formulation (*54*) and it also improves upon the performance of higher substituted versions that give good foaming but poor substantivity and impractical high viscosities.

Polyquaternium-67 is also disclosed as being a preferable thickener for zinc-depositing compositions. Zinc is the second most abundant trace metal in the body and, due to its inclusion in metalloenzymes, it catalyzes nearly every biochemical process in the human system (*55*). Zinc has been used for over 3000 years to treat skin disorders. The consumer acceptance of surfactant-based, zinc-containing topical products is affected by the rheology of the product and it is desirable to add thickening agents to achieve the desired rheological profile. Anionic thickeners should not usually be used for such compounds because they bind with the metal. Therefore, cationic or nonionic thickeners are preferable; but Polyquaternium-67 is appropriate for this purpose.

Guar Hydroxypropyltrimonium chloride is a cationic polygalactomannan that has been used for more than three decades as a hair conditioning polymer that dilution-deposits coacervate phases from anionic surfactant compositions. Another cationic polygalactomannan, cationic cassia gum, has recently been patented (*56*). Polygalactomannans consist of a polymannan backbone with galactose side groups. In guar gum, there is a pendant galactose side group for every two mannan backbone units. These galactose groups sterically hinder the substitutable C-6 hydroxyl unit and this limits the extent of possible cationic substitution on guar gum. In cassia, however, there is less steric hindrance of the C-6 hydroxyl group and, consequently, higher degrees of cationic substitution are possible with cassia (60% for cassia relative to 30% for guar). Cationic

Downloaded by 89.163.34.136 on June 23, 2012 | http://pubs.acs.org
Publication Date (Web): November 17, 2010 | doi: 10.1021/bk-2010-1053.ch001

cassia can be used as a conditioning polymer in shampoos and conditioners to impart cleansing, wet- detangling, dry-detangling and manageability. Maximum coacervate deposition occurs at precise ratios of cationic polymer: anionic surfactant but the optimum ratio for coacervation might not coincide with the best ratios for cleaning and foaming.

Synthetic copolymers of acrylamide and a monomer with three quaternary side groups are postulated to provide improved deposition on hair and improved conditioning performance with respect to wet combing (*57*).

Conditioning shampoos commonly contain dispersed silicone droplets that are expected to deposit on the hair surface during shampooing to confer conditioning benefits. If the silicone is not removed by subsequent shampoos, it can build up on the hair causing 'droop' and flatness. Moreover, the relatively large silicone droplets scatter light and the resultant lack of product clarity is often hidden by adding opacifiers to the shampoo or packaging in an opaque bottle. If pre-gelatinized starch, such as hydroxypropyl distarch phosphate, is included with Polyquaternium-10, suspension of pearlizing agents can be achieved (*58*).

Another way to minimize buildup is to treat the hair with 'water-in-water' emulsions that can be prepared by including cationic polymers with soluble salts in surfactant compositions (*59*). the water-in-water emulsions arise from segregation of the polymer in one phase and the salts in the other phase. These water-in-water emulsions, provide conditioning benefits with good spread of the conditioning phase on the hair and less chance of build-up.

Downloaded by 89.163.34.136 on June 23, 2012 | http://pubs.acs.org
Publication Date (Web): November 17, 2010 | doi: 10.1021/bk-2010-1053.ch001

Cyclodextrins for Controlled Delivery

Cyclodextrins are cyclic polysaccharides made up of common naturally occurring D-(+)-glucopyranose units joined by α-(1,4) linkages. The most common cyclodextrin rings are made up of six units (α-cyclodextrin), seven units (β-cyclodextrin), and eight units (γ-cyclodextrin). The ring structure has an inner apolar cavity which can host other molecules ranging, for example, from odors to fragrances to drug actives. The primary hydroxyl groups are situated on the inner side and the secondary hydroxyl groups are situated on the outer side. Cyclodextrins are useful for the controlled delivery of small molecule therapeutic agents having poor pharmacological profiles. For example, therapeutic agents with low aqueous solubility, or ones in which bioactive forms exist in equilibrium with inactive forms, or agents that must be 'dribbled in' because they are toxic in high doses. The host/ guest inclusion supra-molecular complexes formed by cyclodextrins alter the physical, chemical and biological properties of the conjugated molecules and help in their controlled introduction to the target substrate. Their use in drug delivery is benefited by the enhanced water-solubility, low toxicity and low immune response. The use of conjugates of drug molecules with polymer is another approach that has been used to circumvent the difficulties of delivering 'problem' actives. Polymers such as poly(hydroxypropylmethacrylate), poly(ethyleneglycol), and poly(L-glutamic acid) have been used for this purpose. These approaches have been combined by covalently attaching cyclodextrins moieties to polymers by covalent attachment to polyvinyl alcohol or cellulose, or by copolymerization with vinyl acetate or methyl methacrylate (*60*). There have even been polymers made in which the polymer backbone is threaded though the cyclodextrins rings (*61*). Biocompatible, water-soluble polymers containing covalently attached cyclodextrins moieties can be used for the purpose of conjugating guest molecules by attachment that can be cleaved under biological conditions (*62*). These cyclodextrin-containing polymers improve drug stability and solubility, and reduce toxicity of the small molecule therapeutics when used *in vivo*. Moreover, by selecting from a variety of linker groups and targeting ligands the polymers can provide controlled delivery of therapeutic agents.

Encapsulation

Encapsulation is useful for adding stability to ingredients that could lose efficacy by reacting with other formulation ingredients during storage. Encapsulaton is also useful to protect ingredients against degradation by light, oxidation, heat or extremes of pH. The beneficial agents protected could be sunscreens, skin-lighteners, moisturizers, emollients, perfumes flavors, and oils. Microencapsulation can also be employed as a route to controlled delivery for cosmetics and dermatological therapeutics.

Differential solubility with respect to pH can also be used to encapsulate oils. For example, alkali metal salts prepared from ethylene/maleic anhydride copolymers are soluble in solutions of high pH but insoluble at low pH. Microcapsules can be formed by dispersing oils in aqueous solutions of ethylene/maleic anhydride at high pH and then reducing the pH to the region of 5 to 8 to allow the polymer to precipitate and coat the surface of the dispersed oil droplets (*63*).

Complex coacervates prepared by the interaction of cationic and anionic polyelectrolytes can be employed as encapsulants (*64*). Also, simple coacervates can be formed by the addition of polymers like polyethylene to solutions of ethylcellulose in cyclohexane and this process has been applied to the formation of microencapsulation of pharmaceutical actives for the purpose of taste-masking (*65*).

Polycaprolactone oligomers are insoluble in water and in shea butter. When heated, however, the polymer dissolves up to 10 wt% in the shea butter. This preferential solubility behavior allows the preparation of nanocapsules by heating homogenized dispersions of mixtures of shea butter, water and polycaprolactone oligomers to 80°C then cooling to 20°C to allow coacervate to form at the oil-water interfaces (*66*).

Polysaccharide-zein complexes are appropriate for the delivery of shear sensitive microparticles containing active agents (*67*). Zein is a water-insoluble/alcohol soluble prolamine from corn gluten that is highly resistant to bacterial attack. The advantage of this system is exemplified by a herbal essence/agar-zein complex in a skin cream. The skin cream conferred a distinctive and lingering herbal odor, and it was reported to be non-irritable.

Downloaded by 89.163.34.136 on June 23, 2012 | http://pubs.acs.org
Publication Date (Web): November 17, 2010 | doi: 10.1021/bk-2010-1053.ch001

Downloaded by 89.163.34.136 on June 23, 2012 | http://pubs.acs.org
Publication Date (Web): November 17, 2010 | doi: 10.1021/bk-2010-1053.ch001

Enhanced Delivery

Perfume can be the costliest ingredient in a formulation and economic benefit can be realized by enhancing the deposition of fragrance on target substrates, and prolonging the duration of release of the desirable fragrance. There is also consumer perception benefits that can be derived from controlling the release of the different perfume components with respect to time. For example, "freshness" attributes are usually associated with "top notes" and "middle notes". However, "top notes" can be quickly lost due to evaporation and they tend to dissolve easily in aqueous media and be rinsed away. This challenge has been addressed by particles that selectively adsorb/absorb top notes and middle notes of perfume and enhance deposition from rinse-off personal care products (*68*). These polymeric particles contain a cationic polymer and a perfume having a molecular weight less than 200, a boiling point less than 250°C , and/ or a C log P of less than 3 and/or a Kovats Index value of less than about 1700. The P value is the octanol/water partitioning coefficient of a substance. For large values of this partition coefficient, the value is expressed as log P. Thus, a log P value of 3 indicates that partitioning of the substance is one thousand-fold preferentially into the octanol phase rather than the water phase. The Kovats Index system is an accurate method of reporting gas chromatographic data for inter-laboratory substance identification. The efficacy of the polymer particles in depositing and releasing the different perfume raw materials was measured by a protocol that ultimately tests the amount of perfume released from a fabric by headspace gas chromatography over a period of time specified by a 'longevity test'. Examples of possible 'cationic' monomers are dimethylaminoalkyl acrylates, vinylpyrrolidones, vinyl imidazoyls, vinyl ethers with diethylamino groups, vinylpyridines, alkyl acrylamides, and dialkylaminoalkylacrylamides. The example copolymer comprises methyl methacrylate and dimethylaminoethyl methacrylate cross-linked with ethylene glycol dimethacrylate.

Dendritic Polymer Gels for Iontophoresis

Iontophoresis is a process whereby an electrical potential is applied across the skin to enhance trans-dermal delivery. The intrusion into skin is controlled by containing the active ingredients in a gel within a small reservoir to which the potential is applied. Dendrimer gels have been recommended for this purpose (*69*). The words 'dendrimer' (*70*) coined by Tomalia) and 'arborol' (coined by Newkome) are derived from the Greek *dendro* (meaning tree-like) and the Latin *arbor* (*71*) (meaning tree to describe the fractal-like branched structures of these molecules. Dendrimers and arborols are prepared by a series of iterative steps, each designed to add one sequence of successive segmental units to the outside of the molecule. Each sequence is called a 'generation. Dendrimers can be constructed by a divergent synthesis or a convergent synthesis. Divergent construction starts with the cone of the molecule and builds out generation by generation. In convergent construction the branches are assembled first then they are brought together and bound by the core. Dendrimers and arborols are more precise branched molecules than hyper-branched polymers. Hyper-branched polymers, first patented by Kim in 1987 (*72–74*), are prepared in a single pot process and, as a consequence, the individual molecules within the product vary in molecular weight and structure.

Amphipathic arborols are capable of self-assembling into micelles (*75*). The solubility of one-directional arborols in water decreases dramatically with increasing length of the alkyl hydrophobic group, from 13.0 mmol/L when *n* is 6, to 1.4 mmol/L when *n* is 8, to less than 0.017 mmol/L when *n* is 9. for [9]-n arborols (*76*). At concentrations significantly higher than the critical micelle concentration, there is a possibility that amphipathic arborols would form gels by hydrophobic association and these gels might be expected to have a more uniform pore size than conventional polymer gels. This could be the reason that these interesting tree-like molecules are being proposed for use in iontophoresis reservoirs to enhance the selectivity of delivery of active substances across the skin.

Downloaded by 89.163.34.136 on June 23, 2012 | http://pubs.acs.org
Publication Date (Web): November 17, 2010 | doi: 10.1021/bk-2010-1053.ch001

Polymeric Antimicrobials and Bacteriostats

Small molecule preservatives are coming under increasing scrutiny, especially in Europe and polymeric antimicrobials are being investigated with the hope that they will function effectively to inhibit microbial growth in the product without the possibility of permeating the skin barrier when applied to the human substrate.

In one application, antimicrobial agents, such as silver have been either combined with a crosslinked hydrogel, to create a hydrophilic polymer antimicrobial system that has potential application in the personal care industry, including cosmetic, skin treatment, diapers, and bandages (*77*).

Polymers with antimicrobial properties have been announced. For example, chitosan is readily converted to 3-trimethylammonium-2-hydroxypropyl-N-chitosan (CHI-Q188), N-carboxy-methyl chitosan can be converted to an N′,N′-dimethylammoniopropylcarbamoyl-derivative and further modified by quaternization to produce a series of chitosan aminoamide quaternary compounds. The antimicrobial activity of CHI-Q188 against *Escherichia coli*, *Staphylococcus aureus* and *Pseudomonas aeruginosa* was demonstrated using the minimum inhibitory concentration test. The derivative exhibited biocidal activity at least an order of magnitude higher than previously reported chitosan antimicrobial agents (*78*).

Polyethylenenimine polymers have also been utilized as polymeric antimicrobial agents. For example, an antimicrobial polymer derived from polyethylenenimine was effective against pathogenic gram positive and gram negative bacteria, yeasts and molds, and skin flora bacteria (*79*). Copolymers and derivatives of polyethylenimine with broad spectrum antimicrobial properties are active against microbes on contact. It is believed that the large molecular size of these compounds enables them to resist removal from substrates and also prevents their ingress into the lower layers of skin of humans and animals (*80*).

Polymeric antimicrobials can also be effective against yeasts. Poly(methyl-methacrylate-co-vinylbenzoylchloride) and linear poly(chloroethylvinyl-ether-co-vinylbenzoylchloride) are active against *Candida albicans* and

Candida tropicalis. The poly(methylmethacrylate-co-vinylbenzoylchloride) proved more active against both *C. albicans* and *C. tropicalis* because of its increased cytotoxicity on bacteria and its interference with the cell walls. Poly(chloroethylvinylether-co-vinylbenzoylchloride) also proved effective by increasing the permeability of yeast cell walls.

Finally, old and new antidandruff technologies have been united by combining cationic polymers, such as hydrophobically modified quaternary ammonium cellulose ether, with antimicrobial compounds, such as sodium pyrithione, or zinc pyrithione (*81*). This cationic antimicrobial polymer system displayed effective antimicrobial properties at lower antimicrobial agent concentrations than conventional systems.

Downloaded by 89.163.34.136 on June 23, 2012 | http://pubs.acs.org
Publication Date (Web): November 17, 2010 | doi: 10.1021/bk-2010-1053.ch001

Summary

Today, several thousand different polymers are used as ingredients in personal care products. In many cases these polymers are used to deliver desired attributes to skin and hair and this polymer technology can be the harbinger of polymers that later appear as delivery agents for therapeutic drugs. This review is directed to recent trends in the use of polymers to deliver personal care attributes. The advent of living free radical polymerization has opened the door to synthesis of a wide range of block and graft copolymers and cosmetic formulators have utilized these new materials to simultaneously introduce apparently contradictory mechanical properties and to resolve formulation incompatibilities. Stimuli responsive polymers have been introduced that are hydrophobic below a trigger temperature and hydrophilic above it. Transfer-resistant cosmetics depend upon the detailed molecular structures of silicone resins. Rheology-modifiers for polar and non-polar systems are more precise due to the ability of polymer scientists to control molecular structure, molecular weight and polydispersity. The structure/property relationships of associative thickeners continue to be unraveled with a few surprises in recent years arising from the introduction of semi-hydrophobic monomers to the polymer backbone. Gelling agents have been derived with film-forming properties that confer on them the dual characteristics of thickener and hair-fixative. These polymers are complemented by thermoplastic elastomers that provide durable, styles that are changeable at will and polymers that strengthen permed dyed and relaxed hair. Complex coacervates continue to be the preferred *modus operandi* for stimuli-responsive two-in-one shampoos but delivery by complexes has been extended to fragrances, colors and therapeutic agents such as the antidandruff agent zinc pyridinethiol-N-oxide. Encapsulation and microencapsulation is being utilized to protect ingredients and to deliver them to the desired target substrates.

Finally, polymeric antimicrobials are being introduced with the promise of product preservation without the worry of skin permeation.

References

1. Matyjaszewski, K. General Concepts and History of Living Radical Polymerization. In *Handbook of Radical Polymerization*; Matyjaszewski, K., Davis, T., Eds.; Wiley-Interscience: Hoboken, 2002; Chapter 8, p 361.
2. Farcet, C. U.S. Patent Application 20090047308, 2009.
3. Destarac, M.; Joanicot, M.; Reeb, R. U.S. Patent 6,506,837, 2003.
4. Anthony, O.; Bonnet-Gonnet, C.; Destarac, M.; Farhoosh, R.; Joanicot, M.; Lizarraga, G.; Reeb, R.; Schwob, J.-M. U.S. Patent 6,437,040, 2002.
5. Schmidt, S.; Callais, P.; Macy, N.; Mendolia, M. U.S. Patent Application 2008/0058475, 2008.
6. Stewart, R. F.; Balachander, N.; Bitler, S. P.; Phan, L.; Yoon, V. Y. U.S. Patent 6,199,318, 2001.
7. Bitler, S. P.; Taft, D. D. U.S. Patent 7,449,511, 2008. U.S. Patent Application 20090068133, 2009.
8. Mondet, J.; Blin, X. U.S. Patent Application 20090068133, 2009.
9. Pavlin, M. S. U.S. Patent 20090082460, 2009.
10. Castrogiovanni, A.; Barone, S. J.; Krog, A.; McCulley, M. L.; Callelo, J. F. U.S. Patent 5,505,937, 1996.
11. Brieva, H.; Russ, J. G.; Sandewicz, I. M. U.S. Patent 5,800,816, 1998.
12. Patil, A. A.; Calello, J. F.; Sandewicz, R. W. U.S. Patent Application 20080050328, 2008.
13. Thevenet, L. U.S. Patent Application 20090081261, 2009.
14. Jones, C. E.; Reeve, P. U.S. Patent 5,916,967, 1999.
15. Emmons, W. D.; Stevens, T. E. U.S. Patent 4,079,028, 1978.
16. Eisenhart, E. K.; Howard, P. R.; Randow, R. L.; Aviles, R. G. U.S. Patent 5,281,654, 1994.
17. Hoy, K. L.; Hoy, R. C. U.S. Patent 4,426,485, 1984
18. Sonnabend, L. F. U.S. Patent 4,384,096, 1983.
19. *Aculyn –28; A Cost-Effective Versatile Rheology Modifier*; International Specialty Products Technical Brochure.
20. Hulden, M. *Colloids Surf., A* **1996**, *82*, 263–277.
21. Jones, C. E. *Proceedings of the 4th World Surfactants Congress, CESIO, Barcelona* **1996**, *2*, 439–450.
22. Reeve, P. *Proceedings of International Federation of Society of Cosmetic Chemists, IFSCC, Budapest*, 1997.
23. Jenkins, R. D. U.S. Patent 5,639,841, 1997.
24. Jenkins, R. D.; Bassett, D. R.; Shay, G. D. U.S. Patent 5,292,843, 1994.
25. Hoy, K. L.; Hoy, R. C. U.S. Patent 4,426,485, 1984.
26. English, R. J.; Raghavan, S. R.; Jenkins, R. D.; Khan, S. A. *J. Rheol.* **1999**, *43*, 1175–1194.
27. Dai, S.; Tam, K. C.; Jenkins, R. D. *Macromol. Chem. Phys.* **2002**, *203*, 2312–2321.
28. Jenkins, R. D.; Bassett, D. R.; Shay, G. D. U.S. Patent 5,292,828, 1994
29. Ng, W. K.; Tam, K. C.; Jenkins, R. D. *Polymer* **2001**, *42*, 249–259.
30. Dai, S.; Tam, K. C.; Jenkins, R. D. *J. Polym. Sci., Part B: Polym. Phys.* **2005**, *43*, 3288–3298.

Downloaded by 89.163.34.136 on June 23, 2012 | http://pubs.acs.org
Publication Date (Web): November 17, 2010 | doi: 10.1021/bk-2010-1053.ch001

31. Abdala, A. A.; Wu, W.; Olesen, K. R.; Jenkins, R. D.; Tonelli, A. E.; Khan, S. A. *J. Rheol.* **2004**, *48*, 979–994.
32. Schmucker-Castner, J.; Ambuter, H.; Snyder , M.; Weaver, A. A.; Kotian, S. U.S. Patent 7,217, 752, 2007.
33. *Carbopol® Aqua SF-1 Polymer Technical Data Sheet TDS -294*, July 2007.http://www.personalcare.noveon.com/TechnicalDataSheets/TDS-294_Carbopol_Aqua_SF-1.pdf.
34. Suares, A. J.; Zhang, J. H. U.S. Patent 6,986,895, 2006.
35. Ito, K. ; Mori, Y.; U.S. Patent Application 20060046949, 2006.
36. Sogabe, A.; Kaneda, I. U.S. Patent Application 20070231354, 2007.
37. Morschhauser, R.; Löffler, M.; Maier, I. U.S. Patent 6,964,995, 2005.
38. Morschhäuser, R.; Glauder, J.; Löffler, M.; Kayser, C.; Tardi, A. U.S. Patent 6,891,011, 2005.
39. Water, A.; Birkel, S.; Franzke, M.; Schmitt, K. U.S. Patent Application 20070197704, 2007.
40. *Fixate™ Plus Polymer, TDS-331*, 2007. http://www.personalcare.noveon.com/TechnicalDataSheets/TDS-331_Fixate_PLUS.pdf.
41. *Fixate™ Superhold Polymer, Technical Data Sheet TDS 5565 2007093K*, The Lubrizol Corporation.
42. Krysik, D.; Rafferty, D. W.; Tamareselvy, K.; Zellia, J.; Liu, X.; Shlepr, J. *Cosmet. Toiletries Manufacture Worldwide* **2007**, 11.
43. Drezwinski, M.; Albanese, J.; Yap, E.; Shih, J. S. U.S. Patent Application 2007020264, 2007.
44. Quadir, M.; Burakov, D.; Rollat-Corvol, I. U.S. Patent Application 20070224140, 2007.
45. Singer, J. M.; Baek, J. U.S. Patent Application 20070204871, 2007.
46. Quadir,M.; Burakov, D.; Rollat-Corvol, I. U.S. Patent Application 20070224140, 2007.
47. Vic, G.; Brun ,G.; Gourlaouen, L. U.S. Patent Application 20090155198, 2009.
48. Campain, C.; Devin-Baudoin, P. U.S. Patent Application 2007019008, 2007.
49. Bebot, C. U.S. Patent Application 20070190015, 2007.
50. Pasquet, D.; Bebot, C. U.S. Patent Application 20070190016, 2007.
51. Sabelko, J. J.; Cramm, J. R.; Damyanti, J. U.S. Patent Application 20070207106, 2007.
52. Chrisstoffels, L.; Becker, S.; Volkel, L. U.S. Patent Application 20070191548, 2007.
53. Constantinides, I. C.; Willicut, R. J.; Baker. E. S.; Hutton , H. D.; Felts, T. J.; Schechtman, L. A.; Minko, S.; Motornov, M. U.S. Patent Application 20070196299, 2007.
54. Kreeger, R. L.; Zhou, S. U.S. Patent Application 20070031362 Al, 2007.
55. Neibauer, M. F.; Lane, B. S.; Schwarz, J. R.; Warnke, D. T. U.S. Patent Application 20070009472, 2007.
56. Utz, F.; Lepilleur C. A.; Tamareselvy, K.; Chiarelli, J. A.; Schmucker-Castner, J. F.; Myers, M. P.; Hasman, D. F.; Vondruska, B. J.; Wilber, W. R.; Luo, H; Marchant, N. S.; Shuster, F. U.S. Patent 7,262,157, 2007.

Downloaded by 89.163.34.136 on June 23, 2012 | http://pubs.acs.org
Publication Date (Web): November 17, 2010 | doi: 10.1021/bk-2010-1053.ch001

57. Peffly, M. M.; Brown, M. A.; Staudigel, J. A. U.S. Patent Application 20070207109, 2007.
58. Albrecht, H.; Heitmann, B.; Ruppert, S. U.S. Patent 7,279,449, 2007.
59. Simonet, F.; Nicolas-Morgantini, L. U.S.Patent 20070237733, 2007.
60. Yoshinaga, M. U.S. Patent 5,276,088, 1994.
61. Nobuhiko, Y. U.S. Patent 5,855,900, 1999.
62. Cheng, J.; Davis, M. E.; Khin, K. T. U.S. Patent Application 20080058427, 2008.
63. Allart, P. J.; May, H. B. U.S. Patent 4,124,526, 1978.
64. Viladot Petit, J.-L. EU Patent application 1462157, 2003.
65. Percel, P. J.; Vishnupad, K. S.; Venkatesh, G. M. U.S. Patent 6,451,345, 2002.
66. Simmonet, J.-T.; Biatry, B.; Prigent, F. U.S. Patent Application 20090047, 2009.
67. Baviskar, R. J.; Kini, M.; Pradhan, R. R; Surianarayanan, R. U.S. Patent Application 20090041685, 2009.
68. Dykstra, R.; Gallon, L. S.; Clapp, M. L.; Deckner, G. E. U.S. Patent Application 20080057021, 2008.
69. Smith, G. A. U.S. Patent Application 2008/0058701, 2008.
70. Tomalia, D. A *Polym. J. (Tokyo)* **1985**, *17*, 117–132.
71. Newkome, G. R.; Yao, Z.; Baker, G. R.; Gupta, V. K. *J. Org. Chem.* **1985**, *50*, 2003–2004.
72. Kim, Y. H.; Webster, O. W. *Polym. Prepr.* **1988**, *29*, 310–311.
73. Kim, Y. *J. Polym. Sci., Part A: Polym. Chem.* **1998**, *36*, 1685–1698.
74. Newkome, G. R.; He, E.; Moorefield, C. N. *Chem. Rev.* **1999**, *99*, 1689–1746.
75. Newkome, G. R.; Yao, Z.; Baker, G. R.; Gupta, V. K. *J. Org. Chem.* **1985**, *50*, 2003–2004.
76. Sun, J.; Ramanathan, M.; Dorman, D.; Newkome, G. R.; Moorefield, C. N.; Russo, P. S. *Langmuir* **2008**, *24*, 1858–1862.
77. Chandra, N. S.; McNally, W. F.; Furey, J. M.; Robb, G. J.; Harriton, M. L. U.S. Patent Application 20060062854, 2006.
78. http://chemistry.lsu.edu/chem/facultypages/Faculty.php?chemID=59.
79. Huang, X.; Diesenroth, T. World Patent Application 2007085552, 2007.
80. Huang, X.; Deisenroth, T.; Preuss, A.; Marquis- Bienewald, A.; Hendricks-Guy, C.; Jennings, J. U.S. Patent Application 20070231291, 2007.
81. Annis I.; Gartner C. D. World Patent Application 2007050700, 2007.

Downloaded by 89.163.34.136 on June 23, 2012 | http://pubs.acs.org
Publication Date (Web): November 17, 2010 | doi: 10.1021/bk-2010-1053.ch001

Downloaded by DUKE UNIV on June 23, 2012 | http://pubs.acs.org
Publication Date (Web): November 17, 2010 | doi: 10.1021/bk-2010-1053.ch002

Chapter 2

Polymers in Nano Pharmaceutical Materials

Mustafa Akbulut,[‡] Suzanne M. D'Addio,[†] and Robert K. Prud'homme[†],[*]

[‡]Artie McFerrin Department of Chemical Engineering, Texas A&M University, College Station, TX 77843, USA.
[†]Department of Chemical Engineering, Princeton University, Princeton, NJ 08544, USA.
[*]prudhomm@princeton.edu

With the advent of nanotechnology, research on pharmaceuticals has experienced a paradigm shift. As opposed to traditional materials, new nanomaterials and nanoparticles are currently being investigated as drug delivery systems. This chapter provides an overview of contemporary approaches for producing nano-drugs. The discussion is divided into three parts: (1) the motivation for nano materials in pharmaceutical applications, (2) nano pharmaceuticals produced by "top down" processes that involve size reduction, and (3) processes that use "bottom up" assembly of nano materials from smaller sub units. In the "bottom up" assembly the distinction between thermodynamically controlled assembly and kinetically controlled assembly is presented with emphasis on the kinetically controlled assembly of polymer protected nanoparticles produced by Flash NanoPrecipitation. The advantages and disadvantages of the various approaches are discussed.

Introduction

The development and therapeutic use of a new drug requires more than just a compound with intrinsic pharmacological activity. Of equivalent significance is the path the drug molecules take in getting from the site of administration to site of action; the drug must get to the right place at the right time (*1*). Currently, there is significant effort to find drug delivery systems that facilitate transport of

In Polymeric Delivery of Therapeutics; Morgan, S., et al.;
ACS Symposium Series; American Chemical Society: Washington, DC, 2010.

Downloaded by DUKE UNIV on June 23, 2012 | http://pubs.acs.org
Publication Date (Web): November 17, 2010 | doi: 10.1021/bk-2010-1053.ch002

a drug to its site of action and make it available at the right concentration, at the appropriate time, and for the appropriate duration (*1*). The emerging fields of nanotechnology and nanoscience have an immense potential to fulfill these requirements. For instance, some advantages of drug nanoparticles could be the enhancement of dissolution rate through increased surface area, extending product life, and targeted delivery through novel pathways.

The need for nanoparticle formulations in drug delivery stems from several factors which currently limit the use and efficacy of some drug compounds. (i) Forty percent of all new chemical entities developed by the pharmaceutical industry are poorly water-soluble (*2–5*). Poorly water-soluble drugs have slow dissolution rates, limiting their bioavailability and in some cases, may result in failure to attain desired therapeutic levels in the body (*2*, *3*, *5*). Decreasing the particle radius increases the curvature of the material's interface and leads to an increase in its solubility (*6–8*), according to the Kelvin equation:

$$C(r) = C_\infty \exp\left[2\gamma \frac{V_m}{rRT}\right] \tag{1}$$

where C_∞ is the saturation solubility of the particle, C(r) is the solubility of a particle with radius, r, γ is the surface tension, V_m is the molar volume, R is the universal gas constant, and T is the temperature. Thus, by simply producing smaller and smaller drug particles, the solubility and bioavailability of a drug can be increased. (ii) Nanoparticle formulations can also be beneficial for improving transportation of drug from the site of administration to the systemic circulation. In general, a drug can be administered orally or by direct injection. In the case of oral delivery, only a portion may reach the systemic circulation since the drug may never sufficiently dissolve and pass from the gastrointestinal (GI) track to be absorbed into circulation. To a first approximation, doses delivered by oral administration for a drug limited by dissolution in the GI track can be modeled as follows:

$$dose = [\frac{rate}{area}][\frac{area}{mass}][time] \tag{2}$$

where typical residence times in GI track is ~ 8 hours. The first term in Eq. 2 is determined by the drug solubility and increases as the particle size decreases (inverse of the curvature) as described above. As can be visualized from Fig. 1, the second term is related to the surface area to volume ratio of materials, and increases with decreasing particle size as follows:

$$\frac{\pi R^2}{4/3\pi R^3} \propto \frac{1}{R} \tag{3}$$

(iii) For an injectable therapeutic or diagnostic nanoparticle agent to be of clinical value, prolonged blood circulation is one of the most important requirements. This keeps the drug concentration high enough to be therapeutically effective for as long as possible. One major obstacle to achieve prolonged circulation

Downloaded by DUKE UNIV on June 23, 2012 | http://pubs.acs.org
Publication Date (Web): November 17, 2010 | doi: 10.1021/bk-2010-1053.ch002

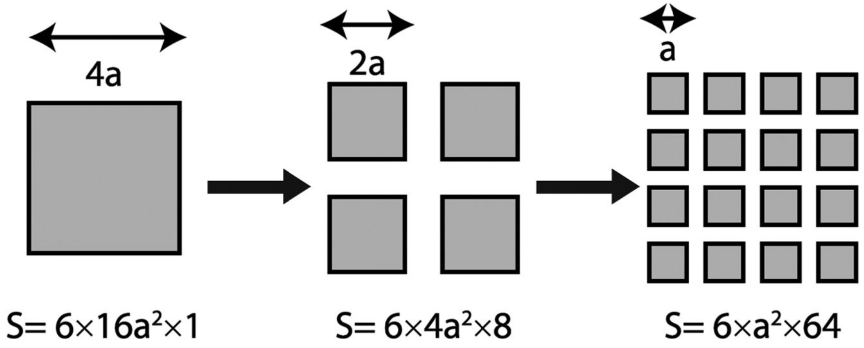

Figure 1. A visualization of showing how surface area, S, increases as the material is broken into smaller and smaller pieces (in 3-D).

is the clearance of foreign particles from the body by the reticulo endothelial system (RES) (*9*). The RES consists of the mononuclear phagocytic cells that circulate in the bloodstream and the matured cells (macrophages) that reside in such organs as the lungs, liver and spleen. The capture of foreign particles is believed to be mediated initially by the adsorption of plasma proteins, such as immunoglobulins, fibronectin or the complement proteins (opsonins), leading to recognition by the phagocytic cells (*9*). Another obstacle for obtaining prolonged circulation is the gradual degradation of drug carriers in blood stream, which can be tuned by changing the molecular weight and structure of a polymer steric stabilizing coating. The traditional method to eliminate circulation problems of NPs arising from the RES is to functionalize nanoparticles with biocompatible polymers: for example, the use of poly(ethylene glycol) (PEG) to coat the surface of nanoparticles has been successful in prolonging substance half lives to several hours in vivo (*10*). Figure 2 shows an example of improved circulation of drugs achieved by the use of lipid-based nanoparticles.

(iv) Nanoparticle formulations can also help drugs to successfully reach the target sites. For example, if the target sites are located outside of the blood compartment, as in the case with solid tumors, a drug-carrier is required to have the capability of penetrating through the blood vessel wall, unless a sustained-release mechanism is adopted (*2*, *11*). Generally, particles with sizes of less than 400 nm can travel through the blood stream without sedimentation or blockage of the microvasculature (*12*, *13*). In addition, such small particles can be taken up by cells through natural means such as endocytosis. But, for extended circulation times, drug particles should not be smaller than 20 nm to avoid renal clearance (*14*, *15*).

Now, we describe the methods to produce such nanoparticles. Drug nanoparticles can be fabricated using either “top-down” or “bottom-up” fabrication approaches. “Top-down” methods start with a bulk material and then break it into smaller pieces using mechanical, chemical or other forms of energy. In bottom-up methods, drug nanoparticles are fabricated from smaller pieces such as atoms or molecules in a controlled manner. The main advantages of top-down methods are: (i) simplicity, and (ii) the ability to separate drug purification (by crystallization) and qualification from the particle size formation

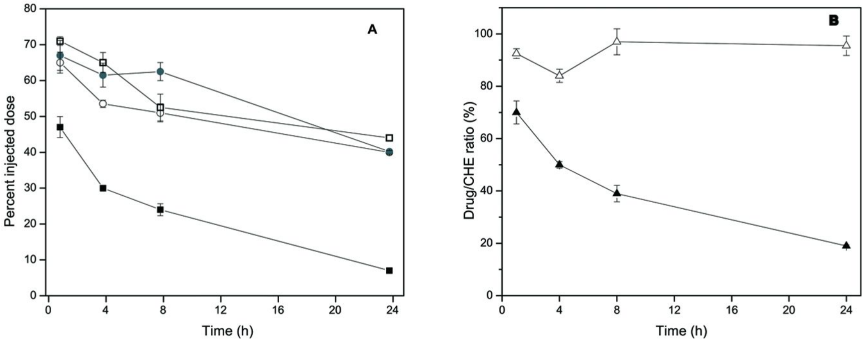

Figure 2. (A) Elimination of 1 (O) and 2 (•) in prodrug/VES/2kPS3k (1:1:2; w/w) formulations labeled with ^{3}H-CHE (□ and ■, respectively) in athymic nude Foxn1^{nu} mice dosed at 35 mg drug/kg doses (n = 3/time point). Drug concentrations were determined by HPLC analysis of plasma recovered at various time points. (B) Relative drug retention was determined using the ratio of drug/^{3}H-CHE in individual mice for 1 (Δ) and 2 (▲) systems (ρ and π, respectively). Error bars represent standard deviation (n = 3). (Adapted from Ref. (10))

process. Bottom-up fabrication offers numerous advantages over the top-down approaches: (i) the possibility of well-defined three-dimensional assembly, (ii) a greater ability to control the size distribution of the resultant particles, (iii) likelihood of inexpensive large scale production, (iv) shorter processing times, and (v) greater flexibility in surface functionalization.

In this review we provide an overview of methodologies for generating drug nanoparticles. These methodologies include milling, solid solution formation, micellar drug formulations, dendrimer formulations, spray drying, supercritical fluid formulations, and Flash NanoPrecipitation (FNP) technology.

Top-Down Approaches

Milling

Milling is a commonly used method for producing micron to sub-micron drug particles. In milling, first the desired material is synthesized, precipitated in pure form as large crystals, then the average particle size is reduced by a combination of energy-intensive methods, such as grinding and ball milling. Finally, the resultant particles are dispersed into the desired fluid media (*3*, *16*).

Drug concentrations up to 400 mg/ml can be produced by milling. Reduction in particle size can require grinding times in the order of hours to days depending on the processing conditions and the drug properties (*3*). The process can be performed either in a batch or recirculation mode and particle sizes from 200 to 1000 nm can be obtained. Figure 3 shows an example of change in the particle size distribution as a result of milling. Pharmacokinetic studies have shown that such naproxen nano-drugs produced by milling compared to traditional tablet formulations have a 2.5-4.5 fold increase in bioavailability.

Downloaded by DUKE UNIV on June 23, 2012 | http://pubs.acs.org
Publication Date (Web): November 17, 2010 | doi: 10.1021/bk-2010-1053.ch002

Downloaded by DUKE UNIV on June 23, 2012 | http://pubs.acs.org
Publication Date (Web): November 17, 2010 | doi: 10.1021/bk-2010-1053.ch002

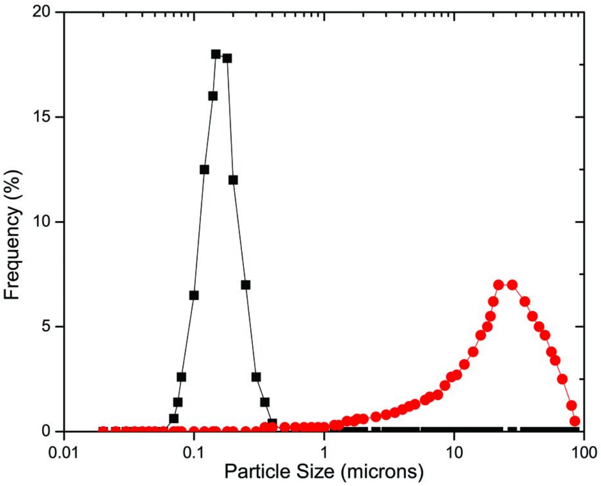

Figure 3. The particle size distribution profile of naproxen crystals before (▲) and after milling (•). Before milling, the drug crystals had a mean particle size of 24.2 microns. After being processed for 30 min in a media mill, the mean particle size of the nanocrystalline dispersion was 0.147 microns with D_{90}=0.205 microns. The particle size measurements were generated using laser light diffraction in a Horiba LA-910 using polystyrene nanospheres ranging in size from 0.1 to 10 microns as standards. (Adapted from Ref. (3))

The challenges of the milling approach include high energy consumption, long processing times, contamination and degradation of the drug by the grinding and milling processes, the requirement of a certain level of brittleness or "friability", and a limited ability to control the size distribution of the resultant particles (*17*). Particles having diameters smaller than 200 nm are very difficult to break down with this method (*17*). Frictional heating and triboelectrification can have significant influence on the processing of drugs in milling media (*18–20*). The frictional heating can result in melting of the drugs, disruption of the stabilizer adsorption, or the thermal degradation of the active (*21*). Another problem with media milling for pharmaceutical applications is the quality and durability of the milling media used in manufacturing (*3*). Crosslinked polystyrene spheres have proven to be effective media with acceptably low level of attrition and contamination of the product erosion of the beads (*3*).

Rapamune, emend, tricor, and megestrol acetate, paliperidone, and palmitate are some commercially marketed examples of drugs prepared by milling methods (*22*).

Solid Solutions

Just as one can make a liquid solution with a solvent and several solutes, one can make a "solid solution" that is one phase with a number of components. Solid solutions of a water insoluble drug are prepared by dissolving a drug in a carrier which has a relatively high aqueous solubility and then solidifying the mixture.

As the solid carrier matrix dissolves in the stomach the “dispersed” hydrophobic drug is now supersaturated in the aqueous media. It may locally combine to form spontaneous nanoparticles or it may be dispersed by dilution. These solid mixtures have shown an ability to improve bioavailability and dissolution rates. By careful selection of a carrier for the solid solution, the dissolution rate of the drug can be increased by up to several orders of magnitude (*23*). Solid solutions can be prepared using two common methods: (i) the hot melt method, and (ii) the solvent method (Fig 4) (*23*, *24*).

In the hot melt method, drug and water-soluble carrier are melted together at a temperature above the eutectic point (Fig. 4). The most common carrier or matrix phase materials are water soluble polymers such as polyvinyl pyrollidone (PVP) (*25*), (polyethylene glycol (PEG) (*26*), hydroxypropylcellulose (HPC) (*27*), chitosan (*28*), and gelatin (*29*). These polymers have the advantages that they are biocompatible, solubilize many hydrophobic drugs in the molten form, and upon cooling they uniformly transition from a liquid to a solid glass. Their high viscosity in the molten state slows diffusional growth process and, even for drugs that phase separate during cooling rather than remaining as true solid solutions, they create solids with finely dispersed drug particles. The liquid solution is then rapidly cooled to induce solidification (*30*). Cooling may lead to supersaturation, but the dispersed drug becomes trapped within the carrier matrix because of rapid solidification (*30*). The resultant solid (solution) is then milled to reduce the particle size, so the final particulate is macroscopic in size. Whether or not a molecular dispersion can be achieved depends on the degree of supersaturation and rate of cooling attained in the process. In other words, the particle size distribution is history dependant i.e. the processing sequence and conditions have an effect on the resultant dispersion and can be varied to optimize the product (*23*). A variant of the traditional hot melt method is hot-melt extrusion by which the drug/carrier mixture is simultaneously melted, homogenized and then extruded and shaped as tablets, granules, pellets, sheets, sticks or powder (*31*). An important merit of the hot melt extrusion method is that the drug/carrier mix is only subjected to an elevated temperature for a short time, which enables drugs that are somewhat thermolabile to be processed (*31*).

An important limitation for the manufacture of solid solutions by the hot melt method is the miscibility of the drug and the carrier in the molten form. When there are miscibility gaps in the phase diagram, this usually leads to a product that is not molecularly dispersed (*23*). In other words, there is phase separation during the quenching stage. Another limitation to the hot melt method is the thermostability of the drug and the carrier (*24*). If too high a temperature is required, the drug may decompose or volatilize during processing. Oxidative reactions can be minimized by processing in an inert atmosphere or under vacuum, while evaporation can be avoided by processing in a closed system, but these additional measures increase the cost of the process.

In the solvent method, the drug and the carrier are dissolved in a common solvent, and then the solvent is evaporated under vacuum to produce a solid mixture (*25*). An important prerequisite for the manufacture of a solid dispersion using the solvent method is that both the drug and the carrier are sufficiently soluble in the solvent, and there is no phase separation during removal of the

Downloaded by DUKE UNIV on June 23, 2012 | http://pubs.acs.org
Publication Date (Web): November 17, 2010 | doi: 10.1021/bk-2010-1053.ch002

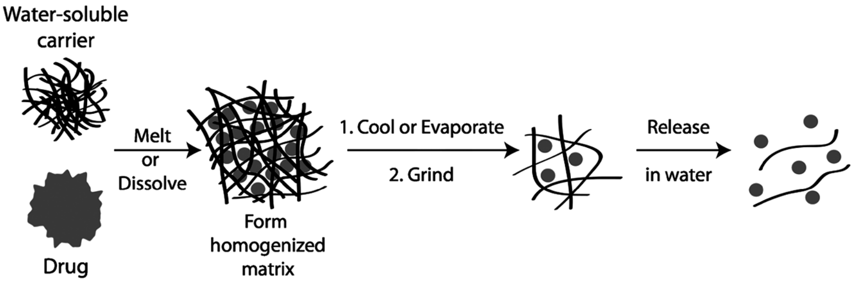

Figure 4. Schematic representation of solid solution strategies. Adapted from Ref (24).

Downloaded by DUKE UNIV on June 23, 2012 | http://pubs.acs.org
Publication Date (Web): November 17, 2010 | doi: 10.1021/bk-2010-1053.ch002

solvent as the composition of the system changes. There are various methods to remove the solvent such as heating, freeze-drying (*32*, *33*), or spray-drying (*34*). Temperatures used for solvent evaporation typically ranges from 25 to 65 °C (*35*).

A griseofulvin-in poly(ethylene glycol) solid dispersion (Gris-PEG, Novartis) and a nabilone-in-povidone solid dispersion (Cesamet, Lilly) are examples of commercial drugs utilizing solid mixture technique. Some other examples of drugs that have been processed into solid dispersions using hot-melting to date include testosterone (*36*), progesterone (*37*), and dienogest (*38*).

Bottom-Up Approaches

Micelles (Self-Assembly)

Controlling the drug form and maintaining chemical and physical stability upon storage gets more difficult as the particle size gets smaller. In the absence of the steric or electrostatic stabilization, the high surface energy of nanometer-particles usually tend to drive aggregation due to attractive van der Waals forces, and the reduction in surface energy per volume as particle size increases (*39*). One technique to overcome aggregation is to protect the drug particles with amphiphilic block copolymers, which can self-associate to form micelles with sizes of 100 nm or less (*40*). The sizes of polymeric micelles not only makes them attractive drug delivery carriers because particles larger than 40 nm avoid renal clearance, but also their size allows permeation through endothelial defects in the vasculature in the vicinity of solid tumors by passive diffusion (*41–43*). It is also possible to form micelles using conventional surfactants; however, surfactant micelles are always smaller than 40 nm. Also, polymeric micelles have advantages over conventional surfactant micelles in that they have better thermodynamic stability in physiological solution, since amphiphilic polymers have remarkably lower critical micellar concentrations than surfactants. If the steric stabilizing layer sufficiently protects the nanoparticle from recognition and clearance by the reticulo-endothelial system (RES), then the NP will have increased circulation time and a higher accumulation of a drug at the target site (*42*).

There are two common methods for preparing polymeric micelles, the direct dissolution method and the dialysis method (Fig 5) (*40*). The selection of which method to use depends mostly on the solubility of the block copolymer in water. If the copolymer is sufficiently soluble in water, the direct dissolution method is utilized. On the other hand, if the copolymer is poorly soluble in water, the dialysis method is usually employed.

The direct dissolution simply involves adding the copolymer to water or other aqueous media, and then mixing the solution thoroughly to achieve a homogenous solution, and waiting for the copolymer to thermodynamically self-assemble into micellar structure. In some cases the polymer and water are mixed at elevated temperatures to facilitate micellization (*40*). For example, using the direct dissolution method, Kabanov et al. (*44*) prepared micelles of poly(oxyethylene-b-oxypropylene-b-oxyethylene) triblock copolymers (Pluronic polymers F68, P85, and F108) in aqueous solutions for drug delivery applications.

The dialysis method is usually used when micelles are to be formed from a copolymer that is poorly soluble in water or aqueous media (*45–47*). In this case, the copolymer and drug are first dissolved in a common organic solvent that is miscible with water, such as dimethylsulfoxide (DMSO), dimethylformamide (DMF), or tetrahydrofuran (THF). Then, the copolymer-drug-solvent mixture is dialyzed against an aqueous phase. As dialysis takes place and system slowly equilibrates, the organic solvent is removed and replaced by the aqueous phase, and micelle formation is induced. During solvent exchange a complicated process of nucleation and precipitation of the drug, micellization of the polymer, and partitioning of the drug into the micelle core occurs. The result may be the formation of large drugs crystals and unfilled micelles, drug loaded micelles or a mixture of both (*48*). For instance, using the dialysis method, methoxy poly(ethylene glycol-b-ε-caprolactone) (PEG-b-PCL) block copolymeric micelles containing indomethacin were prepared by Kim et al. (*49*) and polyethylene oxide-b-polybenzyl L-aspartate (PEO-b-PBLA) micelles were prepared as a novel nano-drug careers by La et al. (*50*).

In both cases, when the solution is water-rich, the hydrophobic blocks of the copolymer form the core of the micelle while the hydrophilic blocks form the outer shell. The hydrophobic micelle core serves as the microenvironment for the incorporation of lipophilic drugs, while the corona shell serves as a stabilizing interface between the hydrophobic core and the external medium.

The loading properties of block copolymer micelles depend largely on the physicochemical properties of the drug, properties of the copolymer, presence of specific interactions between the drug and the core-forming block as well as the method employed for preparation (*48*). In order to understand the relationships between the physicochemical properties of the drug and the copolymer and the drug loading properties of the micelle, it is necessary to first consider the partitioning behavior of the drug between micelles and an external medium. In general, the solubility parameters of the solute (drug) and the core-forming polymer blocks should be of the same order to achieve high loading (*48*).

Some advantages of micellar drugs are (i) the formulation of hydrophobic drugs in these micelle systems provides a significant increase in the water solubility of some compounds, (ii) the administration of drugs micelles can reduce their toxicity and improve their therapeutic efficacy, and (iii) better control of the release profile, and (iv) they can be functionalized to have targeting capabilities. Some

Downloaded by DUKE UNIV on June 23, 2012 | http://pubs.acs.org
Publication Date (Web): November 17, 2010 | doi: 10.1021/bk-2010-1053.ch002

Downloaded by DUKE UNIV on June 23, 2012 | http://pubs.acs.org
Publication Date (Web): November 17, 2010 | doi: 10.1021/bk-2010-1053.ch002

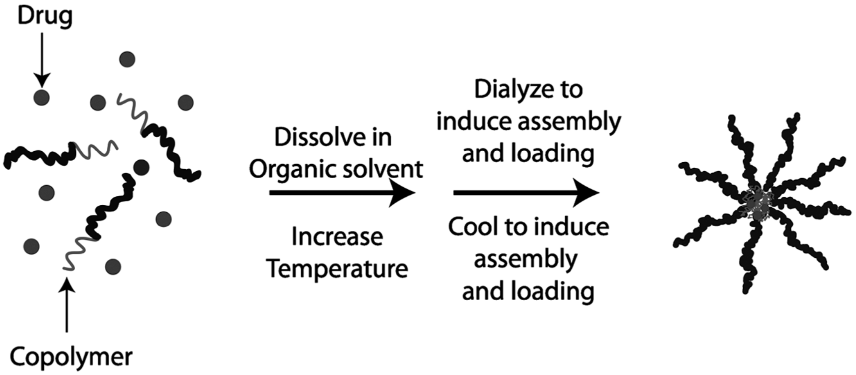
Drug
Copolymer
Dissolve in Organic solvent
Increase Temperature
Dialyze to induce assembly and loading
Cool to induce assembly and loading

Figure 5. A schematic representation of the polymeric micelle formation

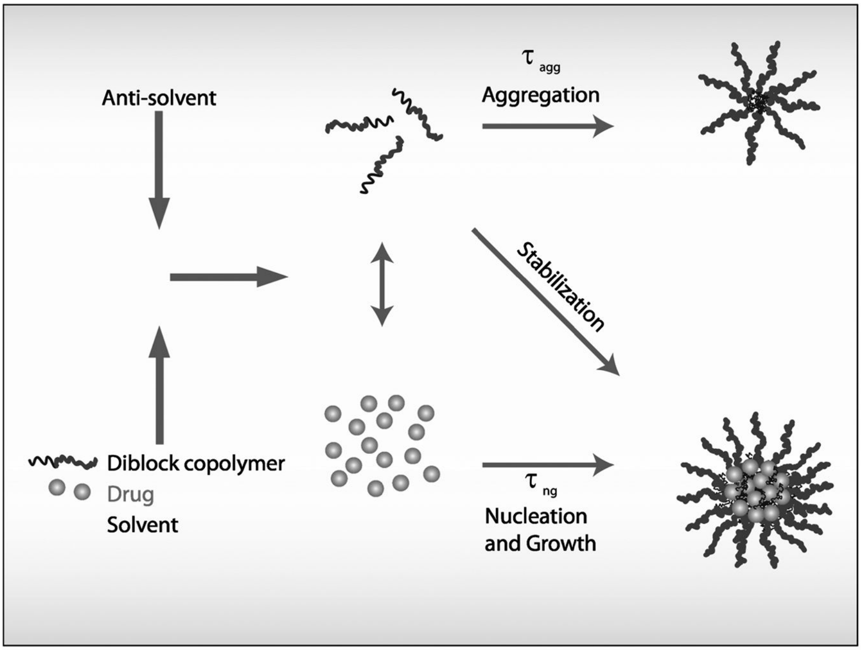
Anti-solvent
τ agg
Aggregation
Stabilization
τ ng
Nucleation and Growth
Diblock copolymer
Drug
Solvent

Figure 6. A schematic representation of the Flash NanoPrecipitation process.

drawbacks are (i) drugs can leave the micelle within a very short period of time following in vivo administration (*10*), and (ii) low loading because of their small size (*48*).

Micellar nanoparticle technology is under clinical study for various applications such as Genexol PM (non-small cell lung cancer, Samyang), Estrasorb (estrogen therapy, Novavax), Medicelle (cancer treatment, NanoCarrier), Flucide (anti-influenza, NanoViricides), Basulin (long acting Insulin, Flamel Technologies), and DO/NDR/02 (paclitaxel delivery- Dabur Research Foundation) (*51*, *52*).

Downloaded by DUKE UNIV on June 23, 2012 | http://pubs.acs.org
Publication Date (Web): November 17, 2010 | doi: 10.1021/bk-2010-1053.ch002

Rapid Precipitation and Directed-Assembly

Rapid precipitation and polymer protection is a simple, rapid, and robust method for producing drug nanoparticles. In these processes, an organic active and amphiphilic diblock copolymer are molecularly dissolved in an organic phase and rapidly mixed against a stream of miscible anti-solvent to precipitate the active with a tunable, narrow, submicron size distribution from 50 nm to 500 nm (Fig 6). When water is the anti-solvent, a hydrophobic active and the hydrophobic portion of the copolymer are simultaneously precipitated to form nanoparticles. They are protected from aggregation and sterically stabilized by the hydrophilic portion of the block copolymer (*53–58*). These differ from traditional micellar nanoparticle formation methods such as direct solution or dialysis methods in terms of the dynamics of the process (*56*): the rapid mixing and precipitation produces nanoparticles that are in a kinetically trapped (frozen) rather than at equilibrium. This non-equilibrium process offers more control and flexibility of size and chemistry because assembly is governed not just by thermodynamic conditions but by the entire process history (*59*).

In terms of loading behavior, there is a fundamental difference between imbibing drugs into a polymeric micelle core, and coating a drug particle with a polymeric stabilizing layer: coating methods lead to much higher drug loading. In rapid precipitation methods, actives are precipitated into particle form, followed by adsorption of stabilizers on the particle surfaces. The result is a pure phase with a surface coating. Thus, precipitation with surface protection, in principle, enables higher drug loadings than can be achieved by imbibing drugs into a polymer matrix (*48*). The loading behavior of FNP can be tuned by controlling aggregation times of polymer and nucleation times of active, which can be adjusted, for example, by changing concentrations of polymer and active. Therefore, it is less dependent on the thermodynamic details and the type of copolymer used.

Rapid mixing can be achieved in several ways. Johnston has relied upon injection into turbulent non-solvent streams in tube flow (*53*, *57*), to produce itraconazole loaded-poly(ethylene oxide-b-propylene oxide-b-ethylene oxide) NPs with sizes of sub-300 nm (*57*). The Prud'homme group has extensively focused on advanced mixing geometries to effect mixing in millisecond times. The mixing processes have been demonstrated both in a confined impinging jet (CIJ) and in a multiple inlet vortex mixer (Fig. 7) (*56*, *60*). We have termed the rapid precipitation and copolymer directed assembly using these advanced mixers Flash NanoPrecipitation (FNP). With the process we have produced NPs from paclitaxel (*10*), β-carotene (*55*, *56*, *60*), bifenthrin (*61*), gold nanoparticles (*62*), and fluorescence imaging dyes (*63*).

FNP contains several key components shown in Fig. 6, first of which is a rapid mixing time, τ_{mix}, shorter than formation time, τ_{ng} for a nanoparticle. The formation processes involve particle nucleation and subsequent growth. This corresponds to a Damkohler number for precipitation, $Da_p = \tau_{mix}/\tau_{ng}$, the ratio of these times, which is less than one. Times, τ_{agg} and τ_{ng} can be tuned effectively by changing the active concentration or the molecular architecture of the diblock copolymer. When the two times are properly tuned to match each other, the insoluble portion of the block copolymer is deposited on the

Downloaded by DUKE UNIV on June 23, 2012 | http://pubs.acs.org
Publication Date (Web): November 17, 2010 | doi: 10.1021/bk-2010-1053.ch002

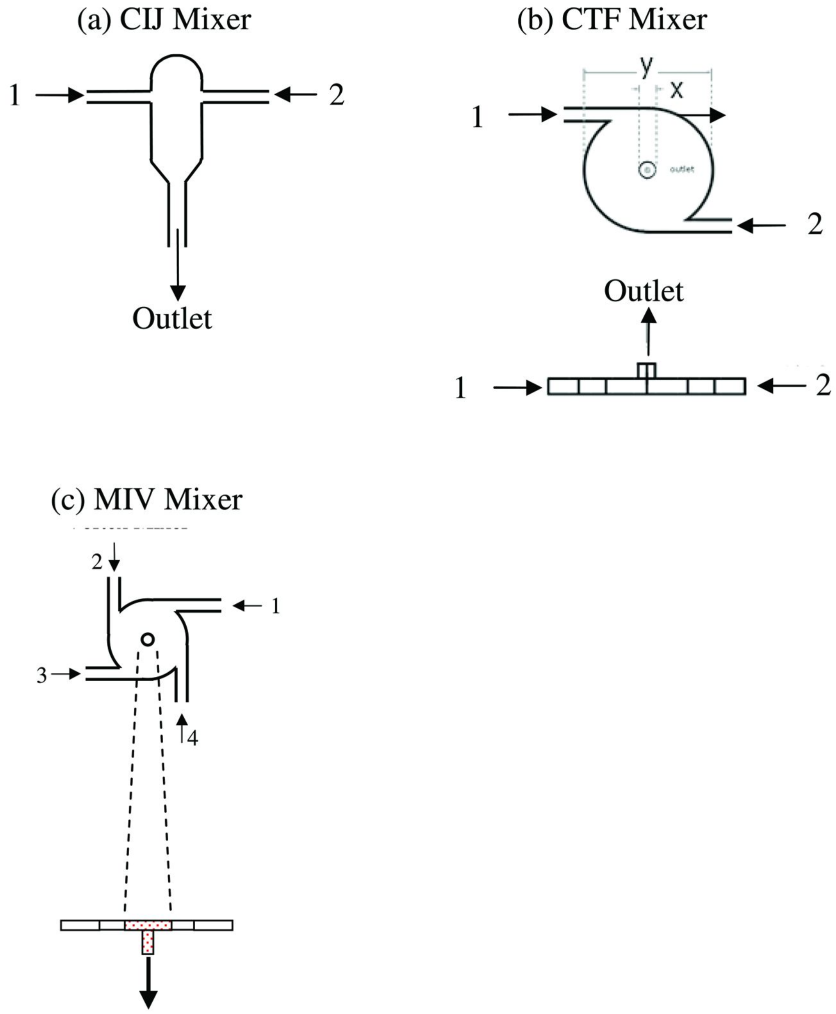

Figure 7. Figures show mixer designs in Flash NanoPrecipitation. Schematic diagram of (a) confining impinging jet mixer (CIJ), (b) confined tangential flow mixer (CTF) and (c) multiple inlet vortex mixer (MIV).

surface of the growing organic particle to freeze the size distribution at that desired for a particular application. In addition, the proper selection of block copolymer can act as a nucleation promoter and further control the production of nanoparticles. Briefly, FNP uncouples micromixing from nucleation and growth, and arrests growth with precisely tailored block copolymers to controllably form nanoparticles with narrow size distributions from 50 - 500 nm.

Fluctuations in concentration due to poor mixing cause dramatic variation in particle formation since nucleation rates depend strongly on supersaturation, $S=C/C_{equil}$ (*64*):

$$J = A \times \exp\left(-\frac{B}{S^2}\right) \tag{4}$$

where coefficients, A, and B depend on the temperature, and the surface energy. In CIJ and MIVM, the segregation length scale of the incoming fluids is rapidly reduced by impinging two or four jet streams. One advantage of the these mixers is that the collision of the incoming jets in the mixer produces a region of high intensity micro-mixing, which can produce a uniformly mixed solution phase prior to nucleation, enabling the preparation of very small particles. Mixing times in the range of milliseconds can readily be achieved by a CIJ or MIVM, enabling the precipitation to occur under a homogenous state at high supersaturation where the effect of mixing is not convoluted with the role of concentration-dependent precipitation. Another important merit of FNP is that the method is scalable (*55*, *56*). Results from small-scale laboratory tests can be directly scaled to larger production volumes.

In FNP, the critical attribute that anti-solvent concentration or temperature drives supersaturation enables the attainment of high supersaturations, $S_0 = C_p/C_{cmc} > 10^2$, where C_p is the initial unimer concentration and C_{cmc} is the critical micelle concentration after the solvent quality jump. The block copolymers and drugs must be soluble at the starting conditions, but have $C_{cmc} \leq 10^{-3}$ wt% at the final conditions. In turn, the free energy penalty required to expel a chain from the nanoparticle core at the final conditions should also be high, $\Delta > 5$ kT (*55*, *56*). The high exchange energy and low C_{cmc} limits solvent mediated unimer exchange between micelles that normally leads to dynamic equilibrium and instability of particle size (*55*, *56*).

Dendrimers

Dendrimers are hyperbranched macromolecules comprising a multifunctional core, several branching points, and outer surface moieties (Fig. 8). Dendrimer size is classified by ‘generation’, wherein each generation corresponds to a layer of branching units (*65*). Synthesis routes are out the scope of this review, but have been extensively reviewed by others (*65–67*). The alternate, step-wise synthesis of dendrimerS, leads to a very low polydispersity, and a defined number of reactive surface groups (*65–67*). Because dentritic molecules contain a hydrophobic interior and yet contain hydrophilic surface groups, they are often referred to as unimolecular micelles. Due to their ability to solubilize hydrophobic drug molecules into their core, they are being considered in drug delivery applications.

The high number of surface functional groups, tailored hydrophobic core created within the branches, and uniform sizes between 5 and 10 nm are their main advantages (*66*). The loading of the dendrimer core is performed by solvent exchange as is done the loading of block copolymer micelles.

Downloaded by DUKE UNIV on June 23, 2012 | http://pubs.acs.org
Publication Date (Web): November 17, 2010 | doi: 10.1021/bk-2010-1053.ch002

Downloaded by DUKE UNIV on June 23, 2012 | http://pubs.acs.org
Publication Date (Web): November 17, 2010 | doi: 10.1021/bk-2010-1053.ch002

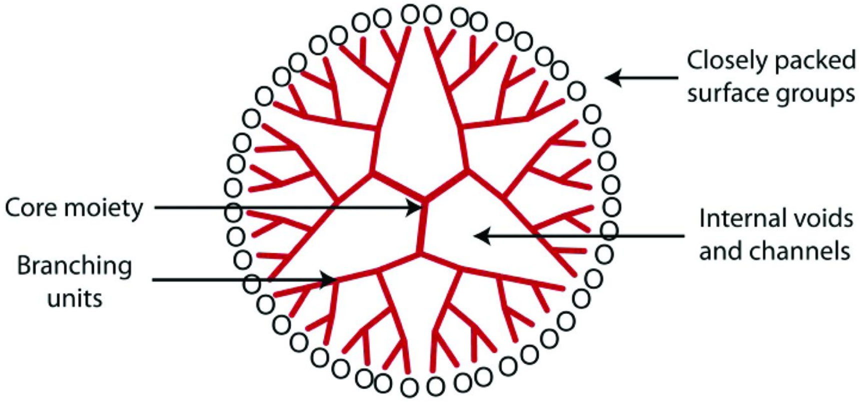

Figure 8. A schematic representation of dendrimer

Supercritical Fluid Methods

Supercritical fluids (SF) have been widely studied as a means towards the creation of uniform powders for pharmaceutical application (*68*). There are two major types of processes which have been developed for the formation of nanoparticles: rapid expansion of supercritical solutions (RESS) and supercritical anti-solvent precipitation (SAS). Both of these processes are capable of producing particles from the micron scale down to the nano-scale (*69*, *70*).

In RESS, the desired drug particulates can be precipitated directly from the SF through a sudden expansion of the fluid through a nozzle into a collection chamber. As the pressure and density of the SF drops during expansion, the solute capacity dramatically decreases, creating supersaturated conditions and inducing homogenous nucleation of particulates (*71*). In a modified RESS process, termed the rapid expansion of a supercritical solution into a liquid solvent (RESOLV), nanpoarticles of both organic and inorganic compounds have been formed (*72*–*74*). However, for water-insoluble organic compounds, stabilizing coatings are necessary to prevent particle aggregation in aqueous media. For example, 400-700 nm nanoparticles of cylcosporin, a water-insoluble drug, formed by the RESOLV process were sterically stabilized after formation by expansion into an aqueous solution of Tween-80, and remained stable over a four month observation period (*75*).

For SAS, precipitation of particles is induced by mixing a solution of the desired drug with a SF or a binary SF mixture, where the SF phase serves as the anti-solvent. For this process to be successful in precipitating particulates, the solvent must be fully miscible in the SF while the drug must be insoluble in the SF. The two fluids are mixed at conditions above the mixture critical point (MCP) which is essential to forming a homogenous mixture and uniform particles. Upon mixing of the drug/solvent phase with the SF phase, solute capacity decreases and drug particulates are precipitated under supersaturated conditions. In SAS the mechanism of particle formation has been found to be dependent on the phase behavior of the binary system and the location of the MCP (*76*, *77*). In concept, this process is no different than anti-solvent precipitations from pure liquid phases. The advantage is that the SF phase can be ultimately removed by depressurization.

Solubility of the drug of interest plays a key role in determining which of the two types of processes is applicable for a given drug molecule. While RESS is a very simple and clean process for the production of powders with high purity, the major limitation is that the solute must have an appreciable solubility in the SF. Otherwise, large volumes of the SF are required to process the drug. This requirement makes this process impractical for many pharmaceutical actives which have low solubility in CO_2, the most commonly used SF.

SAS can be used to form nanoparticles of both hydrophobic and hydrophilic compounds. Since CO_2, the most desirable SF is hydrophobic, hydrophobic compounds are precipitated from a binary mixture of an appropriate organic solvent and the SF. Hydrophilic compounds in aqueous solution are mixed with a SF that must be premixed with an organic solvent in which the aqueous solvent is miscible in order to form a homogenous ternary mixture (*69*, *78*). The temperature, pressure, drug concentration and relative flow rates affect the phase behavior of these systems, which has been shown to affect particle size and polymorphism (*79*). The particle formation pathway in these processes is not well-understood and prediction of the MCP and product properties based on operating conditions is not yet possible. As mentioned previously, the most commonly used SF in both processes, especially for pharmaceutical applications, is SF-CO_2 due to its lack of environmental effects, low cost and mild supercritical conditions. Additionally, SF-CO_2 removal is easily accomplished by reducing the system pressure; though, in SAS, thorough washing of the product with SF to remove solvent is necessary to prevent particle agglomeration. While the exploration of other SFs is an option in order to make the RESS applicable to a greater number of drug compounds, the aforementioned advantages are often lost.

In each of these methods, all processing can be completed in a single, enclosed step resulting high yield, uniform product formation while minimizing energy requirements and contamination risks. However, implementation of SF production methods require semi-batch processes, requiring downtime for product removal and equipment cleaning, which both reduces unit productivity and introduces contamination risks. Further development of these methods is necessary before such implementation can occur on the industrial scale. Key issues which must be overcome including a better understanding of particle formation and how particle size and morphology are affected by process parameters, as well as more practical issues such as proper equipment design and scale up procedures (*68*).

A variant of RESS and SAS processes was developed by Bradford Particle Design (now Nektar) and is shown schematically in Fig. 9. This process uses supercritical CO_2 to enhance the atomization of a solvent stream with a dissolved drug species and, hence, was named solution enhanced dispersion by supercritical fluids (SEDS).

The mixing of the CO_2 stream with the solvent stream occurs at the atomization nozzle where mixing simultaneously produces supersaturation of the drug in the CO_2/solvent mixture and expansion of the CO_2 as the fluid exits the nozzle. The droplet size is smaller than would be achieved with atomization

Downloaded by DUKE UNIV on June 23, 2012 | http://pubs.acs.org
Publication Date (Web): November 17, 2010 | doi: 10.1021/bk-2010-1053.ch002

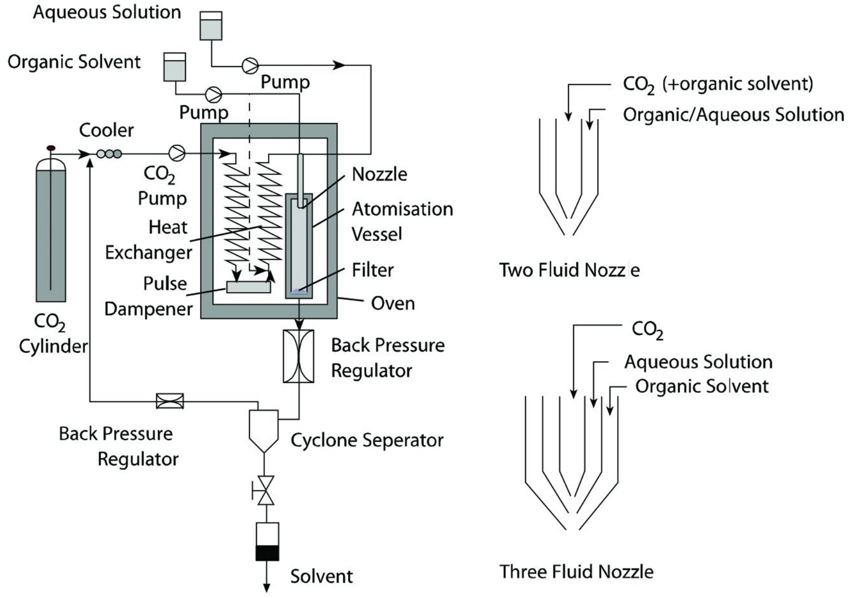
Aqueous Solution
Organic Solvent
Pump
Pump
Cooler
CO_2 Pump
Heat Exchanger
Pulse Dampener
CO_2 Cylinder
Nozzle
Atomisation Vessel
Filter
Oven
Back Pressure Regulator
Back Pressure Regulator
Cyclone Seperator
Solvent
CO_2 (+organic solvent)
Organic/Aqueous Solution
Two Fluid Nozzle
CO_2
Aqueous Solution
Organic Solvent
Three Fluid Nozzle

Figure 9. Schematic of the SEDS process with nozzle arrangements, adapted from Ref. (80).

energy alone because it is augmented by the vaporization of the CO_2. The result is a fine spray which dries to produce high surface area.

The supercritical SEDS process provides high surface area powders that increase the bioavailability of hydrophobic drugs administered by oral or aerosol routes. However, they do not provide discrete particles for parenteral administration. The resulting aggregates are too large to effectively circulate. While elegant and effective, the process has yet to achieve commercial acceptance because of the difficulty and cost of solvent recovery from the CO_2/solvent vapor stream.

Spray Drying

Spray drying techniques are widely employed to produce dry powders of pharmaceutical compounds. The process has been used to directly form nano- and micron-scale particulates from solutions for drug delivery applications, though the majority of work in this field has yielded particles in the 1-10 μm range, which limits their use for parenteral applications (*81–85*). For example, while microcapsules are ideal for aerosol drug delivery, particles this large cannot be used to take advantage of the enhanced permeability and retention (EPR) effect to deliver drugs to tumors (*86*, *87*). The architecture of particles which may be formed by spray drying include core/shell, hollow, and solid foam nanoparticles which may be spherical or collapsed in shape (*88*). Spray drying also may be used as a secondary processing method to encapsulate pre-formed nanoparticles in larger matrices for applications such as controlled release in pulmonary applications (*89*).

Downloaded by DUKE UNIV on June 23, 2012 | http://pubs.acs.org
Publication Date (Web): November 17, 2010 | doi: 10.1021/bk-2010-1053.ch002

Downloaded by DUKE UNIV on June 23, 2012 | http://pubs.acs.org
Publication Date (Web): November 17, 2010 | doi: 10.1021/bk-2010-1053.ch002

In the spray drying process, a feed solution containing the desired components of the powder, including active pharmaceutical ingredients (APIs) and any excipients, is first atomized. A number of atomization methods, such as rotary atomization, pressure atomization, and two-fluid atomization are applicable (*90*). The sprayed droplets then dry while in contact with air or another suitable gas at elevated temperatures. The dry powder must then be separated from the gas stream, which can be recycled or removed from the system (*90*).

A challenge in the formation of nanoparticles by spray drying is controlling particle morphology, which has been found to depend on various process parameters, but with a key emphasis on the evaporation rate (*91–94*). For pharmaceutical applications, both particle size and morphology have been shown to affect drug release rates (*95–97*). A commonly encountered morphology for powders formed by spray drying is a crumpled particle, which has been found to have improved dispersion characteristics for aerosol applications (*95*, *98*). In order to impart some predictability of and control over final product structure, a number of models for droplet drying have emerged (*99*, *100*). In a simplified analytical model, the initial solute concentration and a dimensionless Peclet number, defined as $Pe_i = \frac{\kappa}{8D_i}$, have been used to determine the morphology for a given solute (*101*). This dimensionless group depends on the evaporation rate k, defined as $d^2(t) = d_o^2 - \kappa t$ (*102*), where d is the initial particle diameter and t is evaporation time and the solute diffusivity D_i in the given solvent. Therefore, control over morphology may be attained by modifying the evaporation rate, for a solute of given diffusivity, as well as by controlling the initial solute concentrations.

Another challenge in the formation of nanoparticles by spray drying is efficiently producing particles which are less than a micron in size. At high concentrations, particle size is independent of the concentration and large particles are formed, while at low concentrations, particle size does depends on concentration of solids in the feed (*103*), therefore, dilution of the feed stream may be performed to yield nanoparticles. However, as a consequence of dilution, the overall solids production and the production rate are low. Reduction of droplet size will also yield smaller particles, however this requires an increase in power input in the atomization step. Additionally, recovery of nanometer-sized powders after drying is difficult and may result in significant product losses. Effective separation involves multiple post processing steps, including the use of cyclone separators as well as filters and scrubbers to recover powders from air streams.

Conclusions

We have briefly presented various techniques for the production of nanoparticles in the pharmaceutical industry. The interest in this area is mainly driven by the introduction of new hydrophobic drugs and challenges in making them adequately bioavailable as well as the development of new nanoparticle carriers for drug targeting and controlled release. A review of this type is necessarily cursory -- each specific production process contains a wealth of challenges and details that this review can only briefly allude to. We hope that the references in each section direct you to resources for further study.

As the drug discovery and delivery teams in large and small pharmaceutical companies seek to move laboratory advances into production there will be even more interest in developing and improving processing technologies. Some processes will grow in importance and some will recede. At this time "top down" milling processes are proving more and more successful at producing successful commercial compounds. However, the cost and time involved in milling is a driver for the development of less expensive "bottom up" processes. In addition, "top down" processes cannot produce the sorts of targeted and complex controlled release nanoparticles that are often desired. In "bottom up" processes, the melt solid solution processes, we believe, will continue to evolve as a major means of producing bioavailable compounds for oral delivery. Supercritical fluid processes have been largely unsuccessful at the commercial scale and they are declining in interest. However, for injectable formulations and controlled release we believe that the rapid precipitation with block copolymer directed assembly will be the most successful strategy to produce nanoparticle formulations.

Downloaded by DUKE UNIV on June 23, 2012 | http://pubs.acs.org
Publication Date (Web): November 17, 2010 | doi: 10.1021/bk-2010-1053.ch002

References

1. Hillery, A. M.; Lloyd, A. W.; Swarbrick, J. *Drug delivery and targeting for pharmacists and pharmaceutical scientists*; Taylor & Francis: London, 2001.
2. Kwon, G.; Naito, M.; Yokoyama, M.; Okano, T.; Sakurai, Y.; Kataoka, K. *Langmuir* **1993**, *9* (4), 945–9.
3. Merisko-Liversidge, E.; Liversidge, G. G.; Cooper, E. R. *Eur. J. Pharm. Sci.* **2003**, *18* (2), 113–20.
4. Rogers, T. L.; Gillespie, I. B.; Hitt, J. E.; Fransen, K. L.; Crowl, C. A.; Tucker, C. J.; et al. *Pharm. Res.* **2004**, *21* (11), 2048–57.
5. Verreck, G.; Chun, I.; Rosenblatt, J.; Peeters, J.; Van Dijck, A.; Mensch, J.; et al. *J. Controlled Release* **2003**, *92* (3), 349–60.
6. Harbury, L. *J. Phys. Chem.* **1946**, *50* (3), 190–9.
7. Tang, R. K.; Nancollas, G. H.; Orme, C. A. *J. Am. Chem. Soc.* **2001**, *123* (23), 5437–43.
8. Wu, W. J.; Nancollas, G. H. *J. Solution Chem.* **1998**, *27* (6), 521–31.
9. Brouwer, A.; Knook, D. L. *Mech. Ageing Dev.* **1983**, *21* (3−4), 205–28.
10. Ansell, S. M.; Johnstone, S. A.; Tardi, P. G.; Lo, L.; Xie, S. W.; Shu, Y.; et al. *J. Med. Chem.* **2008**, *51* (11), 3288–96.
11. Kataoka, K.; Kwon, G. S.; Yokoyama, M.; Okano, T.; Sakurai, Y. *J. Controlled Release* **1993**, *24* (1−3), 119–32.
12. Goldberg, M.; Langer, R.; Jia, X. Q. *J. Biomater. Sci., Polym. Ed.* **2007**, *18* (3), 241–68.
13. Staples, M.; Daniel, K.; Cima, M. J.; Langer, R. *Pharm. Res.* **2006**, *23* (5), 847–63.
14. Bai, S. H.; Thomas, C.; Rawat, A.; Ahsan, F. *Crit. Rev. Ther. Drug Carrier Syst.* **2006**, *23* (6), 437–95.

15. Venugopal, J.; Prabhakaran, M. P.; Low, S.; Choon, A. T.; Zhang, Y. Z.; Deepika, G.; et al. *Curr. Pharm. Des.* **2008**, *14* (22), 2184–200.
16. Annapragada, A.; Adjei, A. *Int. J. Pharm.* **1996**, *136* (1-2), 1–11.
17. Brick, M. C.; Palmer, H. J.; Whitesides, T. H. *Langmuir* **2003**, *19* (16), 6367–80.
18. Akbulut, M.; Alig, A. R. G.; Israelachvili, J. *J. Chem. Phys.* **2006**, *124* (17), 174703.
19. Liu, L. X.; Marziano, I.; Bentham, A. C.; Litster, J. D.; White, E. T.; Howes, T. *Int. J. Pharm.* **2008**, *362* (1-2), 109–17.
20. Thommes, M.; Kleinebudde, P. *AAPS PharmSciTech* **2007**, *8*.
21. Watanabe, H.; Ghadiri, M.; Matsuyama, T.; Ding, Y. L.; Pitt, K. G.; Maruyama, H.; et al. *Int. J. Pharm.* **2007**, *334* (1−2), 149–55.
22. Date, A. A.; Patravale, V. B. *Curr. Opin. Colloid Interface Sci.* **2004**, *9* (3−4), 222–35.
23. Leuner, C.; Dressman, J. *Eur. J. Pharm. Biopharm.* **2000**, *50* (1), 47–60.
24. Serajuddin, A. T. M. *J. Pharm. Sci.* **1999**, *88* (10), 1058–66.
25. Mayersoh, M.; Gibaldi, M. *J. Pharm. Sci.* **1966**, *55* (11), 1323–&.
26. Jachowicz, R. *Int. J. Pharm.* **1987**, *35* (1−2), 1–5.
27. Yuasa, H.; Ozeki, T.; Takahashi, H.; Kanaya, Y.; Ueno, M. *Chem. Pharm. Bull.* **1994**, *42* (2), 354–8.
28. Portero, A.; Remunan-Lopez, C.; Vila-Jato, J. L. *Int. J. Pharm.* **1998**, *175* (1), 75–84.
29. Jachowicz, R.; Nurnberg, E. *Int. J. Pharm.* **1997**, *159* (2), 149–58.
30. Sekiguchi, K.; Obi, N. *Chem. Pharm. Bull.* **1961**, *9* (11), 866–&.
31. Elegakey, M. A.; Soliva, M.; Speiser, P. *Pharm. Acta Helv.* **1971**, *46* (1), 31–&.
32. Betageri, G. V.; Makarla, K. R. *Int. J. Pharm.* **1995**, *126* (1−2), 155–60.
33. Makarla, K.; Betageri, G. V. *Pharm. Res. (New York)* **1992**, *9* (Suppl. 10), S129.
34. Lo, W. Y.; Law, S. L. *Drug Dev. Ind. Pharm.* **1996**, *22* (3), 231–6.
35. El-Zein, H.; Riad, L.; El-Bary, A. A. *Int. J. Pharm.* **1998**, *168* (2), 209–20.
36. Dittgen, M.; Fricke, S.; Gerecke, H.; Osterwald, H. *Pharmazie* **1995**, *50* (3), 225–6.
37. Dittgen, M.; Graser, T.; Kaufmann, G.; Gerecke, H.; Osterwald, H.; Oettel, M. *Pharmazie* **1995**, *50* (6), 438–9.
38. Dittgen, M.; Fricke, S.; Gerecke, H.; Osterwald, H. *Pharmazie* **1995**, *50* (7), 507–8.
39. Min, Y. J.; Akbulut, M.; Kristiansen, K.; Golan, Y.; Israelachvili, J. *Nat. Mater.* **2008**, *7* (7), 527–38.
40. Allen, C.; Maysinger, D.; Eisenberg, A. *Colloids Surf., B* **1999**, *16* (1−4), 3–27.
41. Discher, D. E.; Eisenberg, A. *Science* **2002**, *297* (5583), 967–73.
42. Kataoka, K.; Harada, A.; Nagasaki, Y. *Adv. Drug Delivery Rev.* **2001**, *47* (1), 113–31.
43. Torchilin, V. P. *J. Controlled Release* **2001**, *73* (2−3), 137–72.

Downloaded by DUKE UNIV on June 23, 2012 | http://pubs.acs.org
Publication Date (Web): November 17, 2010 | doi: 10.1021/bk-2010-1053.ch002

44. Kabanov, A. V.; Nazarova, I. R.; Astafieva, I. V.; Batrakova, E. V.; Alakhov, V. Y.; Yaroslavov, A. A.; et al. *Macromolecules* **1995**, *28* (7), 2303–14.
45. Kakizawa, Y.; Kataoka, K. *Adv. Drug Delivery Rev.* **2002**, *54* (2), 203–22.
46. Rosler, A.; Vandermeulen, G. W. M.; Klok, H. A. *Adv. Drug Delivery Rev.* **2001**, *53* (1), 95–108.
47. Savic, R.; Luo, L. B.; Eisenberg, A.; Maysinger, D. *Science* **2003**, *300* (5619), 615–8.
48. Kumar, V.; Prud'homme, R. K. *J. Pharm. Sci.* **2008**, *97* (11), 4904–14.
49. Kim, S. Y.; Shin, I. L. G.; Lee, Y. M.; Cho, C. S.; Sung, Y. K. *J. Controlled Release* **1998**, *51* (1), 13–22.
50. La, S. B.; Okano, T.; Kataoka, K. *J. Pharm. Sci.* **1996**, *85* (1), 85–90.
51. Montazeri Aliabadi, H.; Brocks, D. R.; Lavasanifar, A. *Biomaterials* **2005**, *26* (35), 7251–9.
52. Qiu, L. Y.; Zheng, C.; Jin, Y.; Zhu, K. J. E. *Expert Opinion on Therapeutic Patents* **2007**, *17* (7), 819–30.
53. Dixon, D. J.; Johnston, K. P.; Bodmeier, R. A. *AIChE J.* **1993**, *39* (1), 127–39.
54. Hoeben, B. J.; Burgess, D. S.; McConville, J. T.; Najvar, L. K.; Talbert, R. L.; Peters, J. I.; et al. *Antimicrob. Agents Chemother.* **2006**, *50* (4), 1552–4.
55. Johnson, B. K.; Prud'homme, R. K. *AIChE J.* **2003**, *49* (9), 2264–82.
56. Johnson, B. K.; Prud'homme, R. K. *Phys. Rev. Lett.* **2003**, *91* (11), 118302.
57. Matteucci, M. E.; Hotze, M. A.; Johnston, K. P.; Williams, R. O. *Langmuir* **2006**, *22* (21), 8951–9.
58. Young, T. J.; Johnston, K. P.; Mishima, K.; Tanaka, H. *J. Pharm. Sci.* **1999**, *88* (6), 640–50.
59. Pham, K. N.; Puertas, A. M.; Bergenholtz, J.; Egelhaaf, S. U.; Moussaid, A.; Pusey, P. N.; et al. *Science* **2002**, *296* (5565), 104–6.
60. Liu, Y.; Kathan, K.; Saad, W.; Prud'homme, R. K. *Phys. Rev. Lett.* **2007**, *98* (3), 036102.
61. Liu, Y.; Tong, Z.; Prud'homme, R. K. *Pest Manage. Sci.* **2008**, *64* (8), 808–12.
62. Gindy, M. E.; Panagiotopoulos, A. Z.; Prud'homme, R. K. *Langmuir* **2008**, *24* (1), 83–90.
63. Akbulut, M.; Ginart, P.; Gindy, M. E.; Theriault, C.; Chin, K. H.; Soboyejo, W.; et al. *Adv. Funct. Mater.* **2009**, *19* (5), 718–25.
64. Garside J.; Mersmann A.; Nyvlt, J. *Measurement of crystal growth and nucleation rates*, 2nd ed.; Institution of Chemical Engineers: Rugby, 2002.
65. Matthews, O. A.; Shipway, A. N.; Stoddart, J. F. *Prog. Polym. Sci.* **1998**, *23* (1), 1–56.
66. Boas, U.; Heegaard, P. M. H. *Chem. Soc. Rev.* **2004**, *33* (1), 43–63.
67. Vogtle, F.; Gestermann, S.; Hesse, R.; Schwierz, H.; Windisch, B. *Prog. Polym. Sci.* **2000**, *25* (7), 987–1041.
68. Fages, J.; Lochard, H.; Letourneau, J. J.; Sauceau, M.; Rodier, E. *Powder Technol.* **2004**, *141* (3), 219–26.
69. Bustami, H. P.; Hustert, R. *J. Insect Physiol.* **2000**, *46* (9), 1285–93.
70. Reverchon, E. *J. Supercrit. Fluid* **1999**, *15* (1), 1–21.

Downloaded by DUKE UNIV on June 23, 2012 | http://pubs.acs.org
Publication Date (Web): November 17, 2010 | doi: 10.1021/bk-2010-1053.ch002

71. Debenedetti, P. G.; Tom, J. W.; Kwauk, X.; Yeo, S. D. *Fluid Phase Equilibr.* **1993**, *82*, 311–21.
72. Chang, C. J.; Randolph, A. D. *AIChE J.* **1989**, *35* (11), 1876–82.
73. Meziani, M. J.; Pathak, P.; Hurezeanu, R.; Thies, M. C.; Enick, R. M.; Sun, Y. P. *Angew. Chem., Int. Ed.* **2004**, *43* (6), 704–7.
74. Sun, Y. P.; Meziani, M. L.; Pathak, P.; Qu, L. W. *Chem.-Eur. J.* **2005**, *11* (5), 1366–73.
75. Young, T. J.; Mawson, S.; Johnston, K. P.; Henriksen, I. B.; Pace, G. W.; Mishra, A. K. *Biotechnol. Prog.* **2000**, *16* (3), 402–7.
76. Palakodaty, S.; York, P. *Pharm. Res.* **1999**, *16* (7), 976–85.
77. Cardoso, M. A. T.; Monteiro, G. A.; Cardoso, J. P.; Prazeres, T. J. V.; Figueiredo, J. M. F.; Martinho, J. M. G.; et al. *J. Supercrit. Fluid* **2008**, *44* (2), 238–44.
78. Palakodaty, S.; York, P.; Pritchard, J. *Pharm. Res.* **1998**, *15* (12), 1835–43.
79. Tenorio, A.; Gordillo, M. D.; Pereyra, C.; de la Ossa, E. J. M. *J. Supercrit. Fluid* **2007**, *40* (2), 308–16.
80. Palakodaty, S.; Walker, S.; Townend, P.; York, P.; Humphreys, G. *Pharm Contr.* **2000** (August), 60–3.
81. O’Hara, P.; Hickey, A. J. *Pharm. Res.* **2000**, *17* (8), 955–61.
82. Wagenaar, B. W.; Muller, B. W. *Biomaterials* **1994**, *15* (1), 49–54.
83. Fiegel, J.; Garcia-Contreras, L.; Thomas, M.; VerBerkmoes, J.; Elbert, K.; Hickey, A.; et al. *Pharm. Res.* **2008**, *25* (4), 805–11.
84. Grenha, A.; Seijo, B.; Remunan-Lopez, C. *Eur. J. Pharm. Sci.* **2005**, *25* (4−5), 427–37.
85. Vanbever, R.; Mintzes, J. D.; Wang, J.; Nice, J.; Chen, D. H.; Batycky, R.; et al. *Pharm. Res.* **1999**, *16* (11), 1735–42.
86. Portney, N. G.; Ozkan, M. *Anal. Bioanal. Chem.* **2006**, *384* (3), 620–30.
87. Kong, G.; Braun, R. D.; Dewhirst, M. W. *Cancer Res.* **2000**, *60* (16), 4440–5.
88. Vehring, R. *Pharm. Res.* **2008**, *25* (5), 999–1022.
89. Sham, J. O. H.; Zhang, Y.; Finlay, W. H.; Roa, W. H.; Lobenberg, R. *Int. J. Pharm.* **2004**, *269* (2), 457–67.
90. Broadhead, J.; Rouan, S. K. E.; Rhodes, C. T. *Drug Dev. Ind. Pharm.* **1992**, *18* (11−12), 1169–206.
91. Broadhead, J.; Rouan, S. K. E.; Hau, I.; Rhodes, C. T. *J. Pharm. Pharmacol.* **1994**, *46* (6), 458–67.
92. Clarke, N.; O’Connor, K.; Ramtoola, Z. *Drug Dev. Ind. Pharm.* **1998**, *24* (2), 169–74.
93. Conte, U.; Conti, B.; Giunchedi, P.; Maggi, L. *Drug Dev. Ind. Pharm.* **1994**, *20* (3), 235–58.
94. Sen, D.; Spalla, O.; Tache, O.; Haltebourg, P.; Thill, A. *Langmuir* **2007**, *23* (8), 4296–302.
95. Chew, N. Y. K.; Chan, H. K. *Pharm. Res.* **2001**, *18* (11), 1570–7.
96. Fu, Y. J.; Mi, F. L.; Wong, T. B.; Shyu, S. S. *J Microencapsulation* **2001**, *18* (6), 733–47.
97. Sant, S.; Nadeau, W.; Hildgen, P. *J. Controlled Release* **2005**, *107* (2), 203–14.

Downloaded by DUKE UNIV on June 23, 2012 | http://pubs.acs.org
Publication Date (Web): November 17, 2010 | doi: 10.1021/bk-2010-1053.ch002

98. Chan, H. K.; Clark, A.; Gonda, I.; Mumenthaler, M.; Hsu, C. *Pharm. Res.* **1997**, *14* (4), 431–7.
99. Chen, X. Q.; Pereira, J. C. F. *Int. J. Heat Mass Tranfer* **1996**, *39* (3), 441–54.
100. Langrish, T. A. G. *Dry Technol.* **2007**, *25* (4−6), 971–83.
101. Vehring, R.; Foss, W. R.; Lechuga-Ballesteros, D. *J. Aerosol Sci.* **2007**, *38* (7), 728–46.
102. Leong, K. H. *J. Aerosol Sci.* **1987**, *18* (5), 511–24.
103. Elversson, J.; Millqvist-Fureby, A.; Alderborn, G.; Elofsson, U. *J. Pharm. Sci.* **2003**, *92* (4), 900–10.

Downloaded by DUKE UNIV on June 23, 2012 | http://pubs.acs.org
Publication Date (Web): November 17, 2010 | doi: 10.1021/bk-2010-1053.ch002

Downloaded by UNIV OF GUELPH LIBRARY on June 23, 2012 | http://pubs.acs.org
Publication Date (Web): November 17, 2010 | doi: 10.1021/bk-2010-1053.ch003

Chapter 3

Rational Design of Biopolymers via Aqueous Reversible Addition-Fragmentation Chain Transfer Polymerization

Stacey E. York,[1] Adam W. York,[1] and Charles L. McCormick[1,2,*]

[1]Department of Polymer Science, [2]Department of Chemistry and Biochemistry, The University of Southern Mississippi, 118 College Drive, Hattiesburg, MS 39406
[*]charles.mccormick@usm.edu

Over the last decade significant advances in reversible addition-fragmentation chain transfer (RAFT) polymerization have lead to increased opportunities for the tailored design of polymers in the biomedical field. The ensuing discussion provides examples of rationally designed polymers for biomedical applications. Specifically, the synthesis and characterization of responsive shell cross-linked micelles, actively-targeted gene carriers, and temperature-responsive gels are described.

Introduction

The growing need for "smart" polymers in bio-related fields such as targeted drug/gene delivery, diagnostics, and hydrogels has catapulted controlled radical polymerization (CRP) techniques to the forefront for synthesis of biologically relevant systems. The advent of CLRP has allowed researchers to synthesize polymers with narrow polydispersities, controlled molecular weights, and advanced architectures. For example, the most versatile techniques, reversible addition-fragmentation chain transfer (RAFT) polymerization and atom transfer radical polymerization (ATRP) allow the facile production of telechelic di- and triblock copolymers, as well as other architectures. Stimuli-responsive copolymers have potential in various biomedical applications including the controlled delivery of therapeutic agents or the proliferation of cells in three dimensional synthetic tissue scaffolds.

In Polymeric Delivery of Therapeutics; Morgan, S., et al.;
ACS Symposium Series; American Chemical Society: Washington, DC, 2010.

Downloaded by UNIV OF GUELPH LIBRARY on June 23, 2012 | http://pubs.acs.org
Publication Date (Web): November 17, 2010 | doi: 10.1021/bk-2010-1053.ch003

Non-Viral Polymer Based Carriers

Recently, emphasis has been placed on polymeric vehicles for delivery applications due to concerns with viral carriers. Even though viral vectors are efficient at delivering therapeutic agents, significant problems exist including unwanted immunogenic responses by the host, lack of cell specificity, and high manufacturing costs (*1–4*). Non-viral systems can be placed into two general categories, liposome and polymer based carriers. Although liposomes have some of the prerequisites for effective delivery (*2*, *5*) such as cargo protection, straightforward surface modification, and reasonable manufacturing costs, they also have significant deficiencies that include partitioning, physiological instability, and less than optimal pharmokinetics (*6*).

Polymeric vehicles that have been explored for delivery applications include polymer-drug conjugates, micelles, polymersomes, and nanoparticles. To be successful, polymeric carriers should mimic the trafficking ability and the high delivery efficiency that viral vectors provide while avoiding non-specific toxicity and immunogenicity deficiencies associated with viral vectors. In drug/gene delivery several hurdles must be overcome. Specifically, carriers should be biocompatible and degrade or dissociate into smaller components, thus allowing efficient excretion of the macromolecules after delivery has taken place. In addition to the disassembly of polymeric carriers, extracellular and intracellular barriers must also be overcome for successful delivery. Extracellular issues include efficient packaging of the therapeutic agent, increased stability and circulation under physiological conditions, and specific cellular binding. Intracellular requirements involve endosomal release, cytoplasmic transport, and efficient delivery of the therapeutic agent to the nucleus. The development of novel polymers that can efficiently overcome extra- and intracellular barriers has been heavily pursued by the research community.

Polymer based carriers can be passively or actively targeted to specific cellular receptors. Passively targeted carriers do not contain a targeting moiety but rely on increased circulation time, provided by the polymeric carrier. Nontargeted carriers are specifically used for treating tumoral tissues and rely on the enhanced permeability and retention effect (EPR) (*7–14*). The EPR effect occurs because capillaries around tumors have enhanced vascular permeability and limited lymphatic drainage, leading to the accumulation of macromolecules in tumor cells (*7*, *15*). Because normal tissue can remove macromolecules by lymphatic drainage, accumulation of macromolecules occurs only at the tumor site.

As illustrated in Figure 1, actively targeted polymeric carriers have a directing moiety, or moieties, conjugated along the backbone or to an end group of the polymer chain. Targeting moieties include, but are not limited to, folic acid, peptides, proteins, carbohydrates, aptamers, and antibodies. In addition, drugs may be conjugated to the polymer backbone via a degradable linker. The use of actively directed carriers allows the targeting of specific cellular receptors and is not exclusive to cancerous tissues, such as the EPR effect. In addition, research indicates that actively targeted carriers are taken into the cell more efficiently than polymeric carriers lacking targeting ligands (*15–17*).

Downloaded by UNIV OF GUELPH LIBRARY on June 23, 2012 | http://pubs.acs.org
Publication Date (Web): November 17, 2010 | doi: 10.1021/bk-2010-1053.ch003

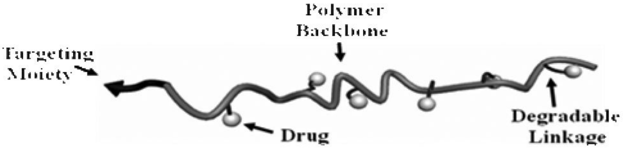

Figure 1. Example of an actively targeted polymeric carrier.

Hydrogels

Hydrogels are used in a variety of biomedically relevant applications, such as controlled release of drugs and tissue engineering. Both natural and synthetic polymers can be utilized to form hydrogels with either chemical or physical cross-links. Depending on the nature of the cross-links, the gel may either be permanently or reversibly cross-linked. Reversibly cross-linked gels may be comprised of either biodegradable chemical cross-links or stimuli-responsive cross-links. Gels bound by stimuli-responsive cross-links may be fully dissociated to the unimeric state within seconds while biodegradable cross-links can be tuned to allow the gel to dissociate on the timescale of days to months. While each system has advantages, this chapter will focus on hydrogels cross-linked via stimuli-responsive polymers which respond quickly to environmental changes. Reversible physical gels are generally comprised of a BAB triblock architecture, where the B block is stimuli-responsive (i.e. pH, salt, or temperature) and the A block is permanently hydrophilic. As seen in Figure 2, the triblock copolymer forms a bridged micellar network at sufficiently high concentration. In addition to bridges spanning between micellar cores, loops may form when both ends of a polymeric chain are incorporated in the same core.

"Smart" Polymers via Controlled Living Free Radical Polymerization for Biological Applications

In order to synthesize advanced architectures required for use in biological applications, a robust polymerization process that can yield well-defined biomacromolecules must be employed. The recent advancements in CRP make these techniques attractive for the construction of such polymers. Although a recent report suggests some opportunities for stable free radical polymerization (*18*), most efforts toward construction of polymeric delivery vehicles with controlled structures and molecular weight have utilized ATRP or RAFT polymerization. While ATRP and RAFT polymerization both have advantages and limitations, RAFT polymerization has proven to be quite robust under diverse reaction conditions (*i.e.* solvent and temperature) with the ability to use a wide variety of functional monomers directly in water without protecting group chemistry. The wide range of functional monomers that can be polymerized provide structopendant functionality while the telechelic nature of the RAFT process provides structoterminal functionality (α and ω). Both pendant and terminal functionality provide conjugation sites for various biological motifs, a prerequisite for drug/gene delivery, biodiagnostics and incorporation of growth factors in three dimensional cell culture scaffolds.

Downloaded by UNIV OF GUELPH LIBRARY on June 23, 2012 | http://pubs.acs.org
Publication Date (Web): November 17, 2010 | doi: 10.1021/bk-2010-1053.ch003

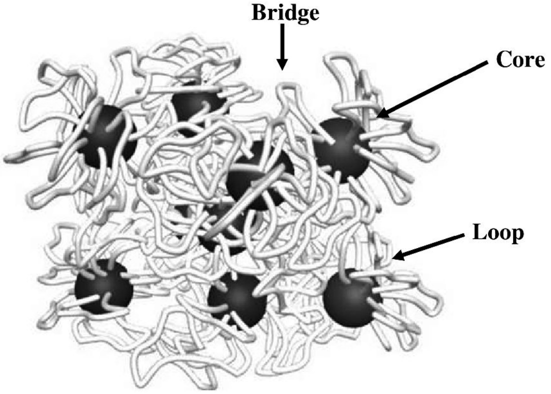

Figure 2. Example of an BAB triblock micellar network.

RAFT polymerization was first reported by the Australian CSIRO group in 1998 (*19–21*). The proposed mechanism of RAFT polymerization operates as a degenerative chain transfer process and specifics of the process including the fate of the intermediate radical and competing side reactions are still heavily debated. The specifics of the RAFT process are beyond the scope of this chapter and the reader is referred to the above reviews for further discussion. RAFT polymerization is similar to conventional free radical polymerizations except for the incorporation of a chain transfer agent (CTA). CTAs typically incorporate a thiocarbonylthio moiety that is reactive towards free radicals. In order to maintain excellent control over the molecular weight careful consideration must be used when selecting CTA, monomer, initiator, and reaction conditions. In order to preserve the thiocarbonylthio functionality the polymerization can be stopped at moderate to low conversions, thus reducing the chance of termination. By maintaining the thiocarbonylthio functional chain end, the resulting polymer, referred to as a macroCTA, can be isolated and subsequently chain extended with a second monomer (*21–24*). The ability of the RAFT process to polymerize a variety of functional monomers while doing so in a controlled/‘living’ fashion allows for the synthesis of an extensive library of polymers.

Polymeric Delivery Vehicles

The ease of synthesizing telechelic block and statistical copolymers via RAFT polymerization has allowed researchers to develop well-defined polymer-drug conjugates, micelles, polymersomes, and polyelectrolyte complexes for delivery based applications. The ability to control the polymerization of a wide variety of functional monomers as well as introduce structoterminal functionality via RAFT polymerization provides a facile route for pre- and post-polymerization biofunctionalization.

Downloaded by UNIV OF GUELPH LIBRARY on June 23, 2012 | http://pubs.acs.org
Publication Date (Web): November 17, 2010 | doi: 10.1021/bk-2010-1053.ch003

Polymer Backbone Conjugation

Polymer backbone conjugation can be achieved through the incorporation of pendant functionality that allows for the construction of multivalent bioconjugates (Figure 1). Activated monomers N-acryloxysuccinimide (NAS) or N-methacryloxysuccinimide (NMS) provide reactive functionality and have been successfully polymerized by both RAFT polymerization (*25–27*) and ATRP (*28*). For example Kane and coworkers (*27*) successfully synthesized narrowly dispersed N-(2-hydroxypropyl) methacrylamide (HPMA)/NMS statistical copolymer via RAFT polymerization in organic media. Incorporation of NMS was kept below 28% and subsequent conjugation of an anthrax inhibitor peptide was demonstrated. The authors reported three orders of magnitude improvement in inhibition by the polymer bioconjugate relative to the free peptide. Recently, Maynard and coworkers (*29*) as well as Kizhakkedathu et al. (*30*) reported the successfully RAFT polymerization of aldehyde protected monomers. The resulting polymers could then be deprotected to yield an aldehyde functionality and subsequently conjugated to either aminoxy containing peptides (*29*) or desferrioxamine an amine containing iron chelator (*30*).

The reactive monomers mentioned above are very useful in the construction of polymer bioconjugates but have to be polymerized in organic solution and in the case of the aldehyde monomers be protected to prevent unwanted side reactions. While protection of the aldehyde-containing monomers is necessary, the tolerance of RAFT to primary amine-containing monomers was demonstrated in the polymerization of as N-(3-aminopropyl)methacrylamide (APMA). McCormick and coworkers reported the successful aqueous RAFT polymerization of APMA and synthesized thermally responsive poly(APMA-*block*-N-isopropylacrylamide) (PAPMA-*b*-PNIPAM) copolymers that formed vesicles upon a temperature increase and could be subsequently "locked" through interpolyelectrolyte complexation between the cationically charged APMA block and the anionic polymer, poly(sodium 2-acrylamido-2-methylpropanesulfonate) PAMPS (*31*).

A method of backbone conjugation introduced by Bulmus and coworkers utilizes a disulfide exchange reaction between thiol-containing small molecule compounds and poly(pyridyldisulfide ethylmethacrylate), a polymer containing pendant disulfide groups (*32*). The small molecules, 3-mercaptopropionic acid (MPA), 4-mercapto-1-butanol (MB), 11-mercapto-1-undecanol (MU), and the model oligopeptide L-glutathione (GLT) were successfully conjugated to the polymer backbone. Depending on the feed ratio and bulkiness of the model compound, disulfide exchange reactions gave yields of 65 to 100%. The feed ratio and molar incorporation were nearly identical for MPA and MB while the bulkiness of GLT limited incorporation to 65% when the feed rationof disulfide to GLT was 1.

Polymer End-Group Conjugation

The inherent nature of RAFT polymerization to yield telechelic polymers has resulted in numerous polymer bioconjugates for potential biodiagnostics, substrate/enzyme interactions, and targeted delivery. The CTA, which usually contains a thiocarbonylthio moiety, can be chemically modified by a number of facile processes. The reduction of the ω-terminal thiocarbonylthio chain end produces thiol end-groups which may then be easily converted to other functionalities. For example, the ω-terminal chain end of PHPMA-*b*-N-[3-(dimethylamino) propyl] methacrylamide) (PHPMA-*b*-PDMAPMA) was reduced from a thiocarbonylthio moiety to a tertiary thiol utilizing sodium borohydride ($NaBH_4$). Subsequently, the tertiary polymeric thiol was converted to a primary amine, yielding an end-functional polymer with high reactivity. As a proof of concept, the activated fluorescent compound, 6-(fluorescein-5-carboxamido)hexanoic acid, succinimidyl ester (5-SFX) was conjugated to the polymer end group.

Downloaded by UNIV OF GUELPH LIBRARY on June 23, 2012 | http://pubs.acs.org
Publication Date (Web): November 17, 2010 | doi: 10.1021/bk-2010-1053.ch003

Polyelectrolyte Complexes

Polyelectrolyte complexes (PC), often called interpolyelectrolyte complexes (IPECs), consist of electrostatically bound polyanions and polycations. Complexes between polycations and polynucleotides, which contain an anionically charged phosphate backbone, have been widely studied due to the potential applications in gene therapy. Complexation of polynucleotides with polycations offers protection against degradative enzymes while increasing the circulation half-life. The charge ratio of these complexes is generally described by the nitrogen to phosphate ratio (N:P), where most polycations utilized have either tertiary or quaternary amines. The N:P ratio plays an important part in the ability of the complex to transverse the cell membrane. Negatively charged complexes (N:P < 1) have difficulties in transfecting cells due to electrostatic repulsions between the anionically charged cell membrane and PC. Positively charged complexes (N:P > 1) tend to bind strongly to cell membranes, and thus lack cell specificity, leading to uptake of the PC in both healthy and diseased tissue. Neutral complexes (N:P=1) circumvent these problems but often have poor solubility in aqueous solution due to charge neutralization, thus their applications in drug delivery is limited.

Alternatively, a poly(cationic-*b*-hydrophilic) block copolymer can be complexed with a polynucleotide in order to form a water-soluble neutral PC. The cationic block provides a means of complexation with the polynucleotide while the hydrophilic block provides steric stabilization. A controlled polymerization technique, such as RAFT polymerization, is required to obtain a well-defined block copolymer. Shortly after our group reported the controlled synthesis of PHPMA (*33*), a nonimmunogenic biocompatible polymer, we reported the synthesis and characterization of a series of poly(HPMA-*b*-N-3-dimethylaminopropyl methacrylamide) P(HPMA-*b*-DMAPMA) which formed neutral water-soluble complexes with a 43 nucleotide small interfering ribonucleic acid (siRNA) (*34*). With the ability to control HPMA and DMAPMA block length, we were able to study their affect on complex stability. DMAPMA block length appeared to be the major contributing factor in protecting siRNA from enzymatic degradation (*34*). As seen in Figure 3, the degradation of complexed siRNA in the presence of RNase A was measured at 260 nm. Degradation of siRNA was indicated by an increase in UV absorbance due to the hyperchromic effect. The positive control, unbound siRNA, rapidly degraded under physiological conditions while the siRNA complexed with P($HPMA_{258}$-*b*-$DMAPMA_{23}$) (*34*).

The P(HPMA-*b*-DMAPMA) system discussed above would rely on the EPR effect to deliver siRNA since no targeting ligand is present. Although, macromolecular species have been shown to accumulate in tumoral tissue through the EPR effect or passive delivery, it has been demonstrated that the presence of a targeting ligand provides an increase in cellular internalization when compared to macromolecular vehicles that solely rely on the EPR effect. Building on our previous report we developed a multivalent terpolymer capable of forming neutral complexes with siRNA while providing multiple conjugation sites for targeting moieties (*35*). The terpolymer consists of two blocks where the first block is a statistical block containing the monomers HPMA and *N*-(3-aminopropyl)methacrylamide (APMA), while the second block consists of the tertiary amine containing monomer DMAPMA. Synthesis of P(HPMA-*stat*-APMA)-*b*-DMAPMA was achieved using acidic aqueous RAFT conditions according to Scheme 1. This three monomer component system addresses issues related to the effective delivery of siRNA. The packaging and protection of the siRNA is accomplished through the incorporation of a cationic block (DMAPMA), while the aqueous stability and targeted delivery of siRNA is accomplished through the statistical polymerization of a hydrophilic (HPMA) and primary amine containing (APMA) monomer (*35*). The use of RAFT polymerization affords control over the number of conjugation sites and the block lengths for construction of narrowly dispersed polymers designed specifically for siRNA delivery.

Multivalent folate-block copolymer conjugates suitable for targeted siRNA delivery were synthesized by reacting the primary amine containing terpolymer with an *N*-hydroxysuccinimide (NHS) activated folic acid (Scheme 1). In order to avoid side reactions the thiocarbonylthio functionality was removed prior to folate conjugation following an established literature procedure (*36*). Conjugation of folic acid to the APMA functionalities was confirmed utilizing UV-vis and ^1H NMR spectroscopy.

Results of *in vitro* cellular studies demonstrate the ability of the folate conjugated copolymer/siRNA complexes to target folate receptors and lead to gene suppression. KB cells (human epidermal cancer cells) which over-express folate receptors and A549 cells (human lung cancer cells) which have minimal folate receptor expression were both treated to show complex specificity. Real-time polymerase chain reaction (RT-PCR) experiments were conducted to determine the mRNA levels of survivin, the targeted gene sequence. As shown in Figure 4, approximately 60% mRNA down-regulation was observed in the KB cell line while no mRNA down-regulation was observed in the A549 cell line. In addition, KB cells were treated with folate conjugated P($HPMA_{315}$-*stat*-$APMA_{13}$)-*b*-$DMAPMA_{23}$/siRNA complexes in the presence of free folic acid (1 mM) to show inhibition of cellular uptake due to the competition of folate receptor binding. The presence of free folic acid led to negligible mRNA down-regulation indicating minimal cellular uptake of complexes.

Downloaded by UNIV OF GUELPH LIBRARY on June 23, 2012 | http://pubs.acs.org
Publication Date (Web): November 17, 2010 | doi: 10.1021/bk-2010-1053.ch003

Downloaded by UNIV OF GUELPH LIBRARY on June 23, 2012 | http://pubs.acs.org
Publication Date (Web): November 17, 2010 | doi: 10.1021/bk-2010-1053.ch003

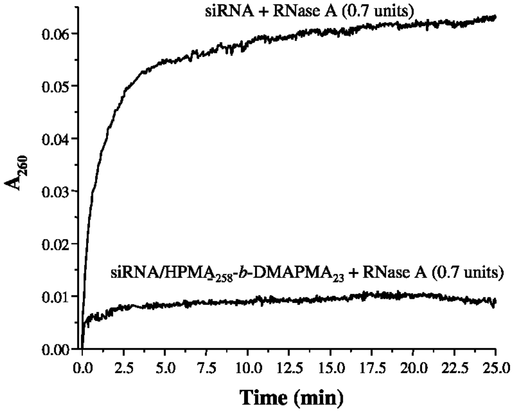

Figure 3. Degradation of free and complexed siRNA as measured by UV absorbance at 260 nm. (Reproduced from reference (34). Copyright 2006 American Chemical Society.)

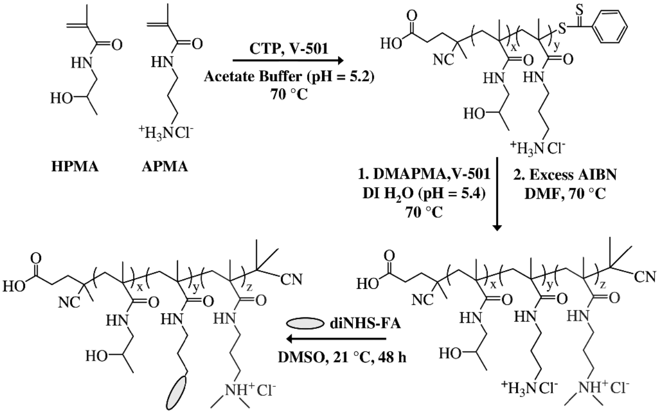

Scheme 1. Reaction pathway for the synthesis of P(HPMA-stat-APMA)-b-DMAPMA and subsequent conjugation of folic acid. (Reproduced from reference (35). Copyright 2009 American Chemical Society.)

Stimuli-Responsive Shell Cross-Linked Micelles and Vesicles

Since 1984, nanostructured materials including synthetic micelles and polymersomes have been studied as potential drug delivery vehicles. These generally consist of amphiphilic diblock or triblock copolymers which self-assemble in water to form a hydrophobic core stabilized by a hydrophilic shell (*37*). Stimuli-responsive-*b*-hydrophilic copolymers can undergo a reversible unimer-to-micelle (vesicle) transition, offering a higher level of sophistication over hydrophobic-*b*-hydrophilic copolymers. Stimuli such as salt, pH, and temperature are often utilized to induce hydrophobic-hydrophilic transitions in biological systems. A wide variety of stimuli-responsive block copolymers have been synthesized via RAFT polymerization. In 2006, our

Downloaded by UNIV OF GUELPH LIBRARY on June 23, 2012 | http://pubs.acs.org
Publication Date (Web): November 17, 2010 | doi: 10.1021/bk-2010-1053.ch003

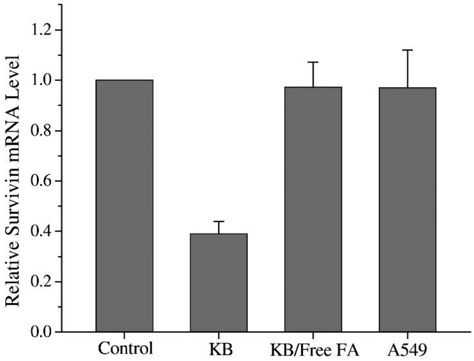

Figure 4. Quantitative RT-PCR analysis of cell specific down-regulation of human survivin messenger RNA (mRNA) by anti-survivin siRNA. The control contained either KB cells/siRNA or A549 cells/siRNA. The other three experiments (marked KB, KB/Free FA and A549) were treated with folate conjugated P(HPMA$_{315}$-stat-APMA$_{13}$)-b-DMAPMA$_{23}$/siRNA complexes in the presence (KB/Free FA) or absence (KB, A549) of 1 mM free folic acid (FA). Error bars represent ± S.D. (Reproduced from reference (35). Copyright 2009 American Chemical Society.)

group reported the successful room temperature aqueous RAFT polymerization of poly(N-isopropylacrylamide) (PNIPAM), a widely studied polymer due to its lower critical solution temperature near physiological conditions (32 °C) (*38*). The dilute solution properties of a series of PNIPAM-*b*-poly(N,N-dimethylacrylamide) (PDMA) di- and triblock copolymers were characterized by dynamic light scattering (*38*). At room temperature the polymers exist in the unimeric state; at elevated temperatures polymers with a sufficiently long PNIPAM block form micelles.

Though stimuli-responsive micelles are promising drug delivery vehicles, the spontaneous dissociation into the unimeric state when diluted below the critical micelle concentration (CMC) limits their practical use. In order to address this problem, a significant amount of research on shell cross-linked micelles and vesicles has been conducted. Since Wooley's seminal report on shell cross-linking (SCL) in 1996 (*39*), a number of significant advancements to the field have been made (*40*). While a larger portion of SCL research has focused on irreversible covalent bond formation, the examples highlighted below utilize reversible linkages via covalent or ionic bonds. A generalized depiction of the assembly-disassembly process for SCL stimuli-responsive micelles is shown in Scheme 2. After rendering the stimuli-responsive block hydrophobic, a cross-linking agent which can react with shell functionality is added. Reversal of the stimulus after cross-linking results in swollen SCL micelles due to an influx of water into the core. In the examples below, the SCL may be reverted back to the unimeric state through a reversible chemical reaction which breaks the cross-links.

In 2006, our group reported the synthesis of a temperature-responsive SCL micelles utilizing a poly(ethylene oxide) (PEO) macroCTA to control the statistical copolymerization of an activated ester monomer, N-acryloyloxysuccinimide (NAS) and DMA. The PEO-*b*-(DMA-*s*-NAS) macroCTA was chain extended with PNIPAM (*25*). The resulting polymers can form micelles at elevated temperatures which can be subsequently cross-linked with ethylenediamine. The SCL micelles can swell to 1.4-1.9 times their original diameters. The PEO outer block is pivotal in providing steric stabilization while preventing interpolymer cross-linking. In a subsequent report, the above polymer was cross-linked with cystamine, a disulfide containing bifunctional amine (*41*). The SCL micelles could be "uncross-linked" with either dithiothreitol (DTT) or tris(2-carboxyethyl)-phosphine (TCEP). Dipyridamole (DIP), a model compound, was loaded into the core of the micelles and SCL micelles. After loading DIP at 45 °C, the temperature was lowered to 25 °C. A burst release occurred from uncrosslinked micelles due to the dissociation back to the unimer state. However, SCL micelles released DIP over the course of several days. In the presence of a reducing agent, DIP release increased significantly (*41*).

Cross-linking through electrostatic interactions also provides a reversible route to obtain SCL micelles. For example, our group formed SCL micelles through the complexation of poly([ar-vinylbenzyl]trimethylammonium chloride) (PVBTAC) with the temperature and pH responsive PDMA-*b*-(NIPAM-*s*-N-acryoylvaline) (AVAL) (*42*). Depending on the solution temperature and pH, a range of micellar sizes could be achieved. In addition, shell-cross-linking could be reversed through the displacement of the polymeric crosslinker, PVBTAC, with the addition of 0.3 M NaCl (*42*).

Our most recent report of shell-cross-linking includes a RAFT synthesized temperature responsive cross-linker and a pH responsive micelle (*43*). Micellization of the ABC triblock copolymer, α-methoxyPEO-*b*-poly[*N*-(3-aminopropyl) methacrylamide]-*b*-poly[2-(diisopropylamino)ethyl methacrylate] (mPEO-*b*-PAPMA-*b*-PDPAEMA), was induced by rendering the PDPAEMA block hydrophobic by increasing the pH above 6.0. The primary amine functionality on PAPMA was then cross-linked utilizing (α,ω-N-hydroxysuccinimidyl ester) PNIPAM (Figure 5). The RAFT synthesized PNIPAM cross-linking contains a reducable trithiocarbonate core, thus providing a route to disassemble the micelle.

Downloaded by UNIV OF GUELPH LIBRARY on June 23, 2012 | http://pubs.acs.org
Publication Date (Web): November 17, 2010 | doi: 10.1021/bk-2010-1053.ch003

Physical Gels for Drug Delivery and Cell Growth Scaffolds

The ability to synthesize complex architectures by RAFT and ATRP has lead to the development of reversibly cross-linked gels. The gels typically consist of a BAB architecture where the B blocks reversibly associate in response to an external stimuli. The mechanical properties, pore size, and availability of adhesion sites for cells are all considerations for the development of cell culture scaffolds while the loading capacity and controlled release of small molecules are concerns for drug delivery applications. In the subsequent section, the synthesis of polymers which address these issues will be discussed.

Downloaded by UNIV OF GUELPH LIBRARY on June 23, 2012 | http://pubs.acs.org
Publication Date (Web): November 17, 2010 | doi: 10.1021/bk-2010-1053.ch003

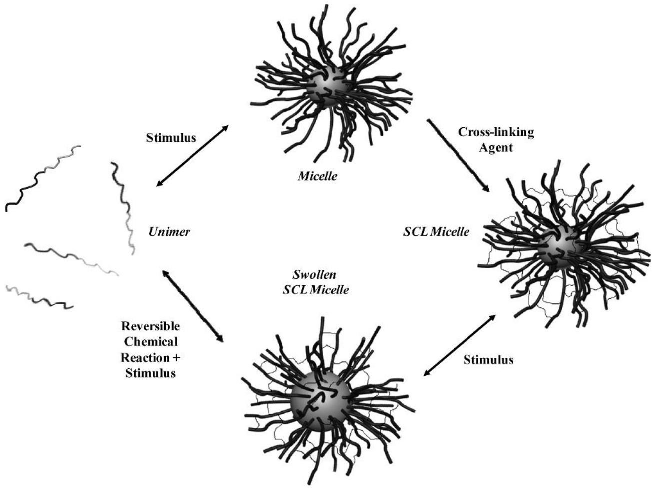

Scheme 2. Reversible shell cross-linking of micelles formed with stimuli-responsive polymers.

pH-Responsive Triblock Copolymer Gels

pH-responsive gels formed from physically associating BAB triblock copolymers have potential use in both cell scaffolding materials and drug delivery. Given the proper pKa, *in situ* gelation of a concentrated polymer solution can occur within the range of physiological pH. The gel could then serve as either a drug loaded scaffold or a platform for cell growth. In 2003, Armes and coworkers presented a proof-of-concept for drug delivery via physical gels by synthesizing a BAB triblock copolymer consisting of 2-methacryloyloxyethyl phosphorylcholine (MPC) A block and 2-(diisopropylamino)ethyl methacrylate (DPA) or 2-(diethylamino)ethyl methacrylate (DEA) B block (*44*). The biocompatible phosphorylcholine functionality present in MPC is widely known to be resistant to protein adsorption and cellular adhesion (*45*). The DPA block provides the pH responsiveness (pKa~6) required to form a reversible gel. Symmetrical triblock copolymers were synthesized through via a difunctional ATRP initiator, diethyl meso-2,5-dibromoadipate. A series of polymers were synthesized with outer block lengths ranging from 30 to 100 while inner blocks of 100 to 300 were utilized. Most of the reported polymers were capable of forming free-standing gels as concentrations were increased to 20 w/v %. DIP was added to an acidic solution of 10 to 20 w/v% polymer. The pH was increased, resulting in a drug-loaded pH responsive gel. Sustained release was achieved for each of the polymer gels at pH 7.4, the triblock gels formed from DPA containing polymers retaining drugs for longer periods of time than DEA containing polymers. A triggered burst release occurred as the gel was dissolved by lowering the pH to 3. Further structural investigations were conducted on $PDPA_{50}$-*b*-$PMPC_{250}$-*b*-$PDPA_{50}$. Small angle neutron scattering studies indicated that free-standing gels could be modeled as a "mesh" of flower micelles in which DPA cores were interconnected through solvated MPC blocks.

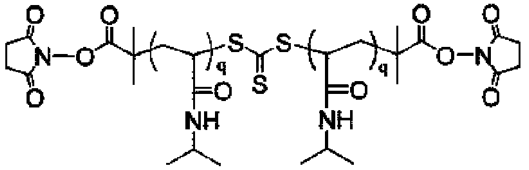

Figure 5. Temperature-responsive polymeric cross-linking agent with reducible functionality.

RAFT polymerization has been utilized extensively to synthesize pH-responsive diblock and triblock copolymers; however, physical characterization has generally been limited to dilute solution studies. The wide range of monomers that may be polymerized by RAFT offers a significant opportunity for further research in this field. Areas which need to be further addressed include the effect of block size, hydrophobicity, and amphiphilic ratio on mechanical properties and release profiles.

Temperature-Responsive Triblock Copolymer Gels

Temperature-responsive polymers offer a unique platform for the design of cell growth scaffolds and drug delivery matrices. Significant research has been conducted on poly(N-isopropylacrylamide) (PNIPAM) due to its lower critical solution temperature at 32 °C. The controlled polymerization of NIPAM in water at room temperature was reported by the McCormick research group in 2006 (*46*). In this report, the difunctional trithiocarbonate 2-(1-carboxy-1-methylethylsulfanylthiocarbonylsulfanyl)-2-methylpropionic acid (CMP) was utilized to synthesize symmetrical ABA triblock copolymers (A = poly(N,N-dimethylacrylamide (PDMA), B = PNIPAM). Variable temperature dynamic light scattering was utilized to demonstrate the unimer-to-micelle transition of these polymers. The polymer morphologies remained completely reversible after several heating and cooling cycles. Following this research, BAB triblock copolymers (A= PDMA, B=PNIPAM) were synthesized and characterized with respect to their ability to form physical gels (*47*). By utilizing the same macroCTA in two chain extension polymerizations, two polymers were synthesized with identical outer block lengths but different inner block lengths [$PNIPAM_{455}$-*b*-$PDMA_{210}$-*b*-$NIPAM_{455}$ (P210) and $PNIPAM_{455}$-*b*-$PDMA_{277}$-*b*-$PNIPAM_{455}$ (P277)] The effect of inner block length, solvent, and polymer concentration on the mechanical properties and pore sizes of the gels were investigated. The critical gelation concentration was 7.5 and 10 wt/vol% for P277 and P210 respectively. When dissolved under physiological conditions the gelation temperature (as defined as the crossover in G' and G") of both gels was depressed by approximately 5 °C. As illustrated in Figure 6, the mechanical properties of the gels at 37 °C could be tuned by varying the polymer concentration. Under physiological conditions, 10 wt/vol% polymer P210 and P277 exhibited mechanical properties comparable to collagen, a commonly used

Downloaded by UNIV OF GUELPH LIBRARY on June 23, 2012 | http://pubs.acs.org
Publication Date (Web): November 17, 2010 | doi: 10.1021/bk-2010-1053.ch003

Downloaded by UNIV OF GUELPH LIBRARY on June 23, 2012 | http://pubs.acs.org
Publication Date (Web): November 17, 2010 | doi: 10.1021/bk-2010-1053.ch003

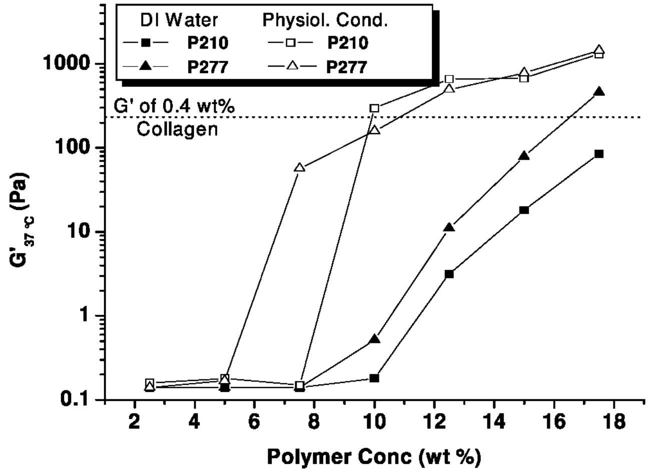

Figure 6. Storage modulus of P210 and P277 at 37 °C as a function of concentration when dissolved in DI water or under physiological conditions (140 mM NaCl/20 mM phosphate buffer, pH 7.4). (Reproduced from reference (46). Copyright 2008 American Chemical Society.)

in vitro cell growth matrix. Initial cytocompatibility tests indicated that the polymers were nontoxic to endothelial cells.

Armes et al. have reported several temperature-responsive triblock copolymers containing PNIPAM outer blocks (*48*, *49*). In addition, the hydrophilic, biocompatible PMPC was utilized as the inner block, thus promoting cell growth (*49*). V79 hamster lung cells incubated on 5 and 10 wt/vol% copolymer gels of $PNIPAM_{81}$-*b*-$PMPC_{200}$-*b*-$PNIPAM_{81}$ for 72 hours showed an increase in cell number as opposed to the 20 wt% gel.

The results discussed in the previous two sections provide the groundwork for numerous investigations into the application of stimuli-responsive physical gels for drug delivery and cell growth scaffolding applications. Further work in the area of conjugating biological motifs, such as cell-adhesive peptides, and fine-tuning the response of the gels will allow the tailoring of systems specialized for specific cell lines.

Acknowledgments

We gratefully acknowledge support received for this research by the U.S. Department of Energy (DE-FC26-01BC15317) and the MRSEC program (DMR-0213883) of the National Science Foundation.

References

1. Marshall, E. *Science* **2000**, *288*, 951–957.
2. Pack, D. W.; Hoffman, A. S.; Pun, S.; Stayton, P. S. *Nat. Rev. Drug Discovery* **2005**, *4*, 581–593.

3. Wong, S. Y.; Pelet, J. M.; Putnam, D. *Prog. Polym. Sci.* **2007**, *32*, 799–837.
4. York, A. W.; Kirkland, S. E.; McCormick, C. L. *Adv. Drug Delivery Rev.* **2008**, *60*, 1018–1036.
5. Park, T. G.; Jeong, J. H.; Kim, S. W. *Adv. Drug Delivery Rev.* **2006**, *58*, 467–486.
6. Napier, M. E.; Desimone, J. M. *J. Macromol. Sci., Polym. Rev.* **2007**, *47*, 321–327.
7. Ulbrich, K.; Subr, V. *Adv. Drug Delivery Rev.* **2004**, *56*, 1023–1050.
8. Tomlinson, R.; Heller, J.; Brocchini, S.; Duncan, R. *Bioconjugate Chem.* **2003**, *14*, 1096–1106.
9. Satchi-Fainaro, R.; Hailu, H.; Davies, J. W.; Summerford, C.; Duncan, R. *Bioconjugate Chem.* **2003**, *14*, 797–804.
10. Nori, A.; Kopecek, J. *Adv. Drug Delivery Rev.* **2005**, *57*, 609–636.
11. Hoste, K.; De Winne, K.; Schacht, E. *Int. J. Pharm.* **2004**, *277* (1-2), 119–131.
12. Etrych, T.; Jelnkova, M.; Rihova, B.; Ulbrich, K. *J. Controlled Release* **2001**, *73*, 89–102.
13. Christie, R. J.; Grainger, D. W. *Adv. Drug Delivery Rev.* **2003**, *55*, 421–437.
14. Maedaa, H.; Wua, J.; Sawaa, T.; Matsumurab, Y.; Hori, K. *J. Controlled Release* **2000**, *65*, 271–284.
15. Pirollo, K. F.; Chang, E. H. *Trends Biotechnol.* **2008**, *26*, 552–558.
16. Bartlett, D. W.; Su, H.; Hildebrandt, I. J.; Weber, W. A.; Davis, M. E. *Proc. Natl. Acad. Sci. U.S.A.* **2007**, *104*, 15549–15554.
17. Kirpotin, D. B.; Drummond, D. C.; Shao, Y.; Shalaby, M. R.; Hong, K.; Nielsen, U. B.; Marks, J. D.; Benz, C. C.; Park, J. W. *Cancer Res.* **2006**, *66*, 6732–6740.
18. Nicolay, R.; Marx, L.; Hemery, P.; Matyjaszewski, K. *Macromolecules* **2007**, *40* (17), 6067–6075.
19. Chiefari, J.; Chong, Y. K.; Ercole, F.; Krstina, J.; Jeffery, J.; Le, T. P. T.; Mayadunne, R. T. A.; Meijs, G. F.; Moad, C. L.; Moad, G.; Rizzardo, E.; Thang, S. H. *Macromolecules* **1998**, *31*, 5559–5562.
20. Moad, G.; Rizzardo, E.; Thang, S. H. *Aust. J. Chem.* **2006**, *59*, 669–692.
21. Moad, G.; Rizzardo, E.; Thang, S. H. *Aust. J. Chem.* **2005**, *58*, 379–410.
22. McCormick, C. L.; Lowe, A. B. *Acc. Chem. Res.* **2004**, *37* (5), 312–325.
23. Lowe, A. B.; McCormick, C. L. *Prog. Polym. Sci.* **2007**, *32* (3), 283–351.
24. Perrier, S.; Takolpuckdee, P. *J. Polym. Sci., Part A: Polym. Chem.* **2005**, *43* (22), 5347–5393.
25. Li, Y.; Lokitz, B. S.; McCormick, C. L. *Macromolecules* **2006**, *39* (1), 81–89.
26. Li, Y.; Lokitz, B. S.; Armes, S.; McCormick, C. L. *Macromolecules* **2006**, *39* (8), 2726–2728.
27. Yanjarappa, M. J.; Gujraty, K. V.; Joshi, A.; Saraph, A.; Kane, R. S. *Biomacromolecules* **2006**, *7*, 1665–1670.
28. Godwin, A.; Hartenstein, M.; Müller, A. H.; Brocchini, S. *Angew. Chem., Int. Ed.* **2001**, *40* (3), 594–597.
29. Hwang, J.; Li, R. C.; Maynard, H. D. *J. Controlled Release* **2007**, *122* (3), 279–286.

Downloaded by UNIV OF GUELPH LIBRARY on June 23, 2012 | http://pubs.acs.org
Publication Date (Web): November 17, 2010 | doi: 10.1021/bk-2010-1053.ch003

30. Rossi, N. A.; Zou, Y.; Scott, M. D.; Kizhakkedathu, J. N. *Macromolecules* **2008**, *41* (14), 5272–5282.
31. Li, Y.; Lokitz, B. S.; McCormick, C. L. *Angew. Chem., Int. Ed.* **2006**, *45* (35), 5792–5795.
32. Wong, L.; Boyer, C.; Jia, Z.; Zareie, H. M.; Davis, T. P.; Bulmus, V. *Biomacromolecules* **2008**, *9* (7), 1934–1944.
33. Scales, C. W.; Vasilieva, Y. A.; Convertine, A. J.; Lowe, A. B.; McCormick, C. L. *Biomacromolecules* **2005**, *6* (4), 1846–1850.
34. Scales, C. W.; Huang, F.; Li, N.; Vasilieva, Y. A.; Ray, J.; Convertine, A. J.; McCormick, C. L. *Biomacromolecules* **2006**, *39* (20), 6871–6881.
35. York, A. W.; Zhang, Y.; Holley, A. C.; Guo, Y.; Huang, F.; McCormick, C. L. *Biomacromolecules* **2009**, *10* (4), 936–843.
36. Perrier, S.; Takolpuckdee, P.; Mars, C. A. *Macromolecules* **2005**, *38*, 2033–2036.
37. McCormick, C. L.; Sumerlin, B. S.; Lokitz, B. S.; Stempka, J. E. *Soft Matter* **2008**, *4*, 1760–1773.
38. Convertine, A. J.; Lokitz, B. S.; Vasileva, Y.; Myrick, L. J.; Scales, C. W.; Lowe, A. B.; McCormick, C. L. *Macromolecules* **2006**, *39* (5), 1724–1730.
39. Thurmond, K. B.; Kowalewski, T.; Wooley, K. L. *J. Am. Chem. Soc.* **1996**, *118*, 7239–7240.
40. Read, E. S.; Armes, S. P. *Chem. Commun.* **2007**, *29*, 3021–3035.
41. Li, Y.; Lokitz, B. S.; Armes, S. P.; McCormick, C. L. *Macromolecules* **2006**, *39*, 2726–2728.
42. Lokitz, B. S.; York, A. W.; Stempka, J. E.; Treat, N. D.; Li, Y.; Jarrett, W. L.; McCormick, C. L. *Macromolecules* **2007**, *40*, 6473–6480.
43. Xu, X.; Smith, A. E.; Kirkland, S. E.; McCormick, C. L. *Macromolecules* **2008**.
44. Ma, Y.; Tang, Y.; Billingham, N. C.; Armes, S. P.; Lewis, A. L. *Biomacromolecules* **2003**, *4*, 864–868.
45. Hayward, J. A.; Chapman, D. *Biomaterials* **1984**, *5*, 135–142.
46. Convertine, A. J.; Lokitz, B. S.; Vasileva, Y.; Myrick, L. J.; Scales, C. W.; Lowe, A. B.; McCormick, C. L. *Macromolecules* **2006**, *39*, 1724–1730.
47. Kirkland, S. E.; Hensarling, R. M.; McConaughy, S. D.; Guo, Y.; Jarrett, W. L.; McCormick, C. L. *Biomacromolecules* **2008**, *9* (2), 481–486.
48. Li, C.; Buurma, N. J.; Haq, I.; Turner, C.; Armes, S. P.; Castelleto, V.; Hamley, I. W.; Lewis, A. L. *Langmuir* **2005**, *21*, 11026–11033.
49. Li, C.; Tang, Y.; Armes, S. P.; Morris, C. J.; Rose, S. F.; Lloyd, A. W.; Lewis, A. L. *Biomacromolecules* **2005**, *6*, 994–999.

Downloaded by UNIV OF GUELPH LIBRARY on June 23, 2012 | http://pubs.acs.org
Publication Date (Web): November 17, 2010 | doi: 10.1021/bk-2010-1053.ch003

Chapter 4

Surface Modification of Positive Contrast Nanoparticle Agents with RAFT Polymers Towards the Targeted Imaging and Treatment of Cancer

**Stephen G. Boyes,[1,*] Misty D. Rowe,[1] Chia-Chih Chang,[1]
Douglas H. Thamm,[2] Susan L. Kraft,[2] Joseph F. Harmon, Jr.,[2]
Natalie J. Serkova,[3] Andrew P. Vogt,[4] and Brent S. Sumerlin[4]**

**[1]Department of Chemistry and Geochemistry, Colorado School of Mines, Golden, Colorado 80401
[2]College of Veterinary Medicine and Biological Sciences, Animal Cancer Center, Colorado State University, Fort Collins, Colorado 80526
[3]Department of Anesthesiology, Biomedical MRI/MRS Cancer Center Core, University of Colorado at Denver and Health Sciences Center, Aurora, Colorado 80045
[4]Department of Chemistry, Southern Methodist University, Dallas, Texas 75275
*sboyes@mines.edu**

A novel surface modification technique was employed to produce a polymer modified positive contrast agent nanoparticle through attachment of well defined polymers synthesized via reversible addition-fragmentation chain transfer (RAFT) polymerization. A range of both hydrophilic and hydrophobic RAFT homopolymers, along with novel multifunctional copolymers of poly(N-isopropylacrylamide)-co-poly(N-acryloxysuccinimide)-co-poly(fluorescein O-methacrylate) were synthesized and subsequently used to modify the surface of gadolinium (Gd) metal-organic framework (MOF) nanoparticles. The succinimide functionality of the copolymer was utilized as a scaffold for attachment of the therapeutic agent, methotrexate, and targeting ligand, H-glycine-arginine-glycine-aspartate-serine-NH_2 peptide. Reduction of the trithiocarbonate RAFT polymer end groups under basic conditions to thiolates provided a means of polymer attachment through vacant orbitals on the Gd^{3+} ions at the surface of the Gd MOF nanoparticles. Magnetic resonance imaging (MRI) confirmed the relaxivity rates of these novel polymer modified structures were easily tuned by changes in the molecular weight and chemical structures of the polymers. In most cases, the relaxivity values were significantly higher than both the unmodified Gd MOF nanoparticles and the clinically employed contrast agents, Magnevist® and Multihance®. These versatile, polymer modified nanoscale scaffolds were shown to provide biocompatibility, cancer cell targeting, diagnostic imaging, through positive contrast in MRI and fluorescence microscopy, and disease treatment capabilities. This unique method provided a simple yet versatile route of producing polymer-nanoparticle theragnostic materials with an unprecedented degree of flexibility in the construct, potentially allowing for tunable loading capacities and spatial loading of targeting/treatment agents, while incorporating bimodal imaging capabilities.

1. Introduction

1.1. Nanoscale Theragnostic Devices

Recently, there has been an explosion in the development of nanomedicine platforms for application in molecular imaging and drug delivery (*1–5*). Nanoscale theragnostic systems (Figure 1) that incorporate molecular targeting, therapeutic agents, and diagnostic imaging capabilities are emerging as the next generation of personalized medicines and have the potential to dramatically improve the therapeutic outcome of drug therapy (*2*, *3*, *5*, *6*). While there is almost unanimous agreement that these next generation, personalized nanomedicines will provide clinically important theragnostic devices, they have yet to reach clinical realization. Arguably, the primary reasons limiting application of these devices are poor design and manufacturing techniques (*1*, *2*, *7*, *8*). Thus, new nanomedicine platforms must be developed for the successful preparation of nanoscale theragnostic devices.

One of the most promising platforms for the formation of new nanoscale theragnostic devices are nanoparticles, where the particle acts as the imaging component of the multifunctional theragnostic device. The use of nanoparticles as the imaging agent for diagnostics is particularly beneficial due to the fact that a large concentration of imaging agent per particle can be delivered to the desired location per targeted biorecognition event. Additionally, these particles have been shown to have longer retention times *in vivo* providing a longer imaging window (*9*). However, in order to produce a nanoparticle based imaging agent that can be easily translated to clinical application, it is important that the nanodevice be useful for application with common and widely utilized diagnostic imaging instrumentation, such as magnetic resonance imaging (MRI), and can

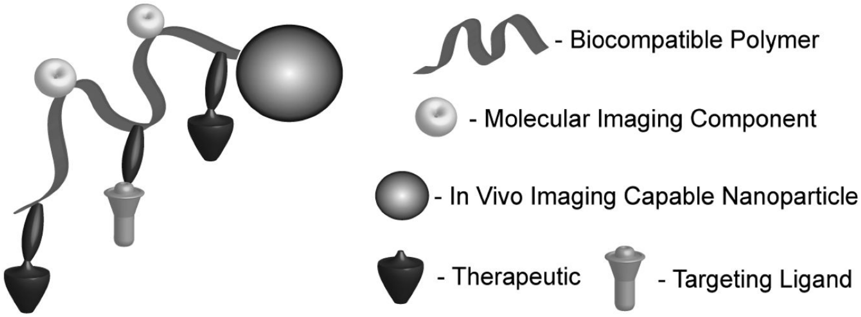
- Biocompatible Polymer
- Molecular Imaging Component
- In Vivo Imaging Capable Nanoparticle
- Therapeutic
- Targeting Ligand

Figure 1. Polymer modified nanoparticle as a nanomedicine construct for targeted diagnostics and therapy.

be modified so as to render the nanostructure biocompatible, while providing a means of biomolecular targeting and disease therapy. Research into the use of inorganic and organo-metallic nanoparticles has shown great promise in regards to the utilization of these structures for theragnostic devices. Due to their inherent physical and optical properties, many nanoparticles have demonstrated the ability to be useful for molecular imaging both in a research and clinical setting. For example, superparamagnetic iron oxide nanoparticles (SPIOs) and gadolinium (Gd) based nanoparticles behave as negative and positive contrast agents, respectively, in MRI, quantum dots have been utilized as markers in fluorescent microscopy, while gold nanorods have been employed in dark field and confocal microscopy (*10–22*).

1.2. Nanoparticles as Diagnostic Imaging Agents for MRI

SPIOs have garnered a majority of the focus on nanoparticle contrast agents for MRI, which has led to current testing of Ferucarbotran and Ferumoxtran in Phases II and III FDA trials, while Ferumoxsil and Ferumoxide are approved for clinical use. Unfortunately, negative contrast agents, such as SPIOs, suffer from a series of drawbacks, including limited *in vivo* cell tracking, MRI cannot distinguish the negative contrast agent from the contrast agent from other signal voids, and negative contrast agents are limited by partial volume effects (*23–25*). Recently, focus on nanoparticle-based MRI contrast agents has shifted to Gd-based nanoparticles (*11*, *12*, *14*, *15*, *17*, *20*, *23*, *26*, *27*) due to their ability to act as a positive contrast agent and their relationship to currently employed MRI contrast agents, such as gadopentetate dimeglumine (Magnevist®) and gadobenate dimeglumine (Multihance®), which are based on Gd chelates. This attention on Gd-based nanoparticle has been mostly driven by limitations with the conventional contrast agents based on Gd chelates, such as a low concentration of Gd per molecule, short retention times *in vivo* due to contrast agent dimensions, limited biostability, and difficulty in functionalization to enable use in more complex diagnostic devices. These Gd-based nanoparticles have been synthesized with both inorganic and organo-metallic compounds of Gd such as gadolinium oxide, gadolinium phosphate, gadolinium fluoride, gadolinium hexanedione and acetylacetenoate mixed with emulsifying wax, and most recently, nanoscale metal-organic frameworks (MOFs) (*11*, *12*, *14–21*, *23*). While Gd-based nanoparticles exhibit relaxivities significantly higher than typical Gd chelates and also provide a contrast agent with higher molecular weights for improved retention times and a high concentration of Gd^{3+} ions per contrast agent particle, their application has been limited due to the difficulty in producing nanoparticles that are biocompatible, stable, and have specific surface functionality (*12*, *23*).

One of the most interesting Gd nanoparticle systems are the nanoscale MOFs, which are constructed from Gd^{3+} ions and organic bridging ligands, such as 1,4-benzenedicarboxylic acid (1,4-BDC), as they have demonstrated exceptional MRI capabilities (*11*, *28*, *29*). However, in order to take advantage of Gd nanoparticles as nanoscale contrast agents for MRI, focus has shifted to overcoming some of their inherent limitations by developing methods to surface modify the nanoparticles (*15–17*). Currently, surface modification methods that have been reported have yielded limited success, as they have resulted in instabilities in the coatings due to their non-covalent nature, poorly defined surfaces, insufficient control over surface functionality, or reduced imaging capabilities due to masking of the underlying Gd nanoparticle. As such, the search for a surface modification technique that provides control over surface functionality and architecture, along with the ability to produce a stable structure without diminishing the inherent imaging properties represents a significant challenge for researchers. Surface modification of Gd-based MOFs through covalent attachment of well-defined polymers offers a means of modifying and/or tuning the relaxation properties of the nanoparticles, incorporating a higher degree of functionality, and increasing the *in vivo* stability and biocompatibility.

1.3. Surface Modification of Nanoparticles with RAFT Polymers

Reversible addition-fragmentation chain transfer (RAFT) polymerization is arguably the most versatile living radical polymerization (LRP) technique with respect to polymerization conditions, along with the ability to produce well-defined, narrow polydispersity index (PDI) polymers with both simple and complex architectures and a high degree of end-group control (*30*, *31*). RAFT polymerization shows great promise in the synthesis of multifunctional polymers due to the versatility of monomer selection and its functional group tolerance. It has been widely employed for the preparation of highly specialized materials for advanced biomedical applications, such as antibody and small interfering ribonucleic acid polymer conjugates, controlled drug delivery vehicles, and bioconjugation (*32–38*). Due to the well defined nature of the RAFT polymerization technique, another advantage of RAFT polymers is the presence of a thiocarbonylthio group on the end of each polymer chain. Literature has shown that the thiocarbonylthio end groups can be reduced to a thiol in the presence of a nucleophile, such as a primary amine or sodium borohydride (*39*, *40*). Because thiols have been shown to react strongly with a variety of metal surfaces, such as gold and silver (*40*), and the surface of semi-conducting nanoparticles, such as CdSe nanoparticles, RAFT polymerization is uniquely placed as one of the premier polymerization techniques to prepare polymers for surface functionalization of a wide range of both planar and nanoparticle substrates (*39–42*).

To date, there are few reports of the utilization of the RAFT polymerization technique to produce well defined polymers that allow for the surface modification of Gd MOF nanoparticles to produce polymer modified positive contrast nanoparticle agent platforms for MRI (*43*, *44*). Herein, we discuss a novel surface modification procedure developed in our research allowing the attachment of well-defined polymers synthesized *via* RAFT polymerization through reduction of the thiocarbonylthio end group under basic conditions to form thiolates and further attachment through coordination chemistry to the Gd MOF nanoparticles (Scheme 1) (*43*, *44*). *In vitro* MRI was employed to determine the relaxivities of the novel polymer modified Gd MOF nanoparticles in comparison to the clinically employed contrast agents, Magnevist® and Multihance®. Furthermore, Gd MOF nanoparticles were surface modified by the covalent attachment of well-defined RAFT copolymers containing a targeting ligand and antineoplastic agent to produce a novel theragnostic nanodevice, with bimodal diagnostic imaging capabilities. Finally, tailoring the functionality and thickness of the polymer coating provided a means of tuning the MRI characteristics of these novel polymer modified positive contrast nanoparticle agents.

2. Experimental Section

2.1. Materials and Characterization

All chemicals were purchased from Sigma-Aldrich, unless otherwise noted. H-glycine-arginine-glycine-aspartate-serine-NH_2 (GRGDS-NH_2) peptide motif was purchased from AnaSpec. *N*-isopropyacrylamide (NIPAM) was doubly recrystallized in hexanes before use. Azobisisobutyronitrile (AIBN) was doubly recrystallized from methanol prior to use. Triethylamine was distilled under pressure and stored in the freezer prior to use. Styrene (styrene) was filtered over basic alumina oxide and then stored in a freezer prior to use. Acrylic acid (AA), *N,N*-dimethylaminoethyl acrylate (DMAEA), and poly(ethylene glycol) methylether acrylate (PEGMEA) were distilled under vacuum and then stored in a freezer prior to use. All other chemicals, unless otherwise discussed, were reagent grade and used as received. S-1-dodecyl S′-(α,α-dimethylacetic acid) trithiocarbonate (DATC) was prepared via Lai et al.'s literature procedure (*45*). N-(2-hydroxypropyl) methacrylamide (HPMA) was synthesized by a procedure in the literature (*46*). A discussion of the characterization of polymers, Gd MOF nanoparticles, and RAFT polymer modified Gd MOF nanoparticles is described in great detail in recent literature (*43*, *44*).

2.2. Formation and Modification of RAFT Polymers

2.2.1. Homopolymer Synthesis via RAFT Polymerization

A range of homopolymers including NIPAM, HPMA, Sty, DMAEA, PEGMEA, and AA were synthesized by RAFT polymerization techniques.

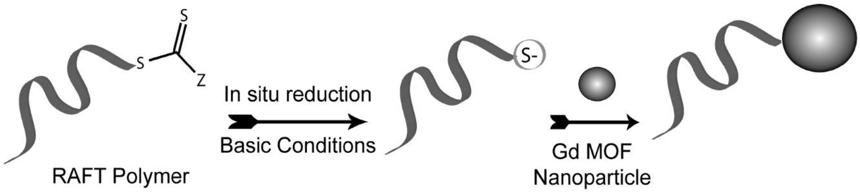

Scheme 1. General route for the modification of gadolinium metal-organic framework nanoparticles with RAFT synthesized polymers.

For example, in order to produce a poly (*N*-isopropyacrylamide) PNIPAM homopolymer with a $M_{n,theoretical}$ of 5,500 g/mol, NIPAM (10.07 g, $8.90x10^{-2}$ mol), N,N-dimethylformamide (DMF) (50 mL), and DATC (0.488 g, $1.34x10^{-3}$ mol) were added to a 150 mL Schlenk flask equipped with a stir bar. The flask was sealed and the solution was gently degassed for 45 min and then left under a high-purity nitrogen atmosphere. The flask was allowed to stir at room temperature until the monomer and DATC were completely dissolved. To a second 150 mL Schlenk flask equipped with a stir bar was added and AIBN (0.0204 g, $1.24x10^{-4}$ mol). This flask was sealed with a rubber septum, subjected to three evacuation-nitrogen purge cycles and left under a nitrogen atmosphere. The monomer solution was then transferred *via* cannula to the initiator containing flask. The reaction was then heated for 1h at 60 °C, after which the polymer was isolated from the solution by evaporating residual solvent under vacuum at 40 °C overnight. Polymer was then purified *via* precipitation to remove residual monomer. Specific RAFT polymerization conditions for each of the other monomer systems can be found in the literature (*43*).

2.2.2. Poly(N-isopropylacrylamide)-co-poly(N-acryloxysuccinimide)-co-poly(fluorescein O-methacrylate) Synthesis via RAFT Polymerization

A range of random copolymers of poly(N-isopropylacrylamide)-co-poly(N-acryloxysuccinimide)-co-poly(fluorescein O-methacrylate) (PNIPAM-co-PNAOS-co-PFMA) were synthesized with 33 wt% monomer in dioxane at 60 °C *via* RAFT polymerization techniques utilizing a 18.75:1 molar ratio of DATC, as the RAFT agent, to AIBN, as the initiator. NIPAM comprised the majority of the copolymer backbone, with NAOS being incorporated into the backbone at 10, 17, 25, 33, and 50 wt% loading to provide a reactive sight for attachment of targeting ligands and/or therapeutic agents. FMA, at approximately 0.5 wt% loading, was added near the end of the polymerization allowing for fluorescent tagging of the biocopolymer for subsequent imaging capabilities in fluorescent microscopy. For example, in order to produce PNIPAM-*co*-PNAOS-*co*-PFMA with a 10 wt% loading of NAOS, anhydrous dioxane (21.9 mL), NIPAM (7.00 g, 61.9 mmol), NAOS (0.700 g, 4.14 mmol), and DATC (0.340 g, 0.931 mmol) were added to a 150 mL Schlenk flask equipped with a stir bar. The flask was sealed and the solution was gently degassed for 45 min and then left under a high-purity nitrogen atmosphere. The flask was allowed to stir at room temperature until the monomer and DATC were completely dissolved. To a second 150 mL Schlenk flask equipped with a stir bar was added AIBN (0.0082 g, 0.050 mmol). This flask was sealed with a rubber septum, subjected to three evacuation-nitrogen purge cycles and left under a nitrogen atmosphere. The monomer solution was then transferred *via* cannula to the initiator containing flask. The reaction was then heated for 24h at 60 °C, at which time a 2 mL sample was taken by syringe for analysis. To a 25 mL Schlenk tube equipped with a stir bar, anhydrous dioxane (10 mL) and fluorescein *O*-methacrylate (0.035 g, 0.087 mmol) were added. The tube was sealed and the solution was gently degassed for 45 min and then left under a high-purity nitrogen atmosphere. The monomer solution was then transferred via cannula to the PNIPAM-*co*-PNAOS copolymer containing flask. The reaction was then heated for an additional 6 h at 60 °C to allow the addition of PFMA to the PNIPAM-*co*-PNAOS copolymer. Polymer was isolated from the solution by evaporating residual solvent under vacuum at 40 °C overnight. Polymer was then purified *via* aqueous extraction to remove residual monomer.

2.2.3. Attachment of GRGDS-NH_2 and MTX to PNIPAM-co-PNAOS-co-PFMA

The PNIPAM-*co*-PNAOS-*co*-PFMA copolymers were subsequently reacted through a condensation reaction of the succinimide groups with primary amine groups of the targeting ligand and/or therapeutic. Reactions were carried out at room temperature in deuterated *N,N*-dimethylsulfoxide (DMSO) with 0.01M triethylamine and stirring at room temperature for 24 h. Unreacted targeting and/or therapeutic agents were then removed *via* silica column chromatography and aqueous/solvent extraction. Methotrexate (MTX) and GRGDS-NH_2 were incorporated into the biocopolymer backbone at 10, 25, and 33 wt% loading capacity. Detailed reaction conditions for the attachment of both the therapeutic and targeting ligand are discussed in the literature (*44*).

2.3. Synthesis of Gd MOF Nanoparticles

Gd MOF nanoparticles were prepared *via* a reverse micro-emulsion synthesis reported by Reiter and coworkers (*11*). Briefly, a water to surfactant ratio of 10 was employed for the reverse microemulsion system containing gadolinium (III) chloride and the bridging ligand, 1,4-BDC (0.075M). Cetyltrimethylammonium bromide (0.05M) was employed as the surfactant, with hexanol as a cosurfactant in a heptane oil phase. The resulting solution was allowed to stir for 24 h at room temperature. Unreacted reagents was removed from the Gd MOF nanoparticles through repeated centrifugation and resuspension in ethanol (2x) and water (2x) followed by drying.

2.4. Surface Modification of Gd MOF Nanoparticles with RAFT Homopolymer and Copolymers

In a typical experiment, RAFT polymer (0.1 g) was added to 25 mL of anhydrous DMF in a 150 mL Schlenk flask equipped with a stir bar, then sealed with a rubber septum. The RAFT polymer solution was purged with high purity nitrogen and then subsequently left under a nitrogen atmosphere. The RAFT agent terminated polymer was then converted to a thiolate terminated polymer, through aminolysis, by the addition of 0.075M hexylamine (0.4 mL) and stirring for 1h at room temperature. Gd MOF nanoparticles (0.01 g) were suspended in an additional 25 mL of DMF in a second 150 mL Schlenk flask equipped with a stir bar, then sealed with a rubber septum. The nanoparticle solution was then purged with high purity nitrogen for 30 min and was subsequently left under a nitrogen atmosphere. The polymer solution was then transferred *via* cannula to the Gd MOF nanoparticle solution. The resulting solution was allowed to stir for 24 h at room temperature under a nitrogen atmosphere. Untethered polymer was removed from the polymer modified Gd MOF nanoparticles through repeated centrifugation and resuspension in DMF (2×) and ethanol (2×), followed by drying.

3. Results and Discussion

3.1. Novel Polymer Modified Gd MOF Nanoparticles as Nanomedicines

Despite the tremendous potential that nanoparticles offer in the booming area of nanomedicines; their modification to provide critical properties such as multimodal imaging, biocompatibility, biomolecular targeting, and a therapeutic outcome is of utmost importance. Developing a method to provide reproducible, well defined, and stable surface modification of nanoparticles is critical. RAFT polymerization techniques offer one of the most versatile routes to enhancing the properties of high surface area nanoparticle structures through modification of nanoparticle surfaces with well-defined RAFT polymers. To date, RAFT polymers have been employed in the modification of a range of surfaces including gold, silver, and CdSe nanoparticles, by reducing the RAFT agent end group to a thiol moiety and employing the ‘grafting to’ approach (*39–42*). Specifically, gold nanorods and Gd nanoparticles, have gained interest due to their potential application as biomedical imaging agents in dark field microscopy and MRI, respectively (*10–12*, *14–19*, *21*, *23*, *26*, *29*, *47–49*).

Recently, focus has intensified on the utilization of Gd nanoparticles as positive contrast agents for diagnostic imaging using MRI (*11*, *12*, *14–21*, *23*). This attention has been driven by limitations with conventional contrast agents based on chelates of Gd^{3+} cations, such as a low concentration of metal ion per molecule, short retention times *in vivo*, and difficulty in functionalization to enable use in nanovectors (*20*, *26*, *29*, *50*). Research into Gd nanoparticles has been focused on overcoming issues related to conventional contrast agents and on taking advantage of the favorable properties of the nanoparticles, such as improved relaxation and in vivo retention times. Due to the strong potential of Gd nanoparticles as theragnostic nanodevices, researchers have attempted to enhance the application of these systems by developing methods to surface modify the nanoparticles (*15–17*). However, despite a great deal of interest, these surface modification methods have demonstrated limited success, as they have resulted in poorly defined surfaces with lack of control over the functionality of the surface of the nanoparticle, instabilities in the coatings due to their non-covalent nature, or reduced imaging capabilities due to masking of the underlying Gd nanoparticle. Furthermore, the modification of Gd nanoparticles with well-defined polymers to provide increased functionality, such as biocompatibility and tunable imaging properties, would be extremely useful for applications such as well-defined nanomedicines. As such, the search for a surface modification technique that provides control over surface functionality and architecture, the ability to incorporate a wide range of both targeting ligands and therapeutics, and produce a stable structure without diminishing the inherent imaging properties represents a significant challenge for researchers in the search for next generation nanomedicines.

3.2. Gd MOF Nanoparticles

The use of Gd MOF nanoparticles as positive contrast agents for MRI should provide several advantages over the clinically employed Gd chelates, such as enhanced imaging through magnetic resonance, increased biostability, and longer *in vivo* retention (*11*, *14–16*, *18–21*, *23*, *26*). Gd-based contrast agents produce a large shortening of the longitudinal relaxation time (T1) and high longitudinal relaxivity (r_1) and are called positive contrast agents, where the relaxivity value, r, is simply defined as the inverse of the relaxation time with respect to the contrast agent concentration (*23*, *50*). The ratio of the transverse relaxivity (r_2) to r_1 is used to provide about the contrast agent, where r_2/r_1 values below 2 show brightening in T1-weighted images, providing a positive contrast agent (*23*). As there is a preference for the use of positive contrast agents at the clinical level, due to their wider dynamic range, contrast agents based on Gd^{3+} chelates are the most widely used.

In this research, Gd MOF nanoparticles were synthesized as described in the literature (*11*, *12*, *51*). The Gd MOF nanoparticles were characterized thoroughly by employing transmission electron microscopy (TEM) (Figure 2) and attenuated total reflectance-Fourier transform infrared spectroscopy (ATR-FTIR) (Figure 3), along with X-ray diffraction and thermogravimetric analysis (TGA). Figure 2a shows the average dimensions of the synthesized Gd MOF nanoparticles to be 122 nm +/- 30 nm in length and 53 nm +/- 12 nm in width. The ATR-FTIR spectrum, Figure 3c, showed a characteristic out-of-plane =C-H aromatic stretch at 725 cm^{-1}, symmetric carboxylate stretch at 1400 cm^{-1}, an asymmetric carboxylate stretch at 1540 cm^{-1}, along with peaks at 2855 cm^{-1}, 2925 cm^{-1}, and 3065 cm^{-1}, which are attributed to the –C-H stretching vibrations of the 1,4-BDC bridging ligand, and 3460 cm^{-1} which was attributed to the –OH stretch of the water ligand. Additionally, TGA was employed and confirmed the empirical formula of the Gd MOF nanoparticles to be $Gd(1,4\text{-}BDC)_{1.5}(H_2O)_2$, as discussed in the literature (*11*).

3.3. Multifunctional Polymers via RAFT Polymerization

3.3.1. Synthesis and Characterization of RAFT Homo- and Copolymers

To demonstrate the versatility of the newly developed procedure to surface modify Gd MOF nanoparticles, poly[*N*-(2-hydroxypropyl) methacrylamide]

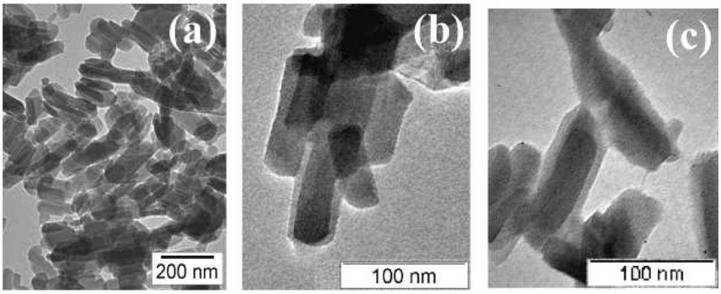

Figure 2. Transmission electron microscopy of (a) unmodified Gd MOF nanoparticles, along with Gd MOF nanoparticles modified with (b) PNIPAM, and (c) PNIPAM-co-PNAOS-co-PFMA polymers synthesized by RAFT polymerization (43, 44).

(HPMA), polystyrene (PSty), PNIPAM, poly[2-(dimethylamino)ethyl acrylate] (PDMAEA), poly[poly(ethylene glycol)methyl ether acrylate] (PPEGMEA), and poly(acrylic acid) (PAA) homopolymers were each synthesized *via* RAFT polymerization techniques employing the RAFT agent, DATC, for subsequent deposition onto the Gd MOF nanoparticles. Trithiocarbonates, such as DATC, have been shown to be effective RAFT agents for the polymerization of a wide range of monomers including acrylates, methacrylates, and acrylamides (*40*, *45*, *52–58*). Each of these polymers, except PSty, were chosen because of their utility as polymers for bio-based applications and positive results towards biocompatibility (*59–62*). PSty was chosen to both demonstrate the inherent flexibility of the surface modification procedure, by using a hydrophobic polymer, and to determine the effect of a hydrophobic coating on the relaxation properties of the Gd MOF nanoparticles. By taking advantage of the living and well defined nature of RAFT polymerization, the molecular weight of the polymers can be easily controlled by simply varying the ratio of monomer to RAFT agent and the extent of conversion of the polymerization. Table 1 shows experimental and theoretical molecular weights for each of the homopolymers synthesized by RAFT polymerization. As can been seen in Table 1, each of the polymerizations showed good agreement between the theoretical and experimental molecular weights. For example, the experimental molecular weight of PNIPAM of 8,600 g/mol corresponded well to the theoretical molecular weight of 8,700 g/mol (Table 1). In conjunction to molecular weight control, well defined RAFT polymerizations typically provide polymers with narrow molecular weight distributions. Table 1 demonstrates that the PDI for each of the homopolymers synthesized was generally low and each gel permeation chromatography (GPC) curve indicated monomodal molecular weight distributions. The good agreement between experimental and theoretical molecular weights and the narrow molecular weight distributions obtained for each of the homopolymers indicates in each case a well defined RAFT polymerization was achieved and that virtually all polymer chains prepared should contain a trithiocarbonate end group, due to the living nature of

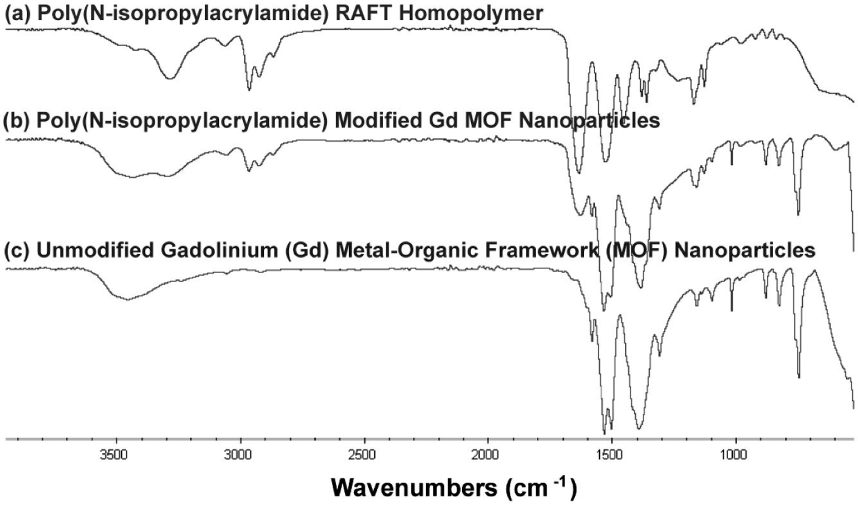

Figure 3. ATR-FTIR spectra of the (a) PNIPAM homopolymer synthesized by reversible addition-fragmentation chain transfer polymerization, (b) PNIPAM homopolymer modified Gd MOF nanoparticles, and (c) unmodified Gd MOF nanoparticles (43).

the polymerization, which can be used to attach the RAFT polymers to the Gd MOF nanoparticles.

3.3.2. Synthesis of Highly Functional Biocompatible Polymers via RAFT Polymerization

Next, highly functional random copolymers of PNIPAM-*co*-PNAOS-*co*-PFMA were synthesized *via* RAFT polymerization employing the RAFT agent, DATC. The NIPAM monomer was chosen because of its extensive use in polymers for bio-based applications and the overall biocompatibility of PNIPAM (*59*), which comprises the major component of the prepared random copolymers in most cases. The NAOS monomer was incorporated into the copolymer as a site for the attachment of different targeting and/or therapeutic agents, Scheme 2. It has been widely reported that primary amines and alcohols will react readily with the succinimide functionality present on the NAOS monomer (*32*, *63*). As each of the targeting and therapeutic agents chosen to be used in this work contain either an available primary amine, by introducing the NAOS monomer at different weight percentages into the copolymer, the targeting and/or chemotherapeutic loading can be easily modified. The content of the NAOS monomer was varied between 10 and 50 wt% allowing for control over the concentration of targeting and/or therapeutic attached to the copolymer. The addition of the FMA monomer into the copolymer, at 0.5 wt%, allowed for the introduction of a fluorescence moiety providing *in vitro* cellular-level imaging and making the final polymer modified Gd MOF nanoparticle bimodal with respect to imaging.

Table 1. Molecular weight and polymer coating properties of RAFT homopolymers (*43*)

Polymer Coating	M_n (g/mol)		$PDI^{b,e}$	Coating Thickness (nm)[f]	Grafting Density (chain/nm^2)	
	Theory[a]	Experimental[b]			Theory[g]	Experimental[h,i]
PNIPAM	5,500	5,700	1.23	4.2 +/- 0.3	0.1849	0.1395
	8,700	8,600	1.12	7.0 +/- 0.4	0.1591	0.1037
	17,100	17,800	1.12	10.9 +/- 1.0	0.1070	0.0873
PHPMA	5,100	5,300	1.44	2.4 +/- 1.1	0.1847	0.1379
	9,000	10,200	1.30	3.5 +/- 0.7	0.0957	0.0993
	19,700	19,400	1.24	7.3 +/- 0.6	0.0729	0.0638
PSty	4,900	4,800	1.15	1.6 +/- 0.3	0.1660	0.1839
	9,400	9,000	1.15	5.7 +/- 0.9	0.1341	0.0960
	18,900	15,300	1.13	8.7 +/- 0.9	0.1033	0.0815
PDMAEA	17,400	15,100	1.25	5.1 +/- 0.3	0.1276	0.1111
PPEGMEA	25,900	19,600	1.29	4.4 +/- 1.0	0.0792	0.0636
PAA	14,300	10,800[c]		5.7 +/- 0.7	0.1545	0.1147
		10,900[d]	1.10[d]		0.1538	0.1142

(a) $M_{n,\ \text{theoretical}}$ is defined as the theoretical number average and for each RAFT polymerization was calculated using the equation M_n = (molecular weight of RAFT agent) + (molecular weight of monomer) × ($[\text{monomer}]_0$ / $[\text{RAFT agent}]_0$) × (monomer conversion), (b) determined by gel permeation chromatography, (c) calculated by end-group analysis using proton nuclear magnetic resonance spectroscopy (^{1}H NMR), (d) determined by matrix assisted laser desorption ionization-time of flight mass spectrometry, (e) PDI was calculated using the equation PDI = (M_w / M_n), (f) polymer coating thickness was determined by TEM and is an average of ten measurements, (g) theoretical grafting densities were calculated from equations discussed in the literature using an average Gd MOF nanoparticle length of 122nm and width of 53nm, along with the experimental molecular weight and bulk density of each polymer, (h) experimental grafting densities were calculated using an average Gd MOF nanoparticle length of 122nm and width of 53nm, the experimental molecular weight of each polymer, a bulk density of 2.529g/cm^3 for the Gd MOF nanoparticles, along with the mass of polymer per mass of Gd MOF nanoparticle determined by TGA and (i) percent relative standard deviations were determined to be <7% for the experimental grafting density calculations.

As can be seen in Table 2, a range of copolymer molecular weights, from 7,500-10,000g/mol, were prepared and in each case there is very good agreement between the theoretical and experimental molecular weights. RAFT polymerization is arguably the best living radical polymerization technique for the polymerization of functional monomers, such as NIPAM, NAOS, and FMA (*30*, *64*, *65*). As such, the incorporation of a higher weight percentage of NAOS monomer into the initial polymerization system led to copolymers with increased molecular weights, while still maintaining excellent control. This is evidenced by the fact that for every copolymer synthesized, the experimental M_n is comparable to the theoretical M_n values (Table 1). For example, the experimental M_n of PNIPAM-*co*-PNAOS-*co*-PFMA at 10 wt% NAOS of 7,700 g/mol was within 3% of the theoretical M_n of 7,500 g/mol. Furthermore, ^{1}H NMR confirmed the experimental weight percentages of PNAOS, in each of the RAFT copolymers synthesized, to be within 1.5 wt% of their corresponding theoretical values.

Finally, due to the controlled nature of RAFT polymerizations, the PDI for each of the copolymers synthesized was less than 1.12, indicating very narrow molecular weight distributions, and each GPC curve indicated monomodal molecular weight distributions. Additionally, since the copolymerization of NIPAM and NAOS monomers was allowed to proceed to moderate conversions before the addition of the FMA monomer, ^{1}H NMR confirmed the copolymer backbones to have approximately random structures with blocky PFMA characteristics near the chain ends. Control of the molecular weight is imperative as it will provide control over the concentration of targeting/therapeutic agent that can be incorporated into the final polymer, minimize heterogeneity in the polymer, and provide a high degree of chain-end functionality, making these constructs especially effective for incorporation into a nanoscale theragnostic device.

3.3.3. Addition of Therapeutic and Molecular Targeting Agent onto RAFT Copolymer

As mentioned previously, a theragnostic nanodevice must contain an imaging component, molecular targeting ligand, and therapeutic agent. Thus, once the random copolymers were synthesized, the ability to incorporate a targeting ligand and/or therapeutic agent onto the polymer backbone *via* reaction with the NAOS segments was investigated. The peptide GRGDS-NH_2 was chosen as the targeting ligand and MTX was chosen as the antineoplastic chemotherapeutic agent. The GRGDS-NH_2 ligand was chosen due to its ability to target the $\alpha_V\beta_3$ integrin, which is expressed in angiogenic vasculature in a range of cancerous tumors (*66*). The chemotherapeutic, MTX, was chosen as it is known to prevent cell proliferation and to induce apoptosis in multiple types of cancer cells through a variety of mechanisms (*67*).

Attachment of the MTX and/or GRGDS-NH_2 peptide motifs to the copolymer was achieved *via* a condensation reaction between the succinimide group on the NAOS monomer and the primary amine present on each motif in the presence of 0.01M triethylamine (Scheme 2). Successful attachment of the GRGDS-NH_2 motif and MTX was qualitatively confirmed by ^{1}H NMR spectroscopy. The ^{1}H NMR studies also provided information regarding critical characteristics of the multifunctional copolymers including the number of drug molecules per polymer chain and the number of targeting ligands per polymer chain. For example, the RAFT copolymer containing 25 wt% NAOS, with a molecular weight of 12,900 g/mol and PDI of 1.06, contained 15 molecules of MTX and 5 molecules of GRGDS-NH_2 per polymer chain. By varying the amount of NAOS or the concentration of MTX or GRGDS-NH_2 used in the modification steps, the number of molecules of each can easily be modified and controlled. It should be noted that as the RAFT polymerization technique allows for the preparation of well-defined copolymers containing the NAOS monomer, the reactivity of the succinimide group can be used to produce copolymer structures tailored with a wide range of targeting-treatment combinations, *via* post-polymerization modification, for diagnosis and treatment of not only cancer, but a wide range of different diseases.

Table 2. Molecular weight properties of multifunctional RAFT copolymers (*44*)

Polymer Coating	M_n (g/mol) Theory[a]	M_n (g/mol) Experimental[b]	PDI[b]
PNIPAM-*co*-PNAOS-*co*-PFMA at 10% wt. NAOS	7,500	7,700	1.09
PNIPAM-*co*-PNAOS-*co*-PFMA at 17% wt. NAOS	8,900	9,900	1.11
PNIPAM-*co*-PNAOS-*co*-PFMA at 25% wt. NAOS	10,100	12,900	1.06

(a) $M_{n,\ \text{theoretical}}$ for each RAFT polymerization was calculated using the equation M_n = (molecular weight of RAFT agent) + (molecular weight of monomer) × ([monomer]$_0$ / [RAFT agent]$_0$) × (monomer conversion), (b) determined by gel permeation chromatography

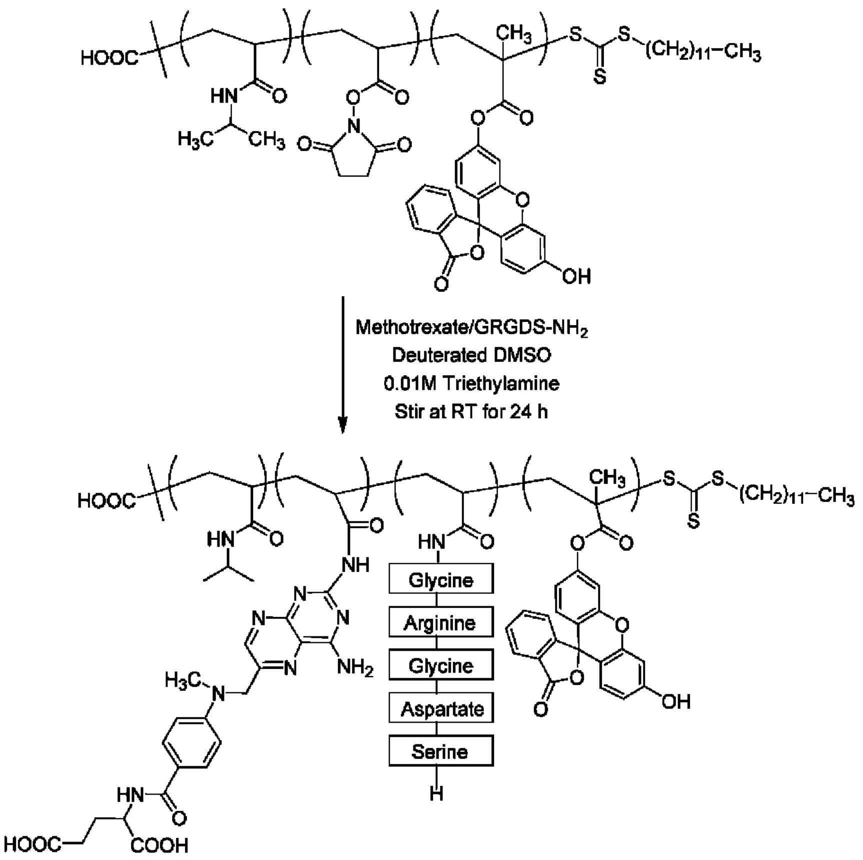
HOOC
HN
O
H3C
CH3
O
O
N
O
O
CH3
S
S
(CH2)11-CH3
S
O
O
O
O
O
OH
Methotrexate/GRGDS-NH2
Deuterated DMSO
0.01M Triethylamine
Stir at RT for 24 h
HOOC
HN
O
O
NH
N
N
N
N
NH2
H3C
N
HN
O
HOOC
COOH
HN
O
Glycine
Arginine
Glycine
Aspartate
Serine
H
CH3
S
S
(CH2)11-CH3
S
O
O
O
O
O
OH

Scheme 2. General route for the modification of PNIPAM-co-PNAOS-co-PFMA copolymer with the chemotherapeutic Methotrexate and targeting ligand, GRGDS-NH$_2$ (44).

3.4. Development of Polymer Surface Modification Technique for Gd MOF Nanoparticles

The limitations inherent with current nanoparticle systems, such as aggregation, *in vivo* toxicity, and poor biostability, have led to a great deal of interest in surface modification with well-defined polymers as a means of incorporating advanced functionality and biocompatibility into nanomedical devices (*20*, *68–71*). To date, the modification of Gd nanoparticles has been focused on either the encapsulation in an emulsifying wax or functionalization of the surface with inorganic materials, such as a silica shell (*12*, *14–19*, *29*, *48*). As such, the development of a surface modification technique for nanoscale Gd MOFs with well-defined polymers synthesized *via* RAFT polymerization offers great potential for the formation of novel nanomedicines. As mentioned above, due to the living nature of RAFT polymerizations, RAFT polymers contain a high degree of chain end functionality, which imparts chain ends with a thiocarbonylthio moiety (*30*).

3.4.1. Gd MOF Surface Modification with Hydrophilic RAFT Polymers

As DATC is employed as the RAFT agent in the formation of RAFT polymers in this study, each of the polymers produced should have trithiocarbonate terminated chains. Surface modification of Gd MOF nanoparticles was achieved by the 'grafting to' technique, which involved an initial aminolysis, using hexylamine, of the trithiocarbonate end group of the RAFT polymers to a thiolate functionality under inert and basic conditions (Scheme 3). Subsequently, it is hypothesized that the thiolate terminated homopolymer was covalently attached to the nanoparticle surface through a coordination reaction between the thiolate end-group moiety and vacant orbitals on the Gd^{3+} ions at the surface of the Gd MOF nanoparticles. Using this procedure, Gd MOF nanoparticles were modified with various RAFT homopolymers (Scheme 3a). It should be noted that after polymer deposition and prior to characterization or use, the nanoparticles were washed several times with a good solvent for the polymer, via repeated washing and centrifugation steps, to remove any untethered polymer from the system.

Prior to attachment of the RAFT polymers to the Gd MOF nanoparticles, ^{1}H NMR, UV-Vis spectroscopy, and ATR-FTIR were used to verify the conversion of the trithiocarbonate end group to a thiolate upon addition of the hexylamine. In each case, the aminolysis reaction resulted in approximately quantitative conversion of the RAFT polymer end groups to thiolates, as had been observed in the literature for similar reactions (*39*, *58*, *72*), with minimal dimerization confirmed by ^{1}H NMR and GPC. Surface modification of the Gd MOF nanoparticles with RAFT homopolymers was characterized through both TEM (Figure 2 b,c and Table 1) and ATR-FTIR spectroscopy (Figure 3). The Gd MOF nanoparticles were first modified with a series of different molecular weight PNIPAM homopolymers synthesized via RAFT polymerization. ATR-FTIR was employed to confirm the addition of the PNIPAM homopolymer onto the surface of the Gd MOF nanoparticles. Several of the characteristic stretches of the free PNIPAM homopolymer, including a broad N-H stretch above 3300 cm^{-1} and a small N-H bend at 1640 cm^{-1} indicating the presence of the acrylamide functionality; an increase in intensity of the $–CH_2$ stretching and C-H stretching vibrations between 2800-3000 cm^{-1} due to backbone methylenes; a peak at 1720 cm^{-1} assigned to the carbonyl stretch of the amide; and a stretch at 1380cm^{-1} attributed to the addition of $–CH_3$ and isopropyl groups, display good transference to the polymer modified Gd MOF nanoparticles, when compared to the unmodified Gd MOF nanoparticles (Figure 3). The TEM image (Figure 2b) shows a relatively uniform coating of the PNIPAM homopolymer around the Gd MOF nanoparticles after deposition with an average coating thickness of about 11nm.

Other hydrophilic homopolymers, such as PHPMA, PDMAEA, PPEGMEA, and PAA synthesized via RAFT polymerization techniques were also employed in the successful modification of Gd MOF nanoparticles. In each case, TEM showed relatively uniform coatings on the surface of the nanoparticles after deposition. Polymer coating thicknesses for these samples are shown in Table 1. Additionally, upon modification of the Gd MOF nanoparticles, several of the respective characteristic stretches of each of the free homopolymers, displayed good transference to the polymer modified Gd MOF nanoparticles, when compared to the unmodified Gd MOF nanoparticles (*43*).

3.4.2. Modification of Gd MOF Nanoparticles with Polystyrene

Three different molecular weight PSty homopolymers synthesized via RAFT polymerizations were next employed to surface modify the Gd MOF nanoparticles. As mentioned above, the use of PSty should result in a more hydrophobic coating on the Gd MOF nanostructure and may dramatically affect the relaxation properties of the particles. The presence of PSty on the Gd MOF nanoparticles was confirmed due to the good transference of aromatic C-H stretching around 3100 cm^{-1} and C=C aromatic doublets at 1420-1480 cm^{-1} from the free polymer to the polymer modified Gd MOF nanoparticles, when compared to the unmodified Gd MOF nanoparticles. Additionally, the PSty modified Gd MOF nanoparticles showed a decreased solubility in aqueous solution with increasing molecular weight. This trend was attributed to the successful modification of the Gd MOF nanoparticles with the highly hydrophobic PSty polymer.

3.4.3. Surface Modification of Gd MOF Nanoparticles with Multifunctional RAFT Copolymers

The surface modification of nanoparticles to incorporate advanced functionality and biocompatibility is a critical step in the development of the next generation of nanoscale theragnostic devices. In a similar procedure as before, modification of the Gd MOF nanoparticles was achieved via initial aminolysis, using hexylamine, of the trithiocarbonate end group of the RAFT copolymers to a thiolate functionality under inert and basic conditions. In each case, both ATR-FTIR and ^{1}H NMR spectroscopy confirmed near quantitative reduction of the trithiocarbonate endgroups of the RAFT copolymers to thiols with the addition of hexylamine, followed by subsequent attachment through thiolate endgroups to the Gd MOF nanoparticle surface. As discussed earlier, after polymer deposition and prior to characterization, the nanoparticles were washed several times with a good solvent for the polymer to remove untethered polymer from the system. Successful modification of the Gd MOF nanoparticles with RAFT copolymers was characterized through both TEM (Figure 2c) and ATR-FTIR spectroscopy (Figure 4). The TEM image (Figure 2c) indicates a relatively uniform coating of polymer around the Gd MOF nanoparticles after deposition, with an average thickness of approximately 9 nm. ATR-FTIR was also utilized to confirm the addition of the polymer onto the nanoparticles without the loss of the copolymer functionality. Several characteristic stretches of the free copolymer, including the carbonyl stretch at 1735 cm^{-1}, succinimide stretch at 1650 cm^{-1}, and methylene stretches from 2810-3000 cm^{-1}, display good transference to the polymer modified Gd MOF nanoparticles when compared to the unmodified Gd MOF nanoparticles (Figure 4).

3.4.4. Molecular Weight Effects on Polymer Coating Thickness and Grafting Density

The different PNIPAM, PHPMA, and PSty samples were also used to examine the effect of molecular weight on grafting density, coating thickness, and relaxivity. As can be seen in Table 1, there is a definite trend of increasing polymer coating thickness with molecular weight of each of the three polymers. For example, the average thickness of the PNIPAM homopolymer with an $M_{n,experimental}$ of 5,700 g/mol is approximately 4.2 nm +/- 0.3 nm (Table 1). The PNIPAM homopolymer with an $M_{n,experimental}$ equal to 8,600 g/mol increased the polymer coating thickness to 7.0 nm +/- 0.4 nm, while an $M_{n,experimental}$ of 17,800 g/mol further raised the thickness to 10.9 nm +/- 1.0 nm (Table 1). Similar results were seen for the PHPMA samples. For example, the average thickness of the PHPMA homopolymer with an $M_{n,experimental}$ of 5,327 g/mol is approximately 2.4 nm +/- 1.1 nm (Table 1). The PHPMA homopolymer with an $M_{n,experimental}$ equal to 10,281 g/mol increased the polymer coating thickness to 3.5 nm +/- 0.7 nm, while an $M_{n,experimental}$ of 5,327 g/mol further raised the thickness to 7.3 nm +/- 0.6 nm (Table 1). Finally, the average thickness of the PSty homopolymer with an $M_{n,experimental}$ of 4,802 g/mol is approximately 1.6 nm +/- 0.3 nm (Table 1). The PSty homopolymer with an $M_{n,experimental}$ equal to 8,972 g/mol increased the polymer coating thickness to 6.7 nm +/- 0.9 nm, while an $M_{n,experimental}$ of 15,245 g/mol further raised the thickness to 8.7 nm +/- 0.9 nm (Table 1). This trend suggests the ability to tailor the polymer coating thickness by simply changing the molecular weight characteristics of the RAFT polymer used for modification.

3.4.5. Calculation of Polymer Grafting Density per Gd MOF Nanoparticle

The development or application of any surface modification technique using polymers requires knowledge of critical elements such as the mode of modification and evidence of the polymer on the surface, both of which have been discussed above. Another element which is critical in all surface modification technique is an understanding of the amount of polymer attached to the surface, as this has a vital role in determining the conformation of the polymer on the surface. As such, the grafting density (σ), defined as number of chains tethered per unit area, was calculated utilizing both theoretical and experimental equations from the literature (*73–79*). First, the average volume and surface area of a Gd MOF nanoparticle was determined assuming a rod-like shape based on the average length of 122nm and width of 53nm, which were determined from TEM images. Secondly, the experimental number average molecular weight of each polymer sample (Table 1) was employed for both the experimental and theoretical grafting calculations. Next, the bulk density of the Gd MOF nanoparticles was determined by XRD to be approximately 2.529 g/cm^3, which compared well to literature values (*11*, *70*). Finally, the bulk density of each polymer was determined from literature values (*73*, *80–82*). Table 1 shows both the theoretical and experimental grafting density values for each of the polymer modified Gd MOF nanoparticle samples calculated from equations discussed in the literature (*43*). As can be seen in Table 1, the theoretical and experimental grafting densities for each of the polymers used for surface modification of the Gd MOF nanoparticles correlated quite well, with nearly all of the experimental calculations being within 25% of their theoretical grafting densities. For example, the PHPMA homopolymer with a molecular weight of 5,327 g/mol was employed to modify Gd MOF nanoparticles providing comparable theoretical and experimental polymer grafting densities of 0.1847 chains/nm^2 and 0.1379 chain/nm^2, respectively. In each case the grafting densities are relatively high for use of a ‘grafting to’ technique, as most of the samples have values around 0.1chains/nm^2, providing modification of the Gd MOF nanoparticles with each polymer in the ‘brush’ regime (*76*, *78*, *83*). However, though the values obtained are quite high, similar experimental grafting densities have been documented in the literature for the ‘grafting to’ technique (*75*, *84–86*). Despite the high grafting density values, a definite trend was seen, which showed a decrease in the grafting density with increased molecular weight of the grafted polymer (Table 1). For example, as the molecular weight of the PHPMA increased from 5,327 g/mol to 10,281 g/mol, the experimental grafting density decreased from 0.1379 chains/nm^2 to 0.0993 chains/nm^2. The experimental grafting density further decreased to 0.0638 chains/nm^2 with modification of the Gd MOF nanoparticles using the PHPMA homopolymer with an experimental molecular weight of 19,370 g/mol. This trend of decreasing grafting density with increasing polymer molecular weight has been discussed extensively in the literature with the ‘grafting to’ technique and is a result of limited diffusion of polymer chains to reactive sites on the nanoparticle surface due to increased steric hindrance of polymer chains that are already attached to the surface (*76*, *78*, *83*). As such, as the molecular weight of the chains increases it becomes more difficult for chains to diffuse to the surface providing lower polymer grafting densities.

The advantage of determining the grafting density of the multifunctional copolymer modified Gd MOF nanoparticles is the fact that it yields both the number of targeting and therapeutic agents on a per particle basis. For the PNIPAM-co-PNAOS-co-PFMA copolymer modified Gd MOF nanoparticles, the grafting density was determined to be approximately 0.97 chains/nm^2, which corresponds to approximately 25,000 polymer chains per Gd MOF nanoparticle. Using the previously determined concentration of MTX and GRGDS-NH_2 for the 25 wt% NAOS RAFT copolymer, this corresponds to approximately 37.5 x 10^4 molecules of MTX and 12.5 x 10^4 molecules of GRGDS-NH_2 per Gd MOF nanoparticle. Due to the narrow molecular weight distributions produced in RAFT polymerization, approximately the same concentration of therapeutic/targeting agents will be incorporated to each polymer chain, making each of the polymer modified Gd MOF nanoparticles very similar in composition. To the best of our knowledge, this is the first time Gd MOF nanoparticles have been successfully surfaced modified with well-defined, highly functional RAFT copolymers for the production of multifunctional nanodevices for image guided cancer intervention. The developed method has the added advantage that the copolymers can be well characterized through common spectroscopic and chromatographic techniques and modified with a wide variety of targeting ligands or therapeutics before surface functionalization. This provides tremendous flexibility in controlling the loading capacity of the molecular targeting agent and the chemotherapeutic, on a per particle basis, while allowing for a wide range of different therapeutic and target ligand combinations.

3.4.6. Hypothesized Surface Modification Mechanism

As discussed in the beginning of this section, we have hypothesized that attachment of the RAFT polymers to the surface of the Gd MOF nanoparticles is via coordination of the thiolate end group of the polymer with vacant orbitals on the Gd^{3+} ions at the surface of the nanoparticles (Figure 3). In an attempt to confirm this hypothesis, the attachment of the RAFT polymers to the surface of the Gd MOF nanoparticles was investigated without the addition of hexylamine. This involved conducting exactly the same procedure described above for attachment of PNIPAM prepared by RAFT polymerization, except no hexylamine was added to the system. TEM was employed to monitor modification of the Gd MOF nanoparticles and confirmed that the attachment of the trithiocarbonate end-functional PNIPAM RAFT homopolymer was unsuccessful as no polymer coating was visible in the microscopy images. ATR-FTIR spectroscopy also demonstrated that the modification of Gd MOF nanoparticles without the addition of a reducing agent was unsuccessful as there were nominal changes between the unmodified and modified Gd MOF nanoparticles. Without the addition of a nucleophile to form thiolate polymer end groups, Gd MOF nanoparticles were not successfully modified. This was attributed to the inability of the trithiocarbonate polymer end group to coordinate itself with the empty orbitals of the Gd^{3+} of the Gd-based nanoscale MOF. This confirmed that the thiolate end groups of the RAFT polymer, formed after aminolysis, were critical for attachment of the polymers and suggested that the thiolate end groups were coordinating to empty orbitals of the Gd^{3+} of the Gd NP surface, as hypothesized in Scheme 4 (*87*, *88*).

Next, a small molecule model, dodecanethiol, was employed to modify the surface of the Gd MOF nanoparticles under basic conditions in an attempt to provide further evidence that the thiolate moiety was indeed allowing attachment of the RAFT polymers to the surface of the Gd MOF nanoparticles. The surface modification technique was employed, as was used in the modification of the Gd MOF nanoparticles, with the difference of the addition of dodecanethiol instead of the RAFT polymer. The ATR-FTIR spectra for the modification of Gd MOF nanoparticles with dodecanthiolate showed an increase in intensity of the C-H stretching attributed to the $-CH_2$ and $-CH_3$ moieties. Due to the small size of the dodecanethiol molecule, TEM images did not show changes to the surface of the Gd MOF nanoparticles after modification. However, similar to the hydrophobic PSty modified Gd MOF nanoparticles, the dodecanthiolate modified Gd MOF nanoparticles showed a high degree of insolubility in water. This was attributed to the incorporation of a hydrophobic dodecyl group attached to the Gd MOF nanoparticles. These results confirmed the successful modification of the Gd MOF nanoparticles and substantiated the hypothesis that the thiolate of the dodecanethiol provided an attachment point to the Gd MOF nanoparticles through an analogous route, as described in Scheme 4, to the polymer modification.

3.4.7. Stability Studies of Unmodified and RAFT Polymer Modified Gd MOF Nanoparticles

The above results have demonstrated, by employing a wide range of well-defined polymers of different functionality, that the proposed novel surface modification technique for Gd MOF nanoparticles using RAFT polymers provides well defined polymer modified nanoparticles, along with the ability to tune both the polymer coating thickness. However, the stability of the polymer modified Gd MOF nanoparticles produced in this work is of critical importance, as recently there has been an increasing focus on nephrogenic fibrosing dermopathy (*89–91*). This disease affects a subset of patients with renal insufficiency and has been linked to exposure to Gd^{3+} released from conventional MRI contrast agents (*89–91*). Recently, literature has shown a simplified method of determining the concentration of free Gd^{3+} leached from the Gd MOF nanoparticles by employing a combination of dialysis and inductively coupled plasma-atomic emission spectroscopy (*29*, *48*). The unmodified and polymer modified Gd MOF nanoparticles were purified by dialysis using the literature procedure to provide information about their stability in terms of Gd^{3+} leached (*29*, *48*).

In an attempt to investigate the in vitro stability of the unmodified and polymer modified Gd MOF nanoparticles, the nanoparticles were then dialyzed against a range of different aqueous solutions, including: deionized ultra-filtered (DIUF) water, a phosphate buffered saline (PBS) solution, bovine serum, and human plasma for up to one week with the dialysate solution being analyzed at several time increments along the experiment. The results demonstrate that in each case a very small quantity of Gd^{3+} is released over a period of one week

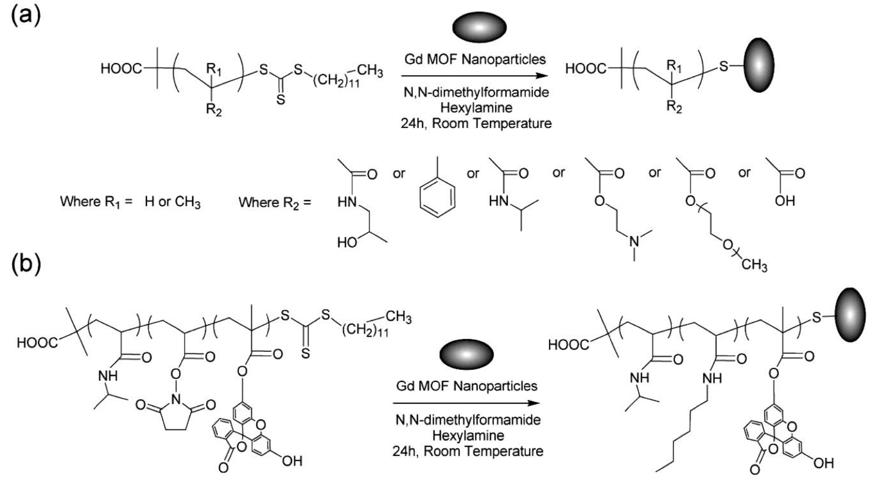
(a)
HOOC
R1
R2
S
S
(CH2)11
CH3
Gd MOF Nanoparticles
N,N-dimethylformamide
Hexylamine
24h, Room Temperature
Where R1 = H or CH3
Where R2 =
or
HN
HO
OH
O
N
CH3
(b)
NH
N
OH
Gd MOF Nanoparticles
N,N-dimethylformamide
Hexylamine
24h, Room Temperature

Scheme 3. Surface modification route for attachment of RAFT (a) homopolymers and (b) multifunctional copolymers to Gd MOF nanoparticles (43, 44).

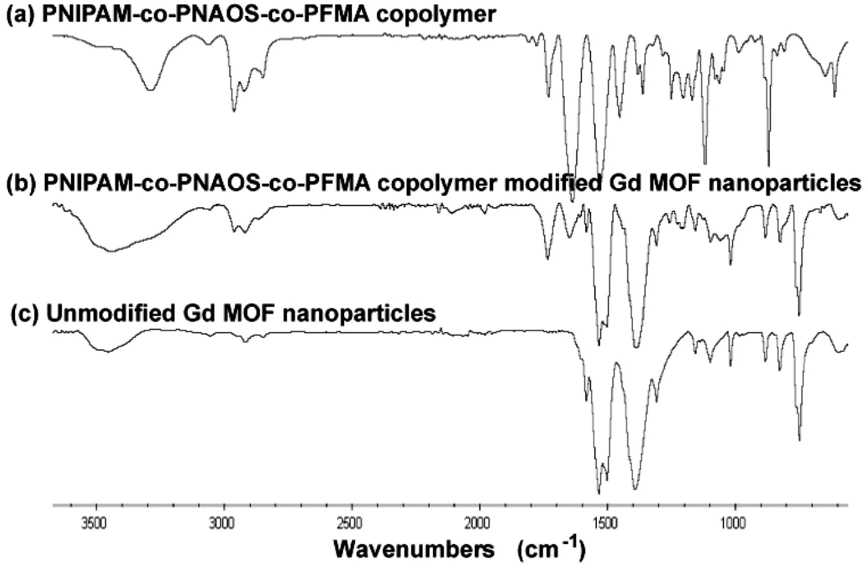

Figure 4. ATR-FTIR spectra of the (a) PNIPAM-co-PNAOS-co-PFMA, (b) PNIPAM-co-PNAOS-co-PFMA copolymer modified Gd MOF nanoparticles, and (c) unmodified Gd MOF nanoparticles (44).

and the vast majority of this release occurred very early in the experiment with no further release of Gd^{3+} seen after the 8 h dialysis period (Table 3). In all of the parallel experiments using the polymer modified Gd MOF nanoparticle, a trend of less Gd^{3+} leaching to the dialysate with polymer modification was seen, suggesting that the polymer modification process improves the stability of the Gd MOF nanoparticles (Table 3). These results demonstrate that the Gd MOF

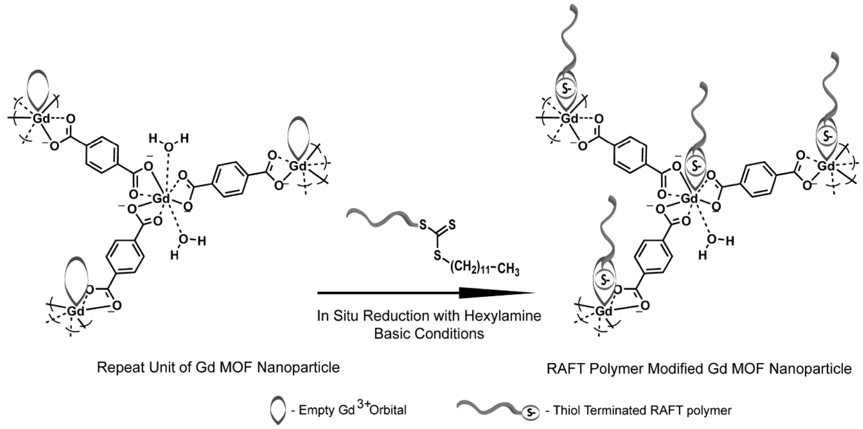
(CH2)11-CH3
In Situ Reduction with Hexylamine
Basic Conditions
Repeat Unit of Gd MOF Nanoparticle
RAFT Polymer Modified Gd MOF Nanoparticle
- Empty Gd3+ Orbital
- Thiol Terminated RAFT polymer

Scheme 4. Proposed 'grafting to' technique for coordination of thiolate polymer chain ends to Gd MOF nanoparticles synthesized by a reverse microemulsion system employing the 1,4-BDC (43).

nanoparticles demonstrate excellent stability over long periods of time and that the polymer modification of the nanoparticles improves the stability in all cases.

Though the results demonstrate the polymer modified Gd MOF nanoparticles show improved stability, with respect to loss of Gd^{3+}, it is also important to discuss the stability of the polymer coating itself. Experimental results have shown that RAFT polymer coating stability is quite robust. TEM and ATR-FTIR have confirmed the persistence of the RAFT polymer coatings on the Gd MOF nanoparticles after being stored in aqueous and organic medium over several months. Furthermore, solutions of polymer modified Gd MOF nanoparticles have been heated near physiological temperatures, 37 °C, for up to one month, which confirmed the continued integrity of the polymer surface modification. These results have further demonstrated that the polymers used to surface modify the Gd MOF nanoparticles demonstrate excellent stability over long periods of time and at physiological temperatures.

3.5. Diagnostic Imaging Properties

3.5.1. Clinical MRI Contrast Agent Properties

MRI has become one of the most important and widely used techniques in medical diagnostics. An MR image is generated from the nuclear magnetic resonance of water protons, with the observed contrast in MRI essentially dependent on factors such as water proton density and the T1 and the transverse relaxation time (T2) values of these protons. Typically contrast agents are used in MRI to aid in diagnostic imaging by increasing the contrast between the particular organ or tissue of interest and the surrounding tissues in the body. Historically Gd chelate compounds have been used as positive contrast agents as they produce a large shortening of T1-relaxation times and r_1, which has become one of the most effective mechanisms to brighten T1-weighted images (*23*, *50*). Relaxivity

Table 3. Concentration of Gd^{3+} Leached from Unmodified and Polymer Modified Gd MOF Nanoparticles During Dialysis (*44*)

Sample Type	Dialysis Solution	Gd^{3+} Leached to Dialysate (mmol/L)[a]			
		2h	4h	8h	1 week
Unmodified Gd MOF NPs	DIUF Water	0.0014	-	-	-
Polymer Modified Gd MOF NPs	DIUF Water	0.0003	-	-	-
Unmodified Gd MOF NPs	PBS	0.0081	0.0065	0.0022	-
Polymer Modified Gd MOF NPs	PBS	0.0023	0.0005	0.0001	-
Unmodified Gd MOF NPs	Serum	0.0013	0.0005	-	-
Polymer Modified Gd MOF NPs	Serum	0.0003	-	-	-
Unmodified Gd MOF NPs	Plasma	0.0023	0.0012	0.0008	-
Polymer Modified Gd MOF NPs	Plasma	0.0005	0.0003	0.0003	-

(a.) Determined by employing inductively coupled plasma-atomic emission spectroscopy.

values, r_1 and r_2, are defined as the inverse of the measured T1 and T2 relaxation values, respectively, in relation to the concentration of Gd^{3+} in the contrast agent. The ratio of r_2/r_1 is used to provide information about the contrast agent, where values between 1 and 2 provide brightening in T1-weighted images, and are employed as positive contrast agents (*23*). Although clinically employed MRI contrast agents, such as Magnevist® and Multihance®, are widely used, recent literature has shown that Gd^{3+} containing nanoscale MOFs could offer specific advantages as positive contrast agents for MRI due to their enhanced relaxivities and improved retention times (*11*, *20*, *21*, *23*, *26*, *29*, *47*, *48*). However, as discussed above, application of Gd nanoparticles has been limited due to the difficulty in producing nanoparticles which are biocompatible, stable, and have specific surface functionality. While researchers have attempted to use surface modification techniques to overcome these limitations, success has been very limited. The surface modification technique presented above potentially provides a method to overcome all of these limitations. To further validate this method and its potential clinical use, it is important to examine the effect of polymer modification and functionality on the MRI properties of these structures.

3.5.2. In Vitro Imaging Capabilities of Hydrophilic RAFT Homopolymer Modified Gd MOF Nanoparticles

In order to provide information about the clinical imaging viability of the polymer modified Gd MOF nanoparticles, as positive contrast nanoparticle agents, *in vitro* MRI was employed to determine relaxation properties of the unmodified and polymer modified Gd MOF nanoparticles. Table 4 compares the relaxivity values collected on a 1.5 T scanner for unmodified Gd MOF nanoparticles, each of the polymer modified Gd MOF nanoparticles, and the clinically employed contrasts agents, Magnevist® and Multihance®. The r_1 values demonstrate that both the unmodified and polymer modified Gd MOF nanoparticles, with the exception of the PSty modified Gd MOF nanoparticles, result in a large shortening of the T1 relaxation time and, thus, behave as positive contrast agents

(Table 4). Of particular note is the fact that the polymer modification of the Gd MOF nanoparticles with the PHPMA, PNIPAM, PDMAEA, PPEGMEA, and PAA RAFT homopolymers demonstrated significantly higher relaxivity values in comparison to both the unmodified Gd MOF nanoparticles and the clinically employed small molecule contrast agents (Table 4). This phenomenon is attributed to increased water retention by the hydrophilic RAFT homopolymer matrices attached to the surface of the Gd MOF nanoparticles. The increased water retention allows for more favorable interactions between the water protons and the free orbitals of the Gd^{3+} containing MOF nanoparticle, thus enhancing T1 relaxation shortening effects. For example, when the highly hydrophilic PHPMA homopolymer, with a molecular weight of 19,370 g/mol, was employed for the modification of the Gd MOF nanoparticles, r_1 and r_2 values of 105.36 $sec^{-1}mM^{-1}$ and 129.63 $sec^{-1}mM^{-1}$, respectively, were determined (Table 4). These values are over 10 times higher than the observed relaxivities of the unmodified Gd MOF nanoparticles and six times higher than the values for the clinically employed Magnevist® and Multihance® (Table 4). Furthermore, in each case the polymer modification of the Gd MOF nanoparticles provided a much lower r_2/r_1 value in comparison to both the unmodified Gd MOF nanoparticles and the clinically employed contrast agents (Table 4), which is advantageous for their use as clinical positive contrast agents. The other hydrophilic polymers, PNIPAM, PDMAEA, PPEGMEA, and PAA, showed similar drastically improved T1 shortening effects and lower r_2/r_1 values in comparison to both the unmodified Gd MOF nanoparticles and the clinical contrast agents (Table 4).

3.5.3. In Vitro Imaging Capabilities of Hydrophobic RAFT Homopolymer Modified Gd MOF Nanoparticles

Next, in order to further establish the effect of chemical structure of the polymer on the relaxivity of the surface modified Gd MOF nanoparticles, the Gd MOF nanoparticles were surface modified with a highly hydrophobic polymer, PSty. The PSty modified Gd MOF nanoparticles showed very low r_1 values and very large r_2 values, which provided relaxivity ratio values more than an order of magnitude higher than the other polymer modified samples (Table 4). For instance, in comparison to the PHPMA homopolymer (19,370 g/mol) modified Gd MOF nanoparticles, which showed an r_2/r_1 value of 1.23, the PSty samples with a comparable molecular weight of 15,245 g/mol yielded an r_2/r_1 value of 31.56 (Table 4). This was attributed to decreased water retention due to the hydrophobic nature of the PSty surface modified Gd MOF nanoparticles, which minimizes interactions between the Gd^{3+} and water molecules and thus lengthens the T1 relaxation times in comparison to the other systems. In each case, the PSty modification provided a small longitudinal relaxivity value, this is most likely due to water that is coordinated Gd^{3+} ions within the interior of the Gd MOF nanoparticle, which is suggested by the nanoparticles repeat structure of $Gd(1,4\text{-}BDC)_{1.5}(H_2O)_2$. The much smaller r_1 and enhanced T2 relaxation properties of the PSty modified Gd MOF nanoparticles make these especially poor scaffolds for positive contrast nanoparticle agents. These experiments

Table 4. Experimental relaxivity data for clinical MRI contrast agents, Multihance® and Magnevist® along with the unmodified and polymer modified Gd MOF nanoparticles (*43*, *44*)

Contrast Agent	r_1 (sec^{-1}mM^{-1})^a	r_2 (sec^{-1}mM^{-1})^a	r_2/r_1
Magnevist ®	13.44	21.40	1.59
Multihance ®	19.45	30.44	1.57
Gd MOF Nanoparticles	9.86	17.94	1.82
PNIPAM (5,700 g/mol) Modified Gd MOF Nanoparticles	20.27	29.73	1.47
PNIPAM (8,600 g/mol) Modified Gd MOF Nanoparticles	46.99	64.10	1.36
PNIPAM (17,800 g/mol) Modified Gd MOF Nanoparticles	62.51	79.90	1.28
PHPMA (5,300 g/mol) Modified Gd MOF Nanoparticles	17.81	25.77	1.45
PHPMA (10,200 g/mol) Modified Gd MOF Nanoparticles	32.94	44.85	1.36
PHPMA (19,400 g/mol) Modified Gd MOF Nanoparticles	105.36	129.63	1.23
PDMAEA (15,100 g/mol) Modified Gd MOF Nanoparticles	37.20	54.17	1.46
PPEGMEA (19,600 g/mol) Modified Gd MOF Nanoparticles	59.93	81.55	1.36
PAA (10,900 g/mol) Modified Gd MOF Nanoparticles	21.30	31.82	1.49
PSty (4,800 g/mol) Modified Gd MOF Nanoparticles	1.17	14.16	12.10
PSty (9,000 g/mol) Modified Gd MOF Nanoparticles	1.20	25.75	21.46
PSty (15,300 g/mol) Modified Gd MOF Nanoparticles	3.91	123.40	31.56
PNIPAM-*co*-PNAOS-*co*-PFMA Modified Gd MOF Nanoparticles	33.43	47.25	1.41
MTX-Copolymer Modified Gd MOF Nanoparticles	38.52	53.92	1.40
GRGDS-NH_2+MTX-Copolymer Modified Gd MOF Nanoparticles	14.45	25.29	1.75

(a.) Longitudinal relaxivity (r_1) and transverse relaxivity (r_2) values, calculated as the reciprocal values of the longitudinal relaxation time (T1) and transverse relaxation time (T2), respectively, of each of the contrast agents were determined with a 1.5T scanner with samples diluted in deionized ultra-filtered water by acquiring signal intensity (I) measurements via region-of-interest analysis of the samples for all pulse sequences with T1 and T2 values being calculated using: $I_i=I_{o,I}\ (1\text{-}\exp^{(-t/T_i)})$.

confirm that the hydrophilic/hydrophobic nature of the polymer employed for the modification of the Gd MOF nanoparticles is extremely important to the MRI capabilities of the constructs.

3.5.4. Polymer Molecular Weight Effects on in Vitro MRI Capabilities

In order to determine the effect of molecular weight of the polymer on the relaxation properties of the polymer modified Gd MOF nanoparticle, three different molecular weights of PHPMA, PNIPAM, and PSty were used to surface modify the nanoparticle constructs. As can be seen in Table 4, both PNIPAM and PHPMA modified Gd MOF nanoparticles showed a trend of enhanced r_1 values and r_2/r_1 values with a respective increase in number average molecular weight of the polymer. For instance, as the PNIPAM molecular weight was increased from 5,700 g/mol to 8,600 g/mol the longitudinal relaxivity increased from 20.27 sec^{-1}mM^{-1} to 46.99 sec^{-1}mM^{-1}, with a decreased r_2/r_1 value of 1.36 from 1.47 (Table 4). Furthermore, as the molecular weight of the PNIPAM was increased to 17,800 g/mol the longitudinal relaxivity value increased to 62.51 sec^{-1}mM^{-1}, while the r_2/r_1 value decreased to 1.28, which is substantially improved in comparison to the clinical employed contrast agents and unmodified Gd MOF nanoparticles (Table 4). Increases in the molecular weight of the PHPMA used for modification of the Gd MOF nanoparticles showed similar enhanced r_1 values

(Table 4). As discussed above, the enhanced T1 relaxation characteristics are expected to be due to the increase in the thickness of the hydrophilic RAFT homopolymer layer on the Gd MOF nanoparticles resulting in increased water retention around the surface of the nanoparticles. This was further confirmed by the stark differences in the relaxivity values determined for the PSty modified Gd MOF nanoparticles. As can be seen in Table 2, an increase in the molecular weight of the PSty, from 4,800g/mol to 15,300 g/mol, resulted in a limited change in the r_1 values, but a large increase in the r_2 values from 14.16 $sec^{-1}mM^{-1}$ to 123.40 $sec^{-1}mM^{-1}$, which is nearly ten times higher than that of the unmodified Gd MOF nanoparticles, Magnevist®, and Multihance®. This apparent decrease in the r_1 values was attributed to the substantial hydrophobic coating of PSty, which prevents interactions of water with vacant orbitals on the Gd^{3+}. This phenomenon is similar to what is seen with other T2-weighted contrast agents, such as SPIOs, which is caused by susceptibility differences of the surroundings of the contrast agent and a strongly varying local magnetic field (*50*, *68*, *69*, *92*). The enhanced T2 relaxation causes a darkening in the MRI contrast media-containing structures, which restricts the use of the PSty modified Gd MOF nanoparticles as positive nanoparticle contrast agents. Therefore, we have demonstrated a straightforward surface modification method which has been shown to tailor the relaxivity properties of our polymer modified Gd MOF nanoparticles by not only modifying the chemical properties of their surface by the attachment of various polymers, but also tuning the relaxivity properties of the nanoparticles by varying the molecular weight of the polymer chains used for surface modification.

3.5.5. *In Vitro Imaging Capabilities of Multifunctional RAFT Copolymer Modified Gd MOF Nanoparticles*

One of the primary requirements of any nanoscale theragnostic device is the ability to image the construct using standard clinical techniques. The PNIPAM-co-PNAOS-co-PFMA copolymer modified Gd MOF nanoparticles prepared in this work provides the specific advantage of multimodal imaging capability. The incorporation of the FMA monomer into the RAFT copolymer allows for cellular level imaging *via* fluorescence microscopy, while the Gd MOF nanoparticle acts as a positive contrast agent for MRI, providing diagnostic imaging at the clinical level. The combination of fluorescence imaging and MRI has received a great deal of attention because they ally the sensitivity of the fluorescence component with the high degree of spatial resolution of MRI (*20*, *48*, *93*). The clinical imaging viability of the copolymer modified Gd MOF nanoparticles as a positive contrast agent was determined through *in vitro* MR imaging. The relaxivity properties of the nanoparticle scaffolds are shown in Table 4. The relaxivity values demonstrate that both the unmodified and the PNIPAM-co-PNAOS-co-PFMA copolymer modified Gd MOF nanoparticles result in a large decrease in the r_1 values and, thus, behave as positive contrast agents. Of particular note is the fact that the copolymer modified Gd MOF nanoparticles increased the longitudinal relaxivity more than triple , r_1 = 33.4 $sec^{-1}mM^{-1}$, that of the values determined for both the unmodified Gd MOF nanoparticles (r_1 = 9.86 $sec^{-1}mM^{-1}$) and clinical contrast agents, Magnevist® and Multihance®, r_1 = 13.44$sec^{-1}mM^{-1}$ and r_1 = 19.45 $sec^{-1}mM^{-1}$, respectively. As discussed before, this phenomenon is attributed to increased water retention by the hydrophilic RAFT copolymer matrix attached to the surface of the Gd MOF nanoparticles, thus enhancing T1 relaxation shortening effects. This data demonstrates the feasibility of achieving clinically useful T1 shortening effects with these novel, multifunctional polymer modified Gd MOF nanoparticles.

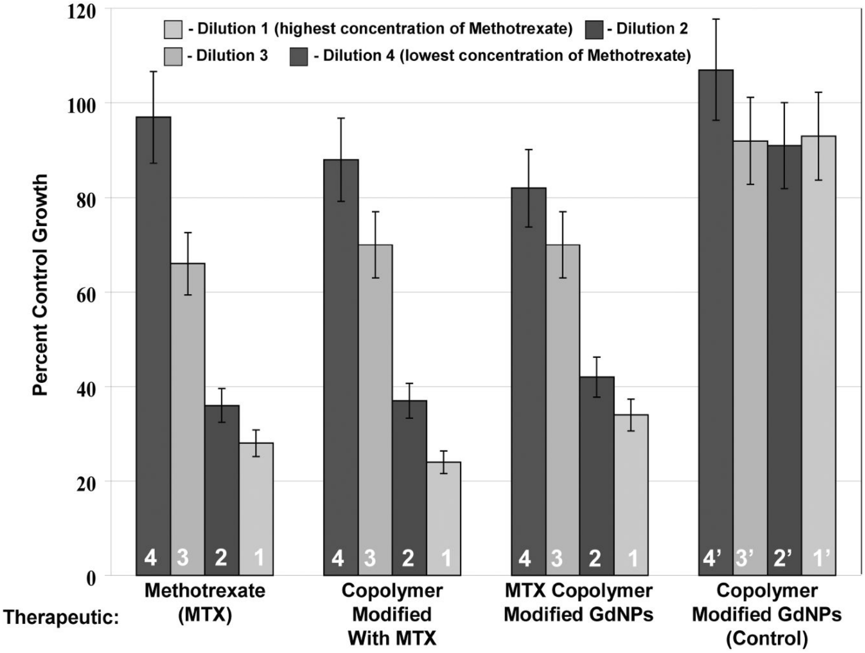

Figure 5. Cell growth inhibition studies for reagents involved in multifunctional nanoparticle formation, including: MTX, PNIPAM-co-PNAOS-co-PFMA tailored with MTX, Gd MOF nanoparticles modified with PNIPAM-co-PNAOS-co-PFMA tailored with MTX. Finally, the control, Gd MOF nanoparticles modified with PNIPAM-co-PNAOS-co-PFMA, without the MTX therapeutic, is shown for comparison. Ten fold dilutions of each sample were carried out with Dilution 1 having the highest concentration of the therapeutic, MTX, and Dilution 4 having the lowest concentration of MTX. The concentration of MTX for each dilution of each therapeutic sample is as follows: Dilution 1 = 1.15mM, Dilution 2 = 0.115mM, Dilution 3 = 0.0115mM, and Dilution 4 = 0.00115M. There is no MTX in Dilutions 1', 2', 3', and 4' (44).

3.6. Molecular Targeting of Multifunctional Copolymer Modified Gd MOF Nanoparticles

In addition to an imaging component, one of the other essential requirements of a successful theragnostic nanodevice is the presence of a molecular targeting component or ligand to increase the targeted selectivity of the system and, in the case of nanoparticles, to take advantage of the large amount of imaging agent that can be delivered to the desired location per targeting biorecognition event, thus reducing the amount of Gd^{3+} required for effective MR imaging (*7*). The synthesized multifunctional copolymer modified Gd MOF nanoparticles have been designed to incorporate dual targeting components. The first targeting component is incorporated by tailoring the PNIPAM-co-PNAOS-co-PFMA copolymer with an active targeting ligand, GRGDS-NH_2. As discussed earlier, GRGDS-NH_2 has been widely used as a molecular targeting agent, as it can specifically bind to over-expressed $\alpha_v\beta_3$ integrins on tumor cells and induce receptor-mediated endocytosis for cellular uptake (*66*). The second potential route of targeting is passive targeting through the enhanced permeability and retention (EPR) effect. This tumor targeting mechanism results from the increased vasculature present in most tumors resulting in preferential extravasation and protracted lodging of particulates of a particular size (*94*). The EPR effect can be taken advantage of due to the controllable size of the Gd MOF nanoparticles used to produce the polymer-modified constructs.

To investigate the ability of the polymer modified Gd MOF nanoparticles to be selectively targeted to cancer cells using the active GRGDS-NH_2 ligand, fluorescence microscopy was used. As mentioned previously, the incorporation of the FMA monomer into the RAFT copolymer provides a means of cellular level fluorescence imaging. To evaluate the ability to selectively target the polymer modified Gd MOF nanoparticles, FITZ-HSA, an $\alpha_v\beta_3$-expressing canine endothelial sarcoma cell line, was incubated with copolymer modified Gd MOF nanoparticles, where the polymer had either been tailored with the GRGDS-NH_2 ligand or contained no GRGDS-NH_2, for 1, 4, or 24 h followed by extensive washing, fixation, and fluorescence microscopy. In the case where the polymer attached to the Gd MOF nanoparticles had been tailored with GRGDS-NH_2 significant cellular surface binding can be visualized after 1h of incubation. This is evidenced by a fluorescent halo forming around the surface of the FITZ-HSA cells after washing of the cells before fluorescence microscopy. After 4h of incubation, the formation of the fluorescent halo becomes even more pronounced. Furthermore, fluorescence microscopy images show internalization of the GRGDS-NH_2 tailored copolymer modified Gd MOF nanoparticles by the cells after an incubation period of 24 h. This was suggested by staining of the nuclei of FITZ-HSA cells with propidium iodide (PI) allowing for visualization of spatial location of the cells. Furthermore, cells stained with the PI showed the same spatial location as the accumulated fluorescent-tagged nanoparticles, confirming selective uptake of the targeted polymer modified Gd MOF nanoparticles by the tumor cells. To demonstrate the importance of the active molecular targeting agent to promote cellular uptake, a control system was analyzed, where the Gd MOF nanoparticles were modified with the PNIPAM-co-PNAOS-co-PFMA copolymer that had not been tailored with GRGDS-NH_2. No significant amount of fluorescence was seen in FITZ-HSA cells that were incubated with Gd MOF nanoparticles that did not contain the GRGDS-NH_2 at 1, 4, or 24 h. This was expected as extensive washing of the cells before fluorescence microscopy should remove all polymer modified Gd MOF nanoparticles and the non-targeted nature of the nanoparticles should provide no attachment mechanism to the cancer cells by means of active targeting. It should be noted that after 24 h, the nuclei of the FITZ-HSA cells that were stained with PI were still present when viewed with the Texas Red filter. These results confirm preferential uptake of the targeted polymer modified Gd MOF nanoparticles was due to active targeting of the $\alpha_v\beta_3$-integrins by the GRGDS-NH_2 ligand. To further confirm specificity of targeting, FITZ-HSA cells were pretreated with free GRGDS-NH_2 peptide, in order to block the $\alpha_v\beta_3$-integrins, before introduction of the targeted polymer modified Gd MOF nanoparticles. The GRGDS-NH_2 targeted polymer modified Gd MOF nanoparticles were then introduced and fluorescent microscopy demonstrated that there was no specific binding for the nanoparticles further exhibiting the targeting specificity of our nanoparticle constructs. These results demonstrate that an active targeting functionality can be added to these Gd MOF nanoparticles, while maintaining the properties required for clinical diagnostic imaging. In addition, these constructs demonstrated fluorescence capability, which makes the constructs bimodal in regards to imaging, unlike other clinical imaging agents, such as Multihance® or Magnevist®.

3.7. Cell Growth Inhibition of Polymer Modified Gd MOF Nanoparticles

To demonstrate that the multifunctional copolymer modified Gd MOF nanoparticle based platforms contain all the basic requirements of a theragnostic nanodevice, growth inhibition studies were performed using FITZ-HSA tumor cells. Samples were incubated with FITZ-HSA at 37 °C in standard culture medium containing 10% PBS for 72 h in a 5% CO_2 atmosphere. The reagents for nanodevice formation, i.e. gadolinium (III) chloride salt, 1,4-BDC, unmodified Gd MOF nanoparticles, and Gd MOF nanoparticles modified with RAFT copolymers were studied. The gadolinium (III) chloride salt, 1,4-BDC, and the unmodified Gd MOF nanoparticles resulted in significant cell growth inhibition at high concentrations. However, it is important to note that modification of the Gd MOF nanoparticles with the RAFT copolymer, with no MTX, did not reduce cell viability at high concentrations. The increased cell viability is attributed to the coating of the Gd MOF nanoparticles with copolymers consisting of the biocompatible polymer PNIPAM. This infers that the presence of the RAFT copolymer on the surface of the Gd MOF nanoparticles increases the biocompatible nature of the nanodevice. To demonstrate the ability of polymer modified nanoparticles to act as chemotherapeutics, Gd MOF nanoparticles were modified with RAFT copolymers containing MTX and both MTX and GRGDS-NH_2, after which cell growth inhibition studies were performed (Figure 5). As a control, both MTX and the RAFT copolymer modified with MTX, unattached to the nanoparticles, were also used in cell growth inhibition studies (Figure 5). As stated previously, MTX is a widely used chemotherapy agent which has been employed in many drug delivery systems because of its ability to inhibit the folate synthesis metabolic pathway (*67*). Figure 5 demonstrates that the MTX-containing polymer modified Gd MOF nanoparticles show a dose dependent inhibition of growth of the FITZ-HSA tumor cells that was comparable to that of the free MTX drug, on an equal concentration of MTX basis. These results demonstrate that attachment of the MTX drug to the copolymer and subsequent modification of Gd MOF nanoparticles with the MTX copolymer does not affect the overall function of the drug. Addition of the MTX to the theragnostic construct provides similar performance to the free therapeutic, but with the added benefit that the device has targeting ability and bimodal imaging through fluorescence and MR.

4. Conclusions

The development of nanoscale theragnostic devices for the diagnosis and treatment of cancer represents one of the primary targets of the general field of nanomedicine. Despite the fact that the incredible potential of these devices is widely recognized, their clinical application is yet to be realized due to poor design and manufacturing techniques. This research has developed a method for the surface modification of Gd MOF nanoparticles with well defined, highly functional RAFT polymers and demonstrated their applicability towards use as positive contrast nanoparticle agents in MRI. Specifically, a range of RAFT homopolymers, PNIPAM, PHPMA, PSty, PDMAEA, PPEGMEA, and PAA, and novel multifunctional copolymers of PNIPAM-co-PNAOS-co-PFMA were synthesized by employing the RAFT agent, DATC. PNIPAM-*co*-PNAOS-*co*-PFMA copolymers were successfully tailored with both a chemotherapeutic, MTX, and with a targeting ligand, GRGDS-NH_2, to form the multifunctional polymeric structure. Following preparation of the RAFT polymers, quantitative aminolysis of the trithiocarbonate end groups in basic conditions provided thiolate end groups which allowed for the direct attachment of the polymers to the surface of the Gd nanoparticle MOFs. Successful modification was attributed to thiolate attachment through vacant orbitals on the Gd^{3+} ions at the surface of the Gd MOF nanoparticles and long term stability in a range of aqueous medium was confirmed. To evaluate the potential of the RAFT polymer modified nanoparticles as a theragnostic nanodevice, MRI, fluorescence imaging, and cell growth inhibition studies were performed. This research demonstrated the molecular weight and chemical properties of polymers used to modify Gd MOF nanoparticles are intimately connected with their T1 relaxation rates and variation in these properties provides a means to tune the relaxivity of the nanoparticles. In the MRI studies, the unmodified Gd MOF nanoparticles showed a r_1 value comparable to the clinically employed contrast agents, Magnevist® and Multihance®, while the majority of the RAFT polymer modified Gd MOF nanoparticles displayed significantly enhanced r_1 values in comparison to those of conventional clinically used Gd contrast agents. Furthermore, tailoring the chemical and physical properties of the RAFT polymers used for the surface modification of Gd MOF nanoparticles has shown the ability to tailor and tune the

r_1 values thus providing greatly enhanced T1 relaxation values in comparison to the unmodified structure and clinically used small molecule contrast agents. The incorporation of FMA into the multifunctional copolymer constructs provided polymer modified Gd MOF nanoparticles that were successfully used as a bimodal diagnostic imaging device for both MR and fluorescence imaging. Additionally, the use of fluorescence imaging demonstrated that the RAFT copolymer modified Gd MOF nanoparticles containing the targeting moiety, GRGDS-NH_2, showed active targeting towards FITZ-HSA tumor cells which over express $\alpha_v\beta_3$-integrins. Gd MOF nanoparticles modified with the RAFT copolymer containing MTX showed dose-dependent treatment of FITZ-HSA cancer cells established by cell viability measurements. By taking advantage of advancements in nanotechnology and polymer science, this research has effectively prepared new nano-scale multifunctional devices with tumor targeting, treatment, and diagnostic imaging capability. The combination of these technologies has the potential to advance the therapeutic outcome of drug treatment for cancer sufferers and improve the quality of life for patients.

References

1. Ferrari, M. Cancer nanotechnology: Opportunities and challenges. *Nat. Rev. Cancer* **2005**, *5*, 162–171.
2. Panchapakesan, B. Nanotechnology: Part 2 - Tiny Technology - Tremendous Therapeutic Potential. *Oncology Issues* **2005** (November/December), 20–23.
3. Park, K. Nanotechnology: What it can do for drug delivery. *J. Controlled Release* **2007**, *120*, 1–3.
4. Service, R. F. Nanotechnology takes aim at cancer. *Science* **2005**, *310*, 1132–1134.
5. Wickline, S. A.; Lanza, G. M. Nanotechnology for Molecular Imaging and Targeted Therapy. *Circulation* **2003**, *107*, 1092–1095.
6. Nasongkla, N.; Bey, E.; Ren, J.; Ai, H.; Khemtong, C.; Guthi, J. S.; Chin, S.-F.; Sherry, A. D.; Boothman, D. A.; Gao, J. Multifunctional polymeric micelles as cancer-targeted, MRI-ultrasensitive drug delivery systems. *Nano Lett.* **2006**, *6*, 2427–2430.
7. Allen, T. M. Ligand-Targeted Therapeutics in Anticancer Therapy. *Nat. Rev. Drug Discovery* **2002**, *2*, 750–763.
8. Jain, R. K. The Next Frontier of Molecular Medicine: Delivery of Therapeutics. *Nat. Med.* **1998**, *4*, 655–657.
9. Gaumet, M.; Vargas, A.; Gurny, R.; Delie, F. Nanoparticles for drug delivery: The need for precision in reporting particle size parameters. *Eur. J. Pharm. Biopharm.* **2008**, *69* (1), 1–9.
10. Huang, X.; El-Sayed, I. H.; Qian, W.; El-Sayed, M. A. Cancer cell imaging and photothermal therapy in the near-infrared region by using gold nanorods. *J. Am. Chem. Soc.* **2006**, *128*, 2115–2120.
11. Rieter, W. J.; Taylor, K. M. L.; An, H.; Lin, W.; Lin, W. Nanoscale metal-organic frameworks as potential multimodal contrast enhancing agents. *J. Am. Chem. Soc.* **2006**, *128*, 9024–9025.

12. Rieter, W. J.; Taylor, K. M. L.; Lin, W. Surface Modification and Functionalization of Nanoscale Metal-Organic Frameworks for Controlled Release and Luminescence Sensing. *J. Am. Chem. Soc.* **2007**, *129*, 9852–9853.
13. Taboada, E.; Rodriquez, E.; Roig, A.; Oro, J.; Roch, A.; Muller, R. N. Relaxometric and Magnetic Characterization of Ultrasmall Iron Oxide nanoparticles with High Magnetization. Evaluation as Potential T1 Magnetic Resonance Imaging Contrast Agents for Molecular Imaging. *Langmuir* **2007**, *23*, 4583–4588.
14. Oyewumi, M. O.; Mumper, R. J. Gadolinium-Loaded Nanoparticles Engineered from Microemulsion Templates. *Drug Dev. Ind. Pharm.* **2002**, *28*, 317–328.
15. Oyewumi, M. O.; Mumper, R. J. Engineering Tumor-Targeted Gadolinium Hexanedione Nanoparticles for Potential Applications in neutron Capture Therapy. *Bioconjugate Chem.* **2002**, *13*, 1328–1335.
16. Oyewumi, M. O.; Liu, S.; Moscow, J. A.; Mumper, R. J. Specific Association of Thuamine-Coated Gadolinium Nanoparticles with Human Breast Cancer Cells Expressing Thiamine Transporters. *Bioconjugate Chem.* **2004**, *14*, 404–411.
17. Oyewumi, M. O.; Yokel, R. A.; Jay, M.; Coakley, T.; Mumper, R. J. Comparison of Cell Uptake, Biodistribition and Tumor Retention of Folate-Coated and PEG-Coated Gadolinium Nanoparticles in Tumor Bearing Mice. *J. Controlled Release* **2004**, *95*, 613–626.
18. Oyewumi, M. O.; Mumper, R. J. Influence of Formulation Parameters on Gadolinium Entrapment and Tumor Cell Uptake Using Folate-Coated Nanoparticles. *Int. J. Pharm.* **2003**, *251*, 85–97.
19. Oyewumi, M. O.; Yokel, R. A.; Jay, M.; Coakley, T.; Mumper, R. J. Comparison of Cell Uptake, Biodistribution and Tumor Retention of Folate-Coated and PEG-Coated Gadolinium Nanoparticles in Tumor-Bearing Mice. *J. Controlled Release* **2004**, *95*, 613–626.
20. Bridot, J.-L.; Faure, A.-C.; Laurent, S.; Riviere, C.; Billotey, C.; Hiba, B.; Jainer, M.; Josserand, V.; Coll, J.-L.; Vander Elst, L.; Muller, R.; Roux, S.; Perriat, P.; Tillement, O. Hybrid gadolinium oxide nanoparticles: Multimodal contrast agents for in vivo imaging. *J. Am. Chem. Soc.* **2007**, *129*, 5076–5084.
21. Evanics, F.; Diamente, P. R.; van Veggel, F. C. J. M.; Stanisz, G. J.; Prosser, R. S. Water-Soluble GdF3 and GdF3/LaF3 Nanoparticles-Physical Characterization and NMR Relaxation Properties. *Chem. Mater.* **2006**, *18*, 2499–2505.
22. Rosi, N. L.; Mirkin, C. A. Nanostructures in Biodiagnostics. *Chem. Rev.* **2005**, *105*, 1547–1562.
23. Hifumi, H.; Yamaoka, S.; Tanimoto, A.; Citterio, D.; Suzuki, K. Gadolinium-based hybrid nanoparticles as a positive MR contrast agent. *J. Am. Chem. Soc.* **2006**, *128*, 15090–15091.
24. Artemov, D.; Bhujwalla, Z. M.; Bulte, J. W. M. Magnetic Resonance Imaging of Cell Surface Receptors Using Targeted Contrast Agents. *Curr. Pharm. Biotechnol.* **2004**, *5*, 485–494.

25. Rinck, P. A.; Bjørnerud, A. *Magnetic resonance in medicine*; European Magnetic Resonance Forum; Wiley-Blackwell, 2001.
26. Reynolds, C. H.; Annan, N.; Beshah, K.; Huber, J. H.; Shaber, S. H.; Lenkinski, R. E.; Wortman, J. A. Gadolinium-Loaded Nanoparticles: New Contrast Agents for Magnetic Resonance Imaging. *J. Am. Chem. Soc.* **2000**, *122*, 8940–8945.
27. Oyewumi, M. O.; Liu, S.; Moscow, J. A.; Mumper, R. J. Specific Association of Thiamine-Coated Gadolinium Nanoparticles with Human Breast Cancer Cells Expressing Thiamine Transporters. *Bioconjugate Chem.* **2003**, *14*, 404–411.
28. James, S. Metal-organic Frameworks. *Chem. Soc. Rev.* **2003**, *32*, 276–288.
29. Taylor, K. M. L.; Kim, J. S.; Rieter, W. J.; An, H.; Lin, W.; Lin, W. Mesoporous Silica Nanospheres as Highly Efficient MRI Contrast Agents. *J. Am. Chem. Soc.* **2008**, *130*, 2154–2155.
30. Perrier, S.; Takolpuckdee, P. Macromolecular design via reversible addition-fragmentation chain transfer (RAFT)/xanthates (MADIX) polymerization. *J. Polym. Sci., Part A: Polym. Chem.* **2005**, *43*, 5347–5393.
31. Le, T. P., Moad, G., Rizzardo, E., Thang, S. H. SH PCT Int. Appl. WO 98 01478 A1 980115, 1998.
32. Yanjarappa, M. J.; Gujraty, K. V.; Joshi, A.; Saraph, A.; Kane, R. S. Synthesis of copolymers containing an active ester of methacrylic acid by RAFT: Controlled moelcular weight scaffolds for biofunctionalization. *Biomacromolecules* **2006**, *7*, 1665–1670.
33. Hong, C.-Y.; Pan, C.-Y. Direct Synthesis of Biotinylated Stimuli-Responsive Polymer and Diblock Copolymer by RAFT Polymerization Using Biotinylated Trithiocarbonate as RAFT Agent. *Macromolecules* **2006**, *39*, 3517–3524.
34. Nguyen, T. L.; Tey, S. Y.; Pourgholami, M. H.; Morris, D. L.; Davis, T. P.; Barner-Kowollik, C.; Stenzel, M. H. Synthesis of semi-biodegradable crosslinked microspheres for the delivery of 1,25-dihydroxyvitamin D3 for the treatment of hepatocellular carcinoma. *Eur. Polym. J.* **2007**, *43*, 1754–1767.
35. Scales, C. W.; Huang, F.; Li, N.; Vasilieva, Y. A.; Ray, J.; Convertine, A. J.; McCormick, C. L. Corona-Stabilized Interpolyelectrolyte Complexes of SiRNA with Nonimmunogenic, Hydrophilic/Cationic Block Copolymers Prepared by Aqueous RAFT Polymerization. *Macromolecules* **2006**, *39*, 6871–6881.
36. Zelikin, A. N.; Such, G. K.; Postma, A.; Caruso, F. Poly(vinylpyrrolidone) for Bioconjugation and Surface Ligand Immobilization. *Biomacromolecules* **2007**, *8*, 2950–2953.
37. Li, M.; De, P.; Gondi, S. R.; Sumerlin, B. S. Responsive Polymer-Protein Bioconjugates Prepared by RAFT Polymerization and Copper-Catalyzed Azide-Alkyne Click Chemistry. *Macromol. Rapid Commun.* **2008**, *29*, 1172–1176.
38. De, P.; Li, M.; Gondi, S. R.; Sumerlin, B. S. Temperature-Regulated Activity of Responsive Polymer−Protein Conjugates Prepared by Grafting-from via RAFT Polymerization. *J. Am. Chem. Soc.* **2008**, *130*, 11288–11289.

39. Sumerlin, B. S.; Lowe, A. B.; Stroud, P. A.; Zhang, P.; Urban, M. W.; McCormick, C. L. Modification of gold surfaces with water-soluble (co)polymers prepared via aqueous reversible addition-fragmentation chain transfer polymerization. *Langmuir* **2003**, *19*, 5559–5562.
40. Hotchkiss, J. W.; Lowe, A. B.; Boyes, S. G. Surface modification of gold nanorods with polymers synthesized by reversible addition-fragmentation chain transfer polymerization. *Chem. Mater.* **2007**, *19*, 6–13.
41. Zhang, Q.; Gupta, S.; Emrick, T.; Russell, T. P. Surface-Functionalized CdSe Nanorods for Assembly in Diblock Copolymer Templates. *J. Am. Chem. Soc.* **2006**, *128*, 3898–3899.
42. Lowe, A. B.; Sumerlin, B. S.; Donovan, M. S.; McCormick, C. L. Facile preparation of transition metal nanoparticles stabilized by well-defined (co)polymers synthesized via aqueous reversible addition-fragmentation chain transfer polymerization. *J. Am. Chem. Soc.* **2002**, *124*, 11562–11563.
43. Rowe, M. D.; Chang, C.-C.; Thamm, D. H.; Kraft, S. L.; Harmon, J. F., Jr.; Vogt, A. P.; Sumerlin, B. S.; Boyes, S. G. Tuning the Magnetic Resonance Imaging Properties of Positive Contrast Agent Nanoparticles by Surface Modification with RAFT Polymers. *Langmuir* **2009**.
44. Rowe, M. D.; Thamm, D. H.; Kraft, S. L.; Boyes, S. G. Polymer-Modified Gadolinium Metal-Organic Framework Nanoparticles Used as Multifunctional Nanomedicines for the Targeted Imaging and Treatment of Cancer. *Biomacromolecules* **2009**, *10* (4), 983–993.
45. Lai, J. T.; Filla, D.; Shea, R. Functional polymers from novel carboxyl-terminated trithiocarbonates as highly efficient RAFT agents. *Macromolecules* **2002**, *35*, 6754–6756.
46. Kopecek, J.; Bazilova, H. Poly[N-(2-Hydroxypropyl)methacrylamide]. 1. Radical Polymerization and Copolymerization. *Eur. Polym. J.* **1973**, *9*, 7–14.
47. Hartman, K. B.; Laus, S.; Bolskar, R. D.; Muthupillai, R.; Helm, L.; Toth, E.; Merbach, A. E.; Wilson, L. J. Gadonanotubes as Ultrasensitive pH-Smart Probes for Magnetic Resonance Imaging. *Nano Lett.* **2008**, *8*, 415–419.
48. Kim, J. S.; Rieter, W. J.; Taylor, K. M. L.; An, H.; Lin, W.; Lin, W. Self-Assembled Hybrid Nanoparticles for Cancer-Specific Multimodal Imaging. *J. Am. Chem. Soc.* **2007**, *129*, 8962–8963.
49. Allen, M.; Bulte, J. W. M.; Liepold, L.; Basu, G.; Zywicke, H. A.; Frank, J. A.; Young, M.; Douglas, T. Paramagnetic Viral Nanoparticles as Potential High-Relaxivity Magnetic Resonance Contrast Agents. *Magn. Reson. Med.* **2005**, *54*, 807–812.
50. Caravan, P.; Ellison, J. J.; McMurry, T. J.; Lauffer, R. B. Gadolinium(III) Chelates as MRI Contrast Agents: Structure, Dynamics, and Application. *Chem. Rev.* **1999**, *99*, 2293–2352.
51. Lin, W.; Rieter, W. J.; Taylor, K. M. L. Modular Synthesis of Functional Nanoscle Coordination Polymers. *Angew. Chem., Int. Ed.* **2009**, *48*, 650–658.
52. Mayadunne, R. T. A.; Rizzardo, E.; Chiefari, J.; Krstina, J.; Moad, G.; Postma, A.; Thang, S. H. Living Polymers by the Use of Trithiocarbonates as Reversible Addition−Fragmentation Chain Transfer (RAFT) Agents:

ABA Triblock Copolymers by Radical Polymerization in Two Steps. *Macromolecules* **2000**, *33* (2), 243–245.

53. Rowe-Konopacki, M. D.; Boyes, S. G. Synthesis of Surface Initiated Diblock Copolymer Brushes from Flat Silicon Substrates Utilizing the RAFT Polymerization Technique. *Macromolecules* **2007**, *40*, 879–888.
54. Rowe, M. D.; Hammer, B. A. G.; Boyes, S. G. Synthesis of Surface-Initiated Stimuli-Responsive Diblock Copolymer Brushes Utilizing a Combination of ATRP and RAFT Polymerization Techniques. *Macromolecules* **2008**, *41* (12), 4147–4157.
55. Hentschel, J.; Bleek, K.; Ernst, O.; Lutz, J.-F.; Borner, H. G. Easy Access to Bioactive Peptide−Polymer Conjugates via RAFT. *Macromolecules* **2008**, *41*, 1073–1075.
56. An, Z.; Shi, Q.; Tang, W.; Tsung, C.-K.; Hawker, C. J.; Stucky, G. D. Facile RAFT Precipitation Polymerization for the Microwave-Assisted Synthesis of Well-Defined, Double Hydrophilic Block Copolymers and Nanostructured Hydrogels. *J. Am. Chem. Soc.* **2007**, *129*, 14493–14499.
57. Bai, Z.; He, Y.; Young, N. P.; Lodge, T. P. A Thermoreversible Micellization−Transfer−Demicellization Shuttle between Water and an Ionic Liquid. *Macromolecules* **2008**, *41* (18), 6615–6617.
58. Xu, J.; He, J.; Fan, D.; Wang, X.; Yang, Y. Aminolysis of Polymers with Thiocarbonylthio Termini Prepared by RAFT Polymerization: The Difference between Polystyrene and Polymethacrylates. *Macromolecules* **2006**, *39* (25), 8616–8624.
59. Vihola, H.; Laukkanen, A.; Valtola, L.; Tenhu, H.; Hirvonen, J. Cytotoxicity of thermosensitive polymers poly(N-isopropylacrylamide), poly(N-vinylcaprolactam) and amphiphilically modified poly(N-vinylcaprolactam). *Biomaterials* **2005**, *26*, 3055–3064.
60. Lee, K. Y.; Yuk, S. H. Polymeric protein delivery systems. *Prog. Polym. Sci.* **2007**, *32*, 669–697.
61. You, Y.-Z.; Manickam, D. S.; Zhou, Q. H.; Oupický, D. Reducible poly(2-dimethylaminoethyl methacrylate): Synthesis, cytotoxicity, and gene delivery activity. *J. Controlled Release* **2007**, *122*, 217–225.
62. Tugulu, S.; Klok, H.-A. Stability and Nonfouling Properties of Poly(poly(ethylene glycol) methacrylate) Brushes under Cell Culture Conditions. *Biomacromolecules* **2008**, *9*, 906–912.
63. Favier, A.; D'Angosto, F.; Charreyre, M.-T.; Pichot, C. Synthesis of N-acryloxysuccinimide copolymers by RAFT polymerization, as reactive building blocks with full control of composition and molecular weight. *Polymer* **2004**, *45*, 7821–7830.
64. Moad, G.; Chiefari, J.; Chong, Y. K.; Krstina, J.; Maydunne, R. T. A.; Postma, A.; Rizzardo, E.; Thang, S. H. Living free radical polymerization with reversible addition-fragmentation chain transfer (the life of RAFT). *Polym. Int.* **2000**, *49*, 993–1001.
65. Lowe, A. B.; McCormick, C. L. Reversible addition–fragmentation chain transfer (RAFT) radical polymerization and the synthesis of water-soluble (co)polymers under homogeneous conditions in organic and aqueous media. *Prog. Polym. Sci* **2007**, *32*, 283–351.

66. Ye, Y.; Bloch, S.; Xu, B.; Achilefu, S. Design, synthesis, and evaluation of near infrared fluorescent multimeric RGD peptides for targeting tumors. *J. Med. Chem.* **2006**, *49*, 2268–2275.
67. Kojima, C.; Kono, K.; Maruyama, K.; Takagishi, T. Synthesis of polyamidoamine dendrimers having poly(ethylene glycol) grafts and their ability to encapsulate anticancer drugs. *Bioconjugate Chem.* **2000**, *11*, 910–917.
68. Strijkers, G. J.; Mulder, W. J. M.; van Tilborg, G. A. F.; Nicolay, K. MRI Contrast Agents: Current Status and Future Perspectives. *Anti-Cancer Agents Med. Chem.* **2007**, *7*, 291–305.
69. LaConte, L.; Nitin, N.; Bao, G. Magnetic Imaging Probes. *Mater. Today* **2005**, *8* (5), 32–38.
70. Taylor, K. M. L.; Jin, A.; Lin, W. Surfactant-Assisted Synthesis of Nanoscale Gadolinium Metal-Organic Frameworks for Potential Multimodal Imaging. *Angew. Chem., Int. Ed.* **2008**, *47*, 7722–7725.
71. van Schooneveld, M. M.; Vucic, E.; Koole, R.; Zhou, Y.; Stocks, J.; Cormode, D. P.; Tang, C. Y.; Gordon, R. E.; Nicolay, K.; Meijerink, A.; Fayad, Z. A.; Mulder, W. J. M. Improved Biocompatibility and Pharmacokinetics of Silica Nanoparticles by Means of a Lipid Coating: A Multimodality Investigation. *Nano Lett.* **2008**, *8*, 2517–2525.
72. Moad, G.; Chong, Y. K.; Postma, A.; Rizzardo, E.; Thang, S. H. Advances in RAFT polymerization: the synthesis of polymers with defined end-groups. *Polymer* **2005**, *46* (19), 8458–8468.
73. Matsuda, Y.; Kobayashi, M.; Annaka, M.; Ishihara, K.; Takahara, A. Dimensions of a Free Linear Polymer and Polymer Immobilized on Silica Nanoparticles of a Zwitterionic Polymer in Aqueous Solutions with Various Ionic Strengths. *Langmuir* **2008**, *24*, 8772–8778.
74. Roth, P. J.; Theato, P. Versatile Synthesis of Functional Gold Nanoparticles: Grafting Polymers From and Onto. *Chem. Mater.* **2008**, *20*, 1614–1621.
75. Liu, Y.; Klep, V.; Zdyrko, B.; Luzinov, I. Polymer Grafting via ATRP Initiated from Macroinitiator Synthesized on Surface. *Langmuir* **2004**, *20*, 6710–6718.
76. Advincula, R. C.; Brittain, W. J.; Caster, K. C.; Ruhe, J. *Polymer Brushes: Synthesis, Characterization, Applications*; Wiley-VCH Verlag GmbH & Co.: Weinheim, 2004; p 483.
77. Halperin, A.; Tirrell, M.; Lodge, T. P. *Adv. Polym. Sci.* **1992**, *100*, 31–71.
78. Jordan, R., Ed. *Surface initiated polymerization I and II: Advances in polymer science*; Springer: Berlin, Heidelberg, New York, 2006; p 214.
79. Sevick, E. M. Shear Swelling of Polymer Brushes Grafted onto Convex and Concave Surfaces. *Macromolecules* **1996**, *29*, 6952–6958.
80. Dong, H.; Matyjaszewski, K. ARGET ATRP of 2-(Dimethylamino)ethyl Methacrylate as an Intrinsic Reducing Agent. *Macromolecules* **2008**, *41*, 6868–6870.
81. Miller, R. L. In *Polymer Handbook*, 4th ed.; Brandup, J., Immergut, E. H., Grulke, E. A., Eds.; John Wiley & Sons: New York, 1999; VI 1.

82. Furuta, I.; Kimura, S.-I.; Iwama, M. In *Polymer Handbook*, 4th ed.; Brandup, J., Immergut, E. H., Grulke, E. A., Eds.; John Wiley & Sons: New York, 1999; V 1.
83. Boyes, S. G.; Granville, A. M.; Baum, M.; Akgun, B.; Mirous, B. K.; Brittain, W. J. Polymer brushes-surface immobilized polymers. *Surface Science* **2004**, *570*, 1–12.
84. Motornov, M.; Sheparovych, R.; Katz, E.; Minko, S. Chemical Gating with Nanostructured Responsive Polymer Brushes: Mixed Brush versus Homopolymer Brush. *ACS Nano* **2008**, *2*, 41–52.
85. Muthukrishnan, S.; Erhard, D. P.; Mori, H.; Muller, A. H. E. Synthesis and Characterization of Surface-Grafted Hyperbranched Glycomethacrylates. *Macromolecules* **2006**, *39*, 2743–2750.
86. Gao, H.; Matyjaszewski, K. Synthesis of Molecular Brushes by “Grafting onto” Method: Combination of ATRP and Click Reactions. *J. Am. Chem. Soc.* **2007**, *129*, 6633–6639.
87. Larsen, T. H.; Sigman, M.; Ghezelbash, A.; Doty, R. C.; Korgel, B. A. Solventless Synthesis of Copper Sulfide Nanorods by Thermolysis of a Single Source Thiolate-Derived Precursor. *J. Am. Chem. Soc.* **2003**, *125*, 5638–5639.
88. Urano, Y.; Higuchi, T.; Hirobe, M.; Nagano, T. Pronounced Axial Thiolate Ligand Effect on the Reactivity of High-Valent Oxo-Iron Porphyrin Intermediate. *J. Am. Chem. Soc.* **1997**, *119*, 12008–12009.
89. Cowper, S. E. Nephrogenic systemic fibrosis: the nosological and conceptual evolution of nephrogenic fibrosing dermopathy. *Am. J. Kidney Dis.* **2005**, *46*, 763–765.
90. Grobner, T. Gadolinium – a specific trigger for the development of nephrogenic fibrosing dermopathy and nephrogenic systemic fibrosis? *Nephrol., Dial., Transplant.* **2006**, *21*, 1104–1108.
91. High, W. A.; Ayers, R. A.; Chandler, J.; Zito, G.; Cowper, S. E. Gadolinium is detectable within the tissue of patients with nephrogenic systemic fibrosis. *J. Am. Acad. Dermatol.* **2007**, *56*, 21–26.
92. Tanimoto, A. Use of SPIOs for Clinical Liver Imaging. In *Fundamental Biomedical Technologies: Nanoparticles in Biomedical Imaging*; Bulte, J. W. M., Modo, M. M. J., Eds.; Springer: New York, 2008; pp 41−61.
93. Taylor, K. M. L.; Rieter, W. J.; Lin, W. Manganese-Based Nanoscale Metal–Organic Frameworks for Magnetic Resonance Imaging. *J. Am. Chem. Soc.* **2008**, *130*, 14358–14359.
94. Brigger, I.; Dubernet, C.; Couvreur, P. Nanoparticles in cancer therapy and diagnosis. *Adv. Drug Delivery Rev.* **2002**, *54*, 631–651.

Downloaded by CORNELL UNIV on June 23, 2012 | http://pubs.acs.org
Publication Date (Web): November 17, 2010 | doi: 10.1021/bk-2010-1053.ch005

Chapter 5

Iron Chelating Macromolecules for Intravascular Iron Chelation Therapy

Nicholas A. A. Rossi[1,2,*] and Jayachandran N. Kizhakkedathu[1]

[1]Centre for Blood Research and the Department of Pathology and Laboratory Medicine, University of British Columbia, Vancouver, BC V6T 1Z3, Canada
[2]Canadian Blood Services, Life Sciences Centre, University of British Columbia, Vancouver, BC V6T 1Z3, Canada
[*]rossinic@interchange.ubc.ca

The development of an iron chelating macromolecular therapeutic for intravascular delivery is reviewed, with particular emphasis on recent research by our group to design, synthesize, and evaluate a well-defined, intravenoeous, iron-chelating macromolecular therapeutic. Several crucial requirements influenced the design of the polymer to be used as a potentially effective parenteral drug. Firstly, the polymer should contain a therapeutic agent; in this case the ability to effectively chelate iron. Secondly, the polymer drug should be well-defined and easily varied in terms of both its physical characteristics (molecular weight, polydispersity) and its composition in order to influence the resulting pharmacokinetics of the drug. This was achieved using controlled polymerization via reversible addition-fragmentation chain transfer (RAFT) methods. Finally, the macromolecule should be blood compatible and degradable to allow for long circulation times and ease of clearance through the kidney.

Introduction

The presence of excess iron in the body can lead to the oxidation of lipids, proteins, carbohydrates and nucleic acids (*1*). The oxidation-reduction process that is catalyzed by iron and results in the formation of the highly reactive OH•

In Polymeric Delivery of Therapeutics; Morgan, S., et al.;
ACS Symposium Series; American Chemical Society: Washington, DC, 2010.

radical is known as the Haber-Weiss reaction (*2*). The OH• radical initiates a series of chemical reactions with several biologically important molecules and is the driving force for the biological and pathological activity of iron in the body (*3*). These oxidative reactions result in the impairment of cellular functions and can lead to cell death and extensive tissue and organ damage. In humans, iron metabolism and bioavailability is tightly controlled through the dietary absorption, trafficking, and recycling of iron within the body. 'Iron overload' can occur due to the inability of humans to excrete excess iron effectively. Iron overload results from enhanced dietary uptake (hemochromatosis), medical treatment (chronic blood transfusions), destabilized hemoglobin (sickle cell disease), reduced hemoglobin (thalassemia), or as a result of conditions such as cardiomyopathies, hepatic fibrosis and diabetes mellitus (*4*–*7*). Since no iron excretion pathway exists to remove the excess iron normally stored in the liver, spleen, and bone marrow, extensive organ damage can often occur (*8*).

In particular, iron chelation therapy is used to transfusion-associated 'secondary iron overload' (*5*). Over the last 30 years, the most commonly used and clinically effective drug is desferrioxamine (DFO), a bacterial siderophore isolated from *Streptomyces pilosus* (*9*). DFO is a multi-dentate ligand with a very strong iron(III) binding affinity (Figure 1). Interest in DFO and several other iron chelators is also linked to their anti-proliferative activity against aggressive tumors, and clinical trials have been conducted for the treatment of neuroblastoma and leukemia (*10*). However, disadvantages of DFO include its high toxicity, cost, and very short plasma half life (only 5.5 min) (*11*, *12*). Furthermore, the hydrophilicity of the ligand has resulted in its poor absorption through the gastrointestinal tract (*13*). Although alternative low molecular weight ligands have been investigated (*9*, *14*), they all demonstrate levels of toxicity at near therapeutic dosing.

Recent advances in the field of polymer therapeutics have focused on improving the therapeutic index of drugs through the development of novel, drug-polymer conjugates (*15*). In most cases, the drug is attached to a biocompatible polymer such as poly(ethylene glycol) (PEG) via a degradable linkage, such as a hydrolysable ester bond, to ensure release of the drug at a predetermined site of action, with the polymers cleared from circulation upon delivery (*15*). An alternative and less common type of polymer-drug conjugate is the macromolecular therapeutic, in which the drug remains with the polymer support while the therapeutic dose is being delivered (*16*, *17*). One of the few examples of this type of therapeutic involves the conjugation of DFO to a dextran or starch polymer (*15*, *18*, *19*). In this case, DFO chelates iron while attached to a polymeric support to reduce toxicity and increase plasma residence time relative to monomeric DFO.

Until recently, only the work carried out by Hallaway and co-workers have focused on the development of an intraveneous polymer therapeutic. Starch and dextran based polymers are naturally occurring and show good biocompatibility. However, the lack of control over the molecular weight of the macromolecular conjugates is a major drawback since this is one of the properties which influences the pharmacokinetic profiles and dosage of the therapeutic drug *in vivo* (*20*). Over the last few years, our group has utilized reversible addition-fragmention chain

Downloaded by CORNELL UNIV on June 23, 2012 | http://pubs.acs.org
Publication Date (Web): November 17, 2010 | doi: 10.1021/bk-2010-1053.ch005

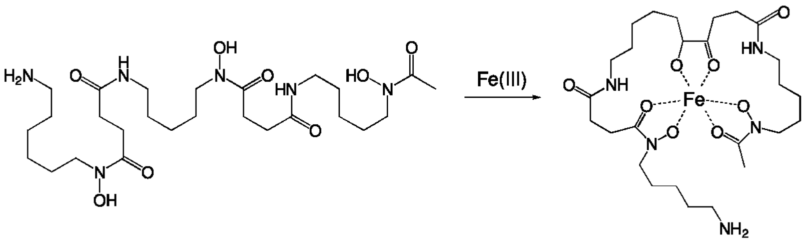

Figure 1. Structure of desferrioxamine (DFO) ligand upon binding to Iron.

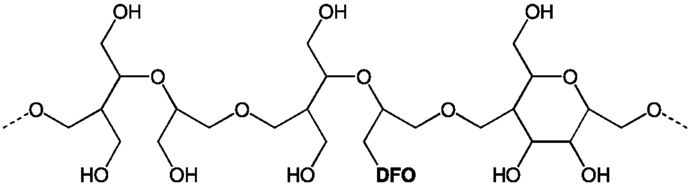

Figure 2. Structure of a starch-DFO conjugate

Downloaded by CORNELL UNIV on June 23, 2012 | http://pubs.acs.org
Publication Date (Web): November 17, 2010 | doi: 10.1021/bk-2010-1053.ch005

transfer (RAFT) (*21*, *22*) methods to synthesize blood compatible copolymers that can be modified to achieve targeted chain length, polydisperisty, and composition (*23*, *24*). Here, recent developments concerning macromolecular iron chelating intraveneous drugs are reviewed.

Dextran and Starch-Based Iron Chelators

Hallaway and co-workers first reported a method for minimizing the toxicity of DFO by attaching the pro-drug to natural, biocompatible dextran and starch polymers in 1989 (*15*). The conjugates were developed by initially generating aldehyde groups on the dextran prior to conjugation to DFO via the reactive primary amine moieties. Addition of $NaCNBH_3$ reduces the Schiff base to form a stable secondary amine linkage (Figure 2). The concentration of DFO on the polymer was determined spectrophotometrically by measuring the characteristic absorption (*15*) of the DFO-Fe(II) complex at λ_{max} 429 nm. Importantly, the iron-binding ability of DFO was not compromised upon conjugation to the polymer.

The toxicity of DFO has been well-documented, with previous cell viability studies showing significant increases in cytotoxicity at 5 μM to 10 μM concentrations (*25*). However, upon conjugation to a biocompatible polymer such as dextran, starch, and hydroxyethyl starch, the toxicity of DFO was greatly reduced (*15*). The distinct lack of toxicity of polymer-bound DFO is due to the inability of the DFO to permeate the cell membrane. Phase I clinical trials involving a starch-based DFO polymer have shown that the drug has a long plasma half-life and results in substantial iron excretion (*26*).

In 2007, Hedlund and co-workers reported that a single infusion of starch-bound DFO provided several days of iron balance and up to a week of unsaturated iron binding capacity in the plasma (*19*). It is hoped that this type of polymer could

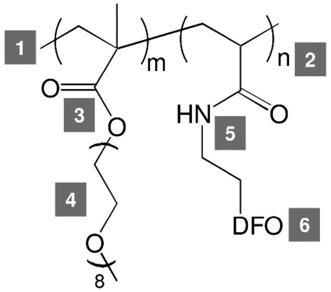

1. Control over molecular weight
2. Control over composition (m, n) and spacing (random) of units
3. Degradability (ester linkages)
4. Biocompatibility (PEG chain)
5. Stable linkage between polymer and therapeutic agent
6. Therapeutic agent (DFO)

Figure 3. Considerations for the design of a well-defined iron-chelating polymer therapeutic

Downloaded by CORNELL UNIV on June 23, 2012 | http://pubs.acs.org
Publication Date (Web): November 17, 2010 | doi: 10.1021/bk-2010-1053.ch005

be infused at the time of transfusion in combination with oral chelators for patients requiring chronic transfusions, while also finding application as a treatment for acute iron poisoning. Clearance from the bloodstream is controlled via cleavage of the starch backbone by circulating α-amylases to create small S-DFO fragments that are filtered into the urine.

In addition, variations in the delivery of polymer-based iron-chelating therapies have been proposed. In 2001, Scott reported the use of an iron shuttle chelating system that utilizes low affinity, smalle molecule, membrane permeable iron binding agents that enter the red blood cell to bind iron. Subsequently, they diffuse out of the cell and 'hand off' iron to high molecular weight, DFO-containing polymers (*27*).

PEG-Based Iron Chelators

Design

The aim of the research conducted by our group was to synthesize, characterize, and evaluate the *in vitro* blood compatibility of a well-defined macromolecular iron chelator (*23*, *24*). Figure 3 highlights our pre-requisites for an effective iron chelating polymer.

First, the molecular weight of the polymer needs to be controlled, since the pharmacokinetic profiles of macromolecular therapeutic agents depend greatly on its structure and size. Similarly, it is essential to control the composition of the copolymer. In this case, the copolymer is made up of two repeat units: poly(ethylene glycol) methyl methacrylate (PEGMA) and a DFO-containing unit. PEGMA is often incorporated to impart a degree of biocompatibility, while the DFO moieties make up the 'functional' or therapeutic aspect of the copolymer. It is especially important that the DFO units be randomly spaced along the backbone (instead of existing as blocks). Furthermore, as the DFO is to remain tethered to the copolymer, it is necessary that it is conjugated to the backbone via a stable linkage such as an amide or amine group. Conversely, a degree of degradability should exist in order for the copolymer to circulate in the body for a period of time, before being excreted through the kidney.

Our group successfully fulfilled these requirements by conjugating DFO to a PEG-containing copolymer. The presence of PEG and the resulting increase

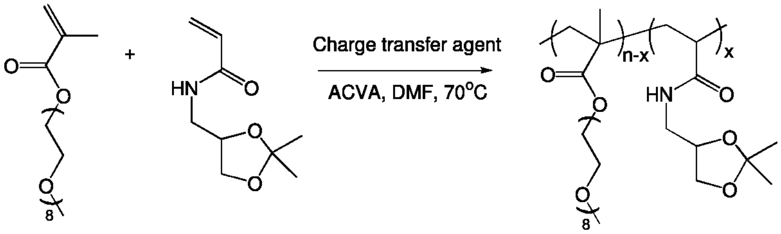

Figure 4. RAFT polymerization of poly(ethylene glycol) methyl ether methacrylate (PEGMA) and (2,2-dimethyl-1,3-dioxolane) methyl acrylamide (DDMAA).

in the Stokes radius of the bound DFO improves vascular retention, making it more suitable for systemic vascular applications (*28*). DFO is conjugated to the polymer support through stable amine linkages, while PEG chains are conjugated via degradable ester bonds. Therefore, DFO remains conjugated to the polymer *in vivo* and chleates excess iron, while cleavage of the PEG side chains (M_n 400) via hydrolysable ester linkages causes the copolymer chelator to decrease in size and eventually be cleared through the kidney at faster rates (*20*). As part of these studies, the *in vitro* properties involving iron-binding, blood compatibility, cytotoxicity, and degradation of the P-DFO copolymers are described. In addition, although the use of DFO was reported as an iron chelating molecule, the modular design of this well-defined copolymer makes it an effective platform for the conjugation of other clinically relevant chelators, organic molecules, peptides, or proteins for potential systemic vascular applications.

Synthesis

By employing the RAFT (*21*, *22*) polymerization method, it was possible to synthesize a range of copolymer precursors with predetermined molecular weights and compositions (*23*). Copolymers of poly(ethylene glycol) methyl ether methacrylate (PEGMA) and a dioxolane-containing monomer, (2,2-dimethyl-1,3-dioxolane) methyl acrylamide (DDMAA), were successfully synthesized (Figure 4).

Control over molecular weight and composition was achieved by altering the chain transfer agent (CTA) concentration and the monomer feed ratio respectively. The resulting copolymers ranged in molecular weight from 21 kDa to 80 kDa and had narrow molecular weight distributions (polydispersity indices typically between 1.2 and 1.3). Kinetic studies revealed that the dioxolane units were randomly distributed along the backbone of the copolymer. The abundance of dioxolane units along the backbone ranged from 10 to 22 % compared to the total number of units (PEG and dioxolane combined).

The precursor copolymers were then modified by first deprotecting the dioxolane functional groups to form 1,2-diol groups and followed by oxidation with periodic acid to form reactive aldehyde groups. These reactive aldehyde groups could then be used to conjugate the amine containing DFO ligands.

Downloaded by CORNELL UNIV on June 23, 2012 | http://pubs.acs.org
Publication Date (Web): November 17, 2010 | doi: 10.1021/bk-2010-1053.ch005

Downloaded by CORNELL UNIV on June 23, 2012 | http://pubs.acs.org
Publication Date (Web): November 17, 2010 | doi: 10.1021/bk-2010-1053.ch005

Conjugation was achieved via an aldamine reaction, followed by a reduction of the resulting Schiff base to a secondary amine (Figure 5) (*23*).

The main advantage of first synthesizing a stable precursor polymer *vs.* direct copolymerization of aldehyde-based monomers is due to the instability and reactivity of aldehydes. For example, it was noted that the aldehyde containing copolymer could not be isolated (i.e. precipitated or lyophilized) since cross-linking of the aldehyde groups was observed (*23*). Therefore, conjugation with amine containing compounds such as DFO was performed immediately after dialysis of the aldehyde-containing copolymer. In contrast, the dialyzed and lyophilized diol form of the copolymer was highly soluble in water and stable over a period of time in the refrigerator at 4°C. The advantage of the current synthesis is that the precursor polymer containing 1,2-diols is much more stable than the corresponding aldehyde polymer. Therefore, it is possible to store the copolymers for extended periods of time, with the aldehyde groups generated under mild conditions immediately prior to conjugation.

Iron-Binding Properties

Several methods were employed to elucidate the copolymer-conjugate structures (*23*, *24*). In particular, UV-Vis absorption spectroscopy was used to determine both the content of DFO contained within each copolymer and the efficiency with which DFO chelates iron before and after conjugation to the copolymer backbone. When the copolymers were dissolved in aqueous $FeSO_4$ solution, a characteristic absorption for iron-complexed DFO was observed (λmax 429 nm), indicating that conjugation was efficient, and that the iron-binding capacity seemed to be intact despite the DFO being tethered to the polymer backbone. In order to confirm these findings, *in vitro* studies showing how DFO and polymer conjugated DFO (P-DFO) inhibit Fe(III)-mediated oxidation of hemoglobin were performed (Figure 6) (*24*). The studies were particularly apt, since Fe(III)-mediated hemoglobin oxidation is a process that underlies the pathology of hemoglobinopathies such as sickle cell anemia and thalassemias (*29*).

Similar to previous DFO-polymer conjugates (*15*), comparison of DFO and P-DFO at various concentrations revealed that DFO behaves similarly whether it is present in the molecular form or whether it is tethered to a polymer. Analysis of various P-DFO samples revealed that changes in molecular weight and composition did not seem to alter the efficacy of Fe(III) binding.

Polymer Degradation Pathway

Ideally, an administered polymer therapeutic should, after circulating in the blood for an optimum length of time, begin to degrade to allow for renal clearance. The kidney has a molecular weight cut off of 50 kDa – 65 kDa (above which compounds are not excreted) depending on the type of polymer or protein (*20*). In the case of the polymer conjugates reviewed here, the PEG side chains (M_n ~ 400) are linked to the copolymer backbone through cleavable ester linkages. As these bonds are cleaved, the molecular weight of the copolymer decreases;

Downloaded by CORNELL UNIV on June 23, 2012 | http://pubs.acs.org
Publication Date (Web): November 17, 2010 | doi: 10.1021/bk-2010-1053.ch005

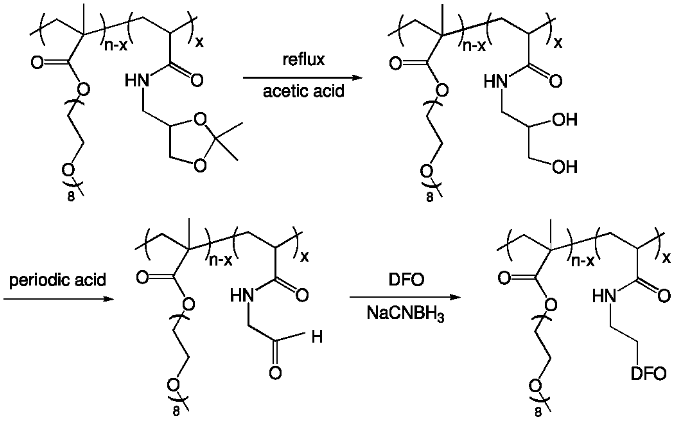

Figure 5. Synthesis of a DFO containing copolymer from a stable precursor.

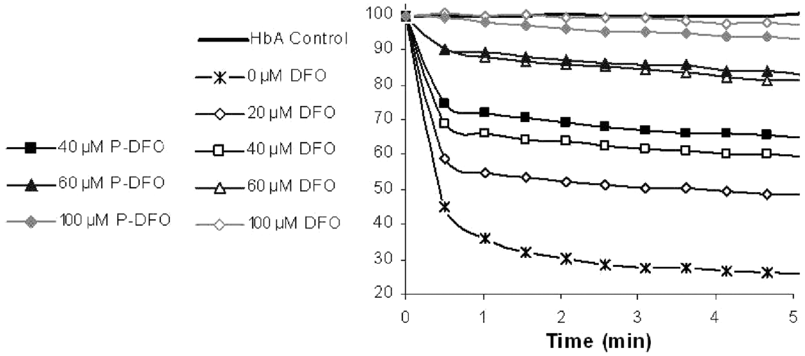

Figure 6. Fe^{3+} mediated hemoglobin oxidation inhibitory effect by DFO and P-DFO. 100 µM Fe^{3+} and 1mM L-Glutathione added to each sample (except control) in hemoglobin. (Adapted from reference (24). Copyright 2009, Elsevier).

for example, if the copolymer has an initial molecular weight of 80 kDa and degradation via ester cleavage occurs *in vivo*, the rate of clearance through the kidney should increase over time. Having synthesized the copolymer using a controlled polymerization technique (RAFT) in which molecular weight can be easily tuned, it should therefore be possible to affect the intial and subsequent rates of clearance through the kidney. Furthermore, since DFO is attached to the copolymer through more stable, amide linkages, degradation of the copolymer to form toxic, single molecule DFO units is greatly reduced. To highlight the degradability of the ester linkages within the copolymer, a simplified experiment whereby degradation was followed using physical (GPC) and chemical (NMR) techniques was performed (*23*). GPC showed that the molecular weight of P-DFO decreased slowly over the course of 4 weeks in slightly basic aqueous solution (pH 9). Proton NMR spectroscopy (^1H NMR) illustrated the partial loss of peaks associated with degradation of the ester bond.

Downloaded by CORNELL UNIV on June 23, 2012 | http://pubs.acs.org
Publication Date (Web): November 17, 2010 | doi: 10.1021/bk-2010-1053.ch005

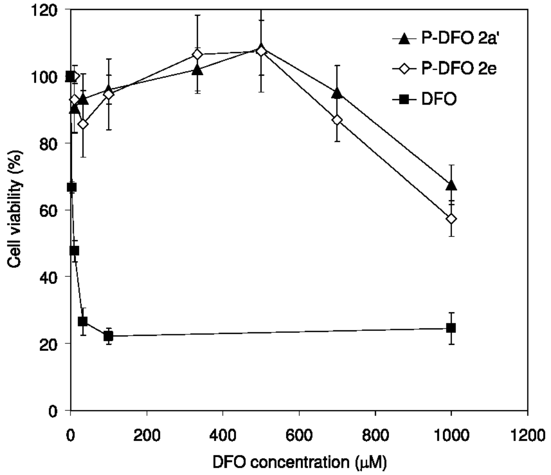

Figure 7. Cell viability of two different P-DFO conjugates (2a' and 2e) and DFO against HUVEC cells at increasing concentrations after incubation for 48 h (MTS assay). (Reprinted from reference (24). Copyright 2009, Elsevier).

In Vitro Cell Toxicity and Blood Compatibility

In order to determine the suitability of the P-DFO samples as possible intravenous polymer therapies, endothelial cells (HUVEC) were used to measure cytotoxicity (*24*). As with the findings conducted on the starch/dextran modified DFO conjugates, the onset of cytoxicity could only be observed at equivalent DFO concentrations of over 500 μM (Figure 7). Conjugation of DFO to the polymer lead to >100 fold improvement in the toxicity profiles of the drug, significantly improving the therapeutic index of the drug *in vivo*. Furthermore, an extensive array of hemo-compatibility experiments including conventional clinical coagulation assays – prothrombin time (PT) and activated partial thromboplastin time (APTT) – as well as more extensive techniques such as thromboelastography (TEG), platelet activation, compliment activation, and whole blood aggregation were conducted to test the *in vitro* suitability of the copolymer. Our conjugates were found to be blood compatible, even at exceptionally high concentrations of up to 10 mg/mL.

Conclusions

Previous reports investigating the use of starch or dextran to conjugate DFO have yielded very promising *in vitro* and *in vivo* results. Recent clinical studies suggest these high molecular weight therapeutics might soon be used as an alternative to toxic and uncomfortable intraveneous treatments currently available. However, there are some disadvantages associated with using poorly-defined polymeric compounds. Since renal clearance rates are inversely proportional to molecular weight, it follows that having a well-defined polymer therapeutic is important in obtaining consistent pharmacokinetic properties. In addition, excretion of higher molecular weight polymers through the urine is unlikely if the polymers are not easily degraded and could result in unwanted tissue accumulation. As a result, we attempted to utilize relatively new controlled polymerization techniques (i.e. RAFT polymerization) to synthesize aldehyde containing copolymers (from a stable copolymer precursors) that can be used to conjugate DFO. The resulting copolymers are well-defined in terms of both the molecular weight characteristics and DFO content and it is possible to control those parameters should the *in vivo* data suggest that polymers with characteristics perform more effectively than others. The *in vitro* data for the copolymers is promising, and *in vivo* studies are currently progressing.

Acknowledgments

This research was funded by the Canadian Institutes of Health Research (CIHR)-Canadian Blood Services (CBS) Partnership Fund and an operating grant from CIHR. The authors thank the LMB Macromolecular Hub at the UBC Centre for Blood Research for the use of their research facilities; the infrastructure facility is supported by the Canada Foundation for Innovation (CFI) and the Michael Smith Foundation for Health Research (MSFHR). N.A.A. Rossi is a recipient of a CIHR/CBS postdoctoral fellowship in Transfusion Science and J.N. Kizhakkedathu is a recipient of a CIHR/CBS new investigator in Transfusion Science.

Downloaded by CORNELL UNIV on June 23, 2012 | http://pubs.acs.org
Publication Date (Web): November 17, 2010 | doi: 10.1021/bk-2010-1053.ch005

References

1. Hebbel, R. P. *Clin. Haematol.* **1985**, *14*, 129–40.
2. Halliwell, B.; Gutteridge, J. M. C. *Free radicals in biology and medicine*; Oxford: Claredon Press, 1989.
3. Bergeron, R. J.; Wiegand, J.; McManis, J. S.; Bussenius, J.; Smith, R. E.; Weimar, W. R. *J. Med. Chem.* **2003**, *46*, 1470–1477.
4. Aisen, P. *Met. Ions Biol. Syst.* **1998**, *35*, 585–631.
5. Hershko, C.; Graham, G.; Bates, G. W.; Rachmilewitz, E. A. *Br. J. Haematol.* **1978**, *40*, 255–263.
6. Batts, K.P. *Modern Pathology* **2007**, *20*, S31–S39.
7. Scott, M. D.; Eaton J. W. In *Free Radical Toxicology*; Wallace, K. B., Ed.; Taylor & Francis: Washington, DC, 1997; pp 401−420.
8. Hentze, M. W.; Muckenthaler, M. U. *Cell* **2004**, *117*, 285–295.
9. Kalinowski, D. S.; Richardson, D. R. *Pharm. Rev.* **2005**, *57*, 547–583.
10. Richardson, D. R. *Crit. Rev. Oncol. Hematol.* **2002**, *42*, 267–281.
11. Hallaway, P. E.; Eaton, J. W.; Panter, S. S.; Hedlund, B. E. *Proc. Natl. Acad. Sci. USA* **1989**, *86*, 10108–10112.
12. Aouad, F.; Florence, A.; Zhang, Y.; Collins, F.; Henry, C.; Ward, R. J.; Chrichton, R. R. *Inorg. Chim. Acta* **2002**, *339*, 470–480.
13. Franchini, M.; Gandini, G.; de Gironcoli, M.; Vassanelli, A.; Borgna-Pignatti, C.; Aprili, G. *Blood* **2000**, *95*, 2776–2779.
14. Liu, Z. D.; Hider, R. C. *Coord. Chem. Rev.* **2002**, *232*, 151–171.
15. Harris, J. M.; Chess, R. B. *Nat. Rev. Drug Discovery* **2003**, *2*, 214–221.

16. Dhal, P. K.; Holmes-Farley, S. R.; Huval, C. C.; Jozefiak, T. H. *Adv. Polym. Sci.* **2006**, *192*, 9–58.
17. Kiick, K. L. *Science* **2007**, *317*, 1182–1183.
18. Dragsten, P. R.; Hallaway, P. E.; Hanson, G. J.; Berger, A. E.; Bernard, B.; Hedlund, B. E. *J. Lab. Clin. Med.* **2000**, *135*, 57–65.
19. Harmatz, P.; Grady, R. W.; Dragsten, P.; Vichinsky, E.; Giardina, P.; Madden, J.; Jeng, M.; Miller, B.; Hanson, G.; Hedlund, B. *Br. J. Haematol.* **2007**, *138*, 374–381.
20. Caliceti, P.; Veronese, F. M. *Adv. Drug Delivery Rev.* **2003**, *55*, 1261–1277.
21. Chiefari, J.; Chong, Y. K.; Ercole, F.; Krstina, J.; Jeffery, J.; Le, T. P. T.; Mayadunne, R. T. A.; Meijs, G. F.; Moad, C. L.; Moad, G.; Rizzardo, E.; Thang, S. H. *Macromolecules* **1998**, *31*, 5559–5562.
22. Moad, G.; Rizzardo, E.; Thang, S. H. *Aust. J. Chem.* **2005**, *58*, 379–410.
23. Rossi, N. A. A.; Zou, Y.; Scott, M. D.; Kizhakkedathu, J. N. *Macromolecules* **2008**, *41*, 5272.
24. Rossi, N. A. A.; Mustafa, I.; Scott, M. D.; Horte, S.; Jackson, J.; Burt, H.; Kizhakkedathu, J. N. *Biomaterials* **2009**, *30*, 638.
25. Poot, M.; Rabinovitch, P. S.; Hoehn, H. *Free Radical Res. Commun.* **1989**, *6*, 323–8.
26. Harmatz, P.; Grady, R. W.; Vichinsky, E.; Giardina, P. J.; Jeng, M.; Madden, J.; Nugent, K. A.; Dragsten, P. *Blood* **2003**, *102*, Abstract 423.
27. Scott, M. D. *Hematology* **2001**, *6*, 73–89.
28. Dhal, P. K.; Holmes-Farley, S. R.; Huval, C. C.; Jozefiak, T. H. *Adv. Polym. Sci.* **2006**, *192*, 9–58.
29. Caliceti, P.; Veronese, F. M. *Adv. Drug Delivery Rev.* **2003**, *55*, 1261–1277.

Downloaded by CORNELL UNIV on June 23, 2012 | http://pubs.acs.org
Publication Date (Web): November 17, 2010 | doi: 10.1021/bk-2010-1053.ch005

Downloaded by PENNSYLVANIA STATE UNIV on June 23, 2012 | http://pubs.acs.org
Publication Date (Web): November 17, 2010 | doi: 10.1021/bk-2010-1053.ch006

Chapter 6

Primary Amine-Functionalized Silicon Surfaces via Click Chemistry with α-Alkynyl-Functionalized Poly(2-aminoethyl methacrylate)

Alp H. Alidedeoglu, Christopher A. Harris, Nemesio Martinez-Castro, Adam W. York, Charles L. McCormick, and Sarah E. Morgan*

School of Polymers and High Performance Materials, The University of Southern Mississippi, 118 College Drive # 10076, Hattiesburg, MS 39406-0001.
***sarah.morgan@usm.edu**

The direct preparation of α-alkynyl-functionalized poly(2-aminoethyl methacrylate) in its hydrochloride salt form (poly(AEMA)) via reversible addition-fragmentation chain transfer (RAFT) polymerization is reported. The controlled "living" polymerization of AEMA was conducted in DMSO at 45 °C using alkynyl-functionalized 4-cyanopentanoic acid dithiobenzoate (CTP) as the chain transfer agent (CTA), and 2,2′-azobis(2,4-dimethyl-4-methoxyvaleronitrile) (V-70) as the initiator. The resulting polymers display values of polydispersity index (PDI) lower than 1.2. Subsequently, the α-alkynyl-functionalized poly(AEMA) was attached to an azide-functionalized silicon wafer via click chemistry. Polymer-modified surfaces were evaluated using characterization techniques including ellipsometry, contact angle measurements, attenuated total reflectance-Fourier transform infrared (ATR-FTIR) spectroscopy and atomic force microscopy (AFM). A grafted polymer layer with average thickness of 15.2 nm and estimated grafting density of 0.39 chains/nm^2 was obtained.

In Polymeric Delivery of Therapeutics; Morgan, S., et al.;
ACS Symposium Series; American Chemical Society: Washington, DC, 2010.

Downloaded by PENNSYLVANIA STATE UNIV on June 23, 2012 | http://pubs.acs.org
Publication Date (Web): November 17, 2010 | doi: 10.1021/bk-2010-1053.ch006

Introduction

Recent advances in controlled radical polymerization (CRP) techniques such as atom transfer radical polymerization (ATRP) (*1*) and RAFT polymerization (*2*, *3*) have resulted in the development of facile routes to obtain telechelic polymers with predetermined MWs and narrow MW distributions. Although CRP has been used for the polymerization of a wide range of monomers, there is intense interest in synthesis of functional polymers with capabilities for post-polymerization modification. This method requires specific end group functionality that must be compatible with polymerization conditions (*4*, *5*). As CRP provides predetermined chain end functionality that is easily controlled, there have been numerous reports of CRP preparation of functional polymers for post-modification applications such as fluorescently labeled chains, polymeric bioconjugates and surface-immobilized polymers (*6*–*12*).

The Cu(I) catalyzed 1,3-dipolar cycloaddition reaction between azide and alkyne groups results in very stable 1,4-disubstituted 1,2,3-triazole products (*13*, *14*). Due to its high thermodynamic driving force, this reaction can be performed in high yield under ambient conditions. This coupling process can be conducted in aqueous or organic media and is compatible with incorporation of a wide range of functional groups. Due to its simplicity and efficiency, the term click chemistry was given to this category of reactions by Sharpless and coworkers in 2001 (*15*).

Extensive reports of the use of click chemistry as a post-polymerization modification technique for functionalizing polymers prepared by CRP methods have appeared in the literature (*16*–*36*). Polymer molecules produced by CRP are generally telechelic, providing an opportunity for the functionalization of polymer chain ends using click chemistry. For example, Agut et al. prepared α-azide- and alkyne-functionalized poly[2-(dimethylamino)ethyl methacrylate] (PDMAEMA) through ATRP using α-ω-functionalized initiators for the preparation of hybrid diblock copolymers (*31*). These blocks were composed of a polypeptide and a poly[2-(dimethylamino)ethyl methacrylate] (PDMAEMA) block that were covalently linked utilizing click chemistry. Lutz et al. reported ATRP-synthesized polymers that were functionalized with azides at the ω-chain end (*32*). These azide functional polymers were subsequently reacted with various alkyne functional compounds to prepare ω-hydroxy, ω-carboxyl and ω-methyl vinyl-functionalized polystyrene. In addition, the combination of ATRP and click chemistry was employed by Vogt et al. to prepare well-defined ω-(meth)acryloyloxy-functionalized poly(*n*-butyl acrylate) and ω-acryloyloxy-functionalized polystyrene macromonomers (*33*). Fewer reports of the use of click chemistry for the post-polymerization modification of polymers synthesized via RAFT polymerization have appeared. One such example was carried out by O'Reilly et al., who reported the synthesis of alkyne-functionalized block copolymers via RAFT polymerization (*34*). An alkynyl-functionalized RAFT CTA was used directly for the sequential polymerization of tetrahydropyran acrylate and styrene, followed by selective cleavage of the tetrahydropyran esters to give α-alkynyl-functionalized block copolymers that are capable of forming surface-functionalized clickable micelles in aqueous solutions. Another example utilizing RAFT polymers was reported by Gondi et al., who synthesized

α-azido terminal polymers using an α-azido-functionalized CTA that allowed the preparation of a range of functional telechelics (*35*).

Click chemistry has also been extensively employed for the modification of surfaces with different types of polymers. Tornoe et al. were the first to demonstrate that click chemistry can be used to modify solid substrates (*14*). They reported the successful synthesis of diversely 1,4-substituted [1,2,3]-triazoles in peptide backbones or side chains upon using the combination of click chemistry and solid-phase peptide synthesis. Given the success of Meldal and coworkers, other researchers began to explore the attachment of polymers prepared via CRP to various surfaces. For example, Ranjan et al. reported the immobilization of an α-alkyne-functionalized polymer, prepared via RAFT polymerization, to azide-functionalized silica nanoparticles via click chemistry (*11*). The same group also demonstrated a 'grafting-from' approach by first attaching alkynyl-functionalized CTA to azide-functionalized silica nanoparticles followed by RAFT surface polymerization of styrene and methyl methacrylate (*36*). They achieved a grafting density of 1.2-1.3 RAFT agent/nm^2 for the immobilization of CTA onto silica nanoparticles, resulting in high-density polymer brushes. Additionally, Ostaci et al. grafted ω-azido-functionalized polymers prepared through ATRP and nitroxide-mediated radical polymerization (NMP) on alkynyl-functionalized silicon wafers using click chemistry (*37*). Polymer brushes with a thickness of 6 nm and grafting densities of 0.2 chains/nm^2 were synthesized.

In 2009, Wang et al. reported a click surface modification of an azide-functionalized gold surface with nitrophenyl groups, resulting in the attachment of the small molecule onto the gold surface creating a monolayer (*38*). Exploiting the presence of the nitro group on the surface, cyclic voltammetry and Raman spectroscopy were used to confirm the identity of the final modified surface, but no estimation of grafting density per unit area was made.

Primary amine-functionalized methacrylates are of interest for their potential utility in post-polymerization modification reactions, such as amide and imine formation, ring-opening reactions and Michael addition reactions, enabling advances in areas that include new approaches for cross-linking micelles and hydrogels, synthesis of novel copolymers for biomimetic scaffold structures, and bioconjugation (*39–48*). However, the controlled polymerization of 2-aminoethyl methacrylate (AEMA) is challenging because it is susceptible to side reactions such as Michael addition in alkaline media (*49*). RAFT polymerization provides a potential route for the controlled polymerization of AEMA without using protecting group chemistry. We recently reported the aqueous RAFT polymerization of AEMA yielding near monodisperse homopolymers (*50*).

Herein, we report the direct synthesis of α-alkynyl-functionalized poly(AEMA) by RAFT polymerization yielding near monodisperse homopolymers. In addition, the successful surface attachment of α-alkynyl-functionalized poly(AEMA) on azide-functionalized silicon wafers was achieved through click chemistry using the 'grafting-to' approach. The resulting poly(AEMA)-modified surfaces were characterized by ellipsometry, contact angle measurements, ATR-FTIR spectroscopy and AFM.

Downloaded by PENNSYLVANIA STATE UNIV on June 23, 2012 | http://pubs.acs.org
Publication Date (Web): November 17, 2010 | doi: 10.1021/bk-2010-1053.ch006

Downloaded by PENNSYLVANIA STATE UNIV on June 23, 2012 | http://pubs.acs.org
Publication Date (Web): November 17, 2010 | doi: 10.1021/bk-2010-1053.ch006

Experimental

Materials

All reagents were used as received without further purification unless otherwise noted. Methacryloyl chloride (>97%), propargyl alcohol (99%), 3-(bromopropyl)trichlorosilane (96%), anhydrous toluene (>99 %), copper sulfate, azidotrimethylsilane ($Si(CH_3)_3N_3$) (95%), sodium ascorbate (>98%) ethanolamine (>98%) and hydroquinone (99%) were purchased from Aldrich. 4-(Dimethylamino)pyridine (99%) (DMAP) and *N,N′*-(dicyclohexyl)carbodiimide (99%) (DCC) were purchased from Acros Organics. Phenylmagnesium bromide solution (3M in diethyl ether) was purchased from Fluka. Dimethylsulfoxide (DMSO), 30% hydrogen peroxide (H_2O_2), sulfuric acid (H_2SO_4), diethylether, ethyl acetate, hexane, and hydrochloric acid were purchased from Fisher. 2,2′-Azobis(2,4-dimethyl-4-methoxyvaleronitrile) (V-70) was purchased from Wako Pure Products and recrystallized from methanol. Silicon wafers were purchased from Silicon Inc., and cut into 1 x 2 cm pieces using a diamond-tipped glass cutter. 4-Cyanopentanoic acid dithiobenzoate (CTP) was synthesized according to literature procedure (*51*). 2-Aminoethyl methacrylate (AEMA) was synthesized using a previously reported procedure (*52*). Alkynyl-functionalized CTP was synthesized according to literature procedure (*53*).

Preparation of α-Alkynyl-Functionalized Poly(AEMA)

α-Alkynyl-functionalized poly(AEMA) hydrochloride was prepared via RAFT polymerization. Note that the hydrochloride salt form of the polymer was synthesized and utilized for surface grafting reactions, and the poly(AEMA) abbreviation used throughout the manuscript refers to the hydrochloride salt. The RAFT polymerization of AEMA hydrochloride was conducted in DMSO at 45 °C using V-70 as the radical initiator and alkynyl-functionalized CTP as the RAFT CTA. An aprotic solvent was used to maintain the AEMA pendant group in hydrochloride salt form in order to avoid possible side reactions such as Michael addition reactions. An initial monomer concentration ($[M]_0$) of 1 M was used with a monomer to CTA ratio ($[M]_0/[CTA]_0$) of 400. The CTA to initiator ratio ($[CTA]_0/[I]_0$) was 10:1. A typical procedure is as follows: in a 30 mL round bottom flask, alkynyl-functionalized CTP (23.8 mg, 0.075 mmol), AEMA (4.952 g, 30.0 mmol) and V-70 (2.31 mg, 0.0075 mmol) were dissolved in 30 mL of DMSO. The flask was sealed with a rubber septum and purged with nitrogen for 30 min at 5 °C, and placed in a 45 °C water bath. The polymerization was allowed to proceed for various time intervals before being quenched by rapid cooling in liquid nitrogen. The polymer solution was purified by dialysis for three days against a pH 5 aqueous solution using a Spectra/Por 7 membrane (molecular weight cutoff of 8000) to remove unreacted monomer, and then lyophilized.

Surface Preparation of Silicon Wafers

Silicon wafers were cleaned using piranha solution (30:70 v/v solution of 30% hydrogen peroxide and concentrated sulfuric acid). The solution was heated for 2 h at 100 °C. *Caution: piranha solution is extremely caustic.* Wafers were rinsed in HPLC water, ethanol and acetone sequentially, characterized by ellipsometry, water contact angle, and atomic force microscopy (AFM), and used immediately for subsequent modification.

Deposition of 3-Bromopropyltrichlorosilane on Silicon Wafers

In a glove box, cleaned wafers were placed in a clean, dry glass 50 mL round bottom flask containing 20 mL of anhydrous toluene. 3-Bromopropyltrichlorosilane (0.2 ml, 1 wt %) was directly added via syringe, and the flask was sealed with a septum. The wafers were removed after 45 minutes and sequentially cleaned with toluene, ethanol, and acetone and dried under a stream of nitrogen.

Downloaded by PENNSYLVANIA STATE UNIV on June 23, 2012 | http://pubs.acs.org
Publication Date (Web): November 17, 2010 | doi: 10.1021/bk-2010-1053.ch006

Synthesis of Azide-Modified Silicon Wafers

The azide-modified silicon wafer was prepared by the substitution of a bromo-terminated monolayer with azidotrimethylsilane ($Si(CH_3)_3N_3$) in a glove box equipped with an integrated, cryostated hexane/heptane bath under nitrogen atmosphere. The bromo-functionalized silicon wafer was placed in a clean, dry glass 50 mL round bottom flask containing 20 mL of anhydrous toluene. $Si(CH_3)_3N_3$ (0.4 ml, 2%) was added directly into the toluene by a syringe and the flask was sealed with a septum. The flask was heated at 80 °C for 48 hours without agitation. The substrate was removed and rinsed with toluene, ethanol, and acetone and dried under a stream of nitrogen.

Click Coupling between Poly(AEMA) and Azide-Modified Silicon Wafers

A previously published procedure for the modification of silica nanoparticles via click chemistry was implemented (*36*). A large excess of poly(AEMA) (0.5 g, 0.017mmol), 0.005 g (0.031 mmol) of $CuSO_4$, 0.015 g (0.75 mmol) of sodium ascorbate and 20 mL of DMSO were combined in a round-bottom flask and stirred until the α-alkynyl-functionalized poly(AEMA) was dissolved. The azide-modified silicon wafer was placed in the flask. The mixture was heated in an oil bath at 80 °C for 2 days. Following the reaction, the silicon wafer was placed in a Soxhlet extractor and extracted with water for 18 h.

Polymer and Surface Characterization

α-Alkynyl-functionalized Poly(AEMA) was characterized by aqueous size exclusion chromatography (ASEC-MALLS) at ambient temperature using Eprogen CATSEC columns (100, 300, and 1000 Å). A Wyatt Optilab DSP interferometric refractometer ($\lambda = 690$ nm) and a Wyatt DAWN DSP multiangle laser light scattering detector ($\lambda = 633$ nm) were employed using a solution of one wt% acetic acid in 0.1 M Na_2SO_4 as the eluent at a flow rate of 0.25 mL/min. Monomer conversions were determined by comparing the area of the UV signal corresponding to monomer at t_0 to the area at t_x. A Polymer Laboratories LC1200

Downloaded by PENNSYLVANIA STATE UNIV on June 23, 2012 | http://pubs.acs.org
Publication Date (Web): November 17, 2010 | doi: 10.1021/bk-2010-1053.ch006

UV/vis detector was employed. Absolute MWs and polydispersities were calculated using the Wyatt ASTRA SEC/LS software package. A Varian 500 MHz NMR equipped with a standard 5 mm 1H/13C probe and operating at 499.77 MHz and 125.68 MHz for proton and carbon, respectively, was utilized to identify the homopolymer structure of α-alkynyl-functionalized poly(AEMA) (number of scans = 64, recycle delay = 3.1 μs, 90 degree pulse width = 16 μs, acquisition time = 1.89 μs). The degree of polymerization (DP) and MW were determined via ^{1}H NMR by integration of the relative intensities of the α-alkynyl-functionalized poly(AEMA) methylene-proton resonances at 3.31 ppm (2 protons labeled "c" in Figure 3) and phenyl-protons of CTP between 7.51 and 7.89 ppm (five protons labeled "1", "2", "3" in Figure 3).

Ellipsometric measurements were carried out on a Gaertner ellipsometer, model L116C, with a 632.8 nm He-Ne laser at a 70° angle of incidence. A nominal refractive index of 1.455 was employed for all modified surfaces.

Contact angle measurements were performed utilizing a Rame-Hart goniometer with a 10.0 μl syringe. Static (θ_a) water contact angles were recorded at 0° horizontal. Five measurements were taken across each sample, with their average being used for analysis.

ATR FTIR spectra were collected using a Bio-Rad FTS-6000 FT-IR single beam spectrometer set at a 4 cm^{-1} resolution equipped with a deuterated triglycine sulfate (DTGS) detector and a 45° face angle Ge crystal. Each spectrum represents 400 co-added scans ratioed against a reference spectrum obtained by recording 400 co-added scans of an empty ATR cell. All spectra were corrected for spectral distortions using Q-ATR software (*54*).

Tapping mode AFM measurements were performed with an Agilent 5500 PicoPlus microscope. Experiments were conducted at room temperature in the presence of air. Images were taken between 500 nm^2 and 5 μm^2 scan areas. Standard silicon probes (RTESP cantilevers, Veeco Probe Center) with a 125μm long cantilever, nominal force constant of 40 N/m, and resonance frequency of 275 kHz for tapping mode surface topography, were used as received. The scan rate was 0.7 Hz, and as an additional precaution to eliminate artifacts, images were obtained from at least three macroscopically separated areas of each sample. All images were processed using PicoView 1.4 AFM software and the Gwyddion 2.9 SPM data analysis framework. All experiments were performed at 22±1 °C in a temperature and humidity controlled room unless specified otherwise. Surface roughness was taken as the root-mean-square average of the 5μm^2 height images for each step of the modification process.

Results and Discussion

Preparation of α-Alkynyl-Functionalized Poly(AEMA)

By virtue of the accepted mechanism for RAFT-mediated polymerization, the degenerative chain transfer process that involves a CTA allows one to prepare polymers that carry the respective "Z" and "R" groups at the α- and ω-termini of the polymer chains (*2*). Thus, by synthetically modifying the R group of the CTA, a variety of end-functionalized polymers can be obtained. Due to its

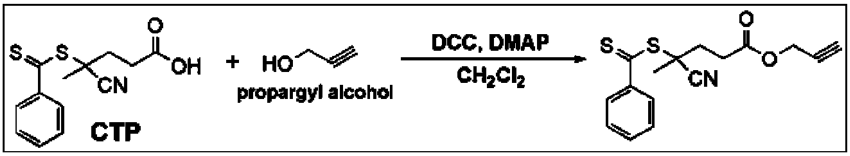

Scheme 1. Preparation of alkynyl-functionalized CTP.

carboxylic acid functionality, CTP has been widely used for modifying the "R" group yielding various functionalized CTAs (*55*). Alkynyl-functionalized CTP was directly synthesized through the esterification reaction between the terminal carboxyl group of CTP and propargyl alcohol using DCC/DMAP coupling agents (70% yield, Scheme 1). Yield was similar to that reported in the literature procedure utilized (*53*). The product structure was determined by ^{1}H NMR as shown in Figure 1 confirming the attachment of propargyl alcohol to CTP.

CTP was chosen based on results reported by our research group for the synthesis of well-defined, low polydispersity homopolymers and diblock copolymers of AEMA via aqueous RAFT polymerization. Specifically, AEMA monomer was polymerized directly in aqueous solution at 50 °C to conversions as high as 95%, resulting in polymers with PDI values lower than 1.2. We also determined that the controlled polymerization of AEMA depends on polymerization temperature. AEMA polymerization performed at 70 °C resulted in loss of CTP activity within 45 minutes leading to an increase in PDI. Our results suggested that the relatively high PDIs reported by previous groups (*52*) are due to the high polymerization temperature, which results in side reactions that lead to broader MW distributions.

To avoid potential side reactions, AEMA polymerizations were carried out in DMSO at 45 °C using V-70 as the radical source and alkynyl-functionalized CTP as the CTA (Scheme 2). DMSO was used to maintain the pendant group of the AEMA hydrochloride in the protonated form during the entire polymerization reaction. For the polymerizations, an initial ratio of $[M]_0$ to $[CTA]_0$ of 400:1 and a $[CTA]_0/[I]_0$ ratio of 10:1 were used. MWs, PDIs and conversion data are shown in Table 1.

ASEC-MALLS traces show unimodal MW distributions, with PDIs below 1.2 and no evidence of high MW termination products (Figure 2). The DP (and thus the MW) was determined via ^{1}H NMR through integration of the relative intensities of AEMA methylene-proton resonance at 3.31 ppm and CTP phenyl-proton resonance between 7.51 and 7.89 ppm (Figure 3). Absolute values of number-average MW (M_n) measured by ASEC are in close agreement with the theoretical values of M_n and the M_n values determined by ^{1}H NMR. The presence of the alkyne group at the end of poly(AEMA) chains was evidenced by the resonance at 2.85 ppm observed in ^{1}H NMR (Figure 3 inset).

Alkyl Azide Modification of Silicon Wafers

Silicon wafers were functionalized with azide groups using a two-step reaction procedure (Scheme 3). In the first step, 3-bromopropyltricholorosilane

Downloaded by PENNSYLVANIA STATE UNIV on June 23, 2012 | http://pubs.acs.org
Publication Date (Web): November 17, 2010 | doi: 10.1021/bk-2010-1053.ch006

Downloaded by PENNSYLVANIA STATE UNIV on June 23, 2012 | http://pubs.acs.org
Publication Date (Web): November 17, 2010 | doi: 10.1021/bk-2010-1053.ch006

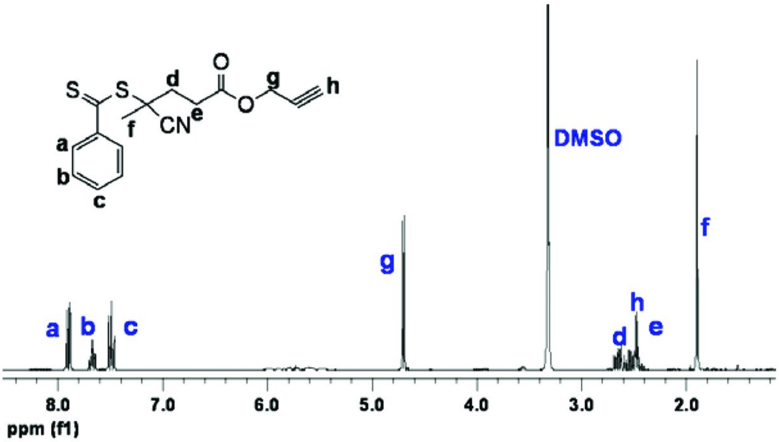

Figure 1. ^{1}H NMR spectrum of alkynyl-functionalized 4-cyanopentanoic acid dithiobenzoate (CTP).

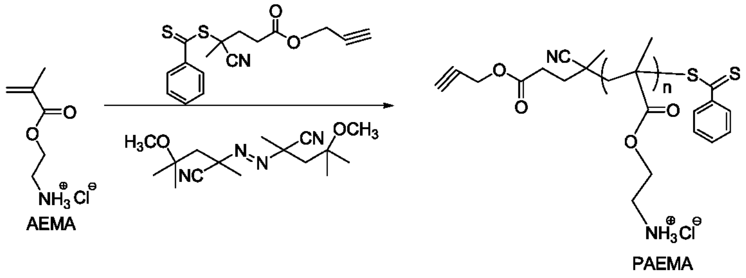

Scheme 2. Preparation α-alkynyl-functionalized poly(AEMA) via RAFT polymerization at 45 °C.

Table 1. Preparation of α-alkynyl-functionalized poly(AEMA) at 45 °C[4]

Time (min)	*M_n[1] (g/mol)*	*M_n[2] (g/mol)*	*M_n[3] (g/mol)*	*PDI[1]*	*Conv.[1] (%)*
150	29000	27000	26000	1.12	42
240	35000	32000	33000	1.13	50
280	39000	36000	37000	1.06	57

[1] Determined by ASEC-MALLS-UV. [2] Determined by ^{1}H NMR. [3] Theoretical molecular weight. [4] [M]:[CTA]:[I] = 400:1:0.1

was used to introduce an alkyl bromide group onto the surface of the silicon wafer. Confirmation of 3-bromopropyltrichlorosilane attachment was achieved by ellipsometry (Table 2), contact angle goniometry (Table 2), and AFM (Table 2 and Figure 4). Ellipsometry data for the alkyl bromide-modified silicon wafer showed a thickness change of 3 nm. This larger than expected thickness indicates that multilayers were obtained, which may be due to the extended reaction time or the trichlorosilane anchoring group having a tendency to undergo surface cross-linking (*56*). The resulting alkyl bromide-functionalized silicon wafer was observed to have a contact angle of 76±0.3°, which is similar to previously reported values (*57*). Tapping mode AFM images of neat silicon wafer and bromide-modified silicon wafer are shown in Figure 4A and Figure 4B. As expected, the neat silicon wafer is smooth with root-mean-square (RMS) roughness value of 0.03 nm (Table 2). There are no visible topographical features. The alkyl bromide-modified silicon wafer surface demonstrates clear morphology changes and surface RMS roughness increases to 0.47 nm (Table 2).

The bromine atoms tethered on the surfaces were substituted with azide groups by the reaction with $Si(CH_3)_3N_3$. In general, this substitution reaction is conducted using sodium azide. However, we found that the limited solubility of sodium azide in DMF leads to a low degree of substitution on the wafers. For this reason, $Si(CH_3)_3N_3$ was used for the substitution reaction, which forms a homogeneous solution in toluene. The modified surfaces were evaluated using ellipsometry, goniometry and AFM (Table 2 and Figure 4). As expected, there was virtually no change in surface layer thickness, contact angle or RMS roughness after azide substitution.

Downloaded by PENNSYLVANIA STATE UNIV on June 23, 2012 | http://pubs.acs.org
Publication Date (Web): November 17, 2010 | doi: 10.1021/bk-2010-1053.ch006

Click Reaction between Alkyl Azide-Functionalized Silicon Wafer and α-Alkynyl-Functionalized Poly(AEMA)

The click reaction is the 1,3-dipolar cycloaddition of azides and alkynes to afford 1,2,3-triazoles (i.e. the Huisgen cycloaddition), often catalyzed with a Cu(I) species (Scheme 4) (*58*). Although 1,3-dipolar cycloaddition reactions are often performed in water to decrease reaction times, we conducted the reaction directly in DMSO to avoid any possible rearrangement reactions of poly(AEMA) at high temperatures. The grafting of α-alkynyl-functionalized poly(AEMA) on azide-functionalized silicon wafer was evaluated through ellipsometry (Table 2), goniometry (Table 2), ATR-FTIR (Figure 5) and AFM (Table 2 and Figure 3). (Note that the reaction was first attempted unsuccessfully in the absence of Cu(I) catalyst, necessitating the reaction scheme shown in Scheme 4.)

The successful modification is evidenced by the appearance of the carbonyl absorbance at 1720 cm^{-1}, indicating the presence of the ester group of α-alkynyl-functionalized poly(AEMA) on the surface (Figure 5). Additional absorbances indicative of polymer surface attachment observed include: the strong absorbances of primary amine at both 1170 cm^{-1} (C-N) and 1620 cm^{-1} (N-H), out of plane ring bending mode absorbances below ~900 cm^{-1}, due to the aromatic ring of the terminal RAFT agent on the poly(AEMA) chains, and aliphatic C-C peaks at ~3000 cm^{-1}. Ellipsometry results provide complimentary evidence of polymer attachment with a surface thickness increase of 15.2 nm between the azide-modified surface and the post-attachment surface (Table 2). Water contact angle measurements indicate a decrease of 29° in the contact angle for the polymer-functionalized surface in comparison to azide-functionalized silicon wafers (Table 2). The tapping mode AFM image of α-alkynyl-functionalized poly(AEMA)-modified silicon wafer shows granular features with an increase of surface RMS roughness to 5.7 nm (Figure 4). Three dimensional (3D) surface topography images of neat silicon wafer and

Downloaded by PENNSYLVANIA STATE UNIV on June 23, 2012 | http://pubs.acs.org
Publication Date (Web): November 17, 2010 | doi: 10.1021/bk-2010-1053.ch006

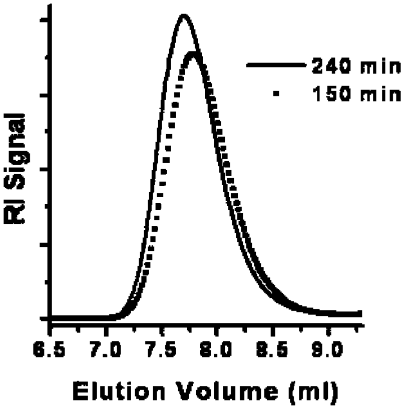

Figure 2. ASEC chromatograms for α-alkynyl-functionalized poly(AEMA) prepared in DMSO at 45 °C.

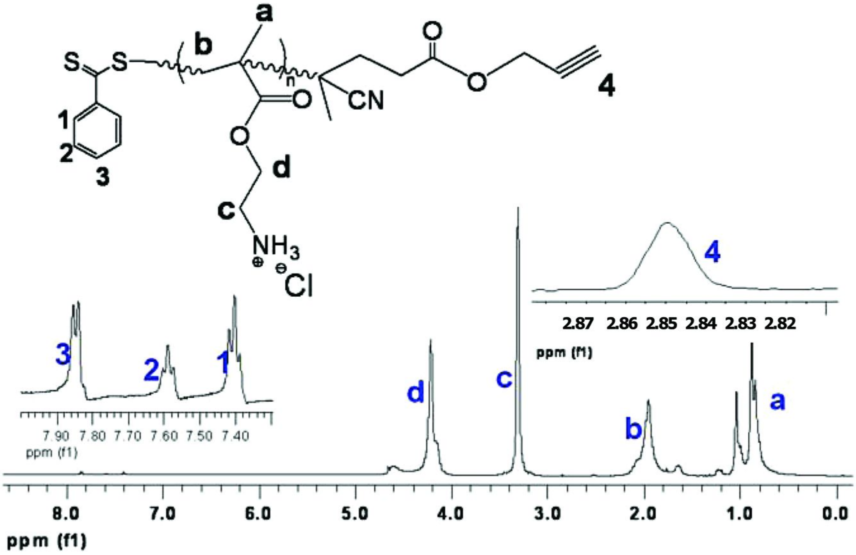

Figure 3. ^1H NMR spectrum of α-alkynyl-functionalized poly(AEMA)

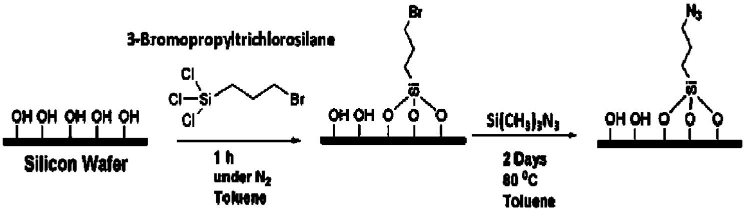
3-Bromopropyltrichlorosilane
Br
N3
Cl
Cl
Si
Cl
Br
OH OH OH OH OH
Silicon Wafer
1 h
under N2
Toluene
OH OH O O O
Si
Si(CH3)3N3
2 Days
80 °C
Toluene
OH OH O O O
Si

Scheme 3. Synthesis of azide-modified silicon wafer.

Downloaded by PENNSYLVANIA STATE UNIV on June 23, 2012 | http://pubs.acs.org
Publication Date (Web): November 17, 2010 | doi: 10.1021/bk-2010-1053.ch006

Table 2. Analysis of Modified Silicon Wafer

Samples	*Surface Thickness[1] (nm)*	*Static Contact Angle[2] (°)*	*RMS Surface Roughness[3] (nm)*
Neat Silicon Wafer (SW)	2.1 ± 0.05	22 ± 0.4	0.03
Alkyl Bromide-Functionalized SW	4.8 ± 0.4	76 ± 0.3	0.47
Alkyl Azide-Functionalized SW	5.1 ± 0.4	82 ± 0.4	0.59
Poly(AEMA)-Modified SW	20.3 ± 3.1	55 ± 0.4	5.70

[1] Determined by ellipsometry. [2] Determined by goniometry. [3] Determined by AFM.

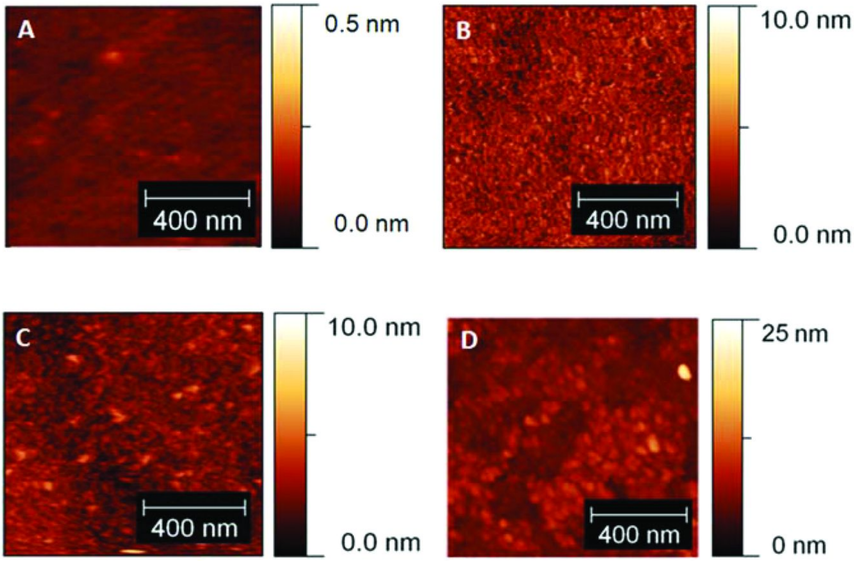

*Figure 4. Tapping mode AFM images of **A.** Neat silicon wafer; **B.** Alkyl bromide-functionalized silicon wafer; **C.** Alkyl azide-functionalized silicon wafer; **D.** Poly(AEMA)-modified silicon wafer.*

the α-alkynyl-functionalized poly(AEMA)-modified silicon wafer are shown in Figure 6. Regular raised features are observed for the polymer-modified surface with continuous surface coverage, indicating the successful surface modification of α-alkynyl-functionalized poly(AEMA) via click chemistry. The relatively high RMS roughness (5.7 nm) in comparison to the average thickness of the polymer layer (15.2 nm) indicates conformational nonuniformity of the tethered polymer chains, i.e. presence of both extended and more tightly coiled or collapsed chains.

The production of the non-uniform grafted polymer surface is the result of the 'grafting-to' approach employed to modify the surface. While this approach is experimentally simple and the synthesis of functionalized polymers in solution provides better control of molecular weight and polymer architecture, the 'grafting-to' method generally yields lower grafting density than the 'grafting-from' method, due to the steric hindrance imposed by the ever-increasing

Downloaded by PENNSYLVANIA STATE UNIV on June 23, 2012 | http://pubs.acs.org
Publication Date (Web): November 17, 2010 | doi: 10.1021/bk-2010-1053.ch006

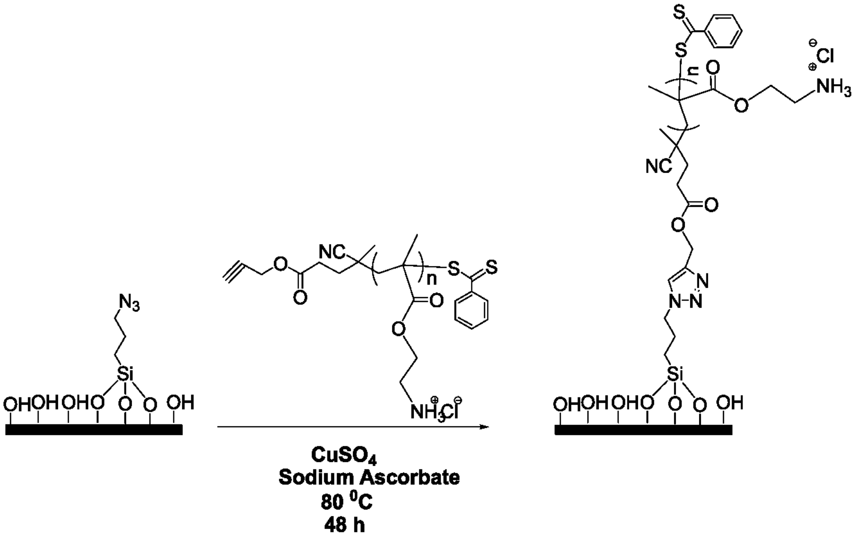

Scheme 4. Surface attachment of α-alkynyl-functionalized poly(AEMA) on alkyl azide-functionalized silicon wafer via click chemistry.

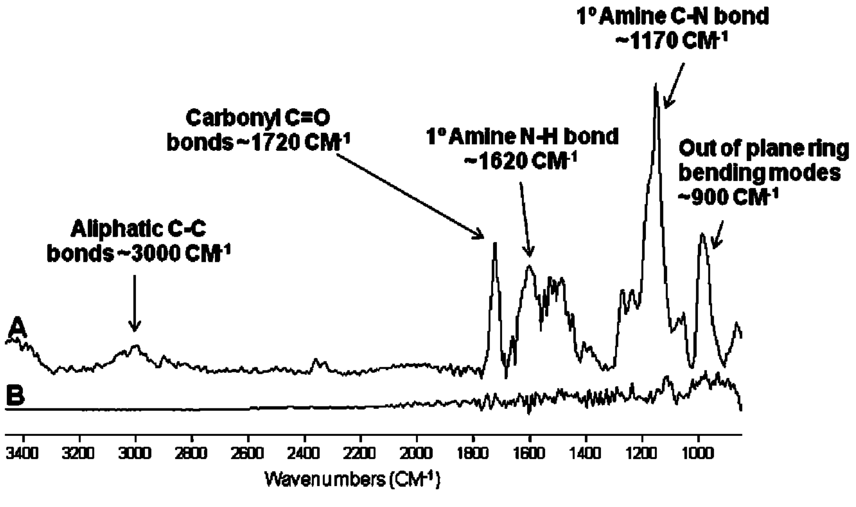

*Figure 5. ATR-FTIR spectra of **A.** Poly(AEMA)-modified silicon wafer surface; **B.** Neat silicon wafer surface.*

density of grafted chains during the progress of the reaction. To determine the coupling efficiency of our system, an estimated grafting density (σ) was calculated using equation (1):

$$\sigma = \Gamma N_A \times 10^{-21} / M = (6.023\Gamma \times 100) / M_n \qquad (1)$$

Downloaded by PENNSYLVANIA STATE UNIV on June 23, 2012 | http://pubs.acs.org
Publication Date (Web): November 17, 2010 | doi: 10.1021/bk-2010-1053.ch006

where Γ is the surface coverage (absorbed amount, mg m^{-2}), M (g/mol) is the molar mass of the attached molecule (measured using ASEC-MALLS) and N_A is Avogadro's number. Γ is calculated according to equation (2):

$$\Gamma = h\rho \qquad (2)$$

where ρ is the bulk density of the attached molecule (g/cm^3) and h is thickness of tethered polymer layer measured via ellipsometry. Using the reported bulk density for AEMA (1.29 g/cm^3) (*59*), a grafting density of 0.39 chains/nm^2 was calculated. This grafting density is relatively high for a 'grafting-to' approach. Ranjan and Brittain recently reported a similar high grafting density of 0.37 chains/nm^2 using click reactions with different polymers for the modification of silica nanoparticles (*11*). Note that Brittain's data was obtained for silica particles, not flat silicon wafers. In general, higher grafting densities are observed with silica nanoparticles, as they are easily suspended in solvent via agitation, resulting in a dynamic system with greater grafting efficiency and more uniform surface modification than that observed in the stationary silicon wafer system.

There is limited data available for 'grafting-to' reactions using click chemistry for attachment of RAFT polymers on silica surfaces. Studies have reported grafting densities varying from a low range of 0.035 to 0.178 polymer chains/nm^2 for immobilization of polymers on a surface, to a high range of 2-5 groups/nm^2 reported for ATRP initiator density on a surface (*60–62*). Specifically pertaining to RAFT polymerization, surface CTA densities have been reported in the range of 0.15-0.54 CTA moieties/nm^2 (*63*, *64*). Brittain and coworkers suggest that RAFT functionalization yields lower grafting densities than ATRP due to the bulky nature of the CTA agent, which limits attachment density during the silanization reaction (*11*). Our calculation of 0.39 chains/nm^2 is consistent with the assumption of steric repulsion.

A theoretical chain length of 30.1 nm was estimated for the fully extended polymer chain employing C—C bond lengths (1.54 Å), sp^3 hybridization angles (109.5°) and measured polymer molecular weight (39,000 amu). The measured polymer layer thickness (avg. thickness 15.2 nm with RMS roughness of 5.7 nm) lies well within the theoretical range. The lower measured polymer thickness value in comparison to the estimate for the fully extended chain results from the presence of varied polymer conformations on the surface (i.e. expanded and collapsed) due to the steric repulsion during the 'grafting-to' process and due to local pH and ionic strength. While the grafting reaction was performed in DMSO with poly(AEMA) in the hydrochloride salt form, the grafted wafers were washed overnight in neutral pH deionized water. Thus it is expected that some of the pendant groups on the grafted chains will exist in the deprotonated form, while others will remain charged. The thickness of the tethered polymer layer depends on electrostatic interactions between the grafted polymer chains, with highly charged chains exisiting in extended conformations due to charge-repulsion, while chains with low charge density adopt collapsed, random coil conformations.

Advantages of the 'grafting-to' approach include experimental simplicity, improved control of polymer architecture prior to attachment to the surface, and commercial availability of solution-based initiators to facilitate the approach.

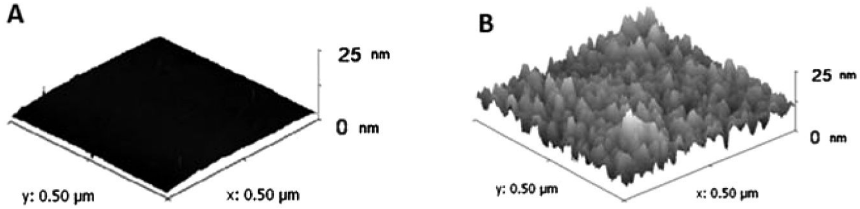

Figure 6. AFM 3D surface topography of ***A.*** *Neat silicon wafer;* ***B.*** *Poly(AEMA)-modified silicon wafer.*

Downloaded by PENNSYLVANIA STATE UNIV on June 23, 2012 | http://pubs.acs.org
Publication Date (Web): November 17, 2010 | doi: 10.1021/bk-2010-1053.ch006

Despite the comparatively lower grafting density in comparison to ATRP surface polymerization, a reasonably high grafting density was obtained using the RAFT polymer/click 'grafting-to' approach.

Conclusion

Herein, we report the synthesis of well-defined, low polydispersity α-alkynyl-functionalized polymers of AEMA via RAFT polymerization. Specifically, AEMA monomer was homopolymerized directly in DMSO using alkynyl-functionalized CTP as the CTA to yield poly(AEMA) with PDI < 1.2. The resulting α-alkynyl-functionalized poly(AEMA) was tethered to alkyl azide-functionalized silicon wafers with a 'grafting-to' method using a click chemistry approach to produce a well-defined primary amine-functionalized surface. The successful surface modification is evidenced through ellipsometry, water contact angle, ATR-FTIR and AFM analysis. An estimated grafting density of 0.39 chains/nm^2 is calculated, indicating an excellent grafting density for the 'grafting-to' method. The pendant primary amine groups on the tethered polymer chains are amenable to a wide range of post-polymerization reactions, such as formation of amides and imines, ring-opening of epoxy groups and Michael addition. The functional surface thus prepared provides a platform for development of materials for applications such as sensors, self-healing materials or stimuli-responsive "smart" films.

Acknowledgments

This research was partially supported by funding from the SBA through award SBAHQ-06-I-0045. It was also supported in part by the MRSEC Program of the National Science Foundation under Award Number DMR 0213883.

References

1. Matyjaszewski, K.; Xia, J. *Chem. Rev.* **2001**, *101* (9), 2921–2990.
2. Moad, G.; Chong, Y. K.; Postma, A.; Rizzardo, E.; Thang, S. H. *Polymer* **2005**, *46* (19), 8458–8468.
3. McCormick, C. L.; Lowe, A. B. *Acc. Chem. Res.* **2004**, *37* (5), 312–325.

4. Coessens, V.; Pintauer, T.; Matyjaszewski, K. *Prog. Polym. Sci.* **2001**, *26* (3), 337–377.
5. Schulz, D. N.; Patil Abhimanyu, O. Functional Polymers: An Overview. *Functional Polymers*; American Chemical Society: Washington, DC, 1998; pp 1−14.
6. Scales, C. W.; Convertine, A. J.; McCormick, C. L. *Biomacromolecules* **2006**, *7* (5), 1389–1392.
7. Mantovani, G.; Ladmiral, V.; Tao, L.; Haddleton, D. M. *Chem. Commun.* **2005**, 2089–2091.
8. Bontempo, D.; Li, R. C.; Ly, T.; Brubaker, C. E.; Maynard, H. D. *Chem. Commun.* **2005**, 4702–4704.
9. Sumerlin, B. S.; Lowe, A. B.; Stroud, P. A.; Zhang, P.; Urban, M. W.; McCormick, C. L. *Langmuir* **2003**, *19* (14), 5559–5562.
10. Lowe, A. B.; Sumerlin, B. S.; Donovan, M. S.; McCormick, C. L. *J. Am. Chem. Soc.* **2002**, *124* (39), 11562–11563.
11. Ranjan, R.; Brittain, W. J. *Macromolecules* **2007**, *40* (17), 6217–6223.
12. York, A. W.; Scales, C. W.; Huang, F.; McCormick, C. L. *Biomacromolecules* **2007**, *8* (8), 2337–2341.
13. Rostovtsev, V. V.; Green, L. G.; Fokin, V. V.; Sharpless, K. B. *Angew. Chem., Int. Ed.* **2002**, *41* (14), 2596–2599.
14. Tornoe, C. W.; Christensen, C.; Meldal, M. *J. Org. Chem.* **2002**, *67* (9), 3057–3064.
15. Kolb, H. C.; Finn, M. G.; Sharpless, K. B. *Angew. Chem., Int. Ed.* **2001**, *40* (11), 2004–2021.
16. Joralemon, M. J.; O'Reilly, R. K.; Hawker, C. J.; Wooley, K. L. *J. Am. Chem. Soc.* **2005**, *127* (48), 16892–16899.
17. O'Reilly, R. K.; Joralemon, M. J.; Wooley, K. L.; Hawker, C. J. *Chem. Mater.* **2005**, *17* (24), 5976–5988.
18. Wu, P.; Malkoch, M.; Hunt, J. N.; Vestberg, R.; Kaltgrad, E.; Finn, M. G.; Fokin, V. V.; Sharpless, B. K.; Hawker, C. J. *Chem. Commun.* **2005**, 5775–5777.
19. Riva, R.; Schmeits, S.; Stoffelbach, F.; Jérôme, C.; Jérôme, R.; Lecomte, P. *Chem. Commun.* **2005**, 5334–5336.
20. Van Steenis, D. J. V. C.; David, O. R. P.; Van Strijdonck, G. P. F.; Van Maarseveen, J. H.; Reek, J. N. H. *Chem. Commun.* **2005**, 4333–4335.
21. Parrish, B.; Breitenkamp, R. B.; Emrick, T. *J. Am. Chem. Soc.* **2005**, *127* (20), 7404–7410.
22. Díaz, D. D.; Punna, S.; Holzer, P.; McPherson, A. K.; Sharpless, K. B.; Fokin, V. V.; Finn, M. G. *J. Polym. Sci., Part A: Polym. Chem.* **2004**, *42* (17), 4392–4403.
23. Tsarevsky, N. V.; Bernaerts, K. V.; Dufour, B.; Du Prez, F. E.; Matyjaszewski, K. *Macromolecules* **2004**, *37* (25), 9308–9313.
24. Opsteen, J. A.; Van Hest, J. C. M. *Chem. Commun.* **2005**, 57–59.
25. Tsarevsky, N. V.; Sumerlin, B. S.; Matyjaszewski, K. *Macromolecules* **2005**, *38* (9), 3558–3561.
26. Sumerlin, B. S.; Tsarevsky, N. V.; Louche, G.; Lee, R. Y.; Matyjaszewski, K. *Macromolecules* **2005**, *38* (18), 7540–7545.

Downloaded by PENNSYLVANIA STATE UNIV on June 23, 2012 | http://pubs.acs.org
Publication Date (Web): November 17, 2010 | doi: 10.1021/bk-2010-1053.ch006

27. Gao, H.; Louche, G.; Sumerlin, B. S.; Jahed, N.; Golas, P.; Matyjaszewski, K. *Macromolecules* **2005**, *38* (22), 8979–8982.
28. Laurent, B. A.; Grayson, S. M. *J. Am. Chem. Soc.* **2006**, *128* (13), 4238–4239.
29. Johnson, J. A.; Lewis, D. R.; Díaz, D. D.; Finn, M. G.; Koberstein, J. T.; Turro, N. J. *J. Am. Chem. Soc.* **2006**, *128* (20), 6564–6565.
30. Ladmiral, V.; Mantovani, G.; Clarkson, G. J.; Cauet, S.; Irwin, J. L.; Haddleton, D. M. *J. Am. Chem. Soc.* **2006**, *128* (14), 4823–4830.
31. Agut, W.; Taton, D.; Lecommandoux, S. B. *Macromolecules* **2007**, *40* (16), 5653–5661.
32. Lutz, J.-F.; Börner, H. G.; Weichenhan, K. *Macromol. Rapid Commun.* **2005**, *26* (7), 514–518.
33. Vogt, A. P.; Sumerlin, B. S. *Macromolecules* **2006**, *39* (16), 5286–5292.
34. O'Reilly, R. K.; Joralemon, M. J.; Hawker, C. J.; Wooley, K. L. *J. Polym. Sci., Part A: Polym. Chem.* **2006**, *44* (17), 5203–5217.
35. Gondi, S. R.; Vogt, A. P.; Sumerlin, B. S. *Macromolecules* **2007**, *40* (3), 474–481.
36. Ranjan, R.; Brittain, W. J. *Macromol. Rapid Commun.* **2008**, *29* (12−13), 1104–1110.
37. Ostaci, R.-V.; Damiron, D.; Capponi, S.; Vignaud, G.; Leger, L.; Grohens, Y.; Drockenmuller, E. *Langmuir* **2008**, *24* (6), 2732–2739.
38. Wang, L.; Tian, Y.; Ran, Q.; Hu, Z.; Xu, J.; Xian, Y.; Peng, R.; Jin, L. *Electrochem. Commun.* **2009**, *11* (2), 339–342.
39. O'Reilly, R. K.; Hawker, C. J.; Wooley, K. L. *Chem. Soc. Rev.* **2006**, *35*, 1068–1083.
40. Read, E. S.; Armes, S. P. *Chem. Commun.* **2007**, 3021–3035.
41. Deming, T. J. *Nature* **1997**, *390* (6658), 386–389.
42. Wong, M. S.; Cha, J. N.; Choi, K.-S.; Deming, T. J.; Stucky, G. D. *Nano Lett.* **2002**, *2* (6), 583–587.
43. Holowka, E. P.; Pochan, D. J.; Deming, T. J. *J. Am. Chem. Soc.* **2005**, *127* (35), 12423–12428.
44. Yuan, J.-J.; Jin, R.-H. *Langmuir* **2005**, *21* (7), 3136–3145.
45. Jin, R.-H.; Yuan, J.-J. *Macromol. Chem. Phys.* **2005**, *206* (21), 2160–2170.
46. Yuan, J.-J.; Mykhaylyk, O. O.; Ryan, A. J.; Armes, S. P. *J. Am. Chem. Soc.* **2007**, *129* (6), 1717–1723.
47. Chen, X.; Armes, S. P. *Adv. Mater.* **2003**, *15* (18), 1558–1562.
48. Chen, X. Y.; Armes, S. P.; Greaves, S. J.; Watts, J. F. *Langmuir* **2004**, *20* (3), 587–595.
49. Housni, A.; Cai, H.; Liu, S.; Pun, S. H.; Narain, R. *Langmuir* **2007**, *23* (9), 5056–5061.
50. Alidedeoglu, A. H.; York, A. W.; McCormick, C. L.; Morgan, S. E. *J. Polym. Sci., Part A: Polym. Chem.* **2009**, *47* (20), 5405–5415.
51. Mitsukami, Y.; Donovan, M. S.; Lowe, A. B.; McCormick, C. L. *Macromolecules* **2001**, *34* (7), 2248–2256.
52. He, L.; Read, E. S.; Armes, S. P.; Adams, D. J. *Macromolecules* **2007**, *40* (13), 4429–4438.

Downloaded by PENNSYLVANIA STATE UNIV on June 23, 2012 | http://pubs.acs.org
Publication Date (Web): November 17, 2010 | doi: 10.1021/bk-2010-1053.ch006

53. Li, Y.; Benicewicz Brian, C. *Polym. Prepr. (Am. Chem. Soc., Div. Polym. Chem.)* **2007**, *48* (1), 524–525.
54. Urban, M. W. *Attenuated Total Reflectace Spectroscopy of Polymers Theory and Practice*; Oxford University Press: 1998; p 256.
55. Patton, D. L.; Advincula, R. C. *Macromolecules* **2006**, *39* (25), 8674–8683.
56. Fadeev, A. Y.; McCarthy, T. J. *Langmuir* **2000**, *16*, 7268–7264.
57. Fadeev, A. Y.; McCarthy, T. J. *Langmuir* **1999**, *15* (21), 7238–7243.
58. Huisgen, R. 1,3-Dipolar Cycloaddition. Introduction, Survey and Mechanism. In *1,3-Dipolar Cycloaddition Chemistry*; Padwa, A., Ed.; Wiley Interscience: 1984; Vol. 1.
59. Krasia, T. Synthesis and Colloidal Properties of a Novel Type of Block Copolymers with beta-Dicarbonyl Groups. University of Postdam, Potsdam, Germany, 2003.
60. Guo, T.-Y.; Liu, P.; Zhu, J.-W.; Song, M.-D.; Zhang, B.-H. *Biomacromolecules* **2006**, *7* (4), 1196–1202.
61. Matyjaszewski, K. Controlled/Living Radical Polymerization. In *Controlled/Living Radical Polymerization From Synthesis to Materials*; Matyjaszewski, K., Ed.; ACS Symposium Series; American Chemical Society: Washington, DC, 2006; pp 2−12.
62. von Werne, T.; Patten, T. E. *J. Am. Chem. Soc.* **2001**, *123* (31), 7497–7505.
63. Li, C.; Benicewicz, B. C. *Macromolecules* **2005**, *38* (14), 5929–5936.
64. Li, C.; Han, J.; Ryu, C. Y.; Benicewicz, B. C. *Macromolecules* **2006**, *39* (9), 3175–3183.

Downloaded by PENNSYLVANIA STATE UNIV on June 23, 2012 | http://pubs.acs.org
Publication Date (Web): November 17, 2010 | doi: 10.1021/bk-2010-1053.ch006

Chapter 7

Synthetic Reactive Polyelectrolytes for Cell Encapsulation

**M. A. Jafar Mazumder,[1,*] Nicholas A. D. Burke,[1] Feng Shen,[2]
Terry Chu,[1] Murray A. Potter,[2] and Harald D. H. Stöver[1,*]**

**[1]Department of Chemistry, McMaster University, 1280 Main Street West,
Hamilton, ON, Canada, L8S 4M1**
**[2]Department of Pathology & Molecular Medicine, McMaster University,
1200 Main Street West, Hamilton, ON, Canada, L8N 3Z5**
[*]mazumdma@mcmaster.ca; stoverh@mcmaster.ca

In this work we studied the synthesis and characterization of reactive polyelectrolytes that are capable of forming covalent cross-links, and that can be used in cell encapsulation. In the first part we outline the synthesis and characterization of these polyelectrolytes, and their use to form covalently cross-linked outer shells around calcium alginate microcapsules. The second part presents the formation of covalently cross-linked networks within the cores of calcium alginate microcapsules. The encapsulation processes, capsule morphology, mechanical strength, permeability and biocompatibility are discussed in some detail. The resulting capsules showed improved mechanical strength yet remain cyto-compatible. This approach to cell-encapsulation may be useful for cell immuno-isolation in therapeutic cell transplants.

Introduction

Encapsulation of cells within semi-permeable polymer shells or beads is a potentially powerful tool for the treatment of enzyme deficiency disorders such as lysosomal storage disorders, neurological disorders, dwarfism, hemophilia, cancer and diabetes. Encapsulation of non-autologous cells can provide mechanical protection and immuno-isolation, permitting the use of standard cell lines that are genetically modified to express key enzymes or other actives missing in patients.

In Polymeric Delivery of Therapeutics; Morgan, S., et al.;
ACS Symposium Series; American Chemical Society: Washington, DC, 2010.

The capsule wall serves as a semi-permeable membrane that allows the exchange of oxygen, metabolites and release of therapeutic proteins, while obscuring the encapsulated cells from the host's immune system (*1–5*). These capsules need to be compatible with both host and implanted cells and should not degrade *in vivo*. This requires capsule walls with suitable molecular weight (MW) cut-off, and ideally some form of cross-linking to enhance resistance to biochemical and mechanical degradation.

The most common cell encapsulation approach involves the alginate/ poly-L-lysine/alginate (APA) capsules as first described by Lim and Sun (*5*). These capsules are primarily composed of alginate, an anionic polysaccharide isolated from marine brown algae. Alginates are linear binary copolymers of β-D-mannuronic acid (M) and α-L-guluronic acid (G) residues. Calcium ions are used to cross-link G-rich regions of the alginate chains, which leads to the formation of firm calcium alginate (CaAlg) hydrogel beads. The resulting CaAlg beads are coated with poly-L-lysine (PLL) to strengthen the outer bead surface and control permeability (*6*). A final coating with Na alginate (Alg) is applied in order to hide the cationic PLL from the host (*4*) and thus make the capsules biocompatible.

While APA capsules meet many of the requirements for immuno-isolation of cells when implanted into mice (*7*), they have at times shown insufficient strength when implanted into larger animals such as dogs, where they collapse within 2 weeks (*8*). This may be due to the destabilization of the alginate core matrix through slow exchange of calcium ions with other physiological ions and/or the loss or degradation of the polyelectrolyte overcoats (*9*, *10*).

A number of studies have attempted to address the challenge of long-term mechanical stability by varying the MW (*11*) or G/M ratio of the alginate (*4*, *12–14*), using uncoated alginate beads (*15*), different cross-linking ions (*14*, *16*) and polyelectrolytes (*17–20*) to coat alginate based capsules. Examples include Alg-chitosan-Alg (*21*), Alg-PLL-poly(acrylic acid) (*19*), Alg-PLL-poly(ethylene glycol), Alg-chitosan-poly(ethylene glycol), and Alg-PLL-poly(ethylene glycol)-Alg (*20*), Alg-poly-L-ornithine-Alg (*17*, *22*), Alg-poly(allylamine)-Alg (*23*), Alg-PEI- poly(acrylic acid)-PEI-Alg, and Alg-PEI-carboxymethylcellulose-PEI-Alg capsules (*24*).

A number of fully synthetic polymers such as poly(hydroxyethyl methacrylate-*co*-methyl methacrylate), p(HEMA-*co*-MMA) (*25*), poly(hydroxyl ethylmethacrylate-*co*-ethyl methacrylate), p(HEMA-*co*-EMA) (*26*) and polyphosphazene (PPP) (*2*) have been studied as biomaterials for microencapsulation.

Several groups have explored ways to improve the capsule strength by photo polymerization of (meth)acrylate-functionalized alginate (*13*, *27–30*) or of other monomers within the alginate core (*31*, *32*). Cross-linking of Alg-chitosan capsules with glutaraldehyde or carbodiimide was shown to improve their mechanical strength (*33*), though these small-molecule cross linkers raise serious toxicity issues. Photo polymerization of monomer-functionalized alginate (*13*, *27–30*), or of monomers within the alginate core (*31*, *32*), was used to strengthen the capsules, though irradiation and the presence of photo initiator and monomers again posed challenges to the encapsulated cells. Recently, Hallé and coworkers

(*34*, *35*) studied APA capsules in which a photoactivatable crosslinker was used to covalently link the PLL chains with other PLL chains and with adjacent alginate chains, in both the surface of the core and the outer coating. These capsules displayed greatly improved mechanical stability while maintaining the cell viability and permeability of standard APA capsules. In addition, these covalently cross-linked capsules prevented the escape of malignant cells into the body of the recipient (*36*).

Another approach has been to examine the use of alternate hydrogel cores (*2*, *37*), including those made of composite materials. Reinforcement of the alginate core through the formation of an interpenetrating network or composite may lead to improved mechanical properties while maintaining most of the desirable properties of Alg.

A number of alginate composite materials have been explored for cell encapsulation (*38*). Compounds added to the alginate forming the bead core were designed to be thermally (agarose (*39*)), ionically (carrageenan (*40*)) or photochemically gelled (*41*), designed to modify viscosity or water content (carboxymethylcellulose (*42*)), act as wall forming materials (cellulose sulphate (*43*), heparin (*42*)), control permeability or provide an improved environment for cell growth (chitlac - lactitol-functionalized chitosan (*44*)). Childs and coworkers formed a composite capsule composed of alginate and poly(sodium acrylate-*co*-N-vinylpyrrolidone) formed by photo polymerization of monomers allowed to diffuse into the CaAlg beads (*31*).

We recently described a pair of polyelectrolytes bearing complementary reactive groups that underwent spontaneous mutual cross-linking to produce a covalently cross-linked polyelectrolyte shell on CaAlg beads (*45*). In contrast to photochemical cross-linking approaches, this cross-linking reaction is based on condensation reactions that occur instantly upon contact. The resulting coated alginate capsules showed enhanced resistance to mechanical and chemical stress, attributed to the cross-linked outer coat. The improvements were however limited, and there was evidence of fibrotic overcoats after implantation, indicating an adverse immune reaction. Analogous four-layer shells, that included outer layers of PLL and alginate, led to improved biocompatibility, and further enhanced mechanical properties (*46*). Recently we investigated amine-bearing polyacrylate as possible replacements for PLL in the preparation of capsules for cell encapsulation. One of the synthetic polycations, poly(N-(3-aminopropyl)methacrylamide) (PAPM), was found to be a promising alternative to PLL (*47*).

We also used reactive polyelectrolytes to reinforce the core of CaAlg capsules. This process involves adding the reactive polyanion to the original alginate solution such that it first becomes trapped in the CaAlg core, and subsequently cross-linked by in-diffusion of PLL of suitable MW (*48*).

This process allows further control over wall thickness and location, compared to the usual sequential layer-by-layer deposition of polyelectrolytes. In one scenario, larger PLL chains (MW ≥ 15-30k) should lead to covalently cross-linked analogs to the conventional APA capsules, as these PLL chains may not penetrate deeply into the CaAlg bead. The second scenario, involving smaller PLL chains (MW < 15k) should lead to covalently core-cross linked capsules, for which loss of alginate due to calcium-sodium exchange or oxidative breakdown (*49*) would be less critical. A third scenario, sequential exposure of the composite beads to high and low MW PLL, may permit separate control over shell and core cross-linking. In all cases the beads would receive a final coat of alginate, or the reactive polyanions (Scheme 1), in order to react surficial excess of polycation, and present an anionic surface to the host.

The first part of this chapter reviews the synthesis and characterization of cationic copolymers composed of methacryloyloxyethyl trimethyl ammonium hydrochloride and aminoethyl methacrylate, and the homopolymer of N-(3-aminopropyl)methacrylamide hydrochloride (APM), as well as reactive anionic copolymers composed of methacrylic acid sodium salts with methacryloyloxy ethyl acetoacetate. This part also describes their assembly and covalent crosslinking in the outer shell of CaAlg capsules. The second part concentrates on the core reinforcement process by the formation of covalent cross-linked networks throughout the core and/or shell of CaAlg capsules. Also, the morphology, mechanical strength and permeability of the capsules, the viability of encapsulated cells and the compatibility of the capsules with a murine host will be discussed in some detail.

Experimental

Materials

The syntheses of cationic copolymer p(MOETAC-*co*-AEM.HCl), C70 (70/30 mol ratio copolymer of [2-(methacryloyloxy)ethyl] trimethyl ammonium hydrochloride and 2-aminoethyl methacrylate) (*45*), its FITC analogs C70*f* (*45*), anionic copolymer p(MAANa-*co*-MOEAA), A70 (70/30 mol ratio copolymer of sodium methacrylate and 2-[methacryloyloxy]ethyl acetoacetate) of variable molecular weight (*48*), and its FITC analogs A70*f*, were described elsewhere (*45*, *48*).

The analogous A60 (THF, yield: 71%) and A50 (1:1 THF/ethanol, yield: 85%) were prepared by free radical polymerization in a similar fashion to A70 (*48*) except for the use of the polymerization solvents shown in brackets. Preparations of poly(sodium methacrylate) A100 (*45*), its FITC analog A100*f* (*48*), poly(2-aminoethyl methacrylate) C0 (*47*), poly(2-(methacryloyloxy)ethyl]trimethyl ammonium hydrochloride) C100 (*45*), poly(N-(3-aminopropyl)methacrylamide hydro chloride) PAPM (*47*), and Rhodamine labelled poly-L-lysine (PLL*r*) (*48*) have been described elsewhere in detail.

Instrumentation

The composition of A70, A60 and A50 was determined by ^{1}H NMR spectroscopy in DMSO-d6 using a Bruker AV 200 spectrometer. The composition of C70, and the pKa values of all amine-based polycations were determined by potentiometric titration with 0.1M NaOH on a PC titrate automatic titrator (Man Tech Associates). The degree of labelling with FITC and Rhodamine was measured on a Varian Cary 50 BIO UV-Vis spectrophotometer. Gel permeation chromatography (GPC) analyses were performed at a nominal flow rate of 0.8 mL/min. The columns were maintained at 35°C and the system was calibrated with commercially available narrow dispersed molecular weight polyethylene glycol (PEG) standards (Waters, Mississauga, ON). The GPC system consisted of a Waters 515 HPLC pump, Waters 717 plus Autosampler, three Ultrahydrogel columns (0-3 kDa, 0-50 kDa, 2-300 kDa), and a Waters 2414 refractive index detector. Dextran-FITC samples were eluted with 0.1 M $NaNO_3$, while for A100, A100*f*,A70, A60 and A50, the mobile phase was 0.3 M $NaNO_3$ in 0.05M phosphate buffer (pH 7). All polyanions were prepared for GPC analysis by the addition of a stoichiometric amount of 1M NaOH to the acid-form precursor polymer, followed by dilution with the mobile phase. An Ubbelohde viscometer (viscometer constant: 0.00314 cSt/s), was used to determine MWs of all polycations dissolves in 1M NaCl at 20 ± 0.1°C. Prior to the measurements, all stock solutions were filtered through a 0.45 μm membrane filter.

Optical microscope images of polyelectrolyte complexes, and capsules were taken using an Olympus BX-51 optical microscope fitted with a Q-Imaging Retiga EXi digital camera and Image Pro software. Phase contrast microscope images were taken using a Wild M40 microscope. A Confocal laser scanning imaging system equipped with air-cooled Argon and HeNe lasers (LASOS; LGK 7628-1) and a ZEISS LSM 510 microscope using LSM Image browser software (version 3.5), was used to study the distribution of FITC and Rhodamine-labeled polymers in the capsules

Preparation of Ca Alg and Ca(A/A70) Beads

The CaAlg and Ca(A/A70) composite beads were prepared using an approach described by Ross et al. (*50*) Briefly, to prepare a Ca(A/A70) composite beads, aqueous solutions of 1.5 wt% Na alginate and 0.5 wt% A70 or A70*f* at pH 7 were filtered through sterile 0.45 μm Acrodisc syringe filters (Pall Corporation, USA). A modified syringe pump (Rassel Mechanical Inc. pump, model # A-99) was used to extrude the Alg-A70 mixture at a rate of 30.1 mL/hr through a 27-gauge blunt needle (Popper & Sons, New York), with a concentric airflow (4 L/min) passing by the needle tip to induce droplet formation. The droplets were collected in a 1.1 wt% calcium chloride, 0.45 wt% sodium chloride gelling bath (10x Alg-A70 volume) causing the formation of Ca(A/A70) composite beads. Twenty minutes after bead formation was complete, the supernatant was removed, and the resulting concentrated Ca(A/A70) composite bead suspension was washed in sequence with four-fold volumes of a) 1.1 wt% $CaCl_2$, 0.45 wt% NaCl for 2 minutes; b) 0.55 wt% $CaCl_2$, 0.68 wt% NaCl for 2 minutes; c) 0.28 wt% $CaCl_2$, 0.78 wt% NaCl for 2 minutes; d) 0.1 wt% CHES, 1.1 wt% $CaCl_2$, 0.45 wt% NaCl for 3 minutes.; and then e) 0.9 wt% NaCl for 2 minutes and stored in saline.

Analogous cell-containing composite beads were prepared by preparing a core solution containing 1.5 wt% sodium alginate, 0.5 wt% A70, and 2 million C_2C_{12} cells per mL of saline. This suspension was extruded to form beads as described above, except for the use of an Orion sage pump, model # M362 located in a sterile laminar flow hood, and a liquid flow rate of 99.9 mL/hour. The cell containing

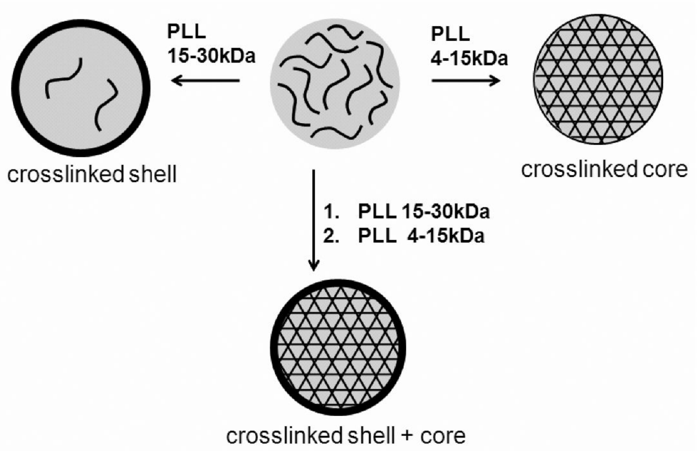

Scheme 1. Schematic representation of the capsule morphologies formed when embedding reactive polyanion within the CaAlg capsule, followed by reaction with high MW PLL, low MW PLL, and sequentially with high and low MW PLL.

capsules were washed as above, and stored in serum free media at 4°C for further use.

The corresponding CaAlg beads were prepared as described above, without adding A70 to the extruding mixture.

Encapsulation Procedure

APA control capsules were prepared by successive exposure to PLL followed by Alg as described elsewhere (*51*). For the 2-layer capsules, CaAlg beads were coated with 0.5 wt% C70 and 0.5 wt% A70 for 10 min each. For 4-layer capsules, the resulting CaAlg-C70-A70 capsules were coated with 0.05 wt% PLL for 6 min, and then with 0.03 wt% Alg for 4 min. Each layering step was followed by sequential washes described elsewhere (*45*, *46*). For some 2-layer capsules, C70 was replaced by PAPM or PLL for comparison. For composite capsules, Ca(A/A70) composite beads were exposed to 0.05 or 0.5 wt% PLL (pH = 8, saline) for 6 minutes, followed by sequential washes (*45*, *46*) and then coated with 0.03 wt% Alg for 4 minutes, followed by three washes with 0.9 wt% NaCl. After the final washing step, in each case the cell containing capsules were cultured in serum free media in a tissue culture incubator at 37°C, while empty capsules were stored in normal saline.

Microcapsules Properties

The chemical and mechanical stress tests for capsule integrity (*47*), the protein (bovine serum albumin) uptake by capsules (*47*), and permeability studies (*48*) were described elsewhere.

C_2C_{12} myoblast cells from the American Type Culture Collection [ATCC] were cultured and encapsulated, and the *in vitro* and *in vivo* cell viabilities measured as described in the literature (*45*).

Mechanical Stabilities

The mechanical properties of individual capsules were measured using a micro compression tester. Single capsules were compressed between a 4 mm^2 silicon wafer attached to a piezo-electric transducer, and a glass microscopy slide mounted on an inverse microscope. The wafer was positioned over one capsule at a time and moved down vertically at a constant speed of 10 μm/s with the help of a stepper motor while plotting the force registered against vertical displacement. Compression data were corrected both for the buoyancy of the silicon wafer, and for the elastic give of the experimental set up. The experiments were performed at room temperature (23 ± 2 °C).

Results and Discussion

The aim of this chapter is to use the oppositely charged reactive polyelectrolytes developed in our lab to strengthen CaAlg beads by the formation of cross-linked interpenetrating networks at the outer shell or throughout the core, and to compare their properties with the conventional APA capsules.

Synthesis of Polyelectrolytes

The synthetic polyelectrolytes were prepared by conventional free radical polymerization. The structure and properties of the natural and synthetic polyelectrolytes used in this research are described in Scheme 2 and Table 1. The composition of copolymers was measured by either titration or ^{1}H NMR, and found to closely match the feed ratio of the two monomers. Typically, monomer to initiator ratios of 50:1 and 100:1 were used for both polycations and polyanions. However, to obtain polyanions (A70) with number average MWs of 22, 42 and 149k, respectively, monomer to initiator ratios of 20:1, 100:1 and 800:1 were used. Attempts to prepare higher MW of A70 resulted in gellation, attributed to covalent cross-linking during polymerization.

Fluorescently labelled versions of the polymers were prepared by reaction with FITC (A70*f*, C70*f*) or via copolymerization with fluorescein O-methacrylate (A100*f*). The final label contents were determined by UV/Vis spectroscopy, with C70*f*, A70*f*-22k, A70*f*-42k, A70*f*-149k, and A100*f* found to have 1.7, 0.22, 0.34, 0.32, and 0.42 mol% of the total monomer units labelled with fluorescein. Unless specifically noted, A70 or A70*f* with a MW of 42k was employed throughout the research. PLL having MWs of 1-4k, 4-15k, and 15-30k were similarly labelled by reaction with rhodamine B isothiocyanate (PLL*r*), leading to label contents of 0.76, 0.77 and 0.62 mol%, respectively.

Physical State of the Polyelectrolyte Complexes (PECs)

Initial model experiments were carried out to understand the interaction between polycations and polyanions, and $CaCl_2$ used in this study.

CaAlg is a solid gel with significant mechanical strength. CaA100, obtained by mixing a 1 wt% solution of A100 with excess 100 mM $CaCl_2$, as well as CaA90 and CaA80 formed liquid coacervate complexes (images not shown), reflecting weaker interactions of Ca^{2+} with these polyanions. CaA70 (22, 42 or 149k), CaA60 and CaA50 showed no macroscopic phase separation, likely due to the lower carboxylate content of these polymers, indicating that these polyanions should retain some mobility even within the CaAlg beads.

Polyelectrolyte complexation between oppositely charged polyanions (Alg, A100, A70) and polycations (PLL, C0, C70, C100, PAPM) at 1 wt% total polymer concentration and pH 7 all gave phase-separated solids. Ionic polyelectrolyte complexes (PECs) formed with the non-reactive analogs, C100 and A100, were shown earlier to dissolve when exposed to [NaCl] > ~500 mM (*52*). In contrast, the solid PECs between primary amine-containing polymers and A70 only swelled upon exposure to 2M NaCl, but did not dissolve (Figure 1), reflecting the presence of covalent cross-links. Formation of such cross-linked complexes throughout or at the surface of CaAlg capsules should lead to capsules better able to resist environmental stresses compared to purely ionic polyelectrolyte complexes.

A model study was also undertaken to further probe the nature and strength of the interactions between the nonreactive polycation, C100 and polyanion, A100 in presence of gelling (Ca^{2+}) and non-gelling (Na^+) ions. It was found that increasing the non-gelling ion (Na^+) changes the solid PEC first into a liquid, and above 350 mM, into soluble species. In contrast, addition of gelling ion (Ca^{2+}) causes displacement of the C100 from the complex, until at $[CaCl_2] \geq 100$ mM the liquid complex consists of almost exclusively CaA100, with only traces of C100 detectable by ^1H NMR (data not shown).

Two-Layer (A-C70-A70) Microcapsules

CaAlg beads as used for cell encapsulation consist of highly hydrated alginate networks that are ionically cross-linked mainly through their guluronic acid residues. Exposure to aqueous solutions of PLL or other polycations, followed by exposure to a biocompatible polyanion, usually alginate, has been a common approach to improve strength as well as permeability control of CaAlg beads containing live cells. Failure modes in long-term implantation may include calcium loss to the host, immune or inflammatory response of the host to the encapsulated cells or to the alginate, loss of polyelectrolytes coating, and/or mechanical degradation.

We have investigated the feasibility of using the synthetic polyelectrolytes C70 and A70 to replace the conventional PLL and outer alginate, respectively, for the preparation of stronger capsules. The key to this approach is that the cross-links are formed between complementary reactive groups that are attached to two different polyelectrolytes. The polycation and polyanion bear amino and acetoacetate groups, respectively, that undergo *in situ* covalent cross-linking

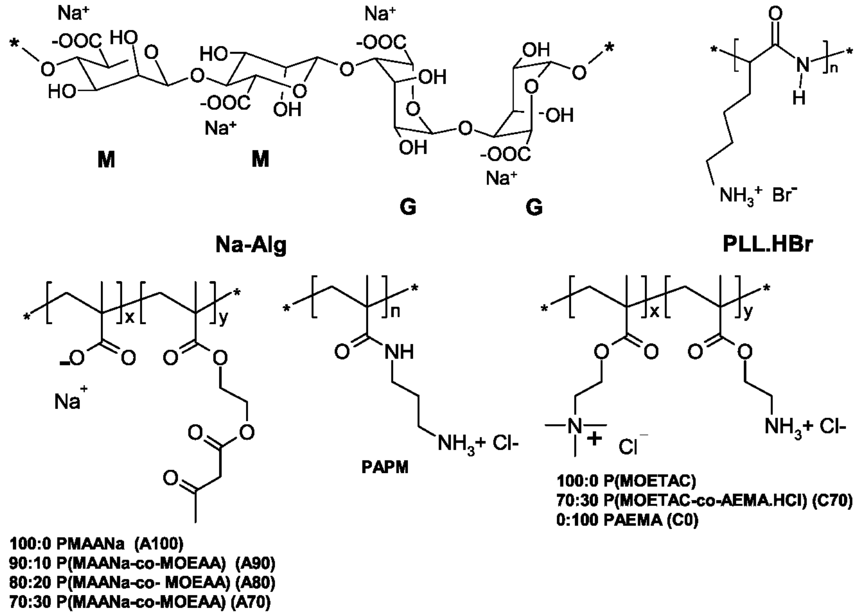
Na-Alg
M
M
G
G
PLL.HBr
PAPM
100:0 PMAANa (A100)
90:10 P(MAANa-co-MOEAA) (A90)
80:20 P(MAANa-co- MOEAA) (A80)
70:30 P(MAANa-co-MOEAA) (A70)
100:0 P(MOETAC)
70:30 P(MOETAC-co-AEMA.HCl) (C70)
0:100 PAEMA (C0)

Scheme 2. Natural and Synthetic Polyelectrolytes Used in this research

reaction once the polyelectrolytes are brought into close proximity by electrostatic interactions, as shown in Scheme 3. The reactive groups are polymer-bound, and their respective polyelectrolyte backbones are designed to reduce their bioavailability and hence their toxicity towards both encapsulated cells and host. Sequential coating of CaAlg beads with these polyelectrolytes (Scheme 3) should lead to a permanently cross-linked skin that may strengthen the capsules, yet have good biocompatibility and permeability.

Narrow-disperse CaAlg beads were first prepared by extruding a 1.5 wt% Na alginate solution, optionally containing C_2C_{12} mouse cells, into a 1.1 wt% $CaCl_2$, NaCl gelling bath. Following a standard washing procedure, these CaAlg beads ("A") were exposed, in sequence, to dilute solutions of the polycation, C70 and the polyanion, A70 to produce AC70A70 capsules. Uncoated CaAlg beads are stiff gels at physiological salt concentrations. Upon treatment with 5 wt% (170 mM) Na citrate to extract the calcium, the beads swell and become almost transparent and difficult to see. In contrast, when the AC70A70 (Figure 2a) and the control APA capsules were exposed to 170 mM Na citrate, the cores of the capsules dissolved, while the shells survived. Subsequent exposure to 2M NaCl completely dissolved the APA control capsules, while the shell of the AC70A70 capsules remained intact (Figure 2b). This indicates that APA shells are held together by ionic bonds that dissociate at high ionic strength, while the AC70A70 capsules have a covalently cross-linked shell that survives at high ionic strength.

Fluorescently labelled AC70A70-type capsules, prepared using either FITC-labelled C70 (designated C70*f*) or A70 (designated A70*f*), show shell thicknesses of up to 35 micron in confocal laser scanning microscopy (CLSM) images (Figure 2c). Shell thicknesses vary with MW of PLL and exposure time, in agreement with

Table 1. Polyelectrolyte Properties

Polyelectrolyte	*Composition*	*M_n (kDa)/PDI*
Na-Alg	G/M, 40:60[a]	428[d]
PLL	-	1-4, 4-15, 15-30[a]
PAPM	-	260[e]
C100	-	300[e]
C70	MOETAC/AEMA, 70:30 (±4)[b]	167[e]
C0	-	299[e]
A100	-	5.4[a]
A100-38k	-	38/2.6[f]
A100f	-	29 / 2.8[f]
A90	MAA/MOEAA, 89:11[c]	29/1.7[f]
A80	MAA/MOEAA, 79:21[c]	41/2.0[f]
A70-22k	MAA/MOEAA, 70:30 (±3)[c]	22/ 3.1[f]
A70-42k	MAA/MOEAA, 70:30 (±3)[c]	42 / 2.4[f]
A70-149k	MAA/MOEAA, 70:30 (±5)[c]	149/ 1.7[f]
A60	MAA/MOEAA, 64:36[c]	32/2.3[f]
A50	MAA/MOEAA, 44:56[c]	31/2.4[f]

[a] Given by supplier. [b] Copolymer composition in mol% determined by titration. [c] Copolymer composition in mol% determined by ^{1}H NMR. [d] See ref (*31*) [e] M_w obtained from viscometry data. [f] M_n and polydispersity index (PDI) determined by GPC.

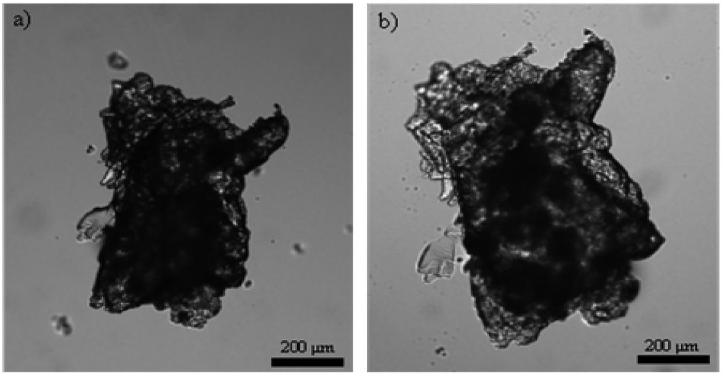

Figure 1. OM image of a piece of self-cross linked polyelectrolyte complex of C70/A70 a) in saline; and b) after exposure to 2M NaCl for 20 minutes.

recent analogous studies (*53*). Layers of similar thickness are observed regardless of which polyelectrolyte is labelled, indicating the presence of a homogeneous

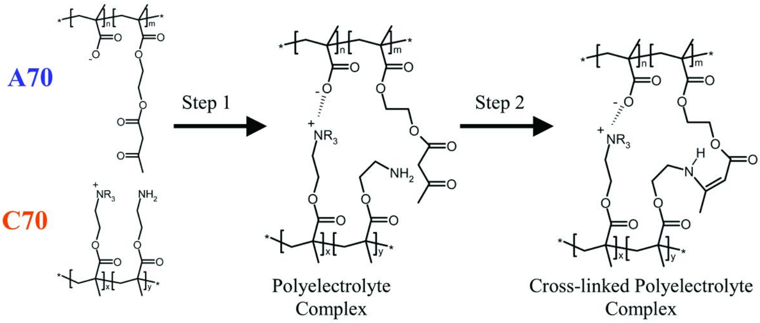

Scheme 3. Reactive copolymers [C70(amino); A70(acetoacetate)] for in-situ cross-linking for the formation of cross linked shell/core in CaAlg beads.

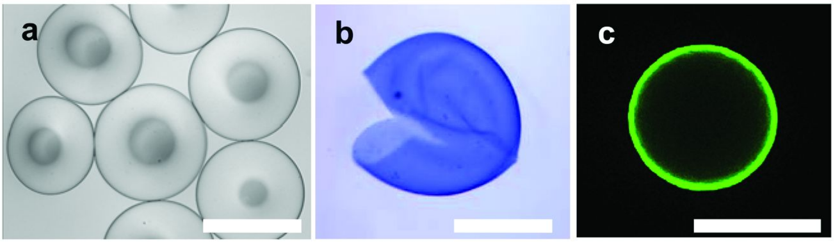

Figure 2. OM image of a) AC70A70 microcapsules, b) Trypan Blue stained shell remaining after exposure to 170 mM citrate and 2M NaCl (cut open to reveal capsular nature), c) CLSM image from the equatorial region of a AC70fA70f microcapsules). Scale bar 500 µm.

mixture of the two polyelectrolytes C70*f* and A70*f* at the surface of the CaAlg bead.

CaAlg beads bearing these cross-linked shells demonstrated greater resistance to osmotic pressure changes compared to conventional beads coated with PLL and Alg (APA). Permeability of such cross-linked hydrogel membranes was studied by GPC analysis of different MWs of poly(ethylene glycol) (PEG) diffusing through analogous flat model membranes. Both APA and AC70A70 membranes were found to have MW cut-offs between 150 kDa and 200 kDa, suitable for exclusion of immuno-related proteins (*54*).

Figure 3 shows a phase contrast microscope image of C_2C_{12} cells encapsulated in APA and AC70A70 capsules, after incubation for one week. Cell viability in *in-vitro* studies of AC70A70 capsules was found to be slightly lower than in the control APA capsules, but the number of live cells remained stable, and the cells were replicating with extended incubation. Preliminary studies of *in vivo* cell viability, after implantation of cross-linked AC70A70 capsules in mice for 1 to 2 weeks, showed fibroid over-coating of many capsules (Figure 4b). This over-coating indicates an immune response of the host that would limit viability of the encapsulated cells. The next section describes one approach to reducing this immune response.

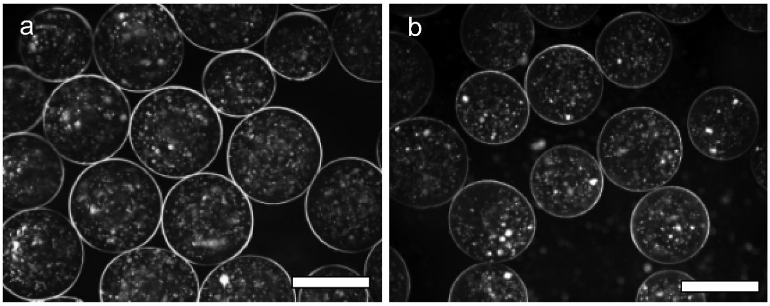

Figure 3. Phase contrast microscope image of C_2C_{12} cells encapsulated in a) APA, b) AC70A70 after incubation for 1 week. Coating conditions: PLL (0.05% w/v in saline, 6 min); Alg (0.03% w/v, 4 min), C70 (0.5% w/v, 10 min), A70 (0.5% w/v, 10 min). Scale bar 500 µm.

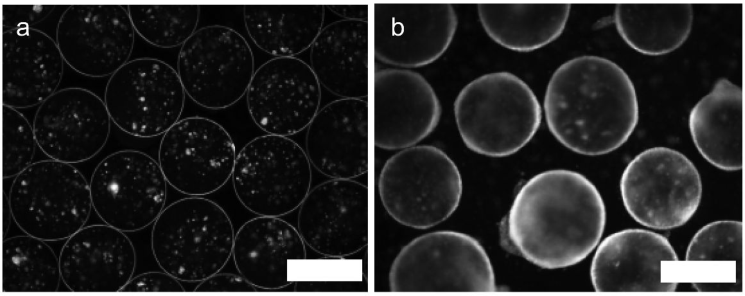

Figure 4. Phase contrast microscope image of C_2C_{12} cells encapsulated in a) APA, b) AC70A70 retrieved from mice after implantation for 1 week. Scale bar 500 µm.

Four-Layer (A-C70-A70-PLL-Alg) Microcapsules

We realized from the above *in vivo* study of 2-layer capsules in mouse models that there is an immune reaction of the host to the capsules or encapsulated cells after implantation. As analogous cell-containing APA capsules prepared from the same alginate do not show this immune reaction, we suspected that C70 and/or A70 might be responsible, by binding components of the BSA-based culture medium used for incubation. To address this issue, we decided to try to hide the C70/ A70 outer layer by additional exposure to PLL followed by Alg, leading to a 4-layer capsule denoted A-C70-A70-PLL-Alg.

The 4-layer capsules show slightly poorer cell viability, which is attributed to the encapsulation process itself. The number of live cells remained stable, and begins to increase shortly after encapsulation. We studied the immune stimulating effect (fibroid overgrowth) of these 4-layer capsules by varying the concentration and compositions of polyelectrolytes, and changing the medium. Binding of FITC labelled BSA (BSA*f*) to the 4-layer capsules was studied by CLSM, as shown in Figure 5. It was found that presence of C70 strongly correlates with protein binding near the capsules surface, while A70 had a lesser effect. Reducing the concentration of C70 and A70 also reduced BSA*f* binding (data not shown). Using serum free medium instead of regular medium to culture the capsules post fabrication eliminates this host reaction. The APA and 4-layer capsules were cultured in serum free media before implantation into the peritoneal cavity of mice, and retrieved after 1 week is shown in Figure 6. The 4-layer capsules are more resistant to the chemical and mechanical stress tests than control APA capsules. The permeability of 4-layer capsules was determined by CLSM and GPC using BSA*f* and narrow dispersed PEGs of different MW. The MW cut-off of the 4-layer capsules was shown to be similar to that of the control APA capsules, and suitable for cell encapsulation. *In vitro* and *in vivo* viability of encapsulated cells of 4-layer capsules was similar to that of APA capsules.

Polycations for Alginate Microcapsules

In our experiments, capsules containing C70 have shown significant undesirable protein binding. In addition, C70 coated capsules are more prone to aggregation during the coating process than PLL coated capsules, and preliminary studies show that primary amine containing methacrylic ester can undergo intra and/or intermolecular amidation in aqueous solution over time that leads to cross-linked gels and interferes with capsule coating. We hence explored other polycations (Scheme 2, Table 1) as possible replacements for C70. Such polyamines should ideally be inexpensive, non-cytotoxic, not elicit protein-binding or a strong host reponse, yet engage in cross-linking with polyelectrophiles such as A70. We synthesized poly(aminopropylmeth acrylamide), (PAPM) and poly(aminoethylmethacrylate) (C0) by free radical polymerization, and compared them with C70 and PLL in the preparation of A-polyamine-A70 capsules for cell encapsulation. CaAlg beads were coated with the four different polycations (C70, C0, PAPM, and PLL), using concentrations from 0.01-0.5 wt% in saline at pH 7.5. The PLL coated capsules were well dispersed for all polycation concentrations. In contrast, CaAlg beads exposed to C70 or C0 in saline, aggregated at polycation concentrations from 0.01 to 0.1 wt%, but stayed dispersed at 0.5 wt%, and CaAlg beads exposed to PAPM in saline aggregated at all PAPM concentrations examined (0.01-0.5 wt%). Using PAPM solutions in 1.1 wt% $CaCl_2$ and 0.45 wt% NaCl solution, a mixture commonly used for the gelling bath, prevented this aggregation during coating. After polycation coating, the beads were coated with A70 in saline, to give capsules with a covalently cross-linked shell, that survive the challenge with citrate and high ionic strength. The representative optical microscopy images of shell cross-linked capsules are shown in Figure 7.

The resulting capsules were then tested for mechanical strength, viability of encapsulated cells and host immune response. These results showed that PAPM is comparable to PLL in terms of shell strength, cell viability and protein binding, in shell cross-linked CaAlg capsules formed with the reactive polyanion A70. They also show better capsule strengths compared to C0 and C70. It was also shown that PAPM as well as PLL are protected from the undesirable intra/intermolecular amidation reactions during storage that were seen for C70 and for C0. In

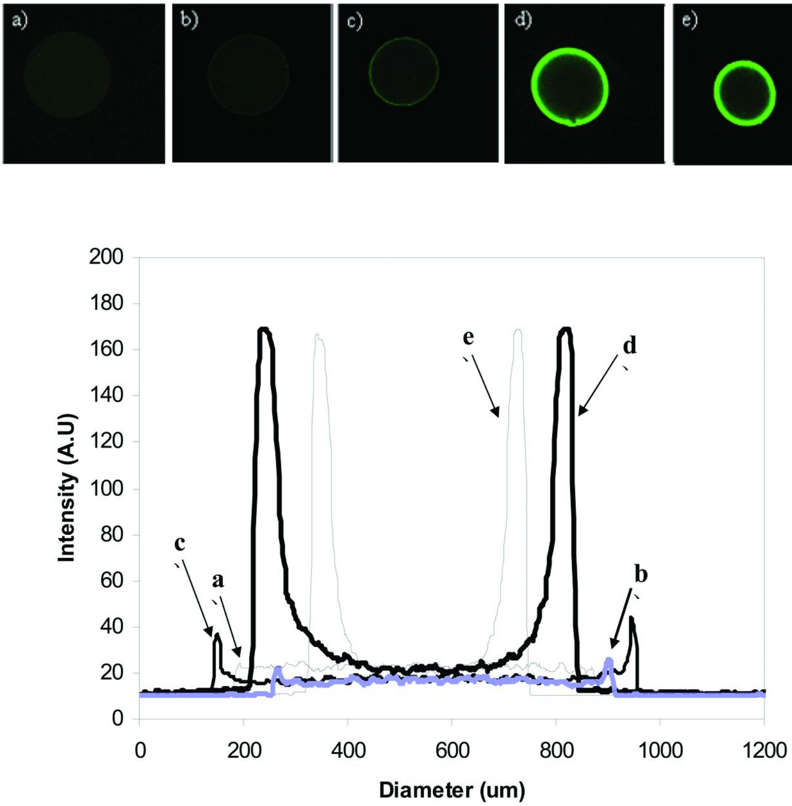

Figure 5. Top – CLSM images, bottom – line profile of a) APA, b) APA100PA, c) APA70PA, d) AC70A100PA and e) 4-layer (AC70A70PA) microcapsules exposed in 0.05 w/v% BSA-FITC at 20 °C for 24 h.

addition, PAPM offers the advantage of controlled MW using controlled radical polymerization techniques, and easy access to copolymers incorporating some of the wide range of acrylic monomers available.

Composite Microcapsules

This work explores the feasibility of using synthetic polyelectrolytes to form cross-linked networks throughout the CaAlg bead, leading to formation of a permanent three-dimensional support structure for cell transplantation and other uses.

This approach involves adding the synthetic reactive polyanion, A70, with the initial Na Alg solution. The resulting Ca(Alg/A70) beads are then covalently crosslinked by exposure to PLL solutions in saline, to form a covalently cross-linked A70-PLL network within the Ca(Alg/A70) composite hydrogel, with morphologies dependent on the MWs and mobilities of the two polyelectrolytes used.

It was found that 15-30k PLL did not penetrate the CaAlg gel matrix past the outer 35 micron (*45*, *46*, *55*) resulting in a shell crosslinked structure similar to that found in the layer-by-layer capsules discussed above (*45*, *46*). On the other hand, 4-15k PLL was able to diffuse in the present Ca(Alg/A70) beads, resulting in core-cross linked networks.

The MW and hence the mobility of the A70 was similarly shown to have significant effects, with higher MW A70 being more efficiently retained in the composite beads.

(A/A70) PA Composite Microcapsules

Ca(A/A70) beads were prepared by dripping saline solutions containing 1.5 wt% Na alginate and 0.5 wt% polyanion A70 (or its fluorescently-labelled analog, A70*f*), adjusted to pH 7, into a $CaCl_2$, NaCl gelling bath (*56*). The composite beads formed had an average diameter of 650 µm and appeared identical to those formed using alginate alone (Figure 8). The beads were subsequently exposed to different concentrations of PLL having different MW, to form shell-crosslinked, and core-crosslinked composite capsules respectively.

Shell-Cross Linked (A/A70)PA Microcapsules

Ca(A/A70) beads exposed to 0.05 wt% PLL (15-30k), washed with saline and then coated with a 0.03 wt% Na alginate solution looked similar to the uncoated beads but the surface was evenly stained by trypan blue indicating the presence of a continuous polycation layer (image not shown). In addition, the surface appeared pink when rhodamine labelled PLL (PLL*r*) was used to coat the composite beads.

The composite bead preparation was repeated with A70*f*, in order to demonstrate the inclusion of the synthetic polyanion and to probe its distribution within the bead. Following bead preparation, the $CaCl_2$ gelling bath and the washing solutions were analyzed by UV-Vis spectroscopy, and showed that 60 ± 5% of the original A70*f*-22k or A70*f*-42k, and 40 ± 5% of the corresponding higher MW A70*f*-149k were lost from the beads, predominantly to the gelling bath (Figure 9). No additional A70*f* loss was observed during the subsequent PLL coating process. Uncoated Ca(A/A70*f*) beads stored in a 6-fold excess of saline at 4 °C lost an additional 3% of the original A70*f* after 2 days, and 16% after 3 months. In contrast, (A/A70*f*)PA capsules did not lose a significant amount of A70*f* to the supernatant over 8 months of storage.

Thus, A70*f* is lost principally in the gellation step during which the droplets were also found to shrink to about 60% of their original volume, a value consistent with other studies (*57*, *58*). Use of higher MW A70 increases the retention of the polymer, possibly due to enhanced entanglement.

CLSM was used to demonstrate the distribution of A70*f* and PLL*r* within the capsules. After gelling in the $CaCl_2$ bath, A70*f* is initially homogeneously distributed within the Ca(A/A70*f*) beads (Figure 10a). Images obtained 1-2 hours after coating these Ca (A/A70*f*) beads with PLL and Alg (Figure 10b), show in

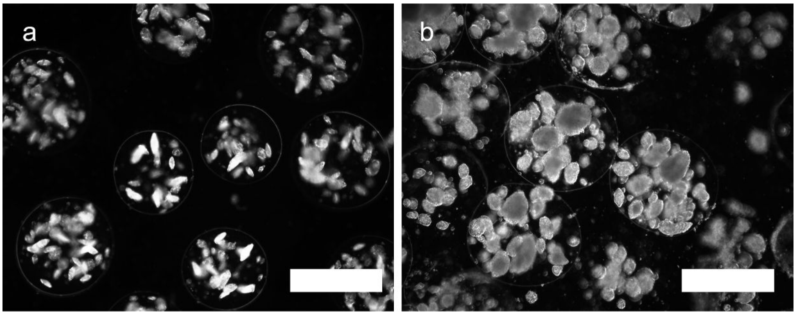

Figure 6. Phase contrast microscope image of C_2C_{12} cells encapsulated in a) APA, b) A-C70-A70-PLL-Alg retrieved from mice after implantation for 1 week. 4-layer-capsules cultured in serum-free medium for 72 hours before implantation. Scale bar is 500 µm.

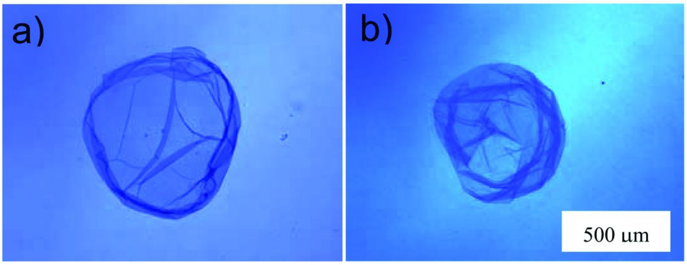

Figure 7. OM images of a) A-PAPM-A70 (0.5/0.5), and b) A-C0-A70 (0.5/0.5) cross-linked capsules shell. After treatment with 170 mM Na citrate and then 2 M NaCl, followed by trypan blue staining. Polycation/polyanion concentrations (wt %) are shown in brackets.

addition a very thin outer shell, perhaps the result of electrostatic or covalent capture of A70*f* by the PLL layer.

After 5 months storage uncoated beads showed considerable fluorescence in the supernatant. However, the retained A70*f* is homogeneously distributed within the capsule. These results suggest that a fraction of the A70*f* chains are short and hence mobile enough to diffuse out of the CaAlg gel, while the remainder are trapped within the gel. The CLSM image of 5-month-old coated capsules is similar to that seen just after preparation (Figure 10b). The A70*f* is retained in the capsules confirming that the PLL coating prevents the loss of A70*f*.

When the coated capsules were treated with excess 170 mM Na citrate for 18 hrs to liquefy the CaAlg core, the capsules swelled (40-50% diameter increase). Mechanical rupture released liquid from the core, indicating that the amount of PLL able to diffuse into the core was not sufficient to effect core crosslnking.Accordingly, Rhodamine-labelled versions of PLL (PLL*r*) of different MW were used to study the effect of PLL MW and concentration on core crosslinking.

CLSM images of capsules coated with 0.05 wt% solutions of PLL*r* show that higher MW PLL*r* (15-30k) remains concentrated near the capsule surface

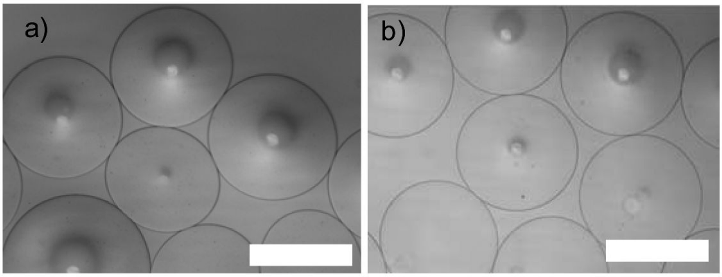

Figure 8. Optical microscope image of a) Ca Alg beads, b) Ca(Alg/A70f) composite beads. The scale bar is 500 μm.

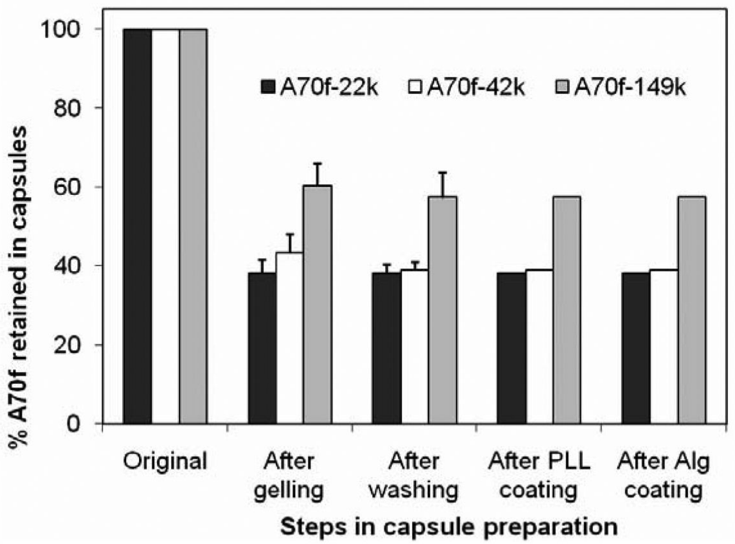

Figure 9. Percentage of A70f remaining in the composite microcapsules at different stages of the capsule preparation. Error bars show the standard deviation for select experiments performed in triplicate.

(Figure 11a). Weak fluorescence is seen in the capsule interior, indicating that a fraction of the PLL*r* is able to diffuse through the CaAlg gel. On the other hand, the lowest MW PLL*r* (1-4k) is evenly distributed throughout the composite capsules (Figure 11c). This is consistent with a number of earlier reports (*4*, *53*, *59–61*). The intermediate MW PLL*r* (4-15k) showed both formation of a distinct shell, and significant in-diffusion to the core of the bead (Figure 11b). The integrity of uncoated and PLL (0.05 wt%) coated Ca(A/A70) composite beads in the presence of Na citrate and NaCl was examined by optical microscopy and compared with that of control APA capsules. Uncoated beads composed of Ca(A/A70) or CaAlg are stable at physiological salt concentrations but dissolve when exposed to 170 mM Na citrate, which extracts the calcium from the gel. In contrast, addition of Na citrate to PLL(4-15k or 15-30k) coated capsules such as APA or Ca(A/A70)PA caused the core of the beads to dissolve, while the shells consisting of the polyelectrolyte complex survived. However, upon addition of 2M NaCl while vigorously agitating, or 0.1M NaOH, the ionically cross-linked APA shells weakened or dissolved while the covalently cross-linked shells of the (A/A70)PA capsules remained intact.

Figure 12a shows a composite bead coated with 0.05 wt% PLL (4-15k). After sequential exposure to 170 mM Na citrate followed by 2M NaCl, the capsule shell was manually cut under the microscope with a micro knife (Figure 12b), revealing both a thin cross-linked shell due to reaction between the higher MW fraction of PLL, and the presence of mobile A70*f* diffusing out through the hole in the shell.The shell is self-supporting, but it is clear that the core of the bead is not cross-linked, likely due to the presence of insufficient amounts of PLL. The resulting capsules hence constitute shell cross-linked shell capsules, analogous to the shell-cross-linked capsules prepared earlier using sequential exposure of CaAlg beads to polycation and A70 (*45*, *46*), except that the reactive A70 is here supplied from the interior of the capsule. The outer surface of the capsule, after coating with alginate, then resembles the conventional APA capsules.

Figure 11c shows a composite bead coated with low MW PLL (1-4k, 0.05 wt%) in which PLL*r* homogeneously distributed throughout the beads. After exposure to Na citrate, the coated capsules dissolved within seconds. This indicates that although this low MW PLL readily penetrates the interior of the beads, at the present concentration of 0.05 wt% it is unable to crosslink the A70 to the extent necessary to give a crosslinked shell or core. The chains may be too short to effectively bridge between A70 and/or Alg chains.

Core-Cross Linked (A/A70)PA Microcapsules

Model experiments, based on combining small aliquots of aqueous solutions of A70 and PLL in different ratios, indicated that formation of cross linked macroscopic complexes required PLL to be present in stoichiometric or larger amounts, relative to A70. Use of sub-stoichiometric amounts of PLL resulted only in formation of turbid solutions, reflecting formation of PLL micro gels, likely coated with A70.

The results above indicated that (A/A70(42k) beads retain roughly 40% of their original loading of A70 or A70*f* at the point of exposure to PLL. These composite beads were exposed to appropriate volume of 0.05 wt% PLL, providing a near stoichiometric *overall* ratio of A70/PLL. However, UV/Vis analysis of a supernatant PLL*r*(15-30k) solution after coating showed that only half of this PLL was actually absorbed by the composite beads. In addition, most of the bound PLL (15-30k and 4-15k), forms a dense shell at the surface as indicated by Figure 11(a and b).

Analysis of the in-diffusion patterns (Figure 11) indicated that the intermediate MW PLL (4-15k) might represent a good compromise between ease of in-diffusion, and a MW high enough to crosslink the A70 in the core, provided it is available in sufficiently high concentration to compensate for incomplete capture and preferential binding to the shell.

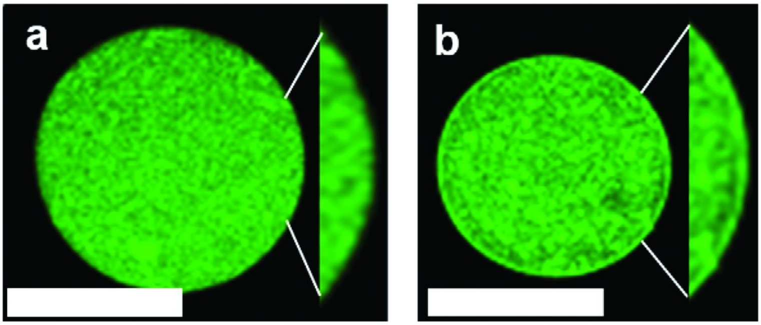

Figure 10. CLSM equatorial optical section of Ca(A/A70f) composite capsule: a) uncoated and b) coated with PLL (15-30 kDa) (0.05 wt%, 6 min) and then alginate (0.03 wt%, 4 min). The scale bar is 500 μm.

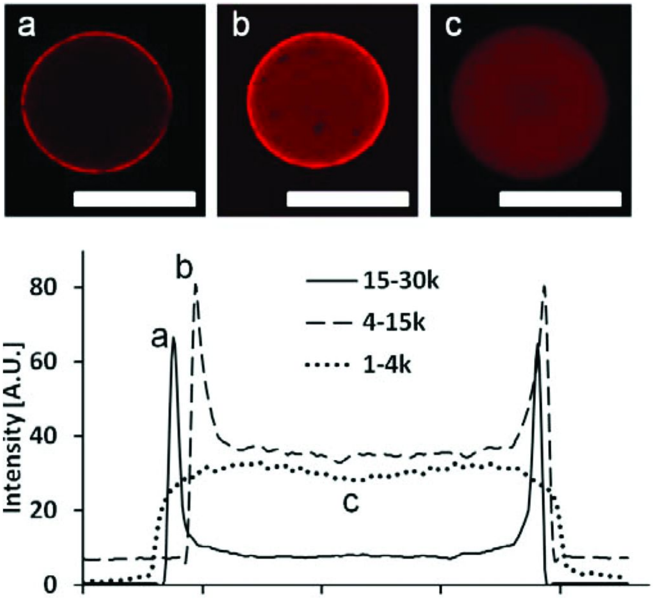

Figure 11. Top: CLSM equatorial optical sections of (A/A70)PA capsules made with PLLr of a) 15-30 kDa; b) 4-15 kDa; and c) 1-4 kDa. Bottom: 25 pixel wide line profiles taken from the images. Coating conditions: PLLr (0.05 wt% in saline, 6 min); Alg (0.03 wt%, 4 min).

Accordingly, we explored increasing the PLL (4-15k) concentration from 0.05 to 0.5 and 1 wt%. Coating using 1 wt% PLL solution resulted in wrinkling of the bead surface, while 0.5 wt% PLL (4-15k) resulted in smooth bead surfaces. Figure 13a shows (A/A70*f*)PA capsules coated with 0.5 wt% PLL (4-15k), followed by Alg (0.03 wt%). The resulting capsules were manually cut, and exposed to 70 mM

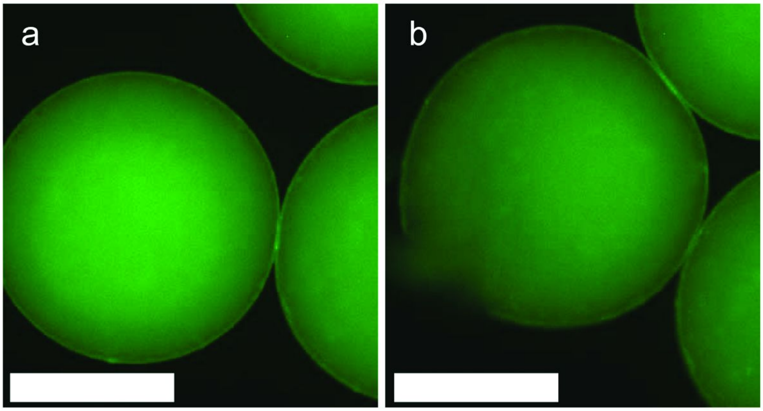

Figure 12. Fluorescence microscopy images of (A/A70f)P(4-15 kDa, 0.05 wt%) A(0.03 wt%) capsules; a) as formed, and b) after being exposed to citrate (170 mM) and NaCl (2 M), and manually cut with a micro-knife. Scale bar: 300 µm

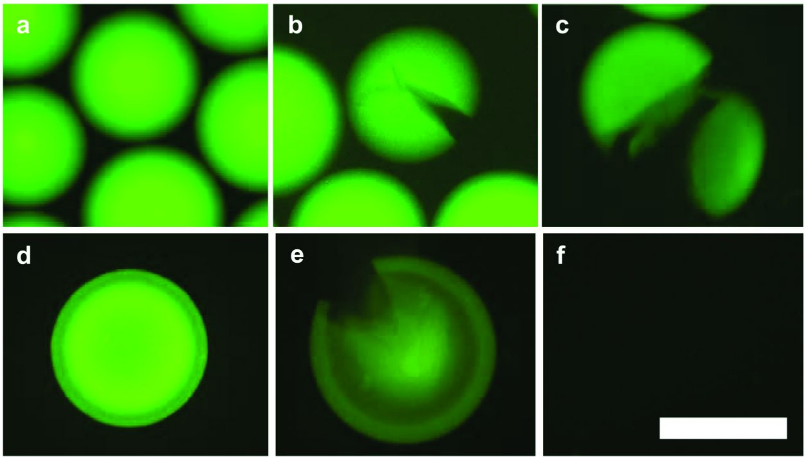

Figure 13. Fluorescence microscopy images of a) (A/A70f)P(4-15k, 0.5 wt%)A(0.03 wt%) and d) (A/A100f)P(4-15k, 0.5 wt%)A(0.03 wt%); e) the beads were manually cut, and then exposed to excess 70 mM Na citrate; c, f) after further treatment with 2 M NaCl. The scale bar is 500 µm.

Na citrate (*62*) (Figure 13b) and then 2M NaCl (Figure 13c). The capsules undergo little swelling and there is minimal loss of A70*f* demonstrating that sufficient PLL has diffused into the core to crosslink the bead throughout. The crosslinked beads also survived subsequent treatment with 0.1M NaOH (not shown).

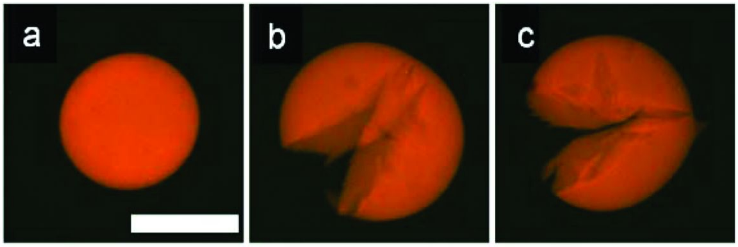

Figure 14. Fluorescence microscopy images of core-cross linked (A/A70)PLLr (4-15k, 0.5 wt%)A (0.03 wt%) composite capsules to show the location of PLLr (4-15 kDa). a) As formed; b) after addition of excess 70 mM Na citrate and crushing; c) following addition of excess 2 M NaCl. The scale bar is 500 µm.

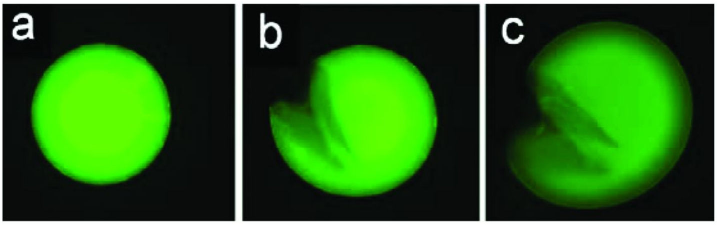

Figure 15. Fluorescence microscopy images of (A/A70f)PA microcapsule prepared by exposure to both high and medium MW PLL. Ca(A/A70f) composite beads were coated with 0.05 wt% PLL (15-30k) (1 min), and then with 0.5 wt% PLL (4-15k) (6 min), followed by 0.03 wt% Alg (4 min). a. As formed, b. After challenge with excess citrate and manual cutting. c. After exposure to excess 2 M NaCl. The scale bar is 300 µm.

Capsules formed using A100*f* (38k) instead of A70*f* (42k) confirmed the role of covalent crosslinking. Figure 13d shows the fluorescence optical microscope image of a (A/A100*f*)P(4-15k, 0.5%)A(0.03%) capsule. Exposure of these capsules to 70 mM Na citrate for about 5 minutes resulted in swelling of the outer layer. Manual cutting confirmed the presence of a swellable shell (Figure 13e) and shows an inner core. Subsequent exposure to 2M NaCl completely dissolved both shell and core within three minutes (Figure 13f), confirming that the permanent structure shown in Figure 13(a-c) is indeed based on covalent cross-linking.

To map the distribution of PLL, Ca(A/A70) composite beads were coated with rhodamine-labelled PLL*r* (4-15k) and examined by fluorescence microscopy (Figure 14). Figures 14a shows an intact capsule, while 14b and c show capsules that were exposed to excess 70 mM Na citrate and then manually crushed, followed by the addition of 2M NaCl revealing both shell and core cross-linking. The presence of a distinct PLL*r* shell in addition to core cross-linking suggests that the higher MW fraction of PLL*r*(4-15k) forms a surface network, while the lower MW fraction diffuses into the core to cross-link with A70. To test if core and shell could be separately crosslinked, CaAlg beads were coated sequentially with two PLL solutions having different MWs, a variation of the approach described by Prokop et al (*38*). Ca(A/A70*f*) composite beads were first exposed to 0.05 wt% PLL (15-30k) for 1 min, followed by exposure to 0.5 wt% PLL (4-15k) for 6 min, and after a saline wash step, by the usual final coat with 0.03 wt% Alg for 4 min. The resulting capsules, after manual cutting and exposure to Na citrate and 2M NaCl, show both the presence of a distinct outer shell formed by reaction of the higher MW PLL with A70*f* near the surface, and core-cross-linking between the lower MW PLL and residual A70*f* remaining in the core (Figure 15, a-c). In contrast, the capsules prepared using only 0.5 wt% PLL (4-15k) did not show a similarly distinct outer shell (Figure 13c). This demonstrates the ability to exert some control over shell and core cross-linking, and may allow independant tuning the MW cut-off and bead strength.

In-Vitro Cell Viability

C_2C_{12} mouse cells were encapsulated in APA, the shell-cross linked (A/A70)P(15-30k, 0.05 wt%)A and the core-crosslinked (A/A70)P(4-15k, 0.5 wt%)A capsules at a rate of 2 million cells per ml capsules. The capsules were then cultured in DMEM (with 10% FBS) *in vitro* for one week. The appearance of cell-containing APA and shell or core-cross linked (A/A70)PA capsules are similar as is shown in Figure 3. The numbers of living cells per microcapsule were monitored versus time of *in vitro* incubation, using the Alamar Blue assay. Figure 16a shows that the average live cell numbers in these shell-crosslinked capsules are initially slightly lower than those in APA microcapsules at day 1 and 4. However, a reasonable number of cells are viable, there is good proliferation and the number of live cells exceed those in APA capsules by day 7, indicating that the A70 in the core of the shell cross-linked (A/A70)PA capsules is not detrimental to cell viability.

Figure 16b shows the cell viability in terms of the average number of live cells per core-cross linked (A/A70)PA and APA capsule after 1, 3, 5 and 7 days. The comparison show that the live cell numbers are higher for APA capsules, though similar relative increases in cell numbers (50-60%) are seen for both types of capsule. Comparison with the good cell viabilities observed in the case of analogous shell-cross linked capsules prepared using only 0.05 wt% PLL (15-30k) (Figure 16a) suggests that the lower initial cell viability in the present core cross-linked capsules is due to the larger amount of lower MW PLL used, perhaps just indirectly through formation of the cross-linked core that interferes with proliferation of the cells.

It was at first surprising that the diffusion of PLL into the capsule core does not have a more negative effect on cell viability. The preferred location of PLL*r* (4-15k) in the shell, compared to the homogeneous distribution of A70*f* (Figure 5) obviously reflects the fact that PLL is applied from the outside, while A70 is found throughout the core. PLL in the bead core should not be very toxic towards the encapsulated cells, as verified by the data in Figure 16b, because most of the PLL diffusing in from the outside should rapidly react with the A70 present throughout the core. Any residual unreacted PLL would likely be complexed by alginate, and thus rendered much less cytotoxic, as reported previously for the complexes formed between polystyrenesulfonate and polycations (*63*).

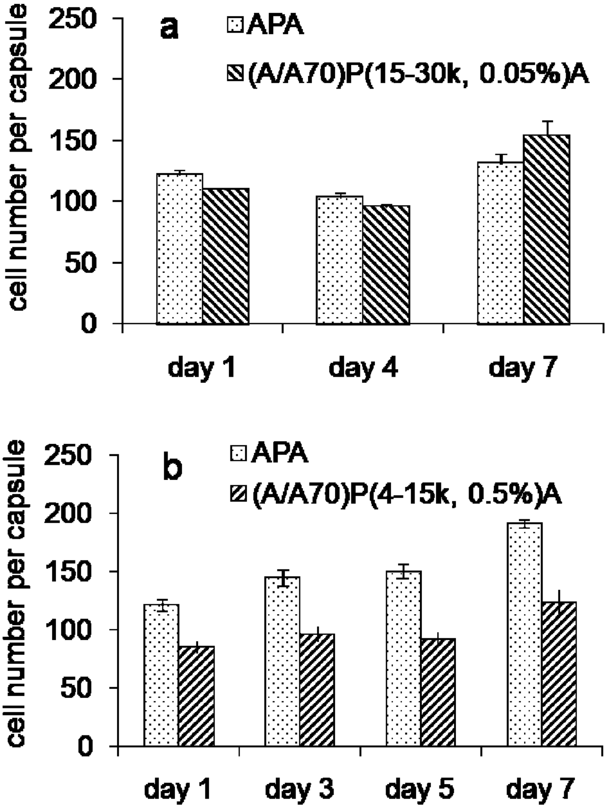

Figure 16. In vitro cell viability of C_2C_{12} cells encapsulated in APA and (A/A70)PA capsules over time. a) APA and shell-cross linked (A/A70)P(15-30k, 0.05 wt %)A capsules and b) APA and core-cross linked (A/A70)P(4-15k, 0.5 wt %)A capsules. Error bars show the standard deviation.

Mechanical Stability of APA and Core-Cross Linked Capsules

The mechanical stability of APA and core cross-linked (A/A70)PA capsule was determined using a high strain rate micro compression tester. It was used to measure the maximum load before rupture, applied through a stepper motor at a constant speed of 10 µm/s to the maximum load while plotting the force registered against vertical displacement. Figure 17 shows a typical force versus displacement curve, for compressing a single APA and core cross-linked (A/A70)PA capsules. During the experiments, the force transducer probe started to move downward at point 1 and touched the capsule at point 2. The compression commenced immediately and the force started to increase until the capsule under went rupture (point 3). Upon compression, the beads deformed to between 2 and 2.5 times their original diameter, and about 20 to 25% of their original height, before cracking. It was noted that the present core-cross linked (A/A70)PA capsules, upon exceeding their maximum compressive loading, do not undergo

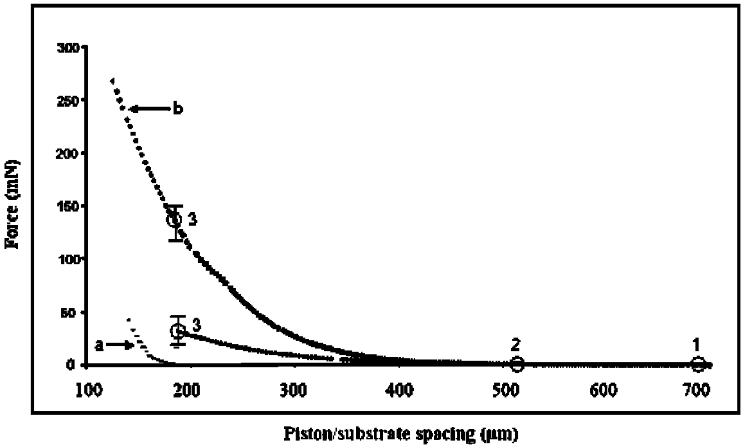

Figure 17. Force versus displacement curve obtained from compression of a) APA, b) core cross-linked (A/A70) PA capsule. The diameter of the microcapsule was about 500 µm.

catastrophic failure, but rather undergo progressive cracking that still provides some matrix isolation for the cells embedded in the fragments. This is in contrast to APA core-shell capsules that fail by a catastrophic bursting mechanism, which exposes all of the bead content to the host.

Typically, core cross-linked capsule exhibited a first crack about 120-150 mNewtons of compressive force (Figure 17). Compression of the same type of capsule after extraction of the calcium in the core with Na citrate shows a slight reduction (data not shown) in load at failure, indicating that most of the bead strength derives from the synthetic polymer network, rather than from the CaAlg matrix. Extraction with citrate is designed to mimic the slow exchange of calcium for sodium known to take place in tissue. The results indicate that the bead strength of these covalently cross-linked capsules should not suffer from such ion exchange. In contrast, typical force at failure for non-cross linked APA capsules described here is between 20 and 40 mNewtons, with the failure mechanism resembling the sudden bursting of a balloon, rather than progressive cracking (Figure 17).

MW Cut-Off of APA and Composite Cross Linked Capsules

It is important that capsules containing cells allow the diffusion of nutrients and metabolites, while preventing the ingress of components of the host immune system. The ideal MW cut-off of the capsule membrane is one that is designed to keep high MW molecules such as antibodies and immunoglobulins out, while allowing exchange of oxygen, nutrients and metabolites including the specific enzymes needed by the patient. The metabolic requirements of various cell types are different and, hence, optimal membrane permeability is expected to depend on the choice of cells, with values of about 100 - 200 kDa commonly considered to be suitable for allografts (*64–67*).

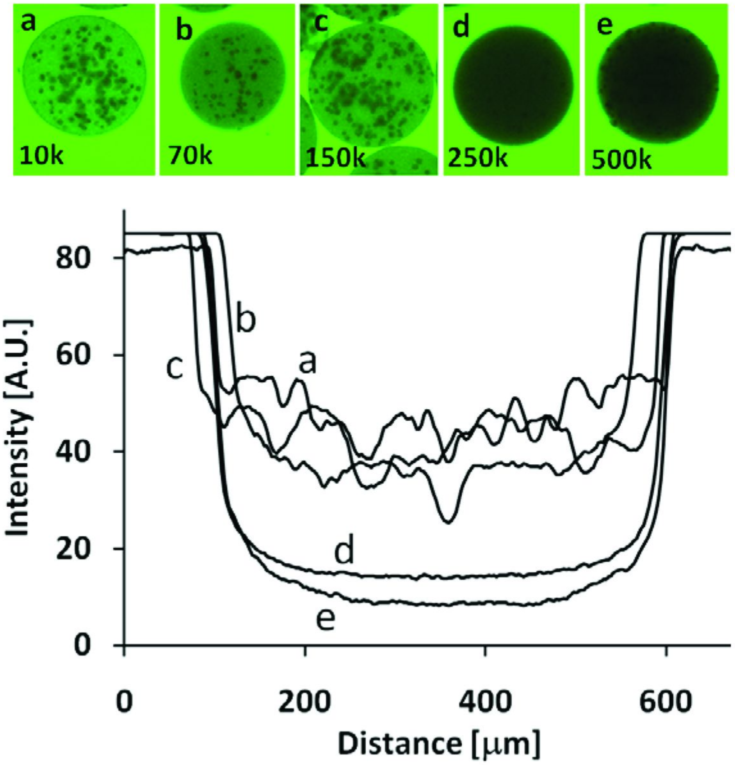

Figure 18. Top: CLSM middle sections of cell containing (A/A70)P(4-15k, 0.5 wt%)A(0.03 wt%) capsules exposed for 24h at room temperature to 0.05 wt% dextran-FITC with nominal MWs of a) 10k, b) 70k, c) 150k, d) 250k, and e) 500k. Bottom: Line profile from images as above.

The MW cut-off of these new shell- and core-cross linked capsules was estimated using a series of commercial dextran-FITC samples with nominal MWs of 10, 70, 150, 250 and 500 kDa (*6*, *68*). Dextran is a polysaccharide composed of glucose units, and fluorescein- labelled dextrans (*69*) have been used to examine the permeability of various membranes, microcapsules and cells. Commercial dextran-FITC samples were analysed by GPC using linear PEG as standard. GPC analysis showed polydispersity indices of about 2 except for the 150 kDa sample, which has a much larger polydispersity index of 4.7. This broad MW distribution led to significant in-diffusion of the low MW fraction. In addition, dextran may behave differently than globular proteins in solution, and as such the use of dextran-FITC provides only a rough indication of the MW cut-off.

The shell-cross linked capsules were exposed to 0.0015 wt% dextran-FITC solutions for 24h and then examined by CLSM. The results showed increasing in-diffusion with decreasing MW, similar to control APA capsules (data not shown). Similarly, core-cross linked capsules containing C_2C_{12} mouse myoblast cells were tested by CLSM following 24h exposure to dextran-FITC (0.05 wt%) having different MWs. Figure 18 shows that dextrans of 500 and 250 kDa are almost completely excluded, while dextrans having MW's of 10 and 70 kDa can diffuse in freely. The 150 kDa dextran has a much broader MW distribution than the other four dextran studied, including a large low MW fraction, which is considered to be responsible for most of the interior fluorescence observed in Figure 18c. Overall, the results indicates that the shell and core cross linked capsules have MW cut offs around 100-200 kDa, similar to APA capsules (data not shown), and is considered suitable for immuno-isolation in allo-transplants.

The permeability of APA and shell-crosslinked capsules containing cells was also assessed by looking for the uptake of BSA*f* (MW 66 kDa) (data not shown). Both types of capsules were permeable to BSA*f*, indicating a MW cut-off greater than 70 kDa, consistent with the dextran-FITC results.

Conclusion

We have shown that covalently cross-linked shells can be formed around CaAlg beads by the sequential deposition of oppositely charged polyelectrolytes bearing complementary amine and acetoacetate reactive groups. We have also shown that internally and externally cross-linked networks can be formed in CaAlg beads by inclusion of A70 in conventional APA-type capsule cores, and exposure to sufficient amounts of PLL having appropriate MW. The distribution of the polyelectrolytes in the capsules was studied using fluorescently labeled analogs. Capsule resistance to citrate and 2M NaCl/0.1M NaOH was used to demonstrate the cross-linked nature of the cores and shells. These capsules also have greater resistance to chemical and mechanical stress tests, compared to control APA capsules. The MW cut-off of cross-linked capsules was shown to be similar to that of the control APA capsules, and is suitable for cell encapsulation. The *in vitro* and *in vivo* viability of encapsulated C_2C_{12} cells within shell and/or core cross-linked capsules was similar to that of conventional APA capsules.

In summary, these results describe promising new approaches to cell encapsulation that offer enhanced capsule resistance to chemical and mechanical stresses, while preserving the desired biocompatibility, and may ultimately be useful for clinical immunosuppressive therapies.

Acknowledgments

The authors of this chapter would like to thank the Canadian Institutes for Health Research (CIHR) and the Natural Sciences and Engineering Research Council (NSERC) of Canada for supporting this work.

References

1. Chang, T. M. S. *Science* **1964**, *146*, 524–525.
2. Bañó, M. C.; Cohen, S.; Visscher, K. B.; Allcock, H. R.; Langer, R. *Nat. Biotechnol.* **1991**, *9*, 468–471.
3. Uludag, H.; Sefton, M. V. *Biotechnol. Bioeng.* **1992**, *39*, 672–678.

4. Thu, B.; Bruheim, P.; Espevik, T.; Smidsrød, O.; Soon-Shiong, P.; Skjåk-Bræk, G. *Biomaterials* **1996**, *17*, 1031–1040.
5. Lim, F.; Sun, A. M. *Science* **1980**, *210*, 908–910.
6. Vandenbossche, G. M. R.; Van Oostveldt, P. V.; Demeester, J.; Remon, J.-P. *Biotechnol. Bioeng.* **1993**, *42*, 381–386.
7. Schneider, S.; Feilen, P. J.; Brunnenmeier, F. *Diabetes* **2005**, *54*, 687–693.
8. Peirone, M. A.; Delaney, K.; Kwiecin, J.; Fletch, A.; Chang, P. L. *Hum. Gene Ther.* **1998**, *9*, 195–206.
9. Van Raamsdonk, J. M.; Cornelius, R. M.; Brash, J. L.; Chang, P. L. *J. Biomater. Sci., Polym. Ed.* **2002**, *13*, 863–884.
10. Rokstad, A. M.; Holton, S.; Strand, B.; Steinkjer, B.; Ryan, L.; Kulseng, B.; Skjak-Braek, G.; Espevik, T. *Cell Transplant.* **2002**, *11*, 313–324.
11. Zimmermann, H.; Zimmermann, D.; Reuss, R. *J. Mater. Sci., Mater. Med.* **2005**, *16*, 491–501.
12. Lanza, R. P.; Kuhtreiber, W. M.; Ecker, D.; Staruk, J. K.; Chick, W. L. *Transplantation* **1995**, *59* (10), 1377–1384.
13. Soon-Shiong, P.; Heintz, R. A.; Skjåk-Bræk, G. Microencapsulation of cells. U.S. Patent 5,762,959, 1998.
14. Zekorn, T.; Siebers, U.; Horcher, A.; Schnettler, R.; Klock, G.; Bretzel, R. G.; Zimmerman, U.; Federlin, K. *Transplant. Proc.* **1992**, *24*, 937–939.
15. Lanza, R. P.; Kuhtreiber, W. M.; Ecker, D.; Staruk, J. K.; Chick, W. L. *Transplantation* **1995**, *59* (10), 1377–1384.
16. Mørch, Y. A.; Donati, I.; Strand, B. L.; Skjåk-Bræk, G. *Biomacromolecules* **2006**, *7*, 1471–1480.
17. Darrabie, M. D.; Kendall, W. F., Jr.; Opara, E. C. *Biomaterials* **2005**, *26*, 6846–6852.
18. Chandy, T.; Mooradian, D. L.; Rao, G. H. R. *J. Appl. Polym. Sci.* **1998**, *70*, 2143–2153.
19. Bünger, C. M.; Gerlach, C.; Freier, T.; Schmitz, K. P.; Pilz, M.; Werner, C.; Jonas, L.; Schareck, W.; Hopt, U. T.; De Vos, P. *J. Biomed. Mater. Res.* **2003**, *67A*, 1219–1227.
20. Haque, T.; Chen, H.; Ouyang, W.; Martini, C.; Lawuyi, B.; Urbanska, A. M.; Prakash, S. *Mol. Pharmaceutics* **2005**, *2*, 29–36.
21. Gaserod, O.; Smidsrod, O.; Skjak-Braek, G. *Biomaterials* **1998**, *19*, 1815–1825.
22. Leung, A.; Lawrie, G.; Nielson, L. K.; Trau, M. *J. Microencapsulation* **2008**, *25*, 387–398.
23. Wang, Y. *J. Mater. Sci. Eng C.* **2000**, *13*, 59–63.
24. Schneider, S.; Feilen, P. J.; Slotty, V.; Kampfner, D.; Preuss, S.; Berger, S.; Beyer, J.; Pommersheim, R. *Biomaterials* **2001**, *22*, 1961–1970.
25. Vallbacka, J. J.; Sefton, M. V. *Tissue Eng.* **2007**, *13* (9), 2259–2269.
26. Mokry, J.; Karbanova, J.; Lukas, J.; Paleckova, V.; Dvorankova, B. *Biotechnol. Prog.* **2000**, *16*, 897–904.
27. Smeds, K. A.; Grinstaff, M. W. *J. Biomed. Mater. Res.* **2001**, *54*, 115–121.
28. Hubbell, J. A.; Pathak, C. P.; Sawhney, A. S.; Desai, N. P.; Hossainy, S. F. A.Gels for encapsulation of biological materials. U.S. Patent 5,529,914, 1996.

29. Soon-Shiong, P.; Desai, N. P.; Sandford, P. A.; Heintz, R. A.; Sojomihardjo, S.Crosslinkable polysaccharides, polycations and lipids useful for encapsulation and drug release. U.S. Patent 5,837,747, 1998.
30. Rokstad, A. M.; Donati, I.; Borgogna, M.; Oberholzer, J.; Strand, B. L.; Espevik, T.; Skjåk-Braek, G. *Biomaterials* **2006**, *27*, 4726–4737.
31. Wang, M.; Childs, R. F.; Chang, P. L. *J. Biomater. Sci., Polym. Ed.* **2005**, *16*, 91–113.
32. Araki, T.; Hitchcock, A. P.; Shen, F.; Chang, P. L.; Wang, M.; Childs, R. F. *J. Biomater. Sci., Polym. Ed.* **2005**, *16*, 611–627.
33. Chandy, T.; Mooradian, D. L.; Rao, G. H. R. *Artif. Organs* **1999**, *23*, 894–903.
34. Dusseault, J.; Leblond, F. A.; Robitaille, R.; Joudan, G.; Tessier, J.; Menard, M.; Henly, N.; Halle, J.-P. *Biomaterials* **2005**, *26*, 1515–1522.
35. Leblond, F. A.; Halle, J.-P. U.S. Patent Appl. Publ., 2005, 22pp, US 2005147594 A1 20050707, CAN 143: 103356 AN 2005: 591961.
36. Dusseault, J.; Langlois, G.; Meunier, M. –C.; Menard, M.; Perreault, C.; Halle, J.-P. *Biomaterials* **2008**, *29*, 917–924.
37. Crooks, C. C.; Douglas, J. A.; Broughton, R. L.; Sefton, M.V. *J. Biomed. Mater. Res.* **1990**, *24*, 1241–1262.
38. Prokop, A.; Hunkeler, D.; Powers, A. C.; Whitesell, R.; Wang, T. G. *Adv. Polym. Sci.* **1998**, *136*, 53–73.
39. Sakai, S.; Hashimoto, I.; Kawakami, K. *Biochem. Eng. J.* **2006**, *30*, 76–81.
40. Prakash, S.; Martoni, C. *Appl. Biochem. Biotechnol.* **2006**, *128*, 1–21.
41. Hertzberg, S.; Moen, E.; Vogelsang, C.; Østgaard, K. *Appl. Microbiol. Biotechnol.* **1995**, *43*, 10–17.
42. Prokop, A.; Hunkeler, D.; Dimari, S.; Haralson, M. A.; Wang, T. G. *Adv. Polym. Sci.* **1998**, *136*, 1–51.
43. Wang, T.; Lacik, T.; Brissova, M.; Anilkumar, A. V.; Prokop, A.; Hunkeler, D.; Green, R.; Shahrokhi, K.; Powers, A. C. *Nat. Biotechnol.* **1997**, *15*, 358–362.
44. Donati, I.; Haug, I. J.; Scarpa, T.; Borgogna, M.; Draget, K.I.; Skjåk-Bræk, G.; Paoletti, S. *Biomacromolecules* **2007**, *8*, 957–962.
45. Mazumder, M. A. J.; Shen, F.; Burke, N. A. D.; Potter, M. A; Stöver, H. D. H. *Biomacromolecules* **2008**, *9*, 2292–2300.
46. Shen, F.; Mazumder, M. A. J.; Burke, N. A. D.; Stöver, H. D. H.; Potter, M. A. *J. Biomed. Mater. Res., Part B* **2009**, *90B*, 350–361.
47. Mazumder, M. A. J.; Burke, N. A. D.; Shen, F.; Potter, M. A.; Stover, H. D. H. To be submitted.
48. Mazumder, M. A. J.; Burke, N. A. D.; Shen, F.; Potter, M. A.; Stover, H. D. H. *Biomacromolecules* **2009**, *10*, 1365–1373.
49. Holme, H. K.; Davidsen, L.; Kristiansen, A.; Smidsrød, O. *Carbohydr. Polym.* **2008**, *73*, 656–664.
50. Ross, C. J. D.; Bastedo, L.; Maier, S. A.; Sands, M. S.; Chang, P.L. *Hum. Gene Ther.* **2002**, *11*, 2117–2127.
51. Li, A. A.; Shen, F.; Zhang, T.; Cirone, P.; Potter, M.; Chang, P. L. *J. Biomed. Mater. Res., Part B* **2006**, *77*, 296–306.

52. Burke, N. A. D.; Mazumder, M. A. J.; Hanna, M.; Stöver, H. D. H. *J. Polym. Sci., Part A: Polym. Chem.* **2007**, *45*, 4129–4143.
53. Bysell, H.; Malmsten, M. *Langmuir* **2006**, *22*, 5476–5484.
54. Shen, F.; Li, A. A.; Gong, Y-K.; Somers, S.; Potter, M. A.; Winnik, F. M.; Chang, P. L. *Hum. Gene Ther.* **2005**, *16*, 971–984.
55. Strand, B. L.; Morch, Y. A.; Espevik, T.; Skjak-Braek, G. *Biotechnol. Bioeng.* **2003**, *82* (4), 386–394.
56. Ross, C. J. D.; Bastedo, L.; Maier, S. A.; Sands, M. S.; Chang, P. L. *Hum. Gene Ther.* **2002**, *11*, 2117–2127.
57. Thu, B.; Gåserød, O.; Paus, D.; Mikkelson, A.; Skjåk-Bræk, G.; Toffanin, R.; Vittur, F.; Rizzo, R. *Biopolymers* **2000**, *53*, 60–71.
58. Velings, N. M.; Mestdagh, M. M. *Polym. Gels Networks* **1995**, *3*, 311–330.
59. Goosen, M. F. A.; O'Shea, M.; Gharapetian, H. M.; Chou, S.; Sun, A. M. *Biotechnnol. Bioeng.* **1985**, *27*, 146–150.
60. King, G. A.; Daugulis, A. J.; Faulkner, P.; Goosen, M. F. A. *Biotechnol. Prog.* **1987**, *3*, 231–240.
61. Gåserød, O.; Smidsrød, G.; Skjåk-Bræk, G. *Biomaterials* **1998**, *19*, 1815–1825.
62. 70 mM Na citrate was found to be sufficient to extract calcium from CaAlg beads.
63. Vogel, M. K.; Cross, R. A.; Bixler, H. J.; Guzman, R. J. *J. Macromol. Sci. Chem. A* **1970**, *4*, 675–692.
64. Morris, P. J. *Trends Biotechnol.* **1996**, *14*, 163–167.
65. Grigorescu, G.; Rehor, A.; Hunkeler, D. *J. Microencapsulation* **2002**, *19*, 245–259.
66. Qi, W.; Ma, J.; Liu, Y.; Liu, X.; Xiong, Y.; Xie, Y.; Ma, X. *J. Membr. Sci.* **2006**, *269*, 126–132.
67. Xing, Z. C.; Huh, M. W.; Kang, I. K. *Key Eng. Mater.* **2007**, *342−343*, 417–420.
68. Vandenbossche, G. M. R.; Oostveldt, P. V.; Remon, J. P. *J. Pharm. Pharmacol.* **1991**, *43*, 275–27.
69. De Belder, A. N.; Granath, K. *Carbohydr. Res.* **1973**, *30*, 375–378.

Downloaded by STANFORD UNIV GREEN LIBR on June 23, 2012 | http://pubs.acs.org
Publication Date (Web): November 17, 2010 | doi: 10.1021/bk-2010-1053.ch008

Chapter 8

Polymer/Dendrimer Supported Organoplatinum Drugs

B. A. Howell[*]

Center for Applications in Polymer Science and Department of Chemistry, Central Michigan University, Mt. Pleasant, MI 48859-0001
[*]bob.a.howell@cmich.edu

Organoplatinum antitumor agents are broad-spectrum, very effective cancer drugs. The simplest of these, Cisplatin [cis-dichlorodiamineplatinum(II)], has long been a prominent component of cancer treatment. However, this drug and others of the class suffer from rather acute toxicity such that side effects associated with its use are significant. While forced-hydration therapy can be practiced to limit the concentration of active organoplatinum species in the extracellular fluid it is not highly effective in minimizing the side effects accompanying drug administration. Release of active platinum drug from a suitable carrier at a low rate might be a better approach to limiting the effective drug concentration to levels below that needed to induce side effects. Hydrophilic, biocompatible polymers have been used as carriers for platinum antitumor compounds. An initial approach involved the formation of noncovalent complexes of appropriate organoplatinum compounds with poly(N-vinylprrolidone). Direct platination of poly(acrylamide)s derived from 1,2-oxazine has been utilized to prepare a range of drug conjugates. However, the greatest potential for the generation of a suitable polymeric prodrug arises from the treatment of a generation 4.5 poly(amidoamine) [PAMAM] dendrimer with diaquo(1,2-diaminocyclohexane) platinum (II). A well-defined dendrimer-platinum conjugate containing forty (1,2-diaminocyclohexane)platinum(II) units coordinated to the dendrimer surface *via* carboxylate groups is formed. This adduct is well-behaved, water-soluble, contains a high loading of platinum units, and displays sustained release

In Polymeric Delivery of Therapeutics; Morgan, S., et al.;
ACS Symposium Series; American Chemical Society: Washington, DC, 2010.

of active platinum species over a twenty-four hour period under physiological conditions.

Keywords: Multivalent antitumor drugs; nanoscule drugs; polymeric prodrugs; sustained-release drug formulations; effective organoplatinum drugs

Downloaded by STANFORD UNIV GREEN LIBR on June 23, 2012 | http://pubs.acs.org
Publication Date (Web): November 17, 2010 | doi: 10.1021/bk-2010-1053.ch008

1. Introduction

Several developments have impacted the formulation of effective, non-toxic, water-soluble, sustained action organoplatinum antitumor drugs. The first was the serendipitous discovery of the remarkable biological activity of *cis*-dichlorodiammineplatinum(II) [Cisplatin] (*1–8*). Cisplatin is a broad-spectrum cancer drug effective against a wide range of tumors. For many years Cisplatin was the most widely used anticancer drug. It is often used in combination with organic antitumor compounds or with Carboplatin [1,1-cyclobutanedicarboxylato(diammine)platinum(II)]; the second platinum anticancer drug to gain widespread commercial use]. Carboplatin displays a somewhat different toxicity profile than does Cisplatin, making it an attractive compliment to Cisplatin (*9–11*).

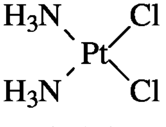

Cisplatin

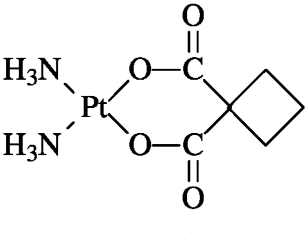

Carboplatin

Both of these compounds reflect the structure required for antitumor activity [two inert *cis* ligands and two labile ligands; chloride displays a near optimum hydrolysis rate under physiological conditions – a pseudo first order half-life of about one hour at 37°C].

The potential of these drugs has been limited because of severe side effects which accompany their administration. Among the most debilitating side effects induced by organoplatinum drugs are severe kidney damage (*12*) and extreme nausea (as a class the platinum compounds are among the most effective nausea producing agents known – to the point that some patients refuse to complete the treatment regimen) (*13*, *14*). In an attempt to identify active but less toxic drugs literally hundreds of platinum compounds in which the structure of the amine ligand has been varied have been synthesized and evaluated for antitumor activity. In the main, this has been a fruitless undertaking. While some ligands impart better solubility, activity, or toxicity than similar properties associated with compounds derived from simple ammonia ligands, no compounds with clearly superior performance have been found. Of the hundreds of compounds synthesized, fewer than thirty have entered clinical trials as antitumor agents (*15*, *16*).

A second development has been huge progress in the utilization of polymeric carriers for a variety of drugs (*17–25*). The use of a polymer-drug conjugate may provide a number of advantages over the drug alone. These may include increased water solubility, sustained delivery of drug, reduced toxicity, enhanced biodistribution, and preferential penetration of abnormal tissue.

A third development has been the discovery of dendritic polymers (*26*, *27*). Dendrimers offer multiple modes of drug incorporation. In particular, the poly(amidoamine) [PAMAM] dendrimers are attractive as drug carriers. They are water-soluble, multivalent, and in general, nontoxic (*28–30*). Dendrimers are highly branched macromolecules with precisely controlled size, shape and end-group functionality. They represent unique core-shell structures consisting of three basic architectural components: a core, an interior of shells (generations) have repeating branch-cell units, and terminal functional groups (the outer shell or periphery). Each generation is built sequentially from a predecessor to form a symmetrical, nearly monodisperse structure of precise molecular weight and nanoscale dimensions (*31*). For PAMAM dendrimers half-generation structures are carboxyl-terminated; full generations are amine-terminated. Both types of functionality are useful for drug conjugation (*32*).

2. Polymer-Supported Organoplatinum Antitumor Agents

Organoplatinum antitumor drugs, particularly Cisplatin, are widely used for the treatment of testicular, ovarian, bladder, head and neck carcinomas. However, the severe side-effects accompanying administration of these drugs has spurred the development of polymer-supported, sustained release formulations. We have, for some time, been using water soluble polymers as platforms on which a platinum drug or prodrug might be supported and from which it might be slowly released into the extracellular fluid (*33–43*). This approach has several major potential advantages over the traditional forced hydration therapy currently practiced. Firstly, the solubility of the drug formulation may be dramatically enhanced such that the volume of the fluid required to introduce a satisfactory dose of drug is strongly diminished [Cisplatin has a solubility of about 10 mg/L in aqueous saline]. More importantly, if the release rate is optimal, the drug is released into the blood stream at a level that is beneath the toxicity threshold such that side effects may be mitigated (*44*). Early attempts involved the formation of noncovalent complexes with poly(N-vinylpyrrolidone) (*33–39*). A strong positive with the respect to the use of this polymer is its long history in biological applications and its approval for use in food and drug applications.

2.1. Noncovalent Complexes of Organoplatinum Antitumor Agents with Poly(N-Vinylpyrollidone)

Poly(N-vinylpyrrolidone) has several properties that make it attractive for use in a sustained-release formulation.

Downloaded by STANFORD UNIV GREEN LIBR on June 23, 2012 | http://pubs.acs.org
Publication Date (Web): November 17, 2010 | doi: 10.1021/bk-2010-1053.ch008

This polymer

1. is readily available in medical grade and in several molecular weight ranges
2. is water soluble
3. has long been used as a blood extender with no known toxicity
4. has FDA approval for use in drug and food applications
5. is widely used as a clarification agent in the beverage industry
6. forms stable molecular complexes with aromatic compounds bearing polar functional groups (*45–48*)

Downloaded by STANFORD UNIV GREEN LIBR on June 23, 2012 | http://pubs.acs.org
Publication Date (Web): November 17, 2010 | doi: 10.1021/bk-2010-1053.ch008

The ability of this material to form molecular complexes with polar aromatic functionality provides a ready means of attachment of compounds containing a labile platinum moiety suitable for hydrolytic release to form an active antitumor species. Compounds of the following type would be suitable for this purpose.

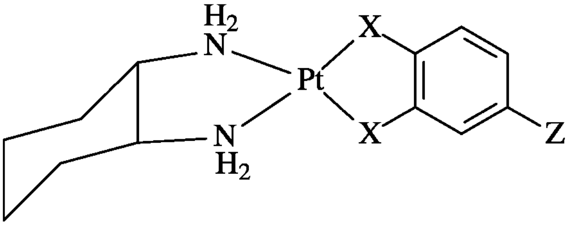

Such compounds contain *trans*-1,2-diaminocyclohexane as an inert ligand and a suitable aromatic ligand bearing a polar group (Z) for complexation with the polymer. The coordinating units (X) should have hydrolytic lability comparable to that of chloride. Complexes of the following kind would be formed.

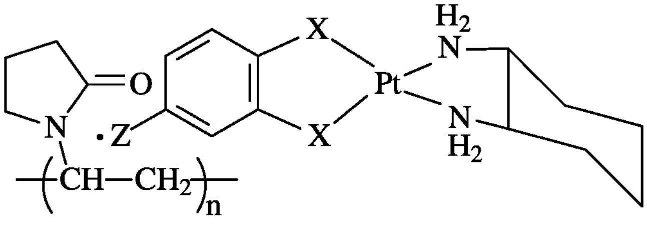

The initial compounds prepared contained 4-substitued catecholato units as labile legands (*38*). In general, the catechol derivatives were prepared by modification of the 2-butanone ketal of catechol followed by removal of the protecting group.

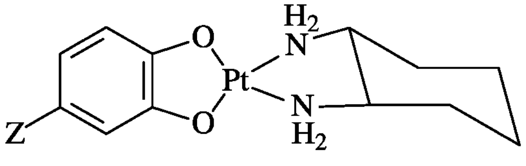

Pertinent infrared absorptions for the platinum compounds are listed in Table I. Initial screening using the inhibition of salmon DNA denaturation as an indicator suggested that the rate of hydrolytic removal of the catecholato ligand of these compounds is too great to permit their use as effective antitumor compounds. Catecholato ligands are considerable better leaving groups than chloride. To reduce the hydrolytic reactivity of the labile ligands corresponding compounds containing substituted phthallato ligands were prepared.

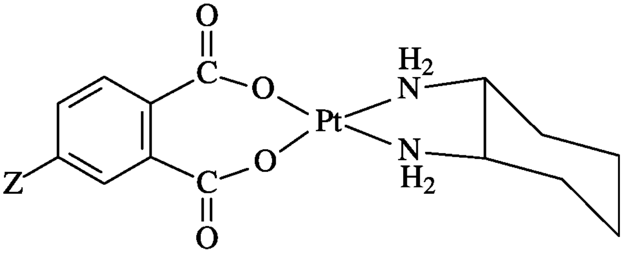

The hydrolytic stability of these compounds is considerably greater than that for the corresponding catecholato compounds. Finally, a series of salicylato compounds with hydrolytic stability intermediate between those of the two earlier sets of compounds was prepared (see Table II) (*39*, *49*).

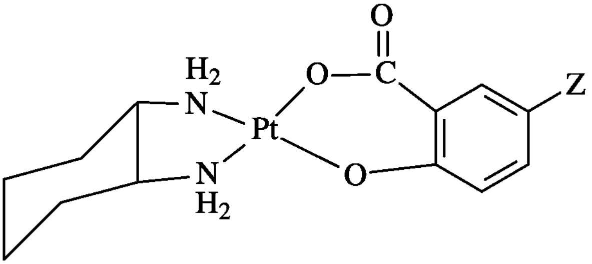

2.2. Poly(acrylamide)s Derived from Tetrahydro-1,2-oxazine as Macroscopic Ligands for Platinum(II) Moieties

Tetrahydro-1,2-oxazine may be generated by synthesis starting from commercially available cyclohexanone oxime (*50*). Chlorination of the oxime affords 1-chloro-1-nitrosocyclohexane which undergoes cycloaddition with 1,3-butadiene to generate an adduct which fragments in the presence of a protic solvent to form dihydro-1,2-oxazine. Mild reduction of this compound provides tetrahydro-1,2-oxazine. Treatment of this compound with acryloyl chloride generates the corresponding acrylamide (Scheme 1). The acrylamide readily undergoes radical polymerization (Scheme 2) to provide a polymer which displays great versatility for the formation of platinum compounds (*51–53*).

Downloaded by STANFORD UNIV GREEN LIBR on June 23, 2012 | http://pubs.acs.org
Publication Date (Web): November 17, 2010 | doi: 10.1021/bk-2010-1053.ch008

Downloaded by STANFORD UNIV GREEN LIBR on June 23, 2012 | http://pubs.acs.org
Publication Date (Web): November 17, 2010 | doi: 10.1021/bk-2010-1053.ch008

Table I. Metal-Ligand Absorption Bands in the Infrared Spectra of Catecholato(1,2-diaminocyclohexane)platinum (II) Compounds

Catechol ligand	*Absorption (cm^{-1})*	
	Pt-N	*Pt-O*
Catechol	537, 482	383, 342
4-Nitrocatechol	506, 421	383, 338
4,5-Dinitrocatechol	504, 439	399, 344
4-Acetylcatechol	510, 440	360
4-Formylcatechol	510, 440	240
2-Sulfo-6,7-dihydroxynapthalene	495, 439	390
3,6-Disulfo-1-nitroso-2-hydroxynaphthalene	486, 442	387

Borane reduction of the amide generates a pendant amine that may interact with platinum species (Scheme 3). More importantly the N-O bond of the oxazine undergoes hydrogenolysis to form a pendant δ-hydroxyamine suitable for interaction with platinum species or chain extension to form a tether of greater length (Scheme 4).

2.3. PAMAM Dendrimers as Supports for Organoplatinum Antitumor Species

2.3.1. Antitumor Activity of PAMAM(G3.5)-Cisplatin

The first preclinical study of a PAMAM dendrimer-platinate conjugate for the delivery of antitumor agents was reported in 1999 (*54*). A generation 3.5 PAMAM dendrimer containing carboxylate surface groups was treated with Cisplatin to generate a dendrimer-platinate (20-25 wt% Pt, about 22 Cisplatin units) which was highly water soluble and had a much higher platinum loading than observed for N-(2-hydroxypropyl)methacrylamide (HPMA) copolymer platinates (3-8 wt% platinum) (*55*). Size exclusion chromatography (GPC) and particle size photon correlation spectroscopy revealed that the PAMAM(G3.5)-Cisplatin conjugate consisted of a number of species including those arising from monodentate and bidentate to carboxylate groups as well as cross-linked dendrimer via platinum bridges, which caused an increase in particle size from 3-4 nm in the parent dendrimer to 30-40 nm diameter of the dendrimer-Cisplatin adduct. Thus, a variety of platinum species, including some physically entrapped Cisplatin, were present in the polymer-drug conjugate. *In vivo* the dendrimer-Cisplatin and Cisplatin administered intraperitoneally (i.p.) were equally active against L1210, and at high dose dendrimer-Cisplatin displayed activity against B16F10 whereas Cisplatin did not. Additionally, when administered intravenously (i.v.) to treat a palpable squamous cell (s.c.) B16F10 melanoma, the PAMAM(G3.5)-Cisplatin adduct displayed antitumor activity whereas Cisplatin was inactive. Measurement of platinum levels in blood and tissues after i.v. injection of Cisplatin (1 mg/kg)

Downloaded by STANFORD UNIV GREEN LIBR on June 23, 2012 | http://pubs.acs.org
Publication Date (Web): November 17, 2010 | doi: 10.1021/bk-2010-1053.ch008

Table II. Metal-Ligand Absorption Bands in the Infrared Spectra of Salicylato(1,2-diaminocyclohexane)platinum(II) Compounds

Salicylate ligand	*Absorption (cm^{-1})*	
	Pt-N	*Pt-O*
4-Amino-2-hydrozybenzoic acid	557, 438	364, 345
4-Bromo-2-2hydroxybenzoic acid	567, 437	365, 349
2-Hydroxybenzoic acid	534, 441	391, 360
2,4,6-Trihydroxybenzoic acid	559, 439	373, 354
2-Hydroxy-3,5-dinitrobenzoic acid	548, 443	366, 351
2-Hydroxy-5-nitrobenzoic acid	515, 440	367, 357
3-Hydroxy-2-naphthoic acid	477, 437	370, 351
2-Hydroxy-5-(3-sulfoxyazaphenyl) benzoic acid	571, 433	373, 352

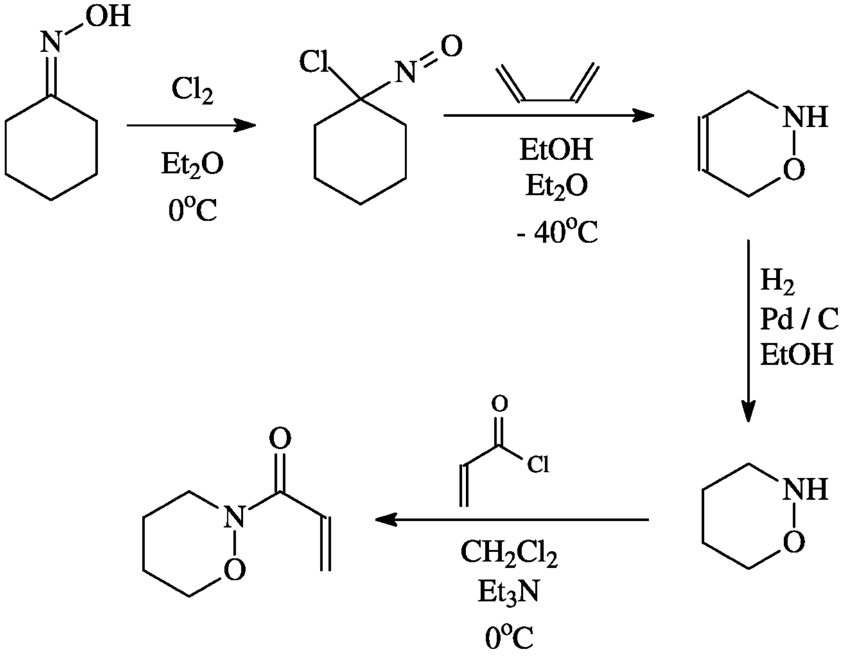

Scheme 1. Synthesis of 2-Acryloyltetrahydro-1,2-oxazine.

or dendrimer-Cisplatin (15 mg/kg) – the maximum tolerated dose (MTD) of these compounds – showed selective accumulation of the dendrimer-Cisplatin in solid tumor tissue by the enhanced permeability and retention (EPR) effect. The improved activity in the s.c. solid tumor model versus the i.p. ascites is indicative of the importance of the EPR effect in tumor targeting. This PAMAM(G3.5)-Cisplatin conjugate was also less toxic (3- to 15-fold) than Cisplatin and thus has potential for further investigation as a novel antitumor approach. However, the release of active platinum species was not detected by atomic absorbance spectrometry (less than 1% of the total platinum released) in pH 7.4 and pH 5.5 buffer solutions over a period of 72 hours. It should also be noted that the exact proportion of the dendrimer-Cisplatin made available as the active diaquo species is not yet known and indeed the time course of platinum liberation is yet to be determined.

2.3.2. Synthesis and Characterization of PAMAM(G4.5)-[(DACH)Pt]

Although the activity of the above polymer-platinum conjugate is impressive, the ill-defined nature of the multiple species present as well as the variable release rates for these entities makes this less than an ideal formulation for the treatment of disease. More recently, a generation 4.5 PAMAM dendrimer nanoconjugate containing (1,2-diaminocyclohexane)platinum(II) [(DACH)Pt] moieties covalently bound to surface carboxylate groups has been prepared (*32*, *56*, *57*). For the preparation of a useful drug formulation, the PAMAM(G4.5) dendrimer has several positive features. Generally, high generation symmetrical dendrimers ($G \geq 4$) have globular structure with peripheral densely-packed terminal groups (*58*). In the case of PAMAM (G4.5), 128 carboxylate groups are closely packed on the dendrimer surface. This strongly facilitates the interaction of carboxylate groups with platinum species to construct a dendrimer-based multivalent platinum conjugate. In addition, the carboxylate functionality should serve as labile ligands for platinum moieties such that release of active platinum species [(DACH)Pt] should occur at a sustained rate over a period of time. Biological studies using PAMAM dendrimers have also demonstrated that high generation PAMAM dendrimers are non-immunogenic and display low mammalian toxicity, while anionic PAMAM dendrimers (surface groups with carboxylate or hydroxylic functionalities) are non-toxic *in vitro* (*59–61*). These intrinsic properties of PAMAM (G4.5) dendrimer make it an interesting multivalent macromolecule that can serve as an exo-receptor for the construction of novel dendrimer-based platinum anticancer agents. The *trans*-1,2-diaminocyclohexane platinum(II) moiety was selected as the active species for the dendrimer-platinum nanoconjugate since 1,2-diaminocyclohexane is known to serve as a superior inert ligand for the preparation of platinum antitumor compounds and to contribute to enhanced antitumor activity. Furthermore, the relative bulky size of $[(DACH)Pt(OH_2)_2](NO_3)_2$ and the hydrophobic nature of DACH inhibit the guest drug from penetrating the sterically-crowded surface to access the interior of the dendrimer.

The synthesis of the PAMAM(G4.5)-[(DACH)Pt] nanoconjugate and a diagram of a structural model are presented in Scheme 5. $[(DACH)PtCl_2]$ was prepared from tetrachloroplatinate as previously described (*40*). This, in turn, was treated with aqueous silver nitrate to generate the corresponding diaquo species. Treatment of this intermediate with a pH 5.0 aqueous solution of PAMAM(G4.5) dendrimer produced the dendrimer-based platinum conjugate with carboxylate groups as the labile ligands at the surface of dendrimer. The PAMAM(G4.5)-[(DACH)Pt] conjugate was purified by dialysis against

Downloaded by STANFORD UNIV GREEN LIBR on June 23, 2012 | http://pubs.acs.org
Publication Date (Web): November 17, 2010 | doi: 10.1021/bk-2010-1053.ch008

Downloaded by STANFORD UNIV GREEN LIBR on June 23, 2012 | http://pubs.acs.org
Publication Date (Web): November 17, 2010 | doi: 10.1021/bk-2010-1053.ch008

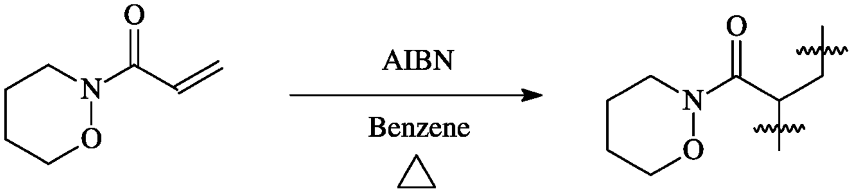

Scheme 2. Polymerization of 2-Acryloyltetrahydro-1,2-oxazine.

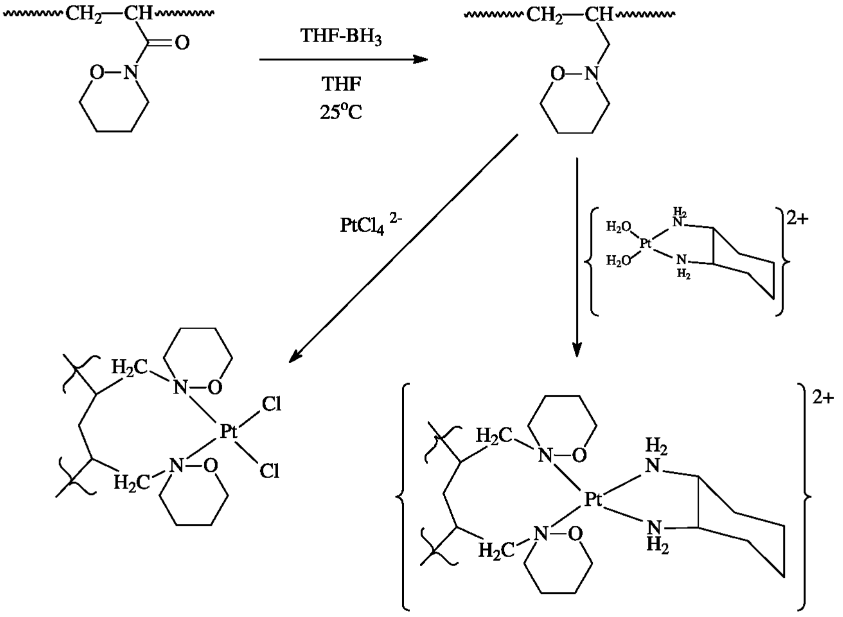

Scheme 3. Formation of Poly[3-(2-tetrahydro-1,2-oxazyl)propylene] and its Interaction with Platinum Species.

deionized water (3500 Da cut-off). The water solubility of the resulting PAMAM(G4.5)-[(DACH)Pt] is extremely good. The resultant sample was checked for purity using thin layer chromatography and dried by lyophilization.

This nanoscale multivalent PAMAM(G4.5)-[(DACH)Pt] conjugate was fully characterized using a variety of spectroscopic, chromatographic and thermal methods. The complexation of surface carboxylate groups by platinum is apparent from the downfield chemical shift of the carboxylate group in the ^{13}C NMR spectrum of the PAMAM(G4.5)-[(DACH)Pt], as shown in Figure 1. Generally, the chemical shift of surface carboxylate of a PAMAM half-generation is smaller than that of interior carbonyl groups (*61*). Here the strong peak at δ 175.2 ppm in Figure 1a corresponds to the 128 surface carboxylates of PAMAM (G4.5). Upon formation of the PAMAM(G4.5)-[(DACH)Pt] conjugate, this absorption is shifted downfield to 177.7 ppm (Figure 1b), reflecting coordination of the surface carboxylate groups with platinum.

Downloaded by STANFORD UNIV GREEN LIBR on June 23, 2012 | http://pubs.acs.org
Publication Date (Web): November 17, 2010 | doi: 10.1021/bk-2010-1053.ch008

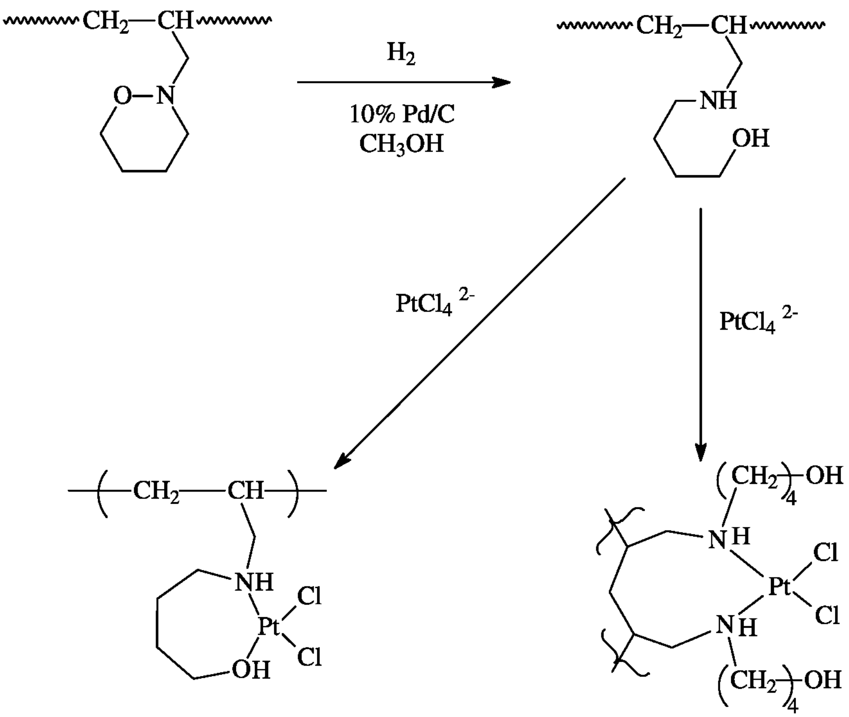

Scheme 4. Formation of Poly[3-(4-hydroxybutylamino)propylene] and its Interaction with Tetrachloroplatinate.

The ^1H NMR spectrum of the conjugate unambiguously shows two characteristic regions representing the ethylene groups (δ 3.60-2.40) of the PAMAM dendrimer and the cyclohexyl portion of the inert ligand (δ 1.80-1.20). It is also important to note that the integration of the signal in the two regions indicates that there are about 40 [(DACH)Pt] units coordinated to each dendrimer. That this is a maximum possible loading of [(DACH)Pt] units per dendrimer is apparent from a series of experiments in which the ratio of $[(DACH)Pt(H_2O)_2](NO_3)_2$ to dendrimer was increased well beyond the theoretical maximum of 64 [(DACH)Pt] units. For example, even when the ratio of $[(DACH)Pt(H_2O)_2](NO_3)_2$ to dendrimer was 192 to 1 (well above that required to saturate the carboxylate surface), the dendrimer-Pt conjugate generated contains 39 (DACH)Pt units. The MALDI-TOF MS data in Table III support this observation and indicate an average of 40 [(DACH)Pt] moieties per dendrimer are bound to the PAMAM(G4.5) surface. This is in close agreement with the results from ^1H NMR spectra and clearly supports the observation that the maximum loading is approximately 40 [(DACH)Pt] moieties per dendrimer molecule. The loading capacity of 40 [(DACH)Pt] units onto the nanocarrier PAMAM(G4.5) is consistent with a recent report of a similar limitation for the interaction of PAMAM (G4, amine surface) with an organic ligand (*62*). Thermogravimetric analyses of the PAMAM(G4.5)-[(DACH)Pt] conjugate was carried out to further ascertain this value. The conjugate begins to decompose at

Downloaded by STANFORD UNIV GREEN LIBR on June 23, 2012 | http://pubs.acs.org
Publication Date (Web): November 17, 2010 | doi: 10.1021/bk-2010-1053.ch008

$$[(DACH)PtCl_2] \xrightarrow[H_2O]{AgNO_3} [(DACH)Pt(OH_2)_2](NO_3)_2$$

$$[(DACH)Pt(OH_2)_2](NO_3)_2 + PAMAM(G4.5) \longrightarrow PAMAM(G4.5)[(DACH)Pt]$$

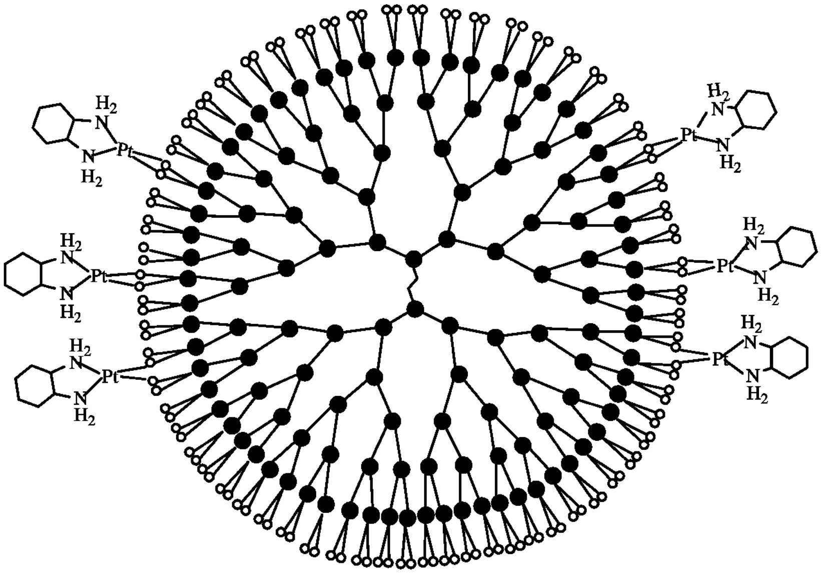

● = —$N(CH_2CH_2CONHCH_2CH_2)_2$ ○ = COO^-

Scheme 5. Synthesis of PAMAM(G4.5)-[(DACH)Pt] Nanoconjugate and a Diagram of its Structure (other [(DACH)Pt] units omitted for clarity).

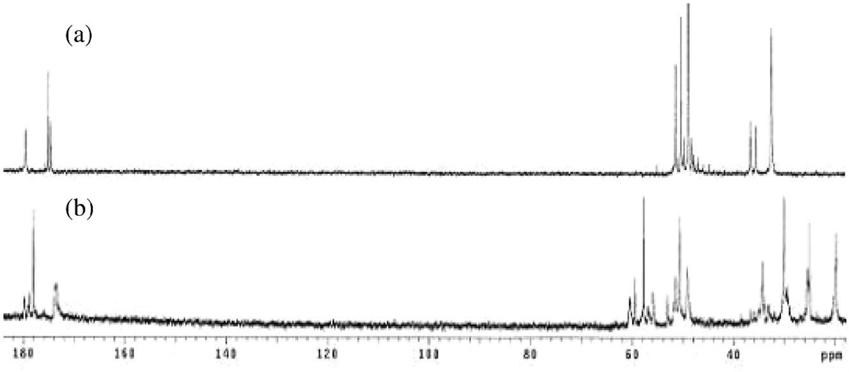

Figure 1. ^{13}C NMR Spectra of (a) PAMAM(G4.5) and (b) PAMAM(G4.5)-[(DACH)Pt] Conjugate in D_2O.

173 °C and a stable residue of platinum oxide is obtained at 910 °C, as shown in Figure 2. The mass of the residual oxide corresponds to 24.1% of the initial sample mass. This is in excellent agreement with that expected (24.7%) for a dendrimer-Pt conjugate containing 40 [(DACH)Pt] moieties. In poly(acrylamide) gel electrophoresis (PAGE), the migration difference between PAMAM(G4.5) and its [(DACH)Pt] conjugate is clearly a result of loading of [(DACH)Pt] moieties onto dendrimer, leading to the increment of the mass value of the conjugate. Remarkably, the drug loading of capacity about 40 [(DACH)Pt] units on PAMAM(G4.5) dendrimer is significantly higher than that observed for the PPI "dendritic-box" (4 large or 8-10 small guest molecules) (*63*) and for a traditional N-(2-hydroxypropyl)methacrylamide (HPMA) copolymer (3-8 wt% platinum) (*55*).

Molecular dynamic simulation is a powerful tool for the theoretical evaluation of the energetic and structural properties of this new class of marcomolecules – dendrimers. There have been numerous molecular dynamics studies for dendrimers which are in good correlation with experimental results. Molecular dynamic simulation has been carried out to investigate the various binding sites for interaction of surface carboxylate groups of PAMAM (G4.5) dendrimers with [(DACH)Pt] species. To some extent, available experimental results have been used to form a base for the computational study. For example, preferred binding sites, in some cases, could be inferred from the results of NMR studies of the binding of platinum moieties to similar polymers, DNA in particular. The available NMR data are not always as useful as might be expected. However, this has proven to be a useful starting point for molecular simulation. Computational simulation has been used to probe the attachment of active organoplatinum fragments to dendrimers, which would serve as a nanocarrier from which the active species might be released over an extended period of time.

The molecular dynamic simulations for the PAMAM(G4.5)-[(DACH)Pt] conjugate were performed using the Forcite module of Accelyrs with universal forcefield [Accelrys Software Inc., San Diego] for 500 psec with 1 femto-second time intervals at 298 K in vacuum after global minimization of 5000 iterations. The minimum energy was then computed for each addition of [(DACH)Pt] to two carboxylates at the PAMAM(G4.5) surface. Various methods have been employed to authenticate the total number of [(DACH)Pt] units which can be attached to the surface carboxylate groups of the dendrimer. The simulation for PAMAM(G4.5)-[(DACH)Pt] shows that the minimum energy for the conjugate is reached when 44 [(DACH)Pt] units are attached to PAMAM(G4.5) dendrimer surface (see Figure 3). This simulation result is in good agreement with the experimental data which demonstrate that about 40 [(DACH)Pt] units are attached to the surface carboxylate groups of the PAMAM(G4.5) dendrimer (*32*).

Dendrimers may be viewed as a unique new class of synthetic nanodevices and PAMAM dendrimers have been generally used as nanoscale building blocks to construct more complex dendritic topologies (*65*, *66*). The dimensions of this PAMAM(G4.5)-[(DACH)Pt] conjugate have been determined using MAC mode atomic force microscopy (AFM). The AFM images of the conjugate on a freshly cleaved mica surface clearly show both individual single molecules and a few aggregates. Detailed cross-sectional measurements on 150 isolated features reflect

Downloaded by STANFORD UNIV GREEN LIBR on June 23, 2012 | http://pubs.acs.org
Publication Date (Web): November 17, 2010 | doi: 10.1021/bk-2010-1053.ch008

Table III. MALDI-TOF Mass Values for Six Preparations of PAMAM(G4.5)-[(DACH)Pt]

Batch	*Molar Ratio of G4.5:[(DACH)Pt]*	*Observed Mass Value*	*No of [(DACH)Pt]**
1	1:48	29271	33
2	1:64	30706	38
3	1:64	31075	40
4	1:72	31538	41
5	1:128	32318	44
6	1:192	30935	39
	Pure PAMAM(G4.5)	20665	-

* No. of [(DACH)Pt] is calculated on the basis of mass value of pure PAMAM(G4.5).

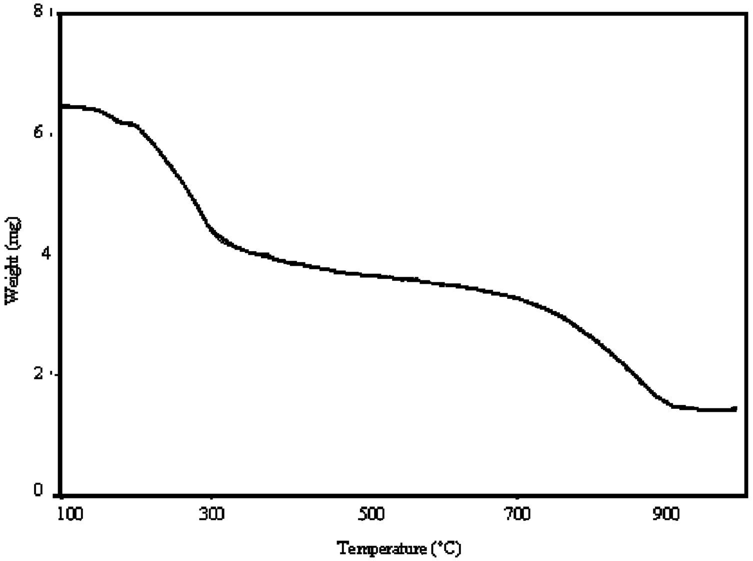

Figure 2. Thermogravimetric Analysis for PAMAM(G4.5)-[(DACH)Pt].

an average height of 0.40 (±0.16) nm and an average diameter of 7.83 (±1.62) nm. The AFM images document the formation of a novel nanoconjugate of the PAMAM(G4.5) and [(DACH)Pt]. The size of the Pt-conjugate is in the nanoscale range as has been observed for other dendrimer species (*67*). The particles depicted in the AFM image appear to be substantially uniform in size and globular in shape.

2.3.3. In Vitro Release of [(DACH)Pt]

The release profile for the active component [(DACH)Pt] was investigated in pH 7.4 phosphate buffer and pH 5.0 phosphate-citrate saline solutions at

Downloaded by STANFORD UNIV GREEN LIBR on June 23, 2012 | http://pubs.acs.org
Publication Date (Web): November 17, 2010 | doi: 10.1021/bk-2010-1053.ch008

Downloaded by STANFORD UNIV GREEN LIBR on June 23, 2012 | http://pubs.acs.org
Publication Date (Web): November 17, 2010 | doi: 10.1021/bk-2010-1053.ch008

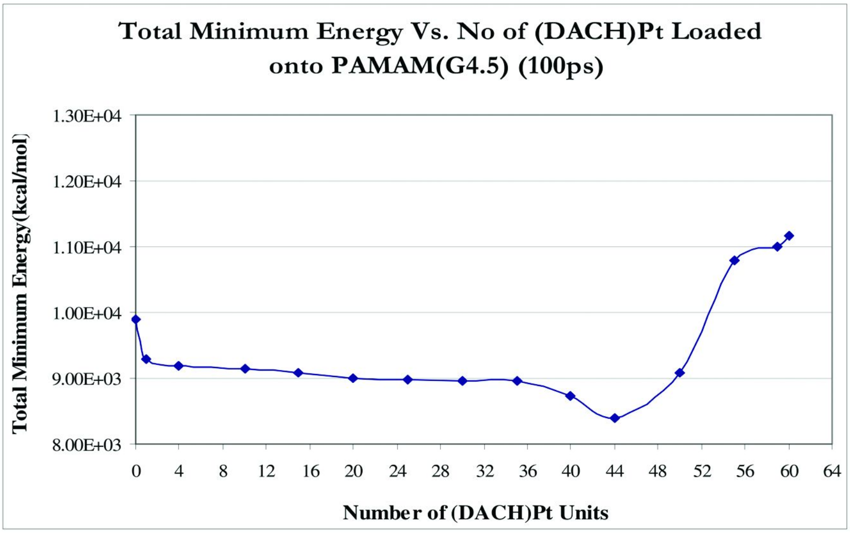

Figure 3. Total Minimum Energy versus Number of (DACH)Pt Units Added Onto PAMAM(G4.5) (using 500 ps simulation).

37° C by measuring the UV-vis absorbance of the dialysis saline at 292 nm, which is the characteristic UV-vis absorbance peak of the [(DACH)Pt] species. The preliminary *in vitro* release tests showed that most of the active species [(DACH)Pt] is smoothly released from the dendrimer nanocarrier over a period of 24 hours. The profile for the release of [(DACH)Pt] from the substrate PAMAM(G4.5) is shown in Figure 4. Overall, the release rate is very good with 76% in pH 7.4 buffer and 85% of the available platinum species in pH 5.0 buffer released in 24 hours, respectively. This behavior suggests that sustainable release should occur inside endosomes at lower pH. The mode of release is probably similar to that observed for other classic platinum drugs in which the labile ligands are carboxylate groups. Generally, under physiological conditions, hydrolysis occurs in a stepwise fashion to form first the monohydrated and subsequently the diaquo platinum species. A study of hydrolysis of Oxaliplatin showed that the ring-opening step has a half-life 16 min and the loss of the oxalate ligand occurs with a half-life of 92 min at 37 °C (*63*). In this case, the [(DACH)Pt] units are released from PAMAM(G4.5)-[(DACH)Pt] nanoconjugate with a half-life of 105 min in pH 5.0 and 310 min in pH 7.4 saline. Therefore, the loss of labile ligand is considerably slower for the PAMAM(G4.5)-[(DACH)Pt] conjugate than that of the similar process for Oxaliplatin and suggests a sustainable release of active drug. These observations suggest that the use of PAMAM(G4.5) nanocarrier for [(DACH)Pt] may be used to generate a drug formulation with water solubility, dosage limitations, and response characteristics superior to those of classical platinum drugs.

Clearly, dendritic polymers may be utilized as nanocarriers for the improved delivery of antitumor agents. They offer several advantages over conventional polymers. Most notably, the nanoscale size, uniform shape, and high surface functionality of these polymers offer the potential for the generation

Downloaded by STANFORD UNIV GREEN LIBR on June 23, 2012 | http://pubs.acs.org
Publication Date (Web): November 17, 2010 | doi: 10.1021/bk-2010-1053.ch008

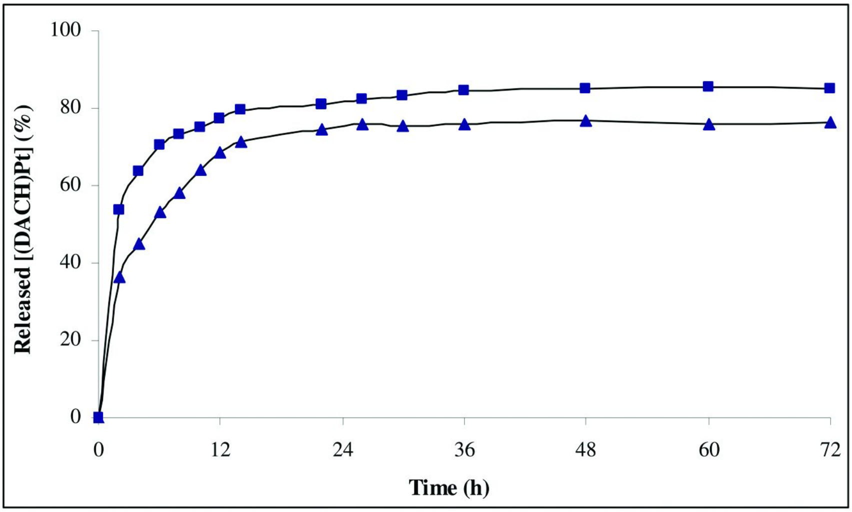

Figure 4. In Vitro Release Profile of [(DACH)Pt] from PAMAM(G4.5)-[(DACH)Pt] in pH 7.4 (▲) and pH 5.0 (■) buffer saline.

of "multivalent" drugs which permit the administration high dosage at low volume and which display enhanced delivery of active agent to the tumor site. In this case, a PAMAM(G4.5) dendrimer has been utilized as a nanocarrier for the generation of a dendrimer-platinum conjugate containing [(DACH)Pt] as the active agent. The dendrimer-platinum conjugate is well-defined with approximately forty [(DACH)Pt] units bound through surface carboxylate groups. This is distinctly unlike an earlier dendrimer-platinum formulation generated from the interaction of a PAMAM(G3.5) dendrimer with Cisplatin in which some platinum species are bound at surface groups, some are bound at interior tertiary nitrogen atoms, and some are physically trapped as unchanged Cisplatin. There are probably at least two reasons for this difference. The first is the more open structure of the smaller generation 3.5 dendrimer. In addition, the large difference in reactivity toward nucleophilic ligands of Cisplatin and diaquo(1,2-diaminocyclohexane)platinum(II) probably limits the effectiveness of the interaction of Cisplatin with surface groups. The loading of active platinum species is much larger than that achieved for earlier PAMAM(G3.5) dendrimer conjugates and considerably higher than that normally observed for linear polymer platinum conjugates. At the same time, the water solubility and release characteristics are superior to those observed for most polymeric platinum drugs. This conjugate displays sustained release of active platinum species over a period of 24 hours under physiological conditions. The PAMAM(G4.5)-[(DACH)Pt] represents a considerable improvement over previous dendrimer-platinum formulations and offers significant opportunity for clinical use.

Downloaded by STANFORD UNIV GREEN LIBR on June 23, 2012 | http://pubs.acs.org
Publication Date (Web): November 17, 2010 | doi: 10.1021/bk-2010-1053.ch008

3. Potential of Polymer/Dendrimer Supported Organoplatinum Antitumor Agents

As in many other area of drug delivery polymer-platinum conjugates offer some significant advantages over use of the unmodified drug. Enhanced water solubility, improved dosage protocols, reduced toxicity, and more effective utilization of the available active agent are all desirable features provided by the polymer-drug conjugate. In particular, the availability of nontoxic, water-soluble dendritic polymers containing high surface functionality offer great potential for the development of novel, highly effective organoplatinum antitumor formulations of toxicity much lower than that characteristic of simple platinum drugs. For the development of well-behaved dendrimer-platinum conjugates, the dendrimer should be large enough so that surface crowding prevents entry of reactive species into the interior of the molecule and the platinum reagent should be sufficiently reactive so as to be readily bound by ligands at the surface of the dendrimer. These conditions seem to be well met by a generation 4.5 PAMAM dendrimer (128 surface carboxylate groups) and diaquo(1,2-diaminocyclohexane)platinum(II). Presumably, because of the steric crowding, the theoretical maximum number of platinum moieties (*64*) cannot be attached to the dendrimer surface. In the case of (1,2-diaminocyclohexane)platinum(II) approximately forty units may be placed at the surface of the dendrimer. This dendrimer-platinum conjugate displays sustained release of active platinum species over 24 hours under physiological conditions. These results offer considerable optimism; for the use of dendrimers in the development of more effective but less toxic organoplatinum antitumor agents.

References

1. Rosenberg, B.; VanCamp, L.; Krigas, T. *Nature* **1965**, *205*, 698.
2. Rosenberg, B.; VanCamp, L.; Grimley, E. B.; Thomson, A. J. *J. Biol. Chem.* **1967**, *242*, 1347.
3. Rosenberg, B.; VanCamp, L.; Trosko, J. F.; Mansour, V. H. *Nature* **1969**, *222*, 385.
4. Rosenberg, B. In *Nuclei Acid-Metal Ion Interactions*; Spiro, T. G., Ed.; John Wiley and Sons, New York, NY, 1980; pp 1−29.
5. Rosenberg, B. *Cancer* **1985**, *55*, 2303.
6. Jamieson, E. R.; Lippard, S. J. *Chem. Rev.* **1999**, *99*, 2467.
7. Wong, E.; Giandomenico, C. M. *Chem. Rev.* **1999**, *99*, 2451.
8. Wang, D.; Lippard, S. J. *Nat. Rev. Drug Discovery* **2005**, *4*, 307.
9. Dabrowiak, J.; Bradner, W. *Prog. Med. Chem.* **1987**, *24*, 129.
10. Kelland, L. *Crit. Rev. Oncol. Hematol.* **1992**, *15*, 191.
11. McKege, M.; Kelland, L. In *Molecular Aspects of Drug-DNA Interactions*; Neidle, S., Waring, M., Eds.; Macmillian: New York, 1992.
12. Jones, T. W.; Chopra, S.; Kaufman, J. S.; Flamenbaum, W.; Trump, B. F. *Lab. Invest.* **1985**, *52*, 363.
13. Rosenberg, B. *Inorganic and Nutritional Aspects of Cancer* **1971**, *91*, 129.
14. Aggrarwal, S. K.; Menon, G. K. *J. Clin. Hematol. Oncol.* **1981**, *11*, 73.

Downloaded by STANFORD UNIV GREEN LIBR on June 23, 2012 | http://pubs.acs.org
Publication Date (Web): November 17, 2010 | doi: 10.1021/bk-2010-1053.ch008

15. Neuse, E. *Polym. Adv. Technol.* **1988**, *9*, 786.
16. Lebwohl, D.; Canetta, R. *Eur. J. Cancer* **1998**, *34*, 1522.
17. Jagur-Grodzinski, J. *Polym. Adv. Technol.* **2009**, *20*, 595.
18. Hoste, K.; DeWinne, K.; Schacht, E. *Int. J. Pharm.* **2004**, *277*, 119.
19. Khandare, J.; Minko, T. *Prog. Polym. Sci.* **2006**, *31*, 359.
20. Duncan, R. *Nat. Rev. Cancer* **2006**, *6*, 688.
21. Duncan, R. *Nat. Rev. Drug Discov.* **2003**, *2*, 347.
22. Batz, H.-G. *Adv. Polym. Sci.* **1977**, *23*, 25.
23. Langer, R. L. *Nature* **1998**, *392*, 5.
24. Langer, R. L. *Science* **2001**, *293*, 58.
25. Allen, T. A.; Cullis, P. C. *Science* **2004**, *303*, 1818.
26. Tomalia, D. A.; Dewald, J. R.; Hall, M. J.; Martin, S. J.; Smith, P. B. Preprint, 1st SPSJ International Polymer Conference, Kyoto, Japan, 1984, p 65.
27. Tomalia, D. A.; Baker, H.; Dewald, J. R.; Hall, M.; Kallos, G.; Martin, S.; Roeck, J.; Ryder, J.; Smith, P. B. *Polym. J.* **1985**, *17*, 117.
28. Tomalia, D. A. *Aldrichimica Acta* **1993**, *26*, 91.
29. Tomalia, D. A., Frechet, J. M. J., Eds. *Dendrimers and Other Dendritic Polymers*; John Wiley and Sons, Inc.: New York, NY, 2001.
30. Tomalia, D. A.; Reyna, L. A. *Biochem. Soc. Trans.* **2007**, *35*, 61.
31. Tomalia, D. A. *Aldrichimica Acta* **2004**, *37*, 39.
32. Howell, B. A.; Fan, D.; Rakesh, L. In *Inorganic and Organometallic Macromolecules: Design and Applications*; Abd-El-Aziz, A. S., Carraher, C. E., Jr., Pittman, C. U., Jr., Zeldin, M., Eds.; Springer Science: New York, NY, 2008; Ch. 11.
33. Howell, B. A.; Walles, E. W. Macromolecular Complexes of Amidocarbonylic Water-Soluble Polymers and Square Planar Platinous and Equivalent Organometalics. U.S. Patent No. 4551502, 1985.
34. Howell, B. A.; Walles, E. W.; Rashidianfar, R.; Glass, J. R.; Hutchinson, B. J.; Johnson, D. A. In *Platinum and Other Metal Coordination Compounds in Cancer Chemotherapy*; Nicholi, M., Ed.; Martinus Nijhoff Publishing: Boston, MA, 1988; pp 670−683.
35. Howell, B. A.; Walles, E. W.; Rashidianfar, R. *Macromol. Chem., Macromol. Symp.* **1988**, *19*, 329.
36. Howell, B. A.; Walles, E. W. *Polym. Prepr.* **1986**, *27* (1), 460.
37. Howell, B. A.; Walles, E. W. *Inorg. Chim. Acta* **1988**, *142*, 185.
38. Howell, B. A.; Walles, E. W.; Rashidianfar, R.; Glass, J. R.; Hutchinson, B. J.; Johnson, D. A. *Inorg. Chim. Acta* **1988**, *142*, 181.
39. Howell, B. A.; Beholz, L. G.; Sastry, B. B. S. *J. Therm. Anal.* **1993**, *40*, 395.
40. Howell, B. A.; Richards, R. M. *Polym. Mater. Sci. Eng.* **1996**, *74*, 274.
41. Howell, B. A.; Sastry, B. B. S. *Polym. Mater. Sci. Eng.* **1996**, *74*, 276.
42. Dysterhouse, R. M.; Howell, B. A.; Squattrito, P. J. *Acta Crystallogr.* **2000**, *C56*, 64.
43. Saltmarsh, J. A.; Howell, B. A.; Squattrito, P. J. *Acta Crystallogr.* **2000**, *C56*, 335.
44. For an excellent review of the development of polymer-based organoplatinum antitumor agents see: Siegmann, D. W.; Carraher, C. E., Jr. In *Macromolecules Containing Metal and Metal-Like Elements, Vol. 3,*

Biomedical Applications, Abd-El-Aziz, A. A., Carraher, C. E., Jr., Pittman, C. U., Jr., Sheets, J. E., Zeldin, M., Eds.; Wiley-Interscience, John Wiley and Sons, Inc.: New York, NY, 2004; Ch. 7, pp 119−192.

45. Takagishi, T.; Yoshikawa, K.; Kuroki, N.; Kozuka, H.; Mitsuishi, M. *J. Polym. Sci., Polym. Chem. Ed.* **1984**, *22*, 185.
46. Higuchi, T.; Kuramoto, R. *J. Am. Pharm. Assoc.* **1954**, *43*, 398.
47. Carpenter, A.; Siggla, S.; Carter, S. *Anal. Chem.* **1976**, *48*, 225.
48. Gustavson, K. H. *Leder* **1963**, *14*, 27.
49. Howell, B. A.; Beholz, L. G. Salicylato(1,2-diaminocyclohexane)platinum(II) Compounds as Potential Antitumor Agents. XIVth International Conference on Organometallic Chemistry, Detroit, MI, August, 1990.
50. Labaziewicz, H.; Howell, B. A.; Lindsfors, K. R.; Mason, R. C. *Heterocycles* **1992**, *34*, 699.
51. Howell, B. A.; Han, G.; Pakyz, D. J. *Polym. Prepr.* **1996**, *37* (1), 601.
52. Howell, B. A.; Southwell, J. E. *Polym. Prepr.* **1997**, *38* (2), 355.
53. Southwell, J. E. Water-Soluble Polymers Containing Coordinating Pentant Groups Derived from 2-Acryloyltetrahydro-1,2-oxazine. M.S. Thesis, Central Michigan University, Mt. Pleasant, MI, 1988.
54. Malik, N.; Evagorou, E. G.; Duncan, R. *Anti-Cancer Drugs* **1999**, *10*, 767.
55. Gianasi, E.; Wasil, M.; Evagorou, E. G.; Keddle, A.; Wilson, G.; Duncan, R. *Eur. J. Cancer* **1999**, *35*, 994.
56. Fan, D.; Howell, B. A.; Rakesh, L. *Polym. Mater. Sci. Eng.* **2005**, *93*, 946.
57. Howell, B. A.; Fan, D. *Proc. R. Soc. A*, in press.
58. Caminati, G.; Turro, N. J.; Tomalia, D. A. *J. Am. Chem. Soc.* **1990**, *112*, 8515.
59. Roberts, J. C.; Bhalga, M. K.; Zera, R. T. *J. Biomed. Mater. Res.* **1996**, *30*, 53.
60. Malik, N.; Wiwattanapatapee, R.; Klopsch, R.; Lorenz, K.; Frey, H.; Weener, J. W.; Meijer, E. W.; Paulus, W.; Duncan, R. *J. Controlled Release* **2000**, *65*, 133.
61. Wiwattanapatapee, R.; Carreno-Gomez, G.; Malik, N.; Duncan, R. *Pharm. Res.* **2000**, *17*, 991.
62. Esfand, R.; Tomalia, D. A. In *Dendrimers and Other Dendritic Polymers* Frechet, J. M. J., Tomalia, D. A., Eds., John Wiley and Sons, Inc.: New York, NY, 2001; Ch. 25, pp 587−604.
63. Deng, S.; Locklin, J.; Patton, D.; Baba, A.; Advincula, R. C. *J. Am. Chem. Soc.* **2005**, *127*, 1744.
64. Jansen, J. F. G. A.; Bradander-van den Berg, E. M. M.; Meijer, E. W. *Science* **1994**, *265*, 1226.
65. Tomalia, D. A.; Mardel, K.; Henderson, S. A.; Holan, G.; Esfand, R. In *Handbook of Nanoscience, Engineering and Technology*; Goddard, W. A., III, Brenner, D. W., Lyshevski, S. E., Iafrate, G. J., Eds.; CRC Press: Boca Raton, FL, 2003; p 2021.
66. Uppuluri, S.; Swanson, D. R.; Piehler, L. T.; Li, J.; Hagnauer, G. L.; Tomalia, D. A. *Adv. Mater.* **2000**, *12*, 796.

Downloaded by STANFORD UNIV GREEN LIBR on June 23, 2012 | http://pubs.acs.org
Publication Date (Web): November 17, 2010 | doi: 10.1021/bk-2010-1053.ch008

67. Jerremalm, E.; Videhult, P.; Alvelius, G.; Griffiths, W. J.; Bergman, T.; Eksborg, S.; Ehrsson, H. *J. Pharm. Sci.* **2002**, *91*, 2116.

Downloaded by STANFORD UNIV GREEN LIBR on June 23, 2012 | http://pubs.acs.org
Publication Date (Web): November 17, 2010 | doi: 10.1021/bk-2010-1053.ch008

Downloaded by DUKE UNIV on June 23, 2012 | http://pubs.acs.org
Publication Date (Web): November 17, 2010 | doi: 10.1021/bk-2010-1053.ch009

Chapter 9

Storage and Release of Nitric Oxide from Molecular Sieve Nanoparticles

Harvey A. Liu, Angelo Lubag, and Kenneth J. Balkus, Jr.[*]

**Department of Chemistry, 800 West Campbell Rd., Richardson,
TX 75080-3021
[*]balkus@utdallas.edu**

The role of nitric oxide (NO) as a vasodilator has long been established. Due to the high reactivity and a lack of a practical delivery system for gaseous NO, its applicability has been limited. In this study, we examine the adsorption of the NO within molecular sieves and demonstrate the ability to fabricate composite materials in the form of electrospun fibrous bandage that can release NO with a controlled rate and in physiological relevant doses. The use of the NO releasing fibers for the preservation of transplant organs was demonstrated on rat hearts.

Introduction

Since the discovery of the diatomic free radical nitric oxide (NO) as the endothelium-derived relaxing factor (EDRF) in the 1980s, there have been many studies aimed at understanding the nitric oxide pathways (*1–3*). The increased interest in NO led to its implication in many physiological processes in the body including vasodilation (*2–4*), the immune response (*5*, *6*), social dysfunction (*7*), wound healing (*8*, *9*), as well as many others. The involvement of the signaling molecule, NO, in many mechanisms suggests that storage and delivery systems capable of generating NO may find utility for many applications. An ability to deliver NO in a controlled manner can be exploited for the anti-aggregation of platelets in implants (*10*, *11*), cancer treatment (*12*), antifungal and/or antibacterial coatings (*6*, *13*, *14*), smart textiles for increased circulation in diabetic patients (*15–18*), as well as organ preservation (*19*, *20*).

While NO has been shown to be involved in many processes, the delivery of NO in its natural gaseous state is impractical for therapeutic applications. This problem has led to the development of many materials that can store NO. These materials can be broadly categorized into two classes of materials. A type of NO storage and delivery system includes the covalent attachment of NO with a secondary amine to form a class of molecules deemed diazeniumdiolates (*4*, *11*, *21–24*). Diazeniumdiolates have been synthesized in many forms such as free powders, ligands to nanoparticles, as well as in electrospun fibers functionalized with secondary amines (*25–32*). While these are the most well studied materials, their application still poses problems including the leaching of the parent amine upon NO release, which may contribute to an increased toxicity (*22*, *23*). Additionally, the mechanism of NO release from diazeniumdiolates require careful regulation of the surrounding conditions. It has been demonstrated that the rate and efficiency of NO release from diazeniumdiolates are not only dictated by the parent secondary amine, but by the relative humidity as well as the pH of the surrounding environment (*22*, *23*, *25*, *33*). Recently, we have addressed these concerns by electrospinning composite fibers within the degradable PLA fibers and controlled the release of NO through changing the fiber morphology. While this has addressed the problems posed by diazeniumdiolates, a slow rate of NO release and the low capacity of NO storage prevents its application for organ tranplant applications (*34*).

The stringent requirements for the optimal conditions in NO delivery from diazeniumdiolates, as well as the requirements for organ preservation applications have led to the development of a more simplified strategy in NO storage and delivery. In this effort, zeolites have been utilized because of their low toxicity as well as high storage capacity (*35–38*). Recently, Wheatley et al. demonstrated the ability to store and release NO from the pores of zeolite A for anti-thrombotic applications (*38*). The mechanism of storage in zeolites involves the coordination of the nitric oxide with the metal ions that reside in the pores of the crystalline structure. It has also been shown by Wheatley et al. that the storage capacity as well as the rate can be tailored by varying the exchangeable metal ion that occupies the pores of the zeolite (*38*). The method of NO release in this system is initiated by its exposure to moisture; because of the higher affinity of the metal ion to water, the nitric oxide is released almost immediately upon the presence of atmospheric moisture (*38*). While the greater storage capacity of NO in zeolites is an integral step in NO delivery for therapeutics, its rapid rate of release as well as its physical state as a powder is not ideal for many physiological applications (*38*).

Recently, we have exploited the high NO storage capacity of zeolite A and embedded them within hydrolysable polylactic acid (PLA) polymer fibers by electrospinning (*39*). In this effort we have demonstrated the ability to well disperse the zeolites within the polymer matrix and show a slightly slower rate of release from the fibers than from the pure powder. By integrating the free powder in a free-standing bandage, we have introduced a facile method of NO administration. Additionally, we have also demonstrated that the integration into a fibrous polymer matrix slows the rate of NO release, which can be further dampened through heat-treatment of the polymer fibers (*39*).

Downloaded by DUKE UNIV on June 23, 2012 | http://pubs.acs.org
Publication Date (Web): November 17, 2010 | doi: 10.1021/bk-2010-1053.ch009

Research in zeolites as vehicles for NO storage has naturally progressed and developed into the study of NO storage in other porous materials, particularly metal-organic frameworks (MOFs) (*35*, *40*). As part of this effort, we found that Cu(4,4′-OOC-Ph-Ph-COO)•1/2 TED (Cu-MOF) exhibited a high NO storage capacity, as high as 5 mmol/g, much higher than that seen in zeolitic materials (1mmol/g). In this study we also demonstrate the application of the NO releasing PLA/Zeolite A bandages for the preservation of procured rat hearts, which showed physiological efficacy through the increase in coronary flow rate after its application.

Downloaded by DUKE UNIV on June 23, 2012 | http://pubs.acs.org
Publication Date (Web): November 17, 2010 | doi: 10.1021/bk-2010-1053.ch009

Experimental Section

Materials

Biphenyl-4,4′-dicarboxylic acid (BPDA, 97%), triethylenediamine (TED, 98%), and copper acetate monohydrate ($Cu(OAc)_2 \cdot H_2O$, >99%) were obtained from Aldrich and used without further treatment. Formic acid (98%, 2% H_2O) was purchased from Fluka and used as received. HPLC grade water was obtained from Fisher and used as received. Molecular sieves 4A 4-8 mesh (Sigma-Aldrich) were washed with HPLC grade water, activated at 400 °C for 1 d, cooled to room temperature in a vacuum oven at low pressure, and stored in capped bottles filled with nitrogen for later use. Chloroform (99.9%, H_2O <0.002%), acetone (99.7%, H_2O = 0.3%), and toluene (99.8%, H_2O = 0.010%) were purchased from Fisher; N,N-dimethylformamide (DMF, 99.8%, H_2O <0.15%) and ethanol were obtained from EMD. All organic solvents were dried over activated 4A molecular sieves for 1 d before use.

Synthesis of Cu-MOF Nanocrystals

Cu-MOF nanocrystals were synthesized in gram quantities by modifying published procedures to control the water content in the reaction mixture, to reduce the synthesis time, and to improve reproducibility (*41–43*). The activated material was dried in a vacuum oven at 90 °C for 1 d and then cooled to room temperature under a blanket of nitrogen before being removed from the vacuum oven.

Electrospinning of Molecular Sieve/Polymer Composite Fibers

The electrospinning of PLA composite fibers was carried out by first dispersing PLA in chloroform to attain a 10% solution. Then the dry molecular sieve was dispersed in 500 µL of chloroform and sonicated until the crystals were well dispersed. This suspension was then combined with the PLA solution with stirring. A syringe was then charged with the composite polymer melt and fed through a 20-gauge needle. Electrospinning was initiated by applying a 10kV voltage to the needle tip. Fibers were collected on a grounded rotating drum to attain aligned fibers.

Nitric Oxide Loading and Release Experiments

The adsorption of NO by the composite fibers was conducted similarly to the previously reported method where nano-zeolite A/PLA composite fibers were infused with NO (*39*). The Cu-MOF (20mg), or zeolite A composite fibers, were first placed in a 50 mL pressure vessel and dehydrated for 3 h at 60 °C under vacuum. The vessel was then purged with a flow of argon for 30 minutes and subsequently exposed to dry NO under pressure (4 atm) for 1 h. After exposure to NO pressure, the vessel was evacuated and the excess NO was flushed out of the vessel by purging with argon for 1h.

During the quantification of NO release, the samples were kept in the infusion vessel to ensure that NO was not released in the transfer process by the contamination from atmospheric moisture. In order to quantify the loading and release of nitric oxide from both the free-molecular sieves as well as the molecular sieves embedded in the polymer fibers, a flow of argon was passed through a vessel containing a saturated salt solution that regulated the relative humidity (magnesium chloride, 33% RH). The argon carried the moisture rich has to the sample to induce NO release. The evolved NO was carried by the argon and subsequently bubbled through a vessel containing 15 mL of deionized water, which served as a water-trapping component where the nitric oxide was oxidized to nitrite. From this solution, 100 µL aliquots were taken at predetermined intervals and the concentration of nitrite determined by UV-vis using the Griess Reagent (*44*, *45*).

Downloaded by DUKE UNIV on June 23, 2012 | http://pubs.acs.org
Publication Date (Web): November 17, 2010 | doi: 10.1021/bk-2010-1053.ch009

Testing of Bandage on Isolated Rat Hearts

The rats sacrificed in this study were first anesthetized with a gas mixture followed by the severing of the spinal cord at the neck. The hearts were then immediately excised from the chest cavity of the rats and cannulated through the aorta where it was fastened with a silk tie. The heart was then perfused at a constant hydrostatic pressure of 50 mmHg with Krebs' buffer at 37°C, which was continuously gassed with 95% O_2 and 5% CO_2. The composition of the perfusion buffer was 118 mM NaCl, 25 mM KCl, 1.2 mM $MgSO_4$, 1.2 mM KH_2PO_4, 25 mM $NaHCO_3$, 10 mM glucose, and, 2.0 M $CaCl_2$. After the perfusing the coronary artery with the buffer solution, the heart was placed in a warming jacket which kept the buffer surrounding the heart at the optimal 37°C. The buffer flows through the coronary arteries and out of the heart, where it accumulated in the fraction collector programmed for one minute intervals. Each of the fractions collected was individually weighed to calculate the flow-rate or the coronary flow. Coronary flow was measured for 20 minutes prior to wrapping with the NO releasing bandage to attain a baseline value. Following the baseline, the heart was removed from the warming water jacket and covered with the reactive NO bandage, then immersed again in the warming media. The flow was allowed to equilibrate for 10 minutes, upon which time the buffer was again collected with the fraction collector.

Downloaded by DUKE UNIV on June 23, 2012 | http://pubs.acs.org
Publication Date (Web): November 17, 2010 | doi: 10.1021/bk-2010-1053.ch009

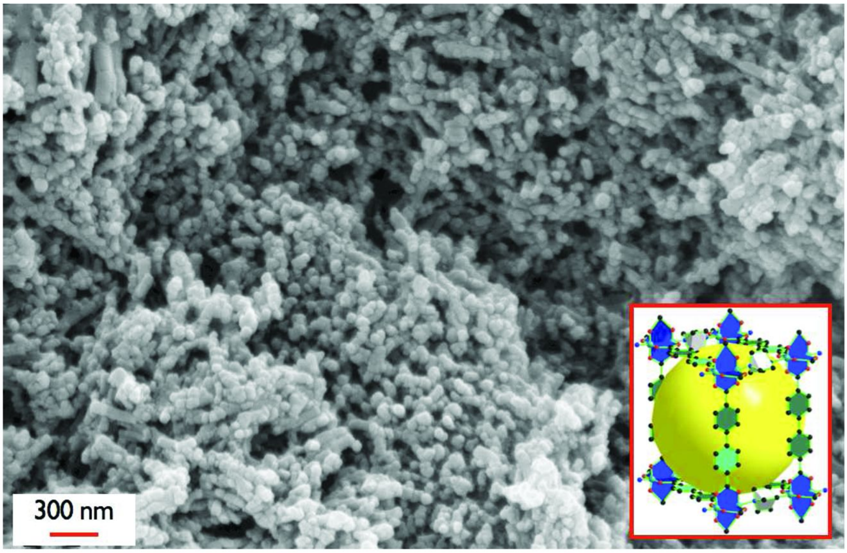

Figure 1. SEM micrograph of Cu-MOF; (inset) proposed crystal structure of Cu-MOF

Instrumentation/Characterization

Samples were evaluated using scanning electron microscopy using a Leo 1530 VP field emission electron microscopy from Au/Pd coated samples. Powder X-ray diffraction (Rigaku Ultima III, CuK_α radiation) was used to characterize the molecular sieves.

Results and Discussion

A SEM micrograph of the as synthesized Cu-MOF and nanozeolite A is shown in Figure 1 and Figure 2, respectively. The inset of figure 1 depicts a plausible three-dimensional structure for Cu-MOF as described by Seki et al. (*41*, *46*) It can be seen from the SEM micrograph that the particles of Cu-MOF synthesized are nanosized, which allows for the incorporation and application of this material into polymeric matrices a facile process. An x-ray diffraction pattern of the as-synthesized Cu-MOF (not shown) matched previously published results. Analysis of the N_2 adsorption isotherms of the Cu-MOF (not shown) yielded BET surface areas of approximately 3000 m^2/g.

The release of nitric oxide from NO infused molecular sieves are shown in Figure 3. A/PLA composite fibers. The shape of the release profile of the free Cu-MOF mimics that of the NO release from zeolite A. An initial burst of nitric oxide is seen within the first 10 minutes followed by a slowing of the rate of NO release. The total capacity of nitric oxide loading was measured to be approximately 5 mmol/g and was expended within 40 minutes upon the influx of moisture.

The mechanism of NO release from zeolites and MOFs has been attributed to the influx of moisture, which displaces the NO adsorbed in the pores of the MOF.

Downloaded by DUKE UNIV on June 23, 2012 | http://pubs.acs.org
Publication Date (Web): November 17, 2010 | doi: 10.1021/bk-2010-1053.ch009

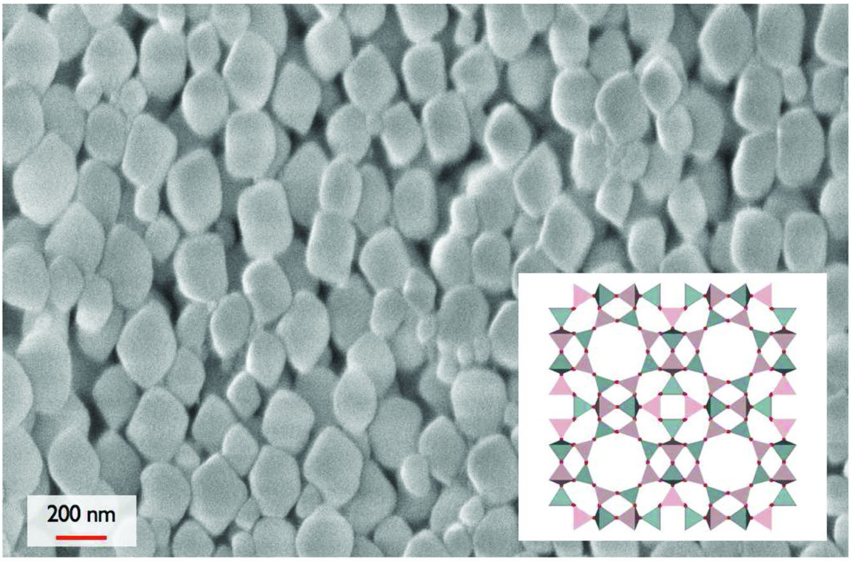

Figure 2. SEM micrograph of Zeolite A; (inset) crystal structure of Cu-MOF

After the infusion of NO within the pores of the Cu-MOF, the excess NO was purged for 1 hour with the flow of argon. Before the influx of moisture a sample was taken and did not reveal evidence of NO release. Nitrite production was not seen until exposure to moisture, releasing NO release from the pores of the MOF.

The storage capacity of NO within the Cu-MOF was up to five times greater than that seen in zeolite A, exhibiting a storage capacity of 5 mmol/g. The storage capacity of the NO was attributed to the high surface area of metal-organic frameworks in comparison to zeolitic materials. This high storage capacity is typical of metal organic frameworks as first demonstrated by McKinlay et al. (*40*).

While the Cu-MOF or zeolite A nanocrystals store and release NO, the powder form is not a practical configuration for the preservation of transplant organs, therefore composites of the fibers were fabricated through electrospinning to attain free-standing NO releasing bandages.

SEM micrographs of the as-spun composite fibers of the nanozeolite-A/PLA and the Cu-MOF/PLA are shown in Figure 4a and b, respectively. The electrospinning of the composite fibers result in free-standing papers that are easily handled and manipulated. Through electrospinning these composite materials, we have been able to exploit the high storage capacity of NO within molecular sieves in the form of a bandage that has a much greater NO storage capacity than previous diazeniumdiolates fibers (*41*).

The release profile of the composite zeolite A and Cu-MOF is shown along with the free-powder in Figure 3. It can be seen that the amount of NO stored within the fibers is comparable to the amount exhibited in the free-MOF. A distinct feature seen in the release profile of the MOF-composite is the delay in the NO release seen in the fibers. This delay in NO release can be attributed to the embedding of the Cu-MOF within the polymer matrix of the fibers, which shields the molecular sieves from the flow of moisture. A slight increase in

Downloaded by DUKE UNIV on June 23, 2012 | http://pubs.acs.org
Publication Date (Web): November 17, 2010 | doi: 10.1021/bk-2010-1053.ch009

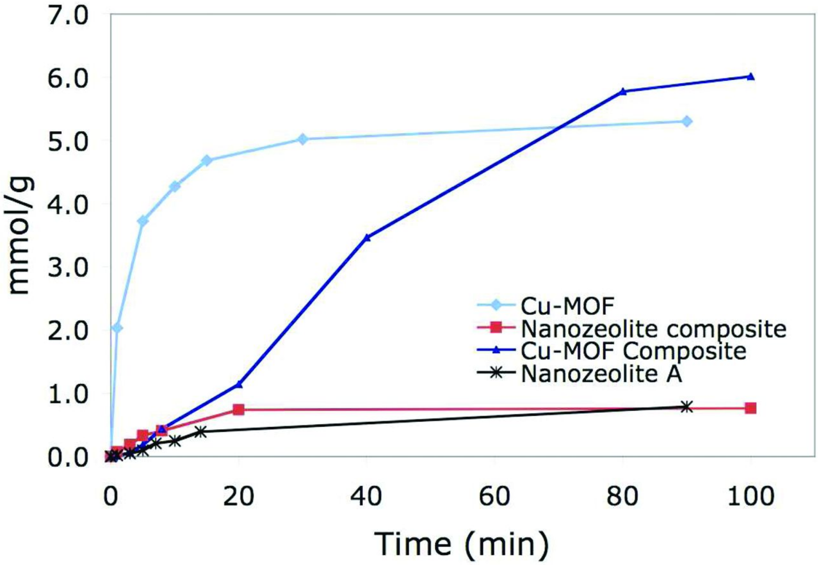

Figure 3. Release profile of NO from molecular sieves and molecular sieve composite fibers

NO loading and release is observed in the Cu-MOF composite, which may be attributed to the electrospinning process. While a homogenous solution is used for electrospinning, some of the fibers and materials are not all collected on the target, but upon electrospinning setup, slightly altering the calculations of the amount of molecular sieves embedded within the polymer.

Application of Molecular Sieve Composites Fibers

As previously discussed, NO stimulates smooth muscles to relax, leading to local vasodilation and an increased blood flow. In order to quantify the effects of the nitric oxide evolved from the fabricated bandage, the coronary flow of rat hearts were studied. A constant flow of perfusion buffer is introduced into the heart through the aorta, though the buffer does not enter any of the chambers of the heart due to the aortic valve that prevents the flow from entering the left ventricle. Instead, the buffer is shunted towards the coronary arteries, which flow to the outside muscles of the heart. From here the buffer is flowed through the coronary arteries and eventually flows out of the heart. The flow rate is measured by the amount of buffer expelled by the heart, which is collected at one-minute intervals. Digital images of the heart before and after wrapping with the bandage are shown in Figure 5a and 5b. An increase in flow rate can be seen from the plot of the flow rate before and after exposing the heart to the NO releasing fibers (Figure 6). It is important to note here that the NO releasing bandage was applied to a healthy heart and a significant change in flow rate was observed. Future tests will be performed on ischaemic hearts, where we believe the effects of NO will help preserve damage from the lack of nutrient flow. This is the first example of an NO releasing paper on isolated rat hearts that has implications for heart transplants.

Downloaded by DUKE UNIV on June 23, 2012 | http://pubs.acs.org
Publication Date (Web): November 17, 2010 | doi: 10.1021/bk-2010-1053.ch009

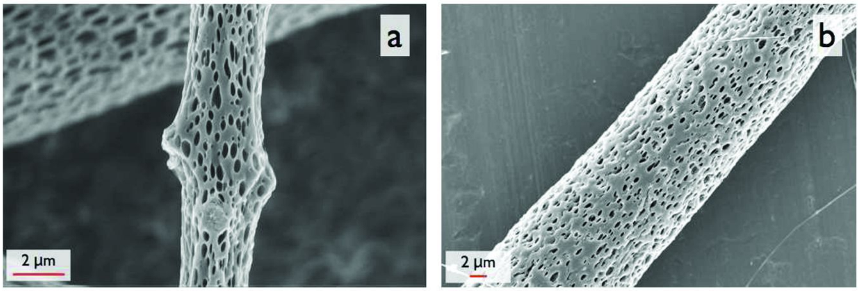

*Figure 4. SEM micrograph of **a.** nanozeolite A/PLA composite fibers and **b.** Cu-MOF/PLA composite fibers*

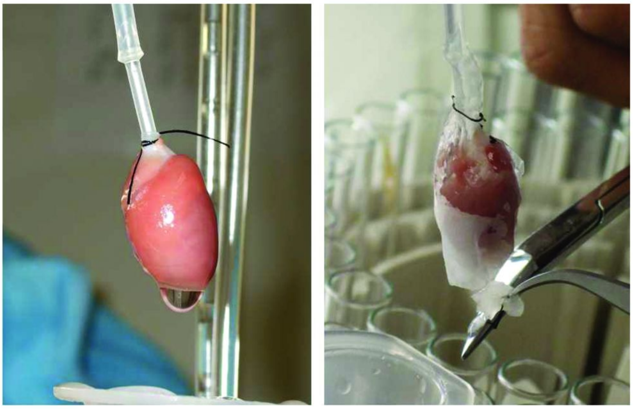

Figure 5. Digital image showing an isolated rat heart with perfusion buffer flowing through the aorta (a) before wrapping and, (b) after wrapping.

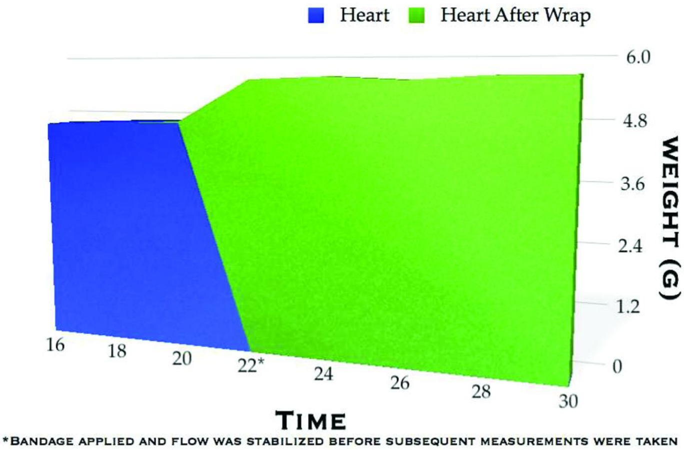

Figure 6. Plot of coronary flow before and after implementation of NO releasing bandage.

Downloaded by DUKE UNIV on June 23, 2012 | http://pubs.acs.org
Publication Date (Web): November 17, 2010 | doi: 10.1021/bk-2010-1053.ch009

Conclusion

Organ transplantation has experienced great advances in the recent past, which has led to the exceptional preservation of the muscle tissue through the use of cold storage and a single flush of cardioplegia. While this process preserves the coronary muscles well, this technique does not address the preservation of the endothelium, the innermost lining of the arteries, which have proven to be the major limiting factor in a successful heart transplant. In the endothelium, nitric oxide serves many functions including: anti-aggregation of platelets, reduction in the aggregation of vascular plaque, vasodilation, a scavenger for oxygen free radicals, as well as an increase in cardiac compliance. Though during heart transplantation, the production of nitric oxide is halted, leading to a poorly preserved endothelium and ultimately a failed heart. The ability to exogenously delivery nitric oxide by simply wrapping the donor organ with a bandage may provide an advantage in the preservation of the endothelium and an increase in the success rate for transplantation.

In this study, we have demonstrated the ability to infuse a high capacity and initiate the delivery of NO from a new metal organic framework,Cu-MOF. While metals in MOFs are not ideal from a toxicological aspect, the high storage capacity of NO is appealing for many applications that require a prolonged release. The inability to reintroduce NO with the porous material upon its application within a subject limits its use, but with a high storage capacity, this issue can be better addressed. Additionally, we present a method to electrospin molecular sieve composite fibers to fabricate bandages that can release NO in a controlled manner. Preliminary results indicating an increase in coronary flow in isolated rate hearts upon wrapping with Zeolite A/PLA papers. Further experiments using molecular sieve composites for organ transplants are in progress.

Acknowledgments

We would like to acknowledge the Robert A. Welch Foundation (Grant AT1153) for financial support for this research.

References

1. Ignarro, L. J.; Lipton, H.; Edwards, J. C. Mechanism of vascular smooth muscle relaxation by organic nitrates, nitrites, nitroprusside and nitric oxide: Evidence for the involvement of S-Nitrosothiols as active intermediates. *J. Pharmacol. Exp. Ther.* **1981**, *218* (3), 739–749.
2. Ignarro, L. J.; Kadowitz, P. J. The pharmacological and physiological role of cyclic GMP in vascular smooth muscle relaxation. *Annu. Rev. Pharmacol. Toxicol.* **1985**, *25*, 171–191.
3. Ignarro, L. J.; Buga, G. M.; Wood, K. S.; Byrns, R. E.; Chaudhuri, G. Endothelium-derived relaxing factor produced and released from artery and vein is nitric oxide. *Proc. Natl. Acad. Sci. U.S.A.* **1987**, *84* (24), 9265–9269.
4. Miller, M. R.; Megson, I. L. Recent developments in nitric oxide donor drugs. *Br. J. Pharmacol.* **2007**, *151* (3), 305–321.

5. Delledonne, M.; Xia, Y.; Dixon, R. A.; Lamb, C. Nitric oxide functions as a signal in plant disease resistance. *Nature* **1998**, *394* (6693), 585–588.
6. Ghaffari, A.; Jalili, R.; Ghaffari, M.; Miller, C.; Ghahary, A. Efficacy of gaseous nitric oxide in the treatment of skin and soft tissue infections. *Wound Repair and Regeneration* **2007**, *15* (3), 368–377.
7. Wass, C.; Klamer, D.; Fejgin, K.; PÂlsson, E. The importance of nitric oxide in social dysfunction. *Behav. Brain Res.* **2009**.
8. Schaffer, M. R.; Tantry, U.; Gross, S. S.; Wasserkrug, H. L.; Barbul, A. Nitric oxide regulates wound healing. *J. Surg. Res.* **1996**, *63* (1), 237–240.
9. Lee, P. C.; Salyapongse, A. N.; Bragdon, G. A.; Shears Ii, L. L.; Watkins, S. C.; Edington, H. D. J.; Billiar, T. R. Impaired wound healing and angiogenesis in eNOS-deficient mice. *Am. J. Physiol. Heart Circ. Physiol.* **1999**, *277* (4 46-4).
10. De Graaf, J. C.; Banga, J. D.; Moncada, S.; Palmer, R. M. J.; De Groot, P. G.; Sixma, J. J. Nitric oxide functions as an inhibitor of platelet adhesion under flow conditions. *Circulation* **1992**, *85* (6), 2284–2290.
11. Raulli, R. Inhibition of human platelet aggregation by diazeniumdiolates: Extent of inhibition correlates with nitric oxide load delivered. *J. Pharm. Pharmacol.* **1998**, *50* (1), 75–82.
12. Fitzhugh, A. L.; Keefer, L. K. Diazeniumdiolates: Pro- and antioxidant applications of the 'NONOates'. *Free Radical Biol. Med.* **2000**, *28* (10), 1463–1469.
13. Hetrick, E. M.; Prichard, H. L.; Klitzman, B.; Schoenfisch, M. H. Reduced foreign body response at nitric oxide-releasing subcutaneous implants. *Biomaterials* **2007**, *28* (31), 4571–4580.
14. Hetrick, E. M.; Schoenfisch, M. H. Antibacterial nitric oxide-releasing xerogels: Cell viability and parallel plate flow cell adhesion studies. *Biomaterials* **2007**, *28* (11), 1948–1956.
15. Lyons, C. R. The role of nitric oxide in inflammation. *Adv. Immunol.* **1995**, *60*, 323–360.
16. De Vriese, A. S.; Verbeuren, T. J.; Van De Voorde, J.; Lameire, N. H.; Vanhoutte, P. M. Endothelial dysfunction in diabetes. *Br. J. Pharmacol.* **2000**, *130* (5), 963–974.
17. Weller, R.; Finnen, M. J. The effects of topical treatment with acidified nitrite on wound healing in normal and diabetic mice. *Nitric Oxide - Biol. Chem.* **2006**, *15* (4), 395–399.
18. Zhu, H.; Ka, B.; Murad, F. Nitric oxide accelerates the recovery from burn wounds. *World J. Surg.* **2007**, *31* (4), 624–631.
19. Pinsky, D. J.; Oz, M. C.; Koga, S.; Taha, Z.; Broekman, M. J.; Marcus, A. J.; Liao, H.; Naka, Y.; Brett, J.; Cannon, P. J.; Nowygrod, R.; Malinski, T.; Stern, D. M. Cardiac preservation is enhanced in a heterotopic rat transplant model by supplementing the nitric oxide pathway. *J. Clin. Invest.* **1994**, *93* (5), 2291–2297.
20. Baker, J. Organ preservation and transportation apparatus and method. U.S. Patent Appl. No. 2006/0121439, 2006.
21. Mowery, K. A.; H. Schoenfisch, M.; Saavedra, J. E.; Keefer, L. K.; Meyerhoff, M. E. Preparation and characterization of hydrophobic polymeric

Downloaded by DUKE UNIV on June 23, 2012 | http://pubs.acs.org
Publication Date (Web): November 17, 2010 | doi: 10.1021/bk-2010-1053.ch009

films that are thromboresistant via nitric oxide release. *Biomaterials* **2000**, *21* (1), 9–21.

22. Keefer, L. K.; Flippen-Anderson, J. L.; George, C.; Shanklin, A. P.; Dunams, T. M.; Christodoulou, D.; Saavedra, J. E.; Sagan, E. S.; Bohle, D. S. Chemistry of the diazeniumdiolates: 1. Structural and spectral characteristics of the [N(O)NO]- functional group. *Nitric Oxide - Biol. Chem.* **2001** (5) (4), 377–394.
23. Hrabie, J. A.; Keefer, L. K. Chemistry of the nitric oxide-releasing diazeniumdiolate ("nitrosohydroxylamine") functional group and its oxygen-substituted derivatives. *Chem. Rev.* **2002**, *102* (4), 1135–1154.
24. Konter, J.; Abuo-Rahma, G. E. D. A.; El-Emam, A.; Lehmann, J. Synthesis of diazen-1-ium-1,2-diolates monitored by the "NOtizer" apparatus: Relationship between formation rates, molecular structure and the release of nitric oxide. *Eur. J. Org. Chem.* **2007** (4), 616–624.
25. Smith, D. J.; Simmons, M. L. Transdermal delivery of nitric oxide from diazeniumdiolates. *J. Controlled Release* **1998**, *51* (2−3), 153–159.
26. Smith, D. J.; Reneker, D. H. Nitric oxide-modified linear poly(ethylenimine) fibers and uses therefor. U.S. Patent No. 6,737,447, 2004.
27. Zhang, H.; Annich, G. M.; Miskulin, J.; Stankiewicz, K.; Osterholzer, K.; Merz, S. I.; Bartlett, R. H.; Meyerhoff, M. E. Nitric Oxide-Releasing Fumed Silica Particles: Synthesis, Characterization, and Biomedical Application. *J. Am. Chem. Soc.* **2003**, *125* (17), 5015–5024.
28. Smith, D. J.; Reneker, D. H. Nitric oxide-modified linear poly(ethylenimine) fibers and uses therefor. U.S. Patent No. 6,855,366, 2005.
29. Jun, H. W.; Taite, L. J.; West, J. L. Nitric oxide-producing polyurethanes. *Biomacromolecules* **2005**, *6* (2), 838–844.
30. Jae, H. S.; Metzger, S. K.; Schoenfisch, M. H. Synthesis of nitric oxide-releasing silica nanoparticles. *J. Am. Chem. Soc.* **2007**, *129* (15), 4612–4619.
31. Polizzi, M. A.; Stasko, N. A.; Schoenfisch, M. H. Water-soluble nitric oxide-releasing gold nanoparticles. *Langmuir* **2007**, *23* (9), 4938–4943.
32. Wan, A.; Gao, Q.; Li, H. Preparation and characterization of diazeniumdiolate releasing ethylcellulose films. *J. Mater. Sci.: Mater. Med.* **2009**, *20* (1), 321–327.
33. Smith, D. J.; Chakravarthy, D.; Pulfer, S.; Simmons, M. L.; Hrabie, J. A.; Citro, M. L.; Saavedra, J. E.; Davies, K. M.; Hutsell, T. C.; Mooradian, D. L.; Hanson, S. R.; Keefer, L. K. Nitric oxide-releasing polymers containing the [N(O)NO]- group. *J. Med. Chem.* **1996**, *39* (5), 1148–1156.
34. Liu, H. A.; Balkus, J., K. J.; Miller, C. Electrospun poly(lactic acid) composites for the delivery of nitric oxide. **2009**, paper submitted.
35. Morris, R. E.; Wheatley, P. S. Gas storage in nanoporous materials. *Angew. Chem., Int. Ed.* **2008**, *47* (27), 4966–4981.
36. Boes, A. K.; Xiao, B.; Megson, I. L.; Morris, R. E. Simultaneous Gas Storage and Catalytic Gas Production Using Zeolites-A New Concept for Extending Lifetime Gas Delivery. *Top. Catal.* **2008**, 1–7.
37. Xiao, B.; Wheatley, P. S.; Morris, R. E. The adsorption, storage and release of nitric oxide using ion exchanged zeolites. In *Studies in Surface Science*

Downloaded by DUKE UNIV on June 23, 2012 | http://pubs.acs.org
Publication Date (Web): November 17, 2010 | doi: 10.1021/bk-2010-1053.ch009

and Catalysis; Xu, R., Chen, J., Yan, W., Gao, Z., Eds.; 2007; Vol. 170, pp 902−909.

38. Wheatley, P. S.; Butler, A. R.; Crane, M. S.; Fox, S.; Xiao, B.; Rossi, A. G.; Megson, I. L.; Morris, R. E. NO-Releasing Zeolites and Their Antithrombotic Properties. *J. Am. Chem. Soc.* **2006**, *128* (2), 502–509.
39. Liu, H. A.; Balkus, J., K. J. A Novel Delivery System for the Bioregulatory Agent Nitric Oxide. *Chem. Mater.* **2009**, *21*, 5032–5041.
40. McKinlay, A. C.; Xiao, B.; Wragg, D. S.; Wheatley, P. S.; Megson, I. L.; Morris, R. E. Exceptional behavior over the whole adsorption-storage-delivery cycle for NO in porous metal organic frameworks. *J. Am. Chem. Soc.* **2008**, *130* (31), 10440–10444.
41. Seki, K.; Mori, W. Syntheses and characterization of microporous coordination polymers with open frameworks. *J. Phys. Chem. B* **2002**, *106* (6), 1380–1385.
42. Traa, Y.; Burger, B.; Weitkamp, J. Zeolite-based materials for the selective catalytic reduction of NOx with hydrocarbons. *Microporous Mesoporous Mater.* **1999**, *30* (1), 3–41.
43. Perez, E. V.; Musselman, I. H. Mixed-Matrix Membranes Containing Metal-Organic Frameworks for Gas Separation. The University of Texas at Dallas, Richardson, TX, 2008.
44. Heines, S. V. Peter Griess - Discoverer of diazo compounds. *J. Chem. Educ.* **1958**, *35* (4), 187–191.
45. Smith, M. A.; Gower, W. R. Peter Griess and the phenylene diamines. *J. Chem. Educ.* **1952**, *29*, 176–177.
46. Seki, K. Design of an adsorbent with an ideal pore structure for methane adsorption using metal complexes. *Chem. Commun.* **2001** (16), 1496–1497.

Downloaded by DUKE UNIV on June 23, 2012 | http://pubs.acs.org
Publication Date (Web): November 17, 2010 | doi: 10.1021/bk-2010-1053.ch009

Downloaded by UNIV OF GUELPH LIBRARY on June 23, 2012 | http://pubs.acs.org
Publication Date (Web): November 17, 2010 | doi: 10.1021/bk-2010-1053.ch010

Chapter 10

Oil Absorption and Delivery System Polymer Technology for Skin and Hair Care

**Susan L. P. Jordan,[1,*] Ashish Batra,[2] Michael Meerbote,[3]
Xiaodong Zhang,[1] Linda Kosensky,[1] and Jennifer Amos[1]**

**[1]The Dow Chemical Company, Bound Brook, NJ 08854
[2]The Dow Chemical Company, Freeport, TX 77541
[3]The Dow Chemical Company, Schkopau, Germany
[*]jordansl@dow.com**

There is a need to provide sustained and targeted release of novel (vitamins and botanical extracts) as well as traditional actives from cosmetic products. In addition, consumers want to control shine and greasiness caused by sebum on skin and hair. Lightly cross-linked co-polymer beads both encapsulate actives for controlled release while imbibing sebum for oil control. The structure of the copolymer affects the rate of oil absorption and delivery of actives and allows formulators to design products that meet specific requirements. The efficacy of oil-imbibing polymer beads to control sebum on *artificial* skin and hair is demonstrated. *In-vivo* panel studies demonstrate a differentiated product that is effective in controlling sebum without excess whitening effects.

Traditional and novel actives such as vitamins, enzymes, sunscreens, fragrances, and botanicals are being introduced in personal care products to give drug-like benefits. These actives are often referred to as “cosmeceuticals” (*1*). In order to gain the most benefit from these actives, formulators require sustained/targeted release. Current delivery systems include liposomes (*2*) which are usually nano size vesicles used to encapsulate either water or oil soluble actives. Liposomes can be difficult to formulate with and usually deliver actives in a burst upon application. Core/shell systems, also known as micro encapsulation (*2*), hold actives in a core. In many cases, the core contains a solid material such

In Polymeric Delivery of Therapeutics; Morgan, S., et al.;
ACS Symposium Series; American Chemical Society: Washington, DC, 2010.

as alginate or CMC to help stabilize the active. The active core is protected by a hard shell (e.g. gelatin, polymethylene urea). These systems typically release their contents upon application by breaking the shell with rubbing. Additional polymers and coatings are sometimes added to the shell to enhance deposition.

A third type of system is the porous polymer particle; a sponge like matrix with extensive channeling (e.g. agar, polystyrene, cross-linked copolymers). The copolymers described here belong to this class of delivery system. These particles typically absorb substances into the porous cavity and slowly release the contents over time when applied (*3*). The release kinetics will depend on the size of the pores, cross-link density, and monomer content. Since they are porous systems, without a hard shell core, they are typically used to hold actives that are not soluble in the solvent used; thus preventing leakage of the active into the solvent (*4*).

In addition to actives delivery, formulators desire products that absorb unwanted sebum from skin and hair. Not only does sebum have negative visual and aesthetic affects, appearing and feeling oily and greasy, but they can also become food for the fungus that causes dandruff as well as perpetuate acne. Sebum control agents are classified into porous (e.g., cross-linked polymers and silica) and non-porous (e.g., talc and stearic alcohols) solutions. The porous materials typically suffer from whitening problems whereas non-porous compounds have low efficiency and can be unstable in formulations. Oil absorbing technology can be tuned to not only absorb oily compounds from the skin and hair, but to deliver oil soluble active ingredients as well.

Lightly cross-linked copolymers of isobornylmethacrylate and laurylmethacrylate were investigated as both oil imbibing polymers and active delivery systems for skin and hair care products. These polymers were previously described (*5*) and patented for acne control (*6*, *7*).

Materials and Methods

Materials

Oil Imbibing Beads

The oil-imbibing beads were prepared by suspension radical copolymerization of isobornylmethacrylate and laurylmethacrylate with divinylbenzene and t-butyl peroctoate as catalyst.

Hair

International Hair Importers and Products, Inc.

Artificial Skin

VITRO-SKIN obtained from IMS, Inc., Portland, ME.

Downloaded by UNIV OF GUELPH LIBRARY on June 23, 2012 | http://pubs.acs.org
Publication Date (Web): November 17, 2010 | doi: 10.1021/bk-2010-1053.ch010

Artificial Sebum

Composition consisting of 62% triolein, 11% squalene and 27% oleic acid.

Formulation Ingredients

METHOCEL™, hydroxyl ethyl cellulose (HEC) and glycerin from The Dow Chemical Company, Midland, MI; Promulgen G and Carbopol from Lubrizol Corp, Wickliffe, Ohio; triolein from Sigma-Aldrich, St. Louis, MO; glydant and Carsoquat SDQ-85 from Lonza, Inc., Basel Switzerland; cetyl alcohol and oleic acid from Cognis, Monheim, Germany; squalene from Robeco Chemical, Inc., New York, NY, pigments from Sun Chemical, Parsippany, NJ; polysorbate 20 and triethanolamine from BASF, Luwigshafen, Germany; isononyl isononate and steric acid from Alzo International Inc., Sayreville, NJ; glyceryl stearate from ISP, Wayne, NJ; NiPaguard from Clariant Corp., Charlotte, NC.

Actives

PPG-10 methyl glucose from Lubrizol Corp, Wickliffe, Ohio; Limonene (L), Carvone (C), Eugenol, 2-phenylethyl alcohol (P), and White Tea Mod 4 from Fragrance Resources, Inc., Clifton, NJ; propylene glycol (PG) from The Dow Chemical Company, Midland, MI; isopropyl alcohol and ethanol from Fischer Scientific, Pittsburg, PA; octylmethoxycinnamate (OMC) from Alzo International Inc., Sayreville, NJ; olive oil from Lipo Chemicals, Patterson, NJ.

Methods

Oil Absorption

Surface oil was measured using a sebum meter (SM 815® from Courage-Khazaka). Model lotions (1% Promulgen G, 0.5% METHOCEL E50-LV, 0.2% neutralized carbopol, 1% glycerin, 5% oil imbibing technology), leave-in-conditioner (1% cetyl alcohol, 1% Permulgen G, 1% Carsoquat SDQ-85, 4% HEC, 5% oil imbibing technology) or liquid foundation (5% glycerin, 0.25% polysorbate 20, 4.35% pigment, 0.2% HEC, 10% Isononyl Isononanate, 2% glyceral stearate, 2% steric acid, 1% NiPaguard, 3% oil imbibing technology) were applied on the substrate and allowed to dry. After drying, artificial sebum (1X, 3X, and 5X the concentration of the beads) was added to the substrate. Sebum meter readings were taken after application of the sebum.

Active Absorption

A 0.15 g sample of beads is placed in small GC vials. The beads fill the vials to a height of 5 mm. The vials are then filled with 1.5 g of the active or solvent of

Downloaded by UNIV OF GUELPH LIBRARY on June 23, 2012 | http://pubs.acs.org
Publication Date (Web): November 17, 2010 | doi: 10.1021/bk-2010-1053.ch010

interest. Increases in the height of the beads are recorded at regular time intervals. The swell factor is defined as the ratio of the final equilibrium height to the starting height of 5 mm.

Active Fragrance Release

1) Fragrance loaded oil-imbibed beads were exposed to various solvents and the amount of fragrance released to solvent characterized by gas chromatography at different intervals of time. 2) Fragrance loaded oil-imbibed beads were incorporated into model lotions and applied to VITRO-SKIN. Multiple head space extraction GC and liquid extraction GC were used to characterize the release profile. 3) Panel studies with human subjects were conducted with samples that showed the most delayed profiles in step one and two.

Downloaded by UNIV OF GUELPH LIBRARY on June 23, 2012 | http://pubs.acs.org
Publication Date (Web): November 17, 2010 | doi: 10.1021/bk-2010-1053.ch010

Direct Injection Gas Chromatography (GC) Conditions

Hewlett Packard GC
Column: 30-m × 0.32-mm ID fused silica, coated with 0.1-µm film of DB-5
Oven: 80°C (hold 1 minute) then ramp at 10°C/minute to 170°C
Injection Port: 290°C
Flame Detector: 300°C
Injection size: 1µL

Multiple Head Space Extraction

In small GC vials, ~ 0.0025g of copolymer beads were allowed to imbibe ~0.0125g of fragrance (5 times the weight of beads) and the vials sealed immediately. Based on loading kinetics study, sufficient time was allowed for equilibrium swelling. Approximately 1.4 g of the solvent was injected with a syringe, the time recorded and vials shaken on a vortex mixer for 1 minute. Immediately (~2 minutes) after mixing, the vial was loaded on the headspace GC and the program was started. The GC was programmed to withdraw an aliquot of sample from the vial every 15 minutes to generate a release profile.

Multiple Head Space Extraction GC Conditions

Perkin Elmer Autosystem GC
Column: 30-m × 0.25-mm ID fused silica, coated with 1-µm film of DB-5
Oven: 100°C (hold 1 minute) then ramp at 10°C/minute to 275°C
Injection Port: 200°C
Flame Detector: 300°C
Headspace Sampler: Thermostat: 65°C; Transfer line: 150°C
Injection time: 0.10 minutes

Downloaded by UNIV OF GUELPH LIBRARY on June 23, 2012 | http://pubs.acs.org
Publication Date (Web): November 17, 2010 | doi: 10.1021/bk-2010-1053.ch010

Pressurization time: 0.5 minutes
Withdrawal time: 0.4 minutes

OMC and Vitamin E Release

OMC or vitamin E (0.1 g) was imbibed in 0.02 g of the oil imbibing beads over night in a tall jar. Approximately 40 g of 50:50 IPA: water (OMC) or ethanol (vitamin E) was added to the jar and mixed on a hand-action shaker for a few minutes. A few drops of this solution were filtered through a syringe filter (0.45 µm pore size) into a UV-cuvette cell and the volume made up to 2 g of 50:50 IPA:water or ethanol. The absorbance at 290 nm was measured for OMC and 293 nm for vitamin E. OMC or vitamin E in a model lotion (1% oil imbibing beads, 5% OMC, 4% Promulgen G, 0.2% Carbopol) or (1% oil imbibing beads, 4% vitamin E, 2% Promulgen G, 0.2% Carbopol) was prepared. Release was monitoring using a Franz diffusion cell and either a silicone membrane (0.005" thick) available from Cardiovascular Instruments Corp. in Boston or a CoTran 7205 PE-co-vinyl acetate membranes with 9% vinyl acetate content (76µm thick) available from 3M. The lotion (~0.3-0.5 g) was applied uniformly to the top of the membrane and allowed to penetrate into a 50:50 IPA:water or ethanol receptor fluid. Samples were removed periodically and absorbance at 290 nm or 293 nm was measured.

Results and Discussion

The copolymer of isobornylmethacrylate (IBMA) and laurylmethacryate (LMA), cross-linked with divinylbenzene, was synthesized at two different monomer compositions (56:44, Polymer A & 40:60, Polymer B; IBMA: LMA) with crosslink density held constant. Polymer A had an average particle size of 22 micron and glass transition (Tg) temperature of 50°C. Polymer B had an average particle size of 122 micron and Tg of 5°C (Figure 1).

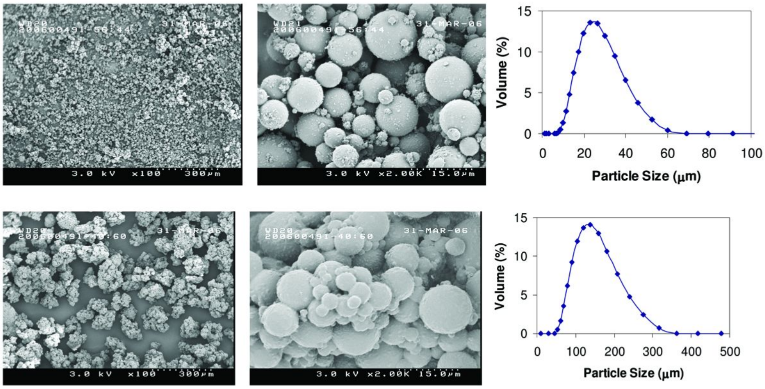

Figure 1. SEM of Polymer A (top) and Polymer B (bottom)

Downloaded by UNIV OF GUELPH LIBRARY on June 23, 2012 | http://pubs.acs.org
Publication Date (Web): November 17, 2010 | doi: 10.1021/bk-2010-1053.ch010

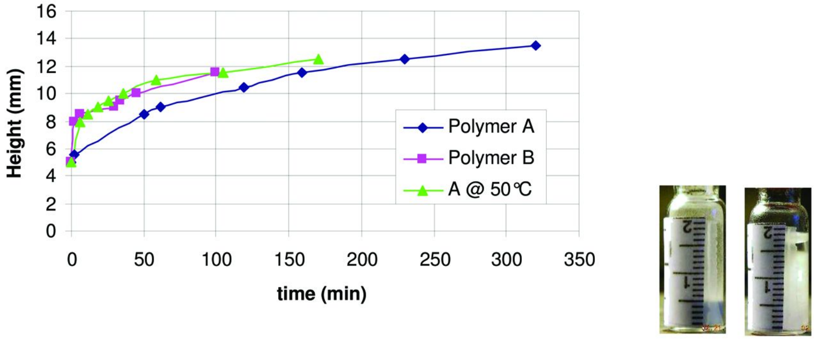

Figure 2. Absorption of artificial sebum by oil imbibing copolymers A & B

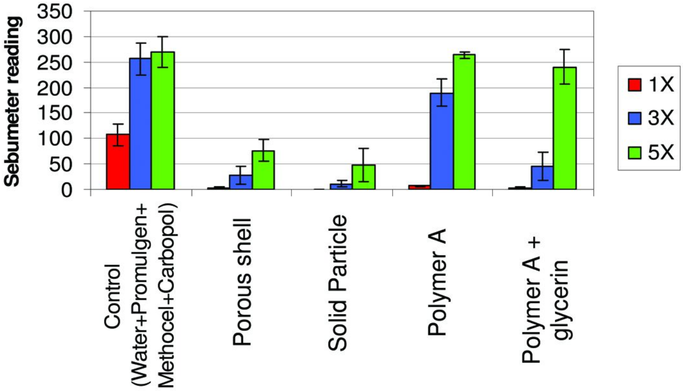

Figure 3. Sebum meter reading on VITRO skin of lotion various oil absorbing technologies plus artificial sebum

As expected, the polymers exhibit different physical properties with different monomer compositions. It would then be expected that the imbibing capabilities will also differ for the two compositions. Figure 2 shows the ability of each polymer to absorb artificial sebum. Although all the sebum is absorbed, copolymer A absorbs the oils slower than copolymer B. This is likely due to the higher hydrophobic character of copolymer B, clearly showing polymer composition is important for performance and can be controlled depending on the desired outcome. Just as the kinetics of absorption can be controlled by polymer composition, active release should also be controllable by altering composition. It should be noted that when heated, copolymer A absorption rate becomes comparable to copolymer B. While not tested, cross-link density should also have an affect on performance properties.

The ability of the polymers to absorb oil from a substrate was investigated using VITRO Skin and hair tresses. Lotion containing polymer A or polymer A plus 1% glycerin was placed on VITRO Skin followed by artificial sebum at either 1, 3 or 5 times the weight concentration of polymer. Figure 3 compares the sebum meter reading of oil on the substrate with a solid (silica shells) oil absorbing material and a commercial porous material. Polymer A with glycerin shows

Downloaded by UNIV OF GUELPH LIBRARY on June 23, 2012 | http://pubs.acs.org
Publication Date (Web): November 17, 2010 | doi: 10.1021/bk-2010-1053.ch010

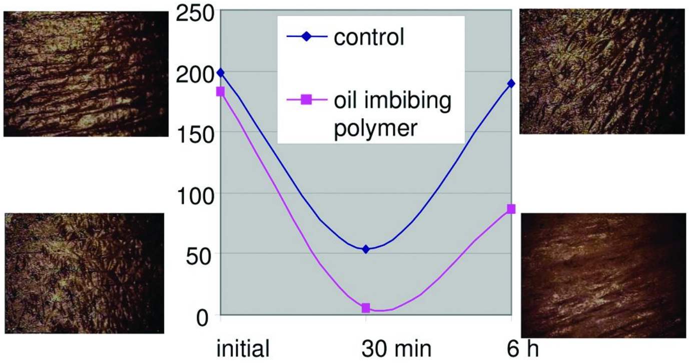

Figure 4. Sebum meter reading (average of 10 panelists) on forehead treated with and without lotion containing 5% Polymer A (bottom squares)

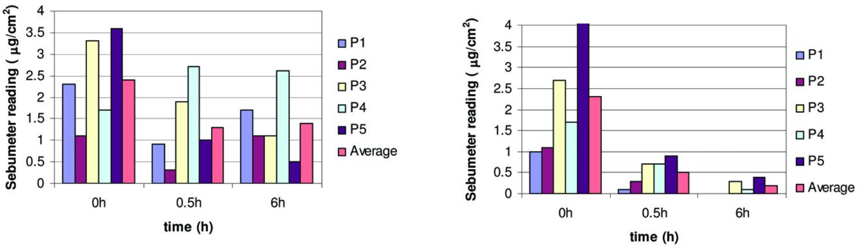

Figure 5. Sebum control of hair tresses treated with leave on conditioner containing polymer A (right) vs. control (left) – 5 panelists.

comparable oil absorption characteristics as current commercial technologies at artificial sebum concentrations up to 3 times the polymer concentration. The more hydrophobic polymer B would be expected to show similar results.

As demonstrated in Figure 4, the oil absorption effect is also seen in an in-vivo panel study with human subjects. Lotion containing Polymer A reduces oil on the fore head (as measured by sebum meter, 10 panelist average) for up to 6 hours compared to a control. As shown in Figure 4, there is no whitening on the skin using a lotion containing 5% polymer. Similar sebum meter readings and panel studies rating oiliness were found for foundation make-up and in half head studies: hair treated with conditioner containing Polymer A (Figure 5).

In addition to sebum control, these polymers are also effective delivery vehicles for oil based active ingredients in personal care formulations. The imbibing kinetics of a series of actives, including solvents and carriers, fragrances, sunscreens and vitamins covering a range of solubility parameters (*8*), into cross-linked beads were characterized (Figure 6). Actives with solubility parameters around 8 such as limonene show significant swelling compared with water soluble actives (high solubility parameters, e.g., phenyl alcohol) that do not imbibe into the beads. This selective imbibing can be used to tailor which actives will be delivered and at what rates.

Downloaded by UNIV OF GUELPH LIBRARY on June 23, 2012 | http://pubs.acs.org
Publication Date (Web): November 17, 2010 | doi: 10.1021/bk-2010-1053.ch010

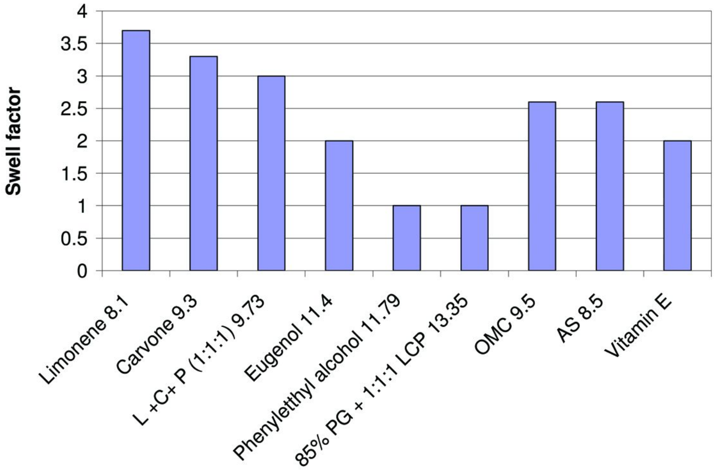

Figure 6. Absorption of several actives, and combination of actives into Polymer A. AS refers to artificial sebum.

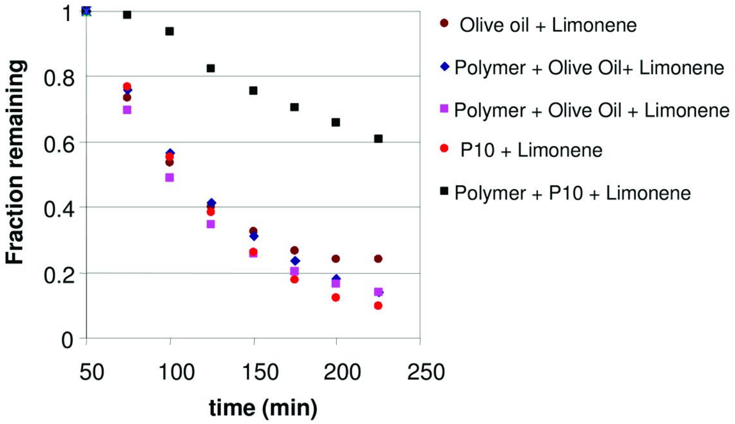

Figure 7. Delayed release of limonene from lotion containing Polymer A and Glucam P10 (top curve) vs. all other combinations.

Release studies from “model” imbibed beads as well as from skin care lotions containing imbibed beads showed considerable delay in release. Figure 7 shows the delayed release of limonene from lotion containing polymer A, limonene (fragrance) and Glucam P-10. The combination of polymer A and Glucam P-10 gives the most dramatic fragrance release profile. A panel study confirmed the enhanced fragrance release over time with fourteen of twenty panelists perceiving more fragrance on a forearm (compared to control) one hour after application.

Figure 8 illustrates the delayed release of octylmethoxycinnamate (OMC, organic sunscreen) from imbibed beads in isopropyl alcohol and water (IPA:Water). As expected, free OMC is immediately released while the imbibed active releases slowly for up to 100 hours.

Downloaded by UNIV OF GUELPH LIBRARY on June 23, 2012 | http://pubs.acs.org
Publication Date (Web): November 17, 2010 | doi: 10.1021/bk-2010-1053.ch010

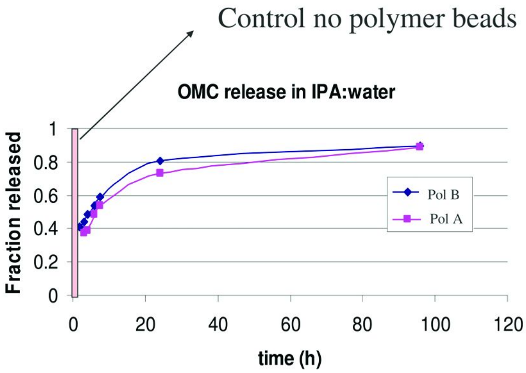

Figure 8. Release kinetics of OMC imbibed in Polymer B and Polymer A in IPA: Water

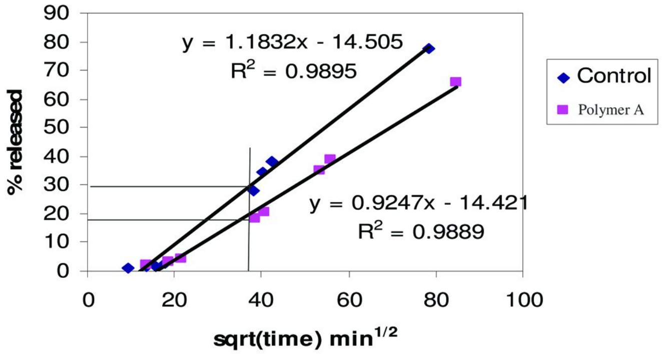

Figure 9. Penetration kinetics of OMC imbibed in Polymer A (squares) vs. free in solution (diamonds).

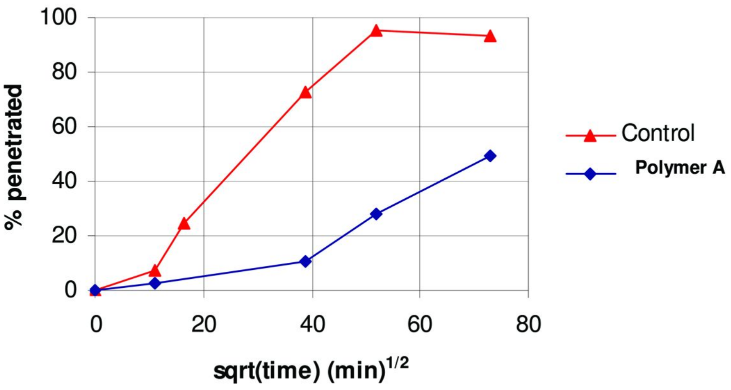

Figure 10. Release kinetics of vitamin E from polymer A in a lotion compared to control.

Because of the difficulty in measuring release of OMC in lotions, Franz cell penetration was used to measure release kinetics of OMC (*9*). As the OMC is

Downloaded by UNIV OF GUELPH LIBRARY on June 23, 2012 | http://pubs.acs.org
Publication Date (Web): November 17, 2010 | doi: 10.1021/bk-2010-1053.ch010

released, it will penetrate the membrane of the Franz cell and can be measured in the IPA/water on the other side. Figure 9 shows that a 60% reduction in OMC imbibed in Polymer A crossing the membrane compared with OMC free in solution.

The release kinetics of vitamin E was similarly measured using the Franz cell. In this case (Figure 10), there is a significant difference in release. It is hypothesized that the larger, bulky molecules such as OMC and vitamin E can more easily be controlled than smaller molecules, such as fragrances.

In studies to determine that sebum control can occur in the presence of polymer imbibed with active ingredients that are to be deposited, lotion containing polymer A imbibed with either OMC or limonene at 1:1 ratio was shown to absorb up to ten times by weight artificial sebum (Figure 11).

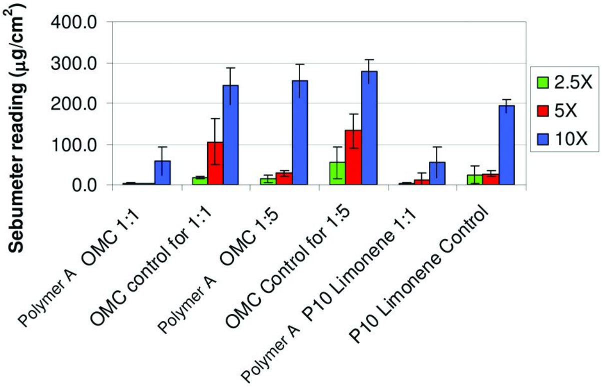

Figure 11. Absorption of sebum from samples containing Polymer A and an OMC or limonene (1:1 ratio – set 1 and 5).

Conclusion

Lightly cross-linked copolymer beads are capable of both imbibing sebum from skin and hair for up to six hours and delivering oily active ingredients. Monomer ratios can affect absorption kinetics and the polymer beads show little or no whitening on application at use levels. The loading kinetics for copolymers A and B was found to be strongly dependent on the composition of the copolymer and temperature for bulky actives such as sunscreens and vitamins and only marginally dependent on composition for fragrances. By altering monomer ratio and cross-link density the polymer can be fine tuned to deliver various actives at different rates as well as absorb unwanted sebum from skin and hair.

References

1. *Cosmeceuticals: Drugs vs. Cosmetics*; Elsner, P., Maibach, H. I., Eds; Marcel Dekker Inc.: New York, NY, 2000.

2. Hawkins, S.; Wolf, M.; Guyard, G.; Greenberg, S.; Dayan, N. In *Delivery System Handbook for Personal Care and Cosmetic Products: Technology, Applications and Formulations*; Rosen, M., Ed.; William Andrews, Inc.: Norwich, NY, 2005; pp 191−213.
3. Saxena, S.; Nacht, S. In *Delivery System Handbook for Personal Care and Cosmetic Products: Technology, Applications and Formulations*; Rosen, M., Ed.; William Andrews, Inc: Norwich, NY, 2005; pp 333−351.
4. Nacht, S. In *Science and Application of Delivery Systems*; Wiecher, J. W., Ed.; Allured Publishing: Carol Stream, IL, 2008; pp 337−351.
5. Haigh, D. H.; Larson, E. G. U.S. Patent 4,529,656, 1985.
6. Lay, G. E.; Haigh, D. H.; Knipstein, R. A. U.S. Patent 4,489,058, 1984.
7. Lay, G. E.; Knipstein, R. A.; Haigh, D. H. U.S. Patent 4,619,826, 1986.
8. *CRC Handbook of Solubility Parameters and Other Cohesion Parameter*; Barton, A. F. M.; CRC Press, Inc.: Boca Raton, FL, 1991.
9. http://www.fda.gov/cder/guidance/1447fnl.pdf.

Downloaded by UNIV OF GUELPH LIBRARY on June 23, 2012 | http://pubs.acs.org
Publication Date (Web): November 17, 2010 | doi: 10.1021/bk-2010-1053.ch010

Chapter 11

Silicone Elastomeric Particles in Skin Care Applications

Donald T. Liles* **and Feifei Lin**

Science & Technology Department, Dow Corning Corporation, Midland, Michigan 48611
***don.liles@dowcorning.com**

Silicone elastomeric particles are spherical particles of vulcanized silicone rubber based on polydimethylsiloxane (PDMS). These particles have a mean particle size distribution of 2-10µm and they are produced commercially via an aqueous emulsion process. Silicone elastomeric particles are used in industrial and personal care applications, the latter include both skin care and hair care. When applied to skin, silicone elastomer particles impart a pleasant sensation and they are also capable of absorbing various liquids such as emollients and sebum. Thus silicone elastomeric particles can be used in skin care applications to deliver certain substances to skin or to control sebum deposition on skin. Described are preparation and properties of silicone elastomeric particles and their uses in some skin care applications.

Introduction

Silicone elastomeric particles, referred to as silicone elastomer powders, E-Powders, or silicone particles, are spherical particles of vulcanized silicone elastomer based on polydimethylsiloxane (PDMS) that have a mean particle size distribution on the order of 2-10µm. Figure 1 depicts the structure for PDMS. A micrograph of silicone elastomer particles is shown in Figure 2. Silicone elastomeric particles were invented in Japan over 20 years ago and have found commercial utility in both industrial and personal care applications (*1–5*). Industrial applications of silicone elastomeric particles include modifying

In Polymeric Delivery of Therapeutics; Morgan, S., et al.;
ACS Symposium Series; American Chemical Society: Washington, DC, 2010.

thermosetting resins for electronics, providing slip to polymeric surfaces and also producing light-diffusing plastic components for electronic video displays.

Silicone elastomeric particles also enjoy a substantial business in the field of personal care. In these applications, silicone powders are used in both skin care and hair care compositions. Silicone elastomer particles provide an extremely pleasant and likable sensation when applied to skin. They also provide conditioning effects when applied to hair. Silicone elastomer particles can absorb significant quantities of liquids such as oils or emollients and still retain a non-wet appearance and consistency. They can also absorb sebum from the skin. Thus silicone elastomer particles are useful in skin care applications where sebum control or addition of certain substances to skin is desired (*6*). This paper describes preparation and properties of silicone elastomer particles. Absorption of various liquids by silicone elastomer particles is also presented and discussed.

Discussion

Preparation

Silicone elastomer particles are composed of spherically shaped, vulcanized silicone rubber that is formed in an aqueous emulsion process. Although there are numerous methods for vulcanizing or curing silicone polymers to form rubber or elastomer, the platinum (Pt) catalyzed, hydrosilylation addition process has emerged as the method of choice for preparing silicone elastomeric powders for personal care applications (*6*). The cure chemistry of this process is depicted by the following equation:

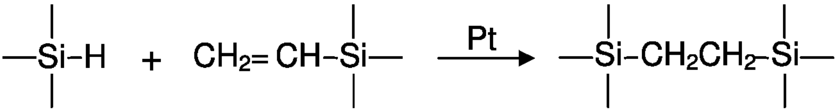

$$-\overset{|}{\underset{|}{\mathrm{Si}}}-\mathrm{H} \quad + \quad \mathrm{CH_2{=}CH}-\overset{|}{\underset{|}{\mathrm{Si}}}- \quad \xrightarrow{\mathrm{Pt}} \quad -\overset{|}{\underset{|}{\mathrm{Si}}}-\mathrm{CH_2CH_2}-\overset{|}{\underset{|}{\mathrm{Si}}}-$$

A chief benefit of hydrosilylation is its rapid reaction rate and its absence of significant byproducts. The fact that Pt catalyzed hydrosilylation is unaffected by water coupled with these features makes it an ideal route for preparing silicone elastomeric particles. The relatively fast reaction kinetics lead to process cycle times that are fairly short thus providing a practical and efficient manufacturing process. Although the reaction will occur at ambient temperature, heat can be applied to increase reaction rate and shorten cycle times if desired.

To carry out the hydrosilylation process and form the silicone elastomeric particles, a vinyl functional siloxane polymer is mixed with a silicon hydride functional siloxane (crosslinker) and the mixture is emulsified in water in the presence of one or more surfactants using high shear. In this process an oil-in-water (o/w) emulsion is formed. In the presence of a Pt catalyst, the composition reacts to form a crosslinked network. Since the particles are dispersed in water, the networks are confined to each individual particle; therefore each particle becomes an elastomer. The emulsion process also leads to spherical particles as emulsion particles typically assume a spherical shape in order to minimize free energy of the dispersed system. It is also possible to control

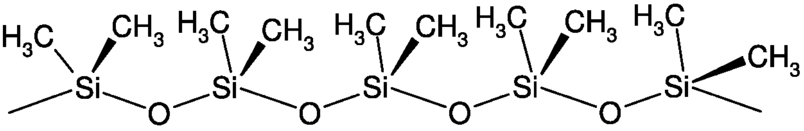

Figure 1. Structure of poly(dimethylsiloxane) (PDMS)

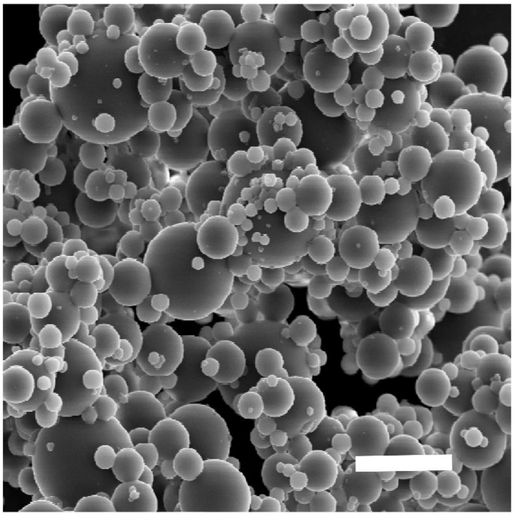

Figure 2. Scanning Electron Micrograph (SEM) image of silicone elastomer particles. White scale bar represents approximately 10 μm.

particle size to some extent by varying certain conditions of the emulsion process. Removal of water leaves silicone elastomeric particles. The process for producing silicone elastomeric particles is shown schematically in Figure 3.

Siloxane Polymers

Modulus, hardness and swelling behavior of cured elastomeric particles are all influenced by crosslink density, which can be controlled to a reasonable extent by choice of the starting siloxane polymer and the crosslinker. Generally higher crosslink densities are preferred over lower crosslink densities. Thus siloxane polymers having somewhat low molecular weights (Mw) are favored over high Mw polymers. Typically viscosities of siloxane polymers under about 1000 cP are preferred for preparing silicone elastomeric powders. This low viscosity also allows for easy preparation of o/w emulsions via high shear. The vinyl functional siloxane polymers actually consist of vinylmethyl/dimethyl siloxane copolymers and are commercially available. Functionality of these siloxane polymers, that is the vinyl groups attached to Si, can be arranged at pendent locations along the polymer chain or at chain ends or both.

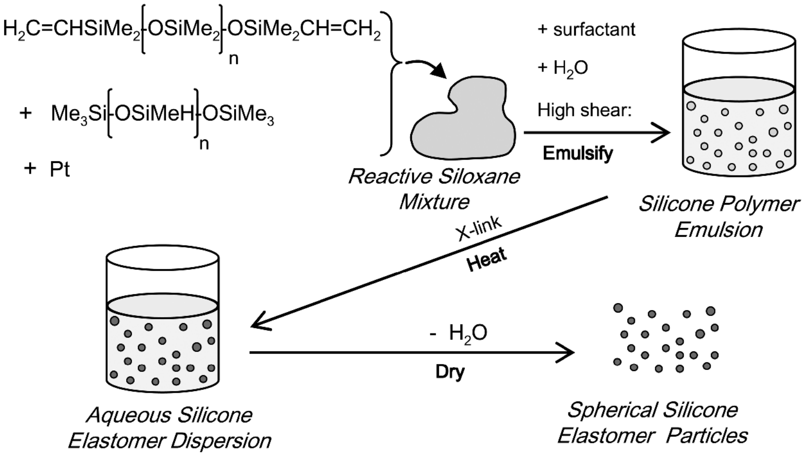
H2C=CHSiMe2[OSiMe2]nOSiMe2CH=CH2
+ Me3Si[OSiMeH]nOSiMe3
+ Pt
Reactive Siloxane Mixture
+ surfactant
+ H2O
High shear:
Emulsify
Silicone Polymer Emulsion
X-link
Heat
Aqueous Silicone Elastomer Dispersion
- H2O
Dry
Spherical Silicone Elastomer Particles

Figure 3. Scheme for preparing silicone elastomeric particles. Vinyl siloxane polymer, SiH crosslinker & Pt catalyst are combined with surfactant & H_2O and emulsified via high shear to produce an emulsion. After x-linking is complete, water is removed leaving spherical silicone elastomeric particles.

Crosslinker

Crosslinking agents for hydrosilylation reactions that form silicone elastomeric powders can be practically any multifunctional silicon hydride (SiH) functional siloxane or silane that is soluble in the vinyl functional-dimethylsiloxane polymer. The most common SiH crosslinkers are methylhydrogen polysiloxanes or methylhydrogen/methyl siloxane copolymers. These copolymers can be either linear or branched. Such siloxanes are readily soluble in the vinyl siloxane polymers and they are also available commercially. Normally a 1:1 stoichometric ratio of SiH to Si-vinyl is used; however, as SiH is capable of reacting with water in the presence of catalysts, in some cases a slight excess of SiH is used to compensate for some SiH to be consumed by water.

Catalyst

As previously stated, a platinum catalyst is used to prepare silicone elastomeric powders used in personal care applications. Pt catalysts effect cure by hydrosilylation in which an SiH adds to a carbon-carbon multiple bond forming an ethylene linkage. The hydrosilylation reaction is used extensively for vulcanizing neat silicone elastomers; numerous attributes including its fast reaction kinetics and absence of significant byproducts make it ideal for forming such elastomers. Although the high cost of Pt is not trivial, it is manageable in silicone elastomer compositions including silicone elastomeric particles since the level of Pt used is on the order of about 2-3ppm to 20ppm based on polymer weight.

The Pt catalyst used to prepare silicone elastomeric particles as well as neat silicone elastomers is in a form that is soluble in the vinyl siloxane polymer.

H_2PtCl_6 dissolved in isopropanol can be used as well as Pt complexes of divnylsiloxanes dissolved in vinylmethylsiloxane/dimethylsiloxane copolymer, the latter of which is preferred and it is commercially available.

With certain vinylsiloxane polymers, cure will begin as soon as all three components of the elastomeric composition have been mixed (catalyst, SiH crosslinker and vinylsiloxane polymer). Since silicone elastomeric particles require additional ingredients (water and surfactant) and another process step (emulsification), a short delay in the cure reaction is desired. If significant cure of the polymer system takes place prior to emulsification, this step may become difficult or impossible to accomplish or emulsion quality may be compromised as well. Thus it is preferred to have cure take place after emulsification of the polymer composition.

In order to accomplish this, less reactive vinylsiloxane polymers can be chosen or a catalyst inhibitor can be used or both. Pt catalyst inhibitors for silicone cure are well known in the industry and they consist of molecules that complex with the Pt compound in a reversible manner such that heat reverses the complex formation and releases an active Pt catalyst. Examples of Pt catalyst inhibitors include acetylenic diols such as 3-methyl-2-butyn-2-ol or 3,5-dimethyl-1-hexyn-3-ol (Surfynol®61) and esters of dibasic carboxylic acids such as diethylfumarate.

Process

The basic concept behind preparing silicone elastomeric particles is to first prepare an aqueous emulsion of polymer particles followed by crosslinking this polymer to form a dispersion of elastomeric particles (*7*). The emulsion process is carried out using standard high shear equipment designed for emulsifying liquids. Such equipment includes homogenizers, Cowles® blade, colloid mills, Sonolators®, or Microfluidizers®. A typical process may consist of preparing a mixture of siloxanes, water and surfactant in one vessel by stirring followed by passing the mixture through a high shear device and into another vessel. The second vessel would also be equipped with a stirrer and perhaps a heater such that the emulsion could be heated if desired. As previously mentioned heat can be optionally applied to the emulsion to speed up cure. This heat would be considered to be moderate heat; emulsions are rarely heated to above 80°C as many emulsions are prone to becoming unstable at or near this temperature. The same is true for silicone elastomer emulsions.

The emulsions formed when preparing silicone elastomeric particles are of the oil-in-water type. Particle size of the emulsion is governed by many factors; some of these include viscosity of the oil phase, type of high shear device, pressure of high shear device (if using a pumping-type high shear device), rotor speed (if using a Cowles® blade or other rotary mixer), and type and level of surfactant. Silicone elastomeric powders appear to have an optimum particle size for best sensory effects, which is approximately 2-10μm. Hence the emulsification process is designed to produce emulsion particles within this range.

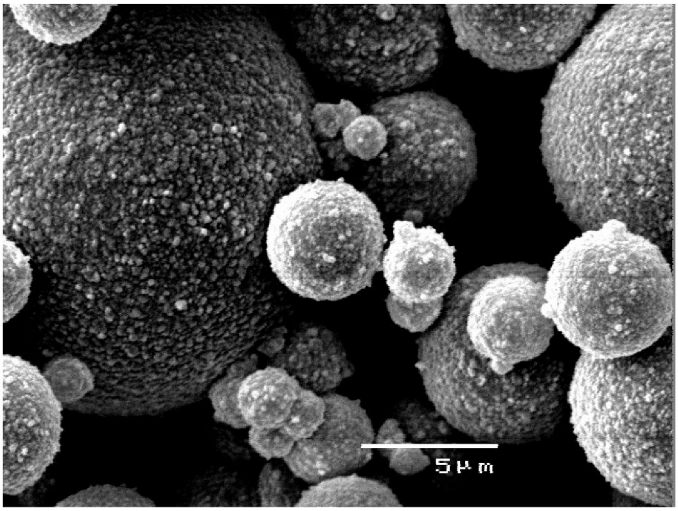

Figure 4. Scanning electron micrograph (SEM) of silicone elastomeric particles treated with Al_2O_3 nanoparticles. Scale bar represents 5 μm. Silicone elastomeric particles treated with inorganic oxides have different sensory and optical properties from untreated particles.

A silicone content or percent solid of the silicone emulsion is not extremely important, but it is typically on the order of 50 percent silicone. Higher solids emulsions would offer the benefit of having less water to remove, but along with higher solids comes higher emulsion viscosity. Difficulties in handling higher viscosity emulsions can outweigh the benefits of having less water to remove.

Since numerous factors affect particle sizes of emulsions, manufacturers of silicone elastomeric particles usually rely on their experience to produce emulsions of the curable elastomeric compositions having desirable particle sizes. It should be noted that particles made by these emulsification procedures described produce a distribution of particle sizes. In other words, they are not unimodal particles. A particle size distribution of a typical sample of silicone elastomeric particles made by conventional emulsification methods is shown in Figure 5.

Microfluidic techniques are used to produce truly unimodal emulsions (*8*). It should be possible to produce unimodal particles of silicone elastomer particles by using such techniques. Such a process would be envisioned to consist of pumping a curable silicone composition through a capillary or orifice into a flowing mixture of water and surfactant under controlled flow conditions. As the silicone emerges from the orifice, it would form spheres of uniform size and cure. In this manner silicone elastomer particles or silicone resins having a spherical shape and a monomodal particle size distribution might be produced.

Once crosslinking is complete, particles are harvested by removal of water. This can be accomplished by filtration, vacuum drying or spray drying. Although filtration would appear to be straightforward, it still requires a drying step (heat) and problems with filter plugging can be significant. Spray drying has become the preferred method for harvesting silicone elastomeric particles.

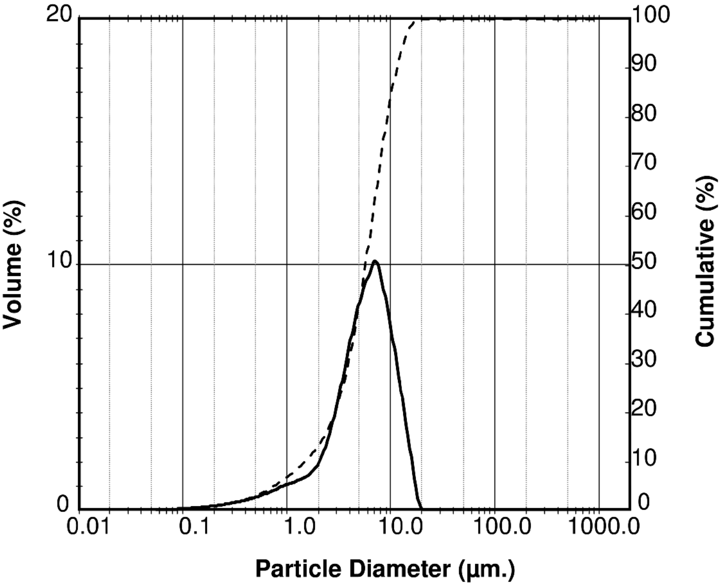

Figure 5. Particle size distribution of a typical silicone elastomeric powder. Volume percent, ($D_{v,\,0.5}$) = 5.71µm. Solid curve is volume % while dashed curve is cumulative %. Results were obtained on a Malvern® Mastersizer S (version 2.81).

Surfactants

One or more surface active agents (surfactants) are used to form a stable aqueous emulsion of the silicone elastomeric composition prior to crosslinking. In most cases, stability of the emulsion is required for relatively short periods of time – 24 hours – so choice of surfactant(s) is not all that critical. As the surfactant remains with the dried silicone elastomeric powder, choice of surfactant is dictated mainly by its compatibility with personal care applications. Namely it should be non-toxic to humans and non-irritating to skin. In addition, the surfactant should also be compatible with Pt catalyzed hydrosilylation reactions. In other words, it should not be a Pt poison.

As a result of these requirements, nonionic surfactants have been selected as surfactants of choice for preparing silicone elastomeric particles. Alcohol ethoxylates (alcohol EO) are the preferred nonionic surfactants and examples of such surfactants include Brij® 35 (lauryl alcohol EO-23) and Genapol® UD-080 (unidecyl alcohol EO-8). It should be realized that numerous other surfactants can be used to prepare silicone elastomeric powders besides these surfactants listed and combinations of surfactants can also be used if desired. The amount of surfactant used to prepare silicone elastomeric powders is also not very critical as the emulsion lifetime is very short. Usually from 0.5 percent by weight to 5 percent by weight of surfactant based on silicone polymer is used.

It also may be desirable to prepare silicone elastomeric powders having ionic surfactants such as anionic or cationic surfactants to achieve certain properties associated with the particles. For example, a cationic surfactant could be used to

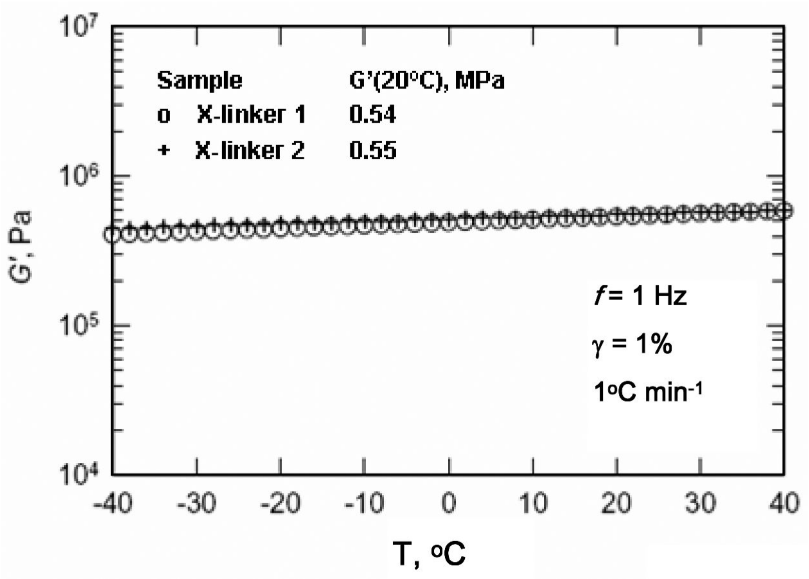

Figure 6. Dynamic shear modulus of two silicone elastomer particle compositions prepared with different crosslinkers. Modulus was determined on elastomeric films cast from the identical elastomer compositions used to prepare silicone elastomer particles. Measurements obtained on an ARES® controlled strain rheometer.

impart a positive charge to silicone elastomeric particles. Examples of anionic or cationic surfactants are Hostapur® SAS-30 (sodium *sec.*-alkane sulfonate) and Arquad® 16-29 (cetyltrimethylammonium chloride), respectively.

It should be mentioned that choice of surfactant and amount can have an impact on particle size of the emulsion and hence the finished silicone elastomeric particles. In addition to varying the emulsification conditions (described above), choice and level of surfactant can be varied to produce an emulsion having a desired particle size.

Silicone Elastomeric Particles with Inorganic Oxides

In the dry state silicone elastomeric particles are usually agglomerated into masses that are much larger than the primary particles. Although these agglomerates can be broken down by shear, it can be difficult in some instances to break down all of the particles into their primary particle state. To overcome this agglomeration phenomenon and also to provide particles with different surface modifications, manufacturers have introduced silicone elastomeric particles treated with various metal oxide particles (*9*). For example, silicone elastomeric particles having their surfaces treated with SiO_2, Al_2O_3 and TiO_2 are commercially available. These oxide treatments not only confer free flowing and non-agglomerating properties to the particles, but they also provide a different sensory feel and different optical properties to the particles as well. Optical properties (light scattering) are discussed in more detain in the section titled soft focus. An electron micrograph of silicone elastomeric particles treated with Al_2O_3 is shown in Figure 4.

Aqueous Dispersions of Silicone Elastomeric Particles

In cases where formulators wish to use silicone elastomeric particle in aqueous cosmetics compositions, it may prove advantageous to use preformed aqueous dispersions of silicone elastomeric particles rather than disperse the dried particles in water. In this case, water is not removed from the aqueous dispersion of silicone elastomer particles during manufacture. Also a surfactant system is chosen that can provide stability towards the dispersion for periods up to several years or more. Normally a suitable antimicrobial agent is added to the aqueous suspension to prevent possible microbial growth during transport and storage. Typically aqueous dispersions of silicone elastomeric particles are supplied with 50-60 percent silicone content.

Properties

Silicone elastomeric particles are spherically shaped, fine particles of silicone elastomer that have excellent thermal stability, and have interesting sensory and lubrication effects. The spherical shape and softness of silicone rubber are believed to contribute to the particles' unique sensory properties. Silicone elastomeric particles can be thought of as having the same properties as do conventional Pt cured silicone elastomers; however most conventional silicone elastomers are filled or reinforced with silica while these particles are unfilled.

Silicone elastomeric particles are characterized by their particle size (distribution), by their modulus and by their hardness. Particle size is normally measured on aqueous dispersions of silicone elastomer particles before removal of water using commercial light scattering instruments. Particle size distribution of a typical silicone elastomeric powder is given in Figure 5. Particle size distribution of silicone elastomeric particles is typically 2-10μm. Modulus and hardness are measured on films or monolithic slabs of cured elastomer prepared from the same composition (excluding surfactant & H_2O) as are the silicone elastomeric particles using a rheometer or durometer, respectively. Hardness of silicone elastomeric particles is in the range of Shore A 30-60. Shear modulus of silicone elastomeric particles is on the order of approximately 50-60MPa @ 20°C/1 Hz. Dynamic shear modulus of two silicone elastomers used to prepare silicone elastomeric particles is given in Figure 6.

Applicatons in Skin Care

Due to their spherical shape, elastic nature, optical and oil absorption properties, silicone elastomer powders are widely used in skin care for benefits

Table I. Absorption of Various Liquids by Different Silicone Elastomer Powders[a]

	Dow Corning® Brand			
Liquid	*9506*[b]	*9701*[c]	*EP-9215*[d]	*EP-9293AL*[e]
Octyl Palmitate	3	1	0.5	0.6
Isopropyl Myristate	5	1.4	0.8	0.6
Mineral Oil	3	1.5	0.6	0.6
Castor Oil	0.5	0.9	0.6	0.4
Sunflower Oil	0.5	0.8	0.5	0.5
Isododecane	2	3	1.5	2
Dow Corning® 245[f]	4	4.1	1.6	2
Water	1	1.1	0.5	0.6
Ethanol	1.3	1.1	0.4	0.4

[a] Values represent g of liquid absorbed per g of powder; composition remains dry to the touch. [b] 9506 is a low hardness particle (Shore A 30). [c] 9701 is a low hardness particle treated with SiO_2. [d] EP-9215 is a higher hardness particle (Shore A 60). [e] EP-9293AL is a low hardness particle coated with Al_2O_3. [f] Dow Corning® 245 is dodecamethylcyclopentasiloxane (D_5).

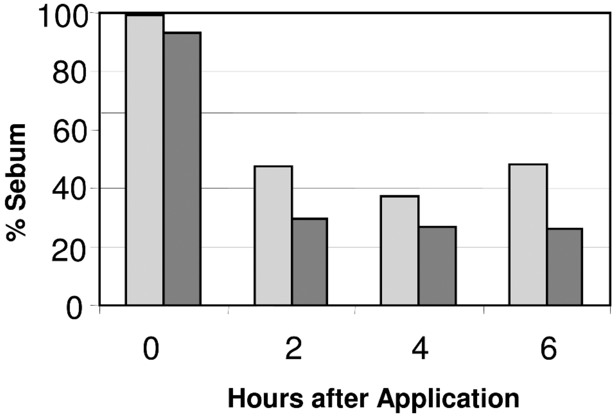

Figure 7. Level of Sebum remaining on human skin after treatment with a formulation containing 23% by weight silicone elastomeric powder. Light bars (left) represent Dow corning® 9506 and dark bars (right) represent Dow Corning 9701. Both silicone powders are low hardness; 9701 has a surface treatment of SiO_2 particles. Values were obtained using a Courage + Khazaka Gmbh. Sebumeter® SM810 and are at a 99% confidence level.

such as silky feel, delivery of actives, sebum absorption, wrinkle masking, matt finish and soft focus.

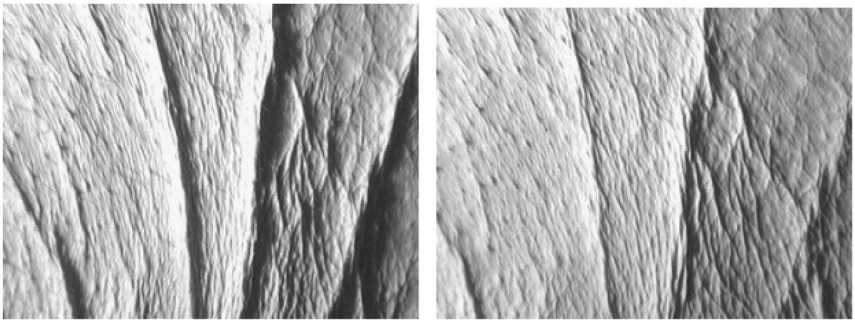

Before Treatment **1 Hour after Treatment**

Figure 8. Before and after treatment of crow's feet wrinkles (facial wrinkles radiating from under or outer corner of eyes) with a water-in silicone composition containing 10% by weight silicone elastomeric powder treated with SiO_2.

Sensory Feel

When silicone elastomeric powders are applied to skin and rubbed, they provide an extremely pleasant and highly agreeable sensation that can be described as soft, silky and velvety. The elastic nature of the particles provides a "cushion" feel while their spherical shape acts as "ball bearings" and roll on the skin surface. These combined effects lead to the extraordinarily pleasant sensation when silicone elastomeric particles are applied to skin. These sensory features are sought after by skin care formulators because of the perception of younger, smoother skin. The threshold level of the perceived benefit for these powders is in the range of 2-5% of a skin care formulation.

Absorption of Liquids; Delivery of Actives

Being crosslinked networks, the elastomer particles are insoluble in all solvents, but they are swellable by certain solvents. The ability of silicone elastomeric particles to swell in certain solvents is an important property in terms of their utility as therapeutic delivery agents for skin. Due to this swelling behavior and also due to their combined surface area, silicone elastomeric particles can take up moderate quantities of various oils and still remain dry to the touch. Thus silicone elastomeric particles can be used to carry certain oily substances or emollients to skin such as mineral oil, glycerides, fatty esters and sunscreens. Table I lists various liquids that are absorbed by several different silicone elastomeric powders and still provide a dry feel.

Absorption of Sebum

Sebum is an oily substance that accumulates on skin and is secreted by sebaceous glands which are found primarily on the scalp, face and upper chest and shoulders of the human body. Human sebum consists of about 57.5% glycerides and free fatty acids, 26% wax esters, 12% squalene, 3% cholesterol esters and 1.5% cholesterol (*10*). Sebum accumulates on skin and its presence can make skin appear shiny, which is undesirable, especially on the face. When applied to skin, silicone elastomeric particles are capable of absorbing sebum and hence causing a reduction in the level of sebum on the surface of skin.

It is possible to quantitatively measure the level of sebum on skin to determine how effective silicone powders are at controlling sebum accumulation on skin. Figure 7 shows the relative amounts of sebum remaining on skin after treatment with two kinds of silicone elastomeric particles.

Acne (*Acne vulgaris*) is a chronic disorder of the skin that is prevalent among adolescents and its treatment usually involves controlling bacterial growth and reducing sebum production (*10*). Although reducing the level of sebum on the surface of skin could be a beneficial strategy for treating acne, it is not know at this time if silicone elastomeric particles offer a therapeutic benefit for treating acne by reducing the level of sebum on the surface of skin.

Optical Properties, Soft Focus and Wrinkle Masking

In an aging population, cosmetic products that hide the effects of aging are highly desirable. Wrinkles and fine lines on skin trap light in crevices and cause the skin tone to look uneven. Pigments from foundations and make-up tend to collect in skin crevices and accentuate fine lines and wrinkles. Simply by covering up the imperfections in some cases creates an unnatural, caked-on appearance. There is a need for materials that can mask the signs of aging, while at the same time project the natural skin tone.

Compositions that coat with transparent materials which give sufficient differences in refractive indices could result in a “soft-focus” effect. The details of the principle and requirements for the soft-focus effect are described by Emmert (*11*). In a simplified description, the soft-focus effect is apparent when the total reflection is minimal (<20% of total light), total transmission is maximal (>75% of total light) while diffused light reflection is maximal (80%) and diffused light transmission is maximal (>50%). When these criteria are met, the total light transmission makes the natural skin tone show through (like a back light) to give a natural glow, while the diffused transmission would even out the skin tone and hide imperfections. Silicone elastomeric particles coated with either Al_2O_3 or TiO_2 nanoparticles have demonstrated the soft-focus effect (*12*, *13*).

Even without quantification of the soft-focus effect potential, a silicone elastomeric powder treated with SiO_2 particles has shown to give the perception of minimized wrinkles. Figure 8 shows before and after facial skin treatment to reduce the appearance of crow’s feet wrinkles (those wrinkles on skin radiating from under or outer corner of eyes) using a water-in-silicone formulation containing 10% silicone elastomer powder treated with SiO_2.

Summary

Silicone elastomeric particles, their preparation, their properties and their uses in skin care applications have been described. Silicone elastomeric particles are spherical particles of silicone rubber having a mean particle size on the order of 2-10μm. These particles are prepared by crosslinking aqueous emulsions of silicone polymer compositions followed by removal of water. Silicone elastomeric particles provide a pleasing sensation when applied to skin. They can absorb various emollients and liquids and deliver them to skin. These elastomeric particles are also capable of reducing the level of sebum on skin. Silicone elastomeric particles can also provide desirable optical properties when applied to skin by providing a perceived benefit of soft and natural glowing skin and also wrinkle reduction.

Acknowledgments

The authors would like to thank the Dow Corning Corporation for supporting their work in the field of silicone elastomer particles and also for support while writing this manuscript. The authors would like to express their appreciation to Jennifer Stasser for obtaining the micrograph of Figure 2 and to Dr. Glenn Gordon for obtaining the rheological data shown in Figure 5.

References

1. Hanada, T.; Morita, Y. U.S. Patent 4,594,134, 1986.
2. Shimizu, K; Hamada, M. U.S. Patent 4,742,142, 1988.
3. Yoshida, K.; Shimizu, K; Hamada, M. U.S. Patent 4,743,670, 1988.
4. Oba, T.; Mihama, T.; Futatsumori, K. U.S. Patent 4,761,454, 1988.
5. Liles, D. T.; Morita, Y.; Kobayashi, K. *Polym. Prepr. (Am. Chem. Soc., Div. Polym. Chem.)* **2001**, *42* (1), 240–241.
6. Liles, D. T.; Lin, F. *Polym. Prepr. (Am. Chem. Soc., Div. Polym. Chem.)* **2008**, *49* (2), 1087–1088.
7. Liles, D. T.; Morita, Y.; Kobayashi, K. *Polymer News* **2002**, *27*, 406.
8. Weitz, D. A.; et al. *Mater. Today* **2008**, *11* (4), 18–27.
9. Morita, Y.; Yokoyama, N. U.S. Patent 5,387,624, 1995.
10. Wilkinson, J. B., Moore, R. J., Eds. *Harry's Cosmeticology*, 7th ed.; Chemical Publishing Co.: New York, NY, 1982; pp 16−18.
11. Emmert, R. Quantification of the Soft-Focus Effect. *Cosmetics & Toiletries Magazine* **1996**, *111*, 57.
12. Dow Corning® EP-9293AL data sheet, 27-1290-01, 2007.
13. Dow Corning® EP-9261TI data sheet, 27-1292B-01, 2008.

Downloaded by PENNSYLVANIA STATE UNIV on June 23, 2012 | http://pubs.acs.org
Publication Date (Web): November 17, 2010 | doi: 10.1021/bk-2010-1053.ch012

Chapter 12

A New Approach to Formulating Mild Cleansers: Hydrophobically-Modified Polymers for Irritation Mitigation

Michael J. Fevola,[*] Russel M. Walters, and Joseph J. LiBrizzi

Johnson & Johnson Consumer & Personal Products Worldwide, Division of Johnson & Johnson Consumer Companies, Inc., Skillman, NJ 08558
[*]mfevola@its.jnj.com

New technical insights into surfactant skin penetration phenomena have led to the control of surfactant micelle penetration as a new approach to mitigating irritation. Polymer-surfactant association using hydrophobically-modified polymers (HMPs) is a practical method for reducing the apparent free micelle concentration in surfactant solutions. Surfactant-based cleansers formulated with HMPs exhibit dramatically lower irritation potential with uncompromised aesthetics. Key design features for irritation mitigating HMPs include strong surfactant binding ability (characterized by the ΔCMC value) and low molecular weight (to minimize rheological consequences of HMP incorporation). HMPs allow for the use of high surfactant loads to achieve high foam performance while maintaining mildness to the skin and eyes. HMPs also enable new levels of mildness for enhanced consumer health and beauty benefits.

Surfactants in Personal Cleansing Products

Surface-active agents, often referred to as *surfactants*, are the primary ingredients in personal cleansing products ranging from bar soaps to shampoos to liquid body washes. Surfactants are amphipathic molecules, that is, they are comprised of both hydrophilic and hydrophobic moieties covalently-linked within the same molecule. This amphipathic nature is the fundamental basis for many of the unique phenomena demonstrated by surfactants in aqueous media,

Downloaded by PENNSYLVANIA STATE UNIV on June 23, 2012 | http://pubs.acs.org
Publication Date (Web): November 17, 2010 | doi: 10.1021/bk-2010-1053.ch012

such as adsorption at air-water and oil-water interfaces and self-assembly into aggregated structures (e.g. micelles or lamellae) (*1*). It is these phenomena that are responsible for the functionality and utility of surfactants in personal cleansing applications. For example, the primary function of the surfactant is to provide the detergency (i.e. the ability to clean) required for removing dirt, oils, sebum, and other residues from the skin and hair (*2*), and this detergency is driven by the interfacial adsorption phenomena exhibited by surfactants (*3*). Cleansing products also rely on surfactant phenomena to build fluid viscosity, to solubilize fragrance oils and active ingredients, and to generate lather and foam in use (*4*). In most cases, a single surfactant type is not sufficient to achieve all of the desired product performance requirements, so multiple surfactants of different chemistries are blended to obtain optimal performance.

Surfactant-Skin Interaction and Negative Consequences

During cleansing, surfactants contact the outermost layer of the skin, the stratum corneum (SC), which is comprised of proteins (e.g. keratin) and lipids (e.g. ceramides, cholesterol, and free fatty acids). Like surfactants, these biological molecules and assemblies tend to exhibit amphipathic character. A significant consequence of this mutual amphipathicity is that surfactants interact quite readily with the SC. Surfactants can adsorb onto and diffuse into the SC and damage its structure by denaturing proteins, disrupting and disorganizing lipid bilayers, and solubilizing and removing lipids (*5*). The indiscriminate nature of detersive surfactants in contact with the skin causes them to damage the skin barrier and increase transepidermal water loss (TEWL), leading to symptoms such as tightening of the skin, dryness, roughness, and scaling (*2*). Prolonged damage of the skin barrier and underlying epidermal tissue may elicit an inflammatory response in the skin, resulting in symptoms that include erythema and pruritis. This combination of barrier damage and inflammation are collectively referred to as *irritation*, and the surfactants typically found in personal cleansing products can exhibit significant irritation potential to the skin.

Assessing Surfactant Irritation Potential

Personal cleansing products should be rigorously tested for safety prior to commercialization to ensure that they are not irritating under normal usage conditions. As animal testing is no longer a standard practice in the personal care and cosmetic industry, final product safety clearance is achieved via the combination of preclinical in vitro studies and in vivo clinical testing on human volunteers. Typical safety testing for personal cleansing products on skin involves exposure of the test subjects to the product under conditions that represent or exceed worst-case consumer usage scenarios (e.g. occlusive patch testing or exaggerated washing). These protocols are designed to maximize the probability of evoking and detecting an irritation response should it occur. Following each exposure to the product, the subjects' responses are evaluated either qualitatively (e.g. by expert and self grading of the exposure site) or quantitatively (e.g. by

Downloaded by PENNSYLVANIA STATE UNIV on June 23, 2012 | http://pubs.acs.org
Publication Date (Web): November 17, 2010 | doi: 10.1021/bk-2010-1053.ch012

instrumental measurements at the exposure site) to assess the product's irritation potential.

While in vivo safety testing on human subjects is a critical prerequisite to product commercialization, it is not practical for evaluating the irritation potential of multiple formula candidates during product development due to the associated time and cost constraints. In addition, human safety testing cannot be conducted until preliminary safety has been demonstrated in nonhuman models. Thus, the personal care and cosmetic industry relies heavily on in vitro methods as a prerequisite to rapidly screen formula candidates for irritation potential prior to in vivo testing, and human-use testing is limited only to those candidates demonstrating safety in vitro and possessing the greatest probability of commercial success.

A variety of in vitro methods have been employed to assess the irritation potential of surfactant-based systems, including the transepithelial permeability (TEP) assay, tissue equivalent assays (e.g. EpiDerm™ and EpiOcular™ by MatTek Corp.), the hen's egg chorioallantoic membrane (HET-CAM) assay, the red blood cell test, and the zein protein solubilization assay (*6*, *7*). While a detailed discussion of each of these methods and their corresponding endpoints is beyond the scope of this chapter, we will discuss the TEP assay in further detail since it is the method employed throughout this work.

TEP Assay

The TEP or fluorescein leakage assay is designed to assess how readily chemicals (primarily surfactants) can induce tissue permeability by damaging or killing epithelial cells (*8–11*). Although the TEP assay is most commonly used to determine the ocular irritation potential of surfactant systems, this sensitive method is nonetheless a good indicator of skin irritation potential as well.

The TEP model comprises a culture of Madine-Darby canine kidney (MDCK) cells that are grown so as to form a cohesive epithelial monolayer on a porous substrate; this monolayer is held together by intercellular *tight junctions*. The monolayer acts as a virtually impermeable barrier to the dye fluorescein; dye leakage will occur if the tight junctions are disrupted or the cells are lysed by the test chemical or formula.

In a typical TEP assay, the MDCK cells are exposed to increasing concentrations of a test formula diluted in a buffer solution, followed by exposure to a fluorescein dye solution. Dye leakage is measured via UV-Vis spectroscopy and recorded as a function of formula concentration (reported as % of original formula concentration). Simulated TEP data are shown in Figure 1: At concentrations ≤ 1.0 %, the tight junctions are undisturbed and little dye leakage is observed. With increasing formula concentration (> 1 %), leakage of dye through the monolayer is detected, indicating the onset of tight junction disruption by the surfactants in the formula. At high formula concentrations (> 5 %), dye leakage plateaus at a maximum value, corresponding to severe disruption of the tight junctions and a major loss of barrier integrity.

TEP results are usually reported as values of EC_{50}, the formula concentration at which 50% of maximum dye leakage occurs. For example, simulated TEP data

Downloaded by PENNSYLVANIA STATE UNIV on June 23, 2012 | http://pubs.acs.org
Publication Date (Web): November 17, 2010 | doi: 10.1021/bk-2010-1053.ch012

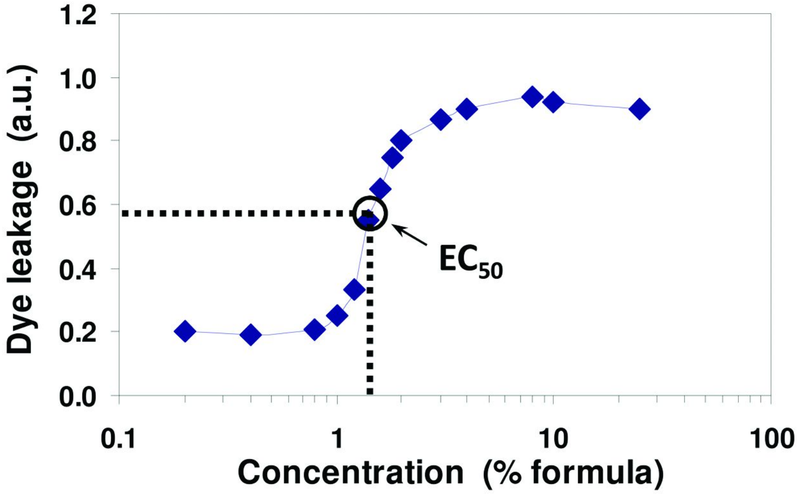

Figure 1. Simulated TEP data, showing fluorescein dye leakage as a function of increasing test formula concentration and the EC_{50} point. (see color insert)

in Figure 1 would yield an EC_{50} value of 1.5 %. Higher EC_{50} values in the TEP assay indicate that greater concentrations of formula are required to induce barrier damage; thus, formula mildness increases with increasing EC_{50}.

Figure 2 shows actual TEP data for three representative cleansing products, an adult shampoo, an adult body wash, and a baby wash (*12*). The adult shampoo generally elicits greater dye leakage compared to the adult body wash at identical formula concentrations, indicating that the shampoo more readily compromises barrier integrity. These data suggest that the shampoo is harsher than the body wash. When compared to the two adult products, the baby wash is observed to be much less aggressive, requiring significantly higher formula concentrations to promote dye leakage.

Mechanistic Approaches to Surfactant Skin Penetration

Surfactant-skin penetration and the ensuing surfactant-tissue interaction are topics of significant interest to both academic and industrial researchers. Tremendous efforts have been made over the past several decades to understand the fundamental nature of these phenomena at the molecular level, and the knowledge gained from this research has led to the continual development of personal cleansing products with ever-increasing mildness. This section will discuss the prevailing theories of surfactant-skin penetration and their implications for the formulation of mild cleansers.

Monomer Penetration Model

The classical *monomer penetration model* of surfactant penetration holds that only surfactant monomers, being of relatively small hydrodynamic size, are able

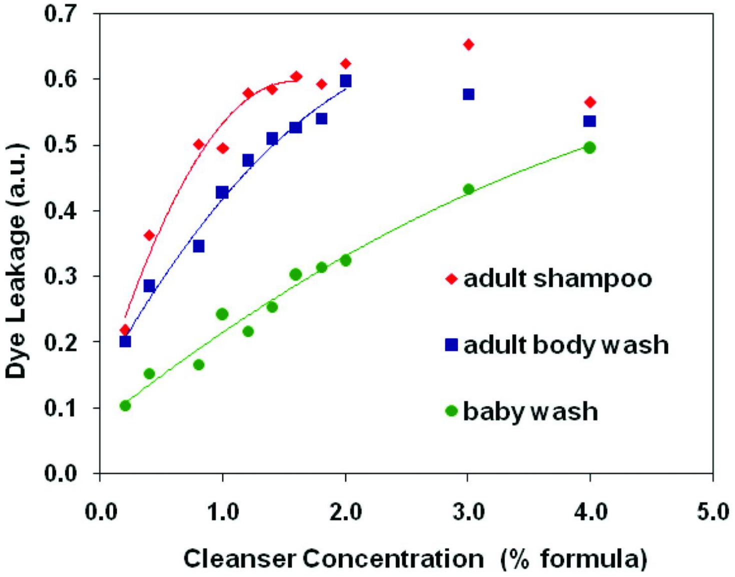

Figure 2. TEP data for representative personal cleansing products. (Reproduced with permission from reference (12). Copyright 2008 Allured Business Media.) (see color insert)

to penetrate into the SC of hydrated skin (*5*, *13*, *14*). The model also assumes that once surfactants self-assemble into micelles at concentrations above the critical micelle concentration (CMC), the resulting micellar species are too large to penetrate into the SC. Thus, for surfactant systems exhibiting low values of CMC, there will be fewer monomeric surfactants available to penetrate into the skin.

Based on this logic, the long-standing approach to formulating mild cleansing systems involves using surfactants with relatively low CMC values and combining surfactants of different chemistries to synergistically lower the CMC of the surfactant blend. Many successful methods for formulating mild cleansers, such as using polyoxyethylene alkyl ether sulfates in place of alkyl sulfates and blending anionic surfactants with nonionic and/or zwitterionic surfactants, can be rationalized in the context of this model. However, the monomer penetration model fails to adequately explain certain phenomena associated with surfactant-induced skin irritation. In particular, the monomer model is not consistent with the dose-dependent irritation response that is usually observed when surfactants such as sodium dodecyl sulfate (SDS) are applied to skin as a function of increasing concentration (i.e. irritation increases with increasing surfactant dose). According to the model, the irritation response should reach a maximum at the CMC of the surfactant system and then remain constant with increasing surfactant concentration, as surfactants in micellar form should not contribute to irritation. This model also does not account for the fact that the SC swells when hydrated, which could allow micelles to penetrate via aqueous domains not normally present in the dry SC.

Downloaded by PENNSYLVANIA STATE UNIV on June 23, 2012 | http://pubs.acs.org
Publication Date (Web): November 17, 2010 | doi: 10.1021/bk-2010-1053.ch012

Downloaded by PENNSYLVANIA STATE UNIV on June 23, 2012 | http://pubs.acs.org
Publication Date (Web): November 17, 2010 | doi: 10.1021/bk-2010-1053.ch012

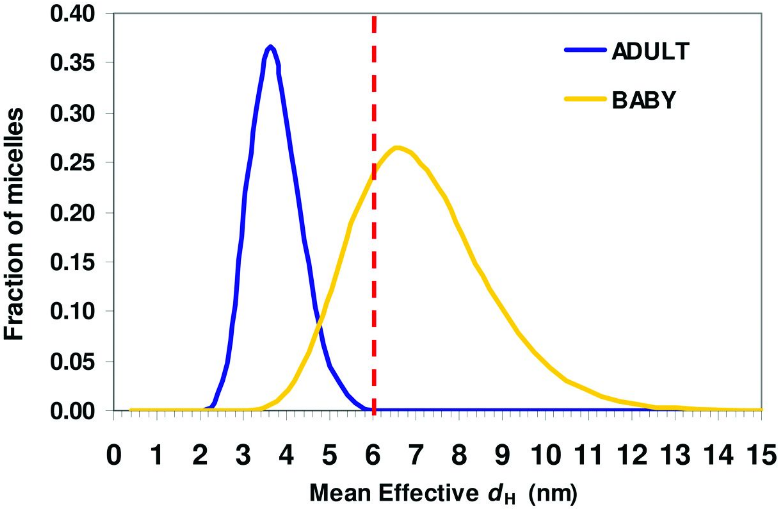

Figure 3. Micelle size distributions for an adult shampoo and a baby shampoo. Sample concentration = 3.0 wt% in deionized water. The dashed red line at 6 nm represents the upper size limit of aqueous pore radii in the SC as measured by Moore et al. (13). (Reproduced with permission from reference (12). Copyright 2008 Allured Business Media.) (see color insert)

Micelle Penetration Model

More recent studies by Blankschtein and coworkers (*13*, *15*, *16*) have provided evidence that surfactant micelles are capable of penetrating the SC into the epidermis, leading them to propose the *micelle penetration model*, which holds that both monomeric *and* micellar surfactant species can contribute to irritation. Moore et al. showed that SDS micelles exhibit an average hydrodynamic radius (R_h) of 20 Å, whereas the average aqueous pore radii of the SC are 10-28 Å, indicating the potential for SDS micelle penetration (*13*). In vitro skin penetration experiments conducted at ambient temperature and using ^{14}C radiolabeled SDS at concentrations in excess of the CMC confirmed that SDS micelles were contributing to SDS skin penetration. Subsequently, it was shown that the addition of low molecular weight polyethylene oxide (PEO) to SDS solutions above the CMC reduced SDS skin penetration. Dynamic light scattering (DLS) analysis revealed the formation of SDS-PEO complexes exhibiting values of R_h = 25 Å; thus, it was concluded that the reduced SDS penetration was due to steric hindrance that inhibited diffusion of the polymer-surfactant complexes into the SC.

In a related study, Moore et al. (*15*) examined the in vitro skin penetration of mixed micelles comprised of SDS and the nonionic surfactant dodecyl hexa(ethylene oxide) ($C_{12}EO_6$) at ambient temperature. SDS penetration was observed to decrease with increasing concentrations of $C_{12}EO_6$ in the SDS solutions. DLS measurements of micelle size showed that values of R_h increased from 20 Å to 27 Å as the concentration of $C_{12}EO_6$ was increased, indicating that the mixed micelles were becoming too large to effectively penetrate the SC. Using this same approach, Ghosh and Blankschtein (*16*) demonstrated that, unlike SDS, sodium cocoyl isethionate (SCI) solutions exhibit a dose-*independent* penetration profile; DLS analysis revealed larger values of R_h for SCI (34 Å), indicating that the SCI micelles are too large to effectively penetrate into the aqueous pores of the hydrated SC.

The micelle penetration model provides an improved theoretical framework for understanding surfactant-induced irritation. Not only does this model account for the dose-dependent irritation response observed for many surfactant systems, it also relates better to the surfactant concentration regimes that are used in clinical studies on surfactant-skin interaction and experienced by consumers when using cleansers (i.e. surfactant concentrations >> CMC).

Whether or not micellar surfactant actually penetrates the SC as *intact* micelles is still open to debate. Neither the monomer penetration model nor the micelle penetration model account for the significant variable of surfactant dynamics (*17*): The facts that 1) monomeric surfactants rapidly exchange into and out of micelles with exchange rate constants on the order of milliseconds to seconds, and 2) micelles are transient species with lifetimes on the order of seconds to tens of seconds, raise the possibility that micellar surfactant could diffuse into and beyond the SC as monomeric species and reform as micelles once the local concentration reaches the CMC. Although further research is required to reach a definitive conclusion, it is nevertheless clear that micellar surfactant contributes to penetration, either by direct micellar penetration or by acting as a reservoir to provide a continual source of monomeric penetrating species.

Downloaded by PENNSYLVANIA STATE UNIV on June 23, 2012 | http://pubs.acs.org
Publication Date (Web): November 17, 2010 | doi: 10.1021/bk-2010-1053.ch012

Application of Micelle Penetration Model

The utility of the micelle penetration model is evident in subsequent work conducted by Blankschtein and coworkers (*18–20*), in which the model has been used to explain phenomena observed during the course of various surfactant skin penetration studies. In one study (*18*), Ghosh and Blankschtein determined that the humectant glycerol effectively decreases the average aqueous pore radius of the hydrated SC, in turn reducing the ability of SDS micelles to penetrate into the skin. Thus, the authors demonstrated an interesting alternative approach to inhibiting surfactant skin penetration by exploiting steric hindrance: Instead of creating larger micelles to reduce penetration into aqueous pores of a given size, the effective size of the aqueous pores in the SC can be reduced to create steric hindrance and inhibit micelle penetration. Additionally, in vitro and in vivo studies (*19*, *20*) of skin barrier perturbation by aqueous surfactant-humectant systems provide further evidence that the micelle penetration model can effectively explain the trends observed when formulations of varying irritation potential are applied to skin.

We have conducted DLS measurements of micelle size and size distribution to demonstrate the applicability of the micelle penetration model to commercially-relevant surfactant systems used in personal cleansers. In one example, a clear adult shampoo (surfactant base comprising Sodium Laureth Sulfate, Sodium Lauryl Sulfate, and PPG-2 Hydroxyethyl Coco/Isostearamide, total product solids = 19

Table I. DLS and TEP Data for Adult and Baby Shampoos. SOURCE: Reproduced with permission from Reference (*12*). Copyright 2008 Allured Business Media

Product	*Average micelle d_H (nm)*	*Fraction of micelles with $d_H < 6$ nm*	*TEP EC_{50} value (% formula)*
Adult shampoo	3.7	100%	0.76 – IRRITANT
Baby shampoo	7.1	31%	3.89 – MILD

wt%) and a clear baby shampoo (surfactant base comprising Cocamidopropyl Betaine, PEG-80 Sorbitan Laurate, and Sodium Trideceth Sulfate, total product solids = 11 wt%) were diluted with deionized water and examined via DLS. Figure 3 shows the micelle size distributions for each product when diluted to 3.0 wt% of the original product concentration; Table I contains DLS results for the diluted shampoos and TEP EC_{50} values for each product.

The baby shampoo exhibits an average micelle hydrodynamic diameter (d_H) of 7.1 nm, nearly twice that of the adult shampoo surfactant (d_H = 3.7 nm). The TEP data indicate that the baby shampoo (EC_{50} = 3.89%) has a lower irritation potential than the adult shampoo (EC_{50} = 0.76%). As TEP is a dilution-based assay, one may normalize the adult shampoo EC_{50} value to account for its higher solids content; nevertheless, the normalized value (EC_{50}' = 1.31%) still indicates that the baby shampoo contains a significantly milder surfactant blend. In accordance with the micelle penetration model, the mildness of the baby shampoo may be attributed to the ability of its surfactant blend to form larger micelles at in-use dilution levels.

In their studies, Blankschtein and coworkers (*13*, *15*, *16*, *18*) based their conclusions on the *average* values of micelle hydrodynamic radii and aqueous pore radii; however, the authors indicated that important conclusions may also be drawn from the size distribution functions of micelles and aqueous pores. Micellar species are typically polydisperse in size, especially in the case of multicomponent surfactant blends, and this fact must be taken into consideration when interpreting data according to the micelle penetration model. For example, Moore et al. (*13*) reported the upper limit of aqueous pore radii in hydrated SC as 28 Å, translating to an aqueous pore diameter of ca. six nm. According to the micelle penetration model, micelles with values of d_H greater than six nm would not be able to penetrate tissue and contribute to irritation. This six nm upper limit is indicated by a dashed red line in Figure 3. In this case, 100% of the micelles in the adult shampoo sample exhibit d_H values below six nm and would therefore have the potential to penetrate into tissue and contribute to irritation. In contrast, only 31% of the micelles in the baby shampoo sample are below the six nm limit, rendering it a formula with reduced irritation potential, a conclusion confirmed by the TEP results in Table I.

Additionally, the above example illustrates a key dilemma associated with attempting to formulate mild cleansers with high foam performance. Although the baby shampoo surfactant blend forms relatively large micelles at in-use dilution levels, solutions of the baby shampoo still contain a significant fraction of smaller micelles that can contribute to irritation. However, the concentration of smaller micelles is sufficiently low enough to not cause irritation because baby

Downloaded by PENNSYLVANIA STATE UNIV on June 23, 2012 | http://pubs.acs.org
Publication Date (Web): November 17, 2010 | doi: 10.1021/bk-2010-1053.ch012

shampoos are typically formulated with relatively low surfactant loads. Yet if one attempts to formulate a high foaming, mild shampoo by simply employing the baby shampoo surfactant blend at higher loadings to boost foam performance, the resulting product will no longer be as mild as the original baby shampoo because the concentration of small penetrating micelles will increase with overall surfactant concentration, thereby increasing irritation potential.

Irritation Reduction Via Polymer-Surfactant Association

Downloaded by PENNSYLVANIA STATE UNIV on June 23, 2012 | http://pubs.acs.org
Publication Date (Web): November 17, 2010 | doi: 10.1021/bk-2010-1053.ch012

Product formulators are often faced with the challenge of crafting cleansers that exhibit maximum performance and consumer appeal while maintaining mildness. More often than not, key performance attributes, such as lather, may suffer at the expense of maintaining mildness. For example, the high foaming desired by consumers in adult cleansing products is driven largely by anionic surfactants (e.g. Sodium Laureth Sulfate, Sodium Lauryl Sulfate, etc.) that tend to be harsh and irritating. To achieve the mildness required for baby cleansers and cleansers for sensitive skin, these anionic surfactants must be used at lower concentrations and combined with less aggressive, lower foaming nonionic and zwitterionic surfactants, resulting in milder cleansers with diminished foam performance. Although these surfactant blends achieve the benefit of increased mildness, their foam performance often falls short of most adult consumers' expectations.

The advancement of the micelle penetration model has provided new technical insight into surfactant-induced irritation, paving the way for new solutions to this classical problem. Building on the understanding that micelles contribute to irritation, the control of micelle penetration has emerged as a new approach to formulating mild cleansers.

One such method for limiting micelle penetration involves the use of water-soluble polymers to bind surfactants via *polymer-surfactant association*, thereby creating polymer-surfactant complexes that are too large to penetrate into living tissue and lowering the concentration of free micelles in solution (Figure 4). Polymer-surfactant association is a well-known phenomenon that has been characterized for many combinations of water-soluble polymers and surfactants (*21*, *22*).

Moore et al. (*13*) demonstrated that polymer-surfactant association is a plausible method for reducing micelle penetration in their study of SDS-PEO systems; however, the work was conducted at surfactant concentrations significantly lower than the levels used in personal cleansing products. Additionally, since PEO is a nonionic and hydrophilic polymer, it cannot bind surfactant efficiently enough to mitigate irritation at practical use levels in personal cleansing products (*23*). For practical irritation mitigation in commercial systems, PEO would need to be added to formulations at levels that would negatively impact both product aesthetics and formula cost.

Goddard et al. (*24*) demonstrated that the cationic cellulose ether Polyquaternium-10 (PQ-10) readily binds high levels of SDS due to the strong electrostatic attractions between the two species and cooperative binding

Downloaded by PENNSYLVANIA STATE UNIV on June 23, 2012 | http://pubs.acs.org
Publication Date (Web): November 17, 2010 | doi: 10.1021/bk-2010-1053.ch012

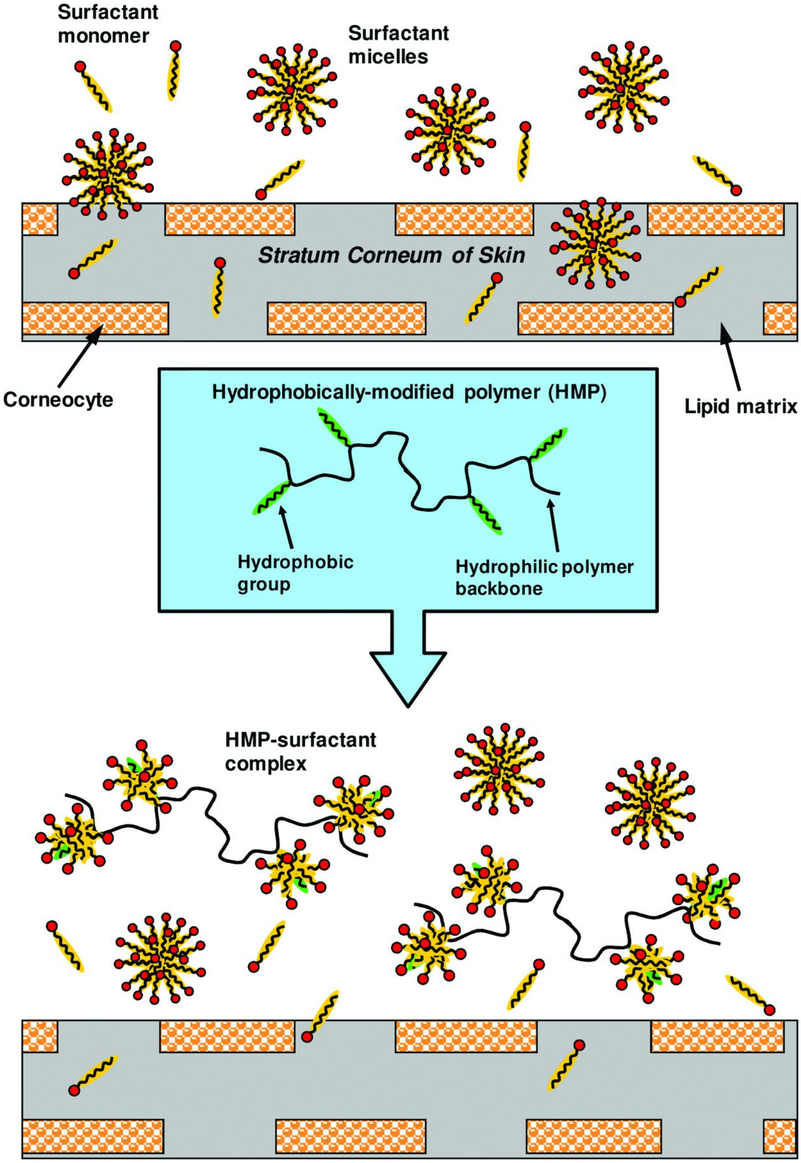
Surfactant monomer
Surfactant micelles
Stratum Corneum of Skin
Corneocyte
Lipid matrix
Hydrophobically-modified polymer (HMP)
Hydrophobic group
Hydrophilic polymer backbone
HMP-surfactant complex

Figure 4. Schematic representation of polymer-surfactant association using HMPs to reduce micelle penetration. (see color insert)

phenomena. It was subsequently shown that the addition of PQ-10 to SDS solutions reduced both SDS penetration into skin and SDS-induced swelling of the SC. These results were interpreted primarily in the context of the monomer penetration model (i.e. PQ-10 reduced the amount of free SDS monomer in the system), yet Goddard also proposed that other mechanisms could be contributing to the observed reduction in SDS penetration and SC swelling (e.g. adsorption of PQ-10 onto keratinous surfaces could interfere with SDS binding and penetration).

Downloaded by PENNSYLVANIA STATE UNIV on June 23, 2012 | http://pubs.acs.org
Publication Date (Web): November 17, 2010 | doi: 10.1021/bk-2010-1053.ch012

The work of Goddard and coworkers demonstrated that PQ-10 was more efficient than PEO at binding SDS and that it could effectively reduce SDS-tissue interaction, but the studies were conducted using relatively high levels of PQ-10 (1 – 2 wt%). These high levels of PQ-10 are approximately an order of magnitude greater than the levels normally employed in commercial use, and again are not practical in terms of cost or product aesthetics. Thus, to effectively employ polymer-surfactant association for the purpose of preventing surfactant penetration, polymers capable of efficiently binding large amounts of surfactant in a cost-effective, aesthetically-pleasing manner are necessary.

Hydrophobically-Modified Polymers for Irritation Mitigation

Surfactant binding efficiency is governed by both polymer and surfactant chemistry, with the electrostatically charged nature (i.e. anionic, cationic, nonionic) and hydrophobicity of each species being the most critical variables. The binding affinity of a polymer for a given surfactant or surfactants may be enhanced by tailoring the polymer's chemistry to include functionalities that promote surfactant association, such as hydrophobic domains, oppositely-charged ionic groups, or dipolar moieties.

HMPs are hydrophilic, water-soluble polymers that contain hydrophobic moieties (Figure 4). These polymers are particularly efficient at binding surfactants due to the strong propensity for aggregation of hydrophobic surfactant tail groups with the hydrophobic domains of the HMP. In some cases, the hydrophobic interactions driving HMP-surfactant association are so prevalent that charged HMPs will efficiently bind surfactants of like charge, despite the repulsive electrostatic interactions.

We have found that the enhanced surfactant binding efficiency of HMPs makes these polymers ideal for irritation mitigation in surfactant-based personal cleansing products (*23*, *25–29*). Because HMPs readily associate large amounts of surfactant, effective irritation mitigation can be achieved by adding relatively low levels of HMP to a surfactant system; these levels are typically low enough such that formula cost and product aesthetics are not negatively impacted.

The ΔCMC concept

To ensure proper HMP selection for effective irritation mitigation in surfactant-based cleansers, one must be able to quantify the amount of surfactant that a given HMP will bind in a specific surfactant system. Surfactant binding efficiency is readily measured via equilibrium surface tensiometry using the Wilhemy plate method (*23*). Figure 5 shows idealized plots of surface tension as a function of surfactant concentration for titrations of surfactant into water and into a HMP solution (*30*). In the absence of a HMP, surface tension initially decreases with increasing surfactant concentration due to surfactant populating the air-water interface. At the CMC, the chemical potential of surfactant adsorbed at the air-water interface equals the chemical potential for micelle formation.

Downloaded by PENNSYLVANIA STATE UNIV on June 23, 2012 | http://pubs.acs.org
Publication Date (Web): November 17, 2010 | doi: 10.1021/bk-2010-1053.ch012

Above the CMC, surfactant added to the solution is solubilized into micellar species, and in turn, the surface tension remains constant.

The surface tension profile for titration of surfactant into an HMP solution is notably different. Surface tension initially decreases as surfactant is added to the solution until reaching the critical aggregation concentration (CAC), where the chemical potential for polymer-surfactant interaction becomes favorable. At concentrations above the CAC, surfactant is preferentially adsorbed onto the HMP instead of existing as monomeric surfactant in the bulk and populating the air-water interface; thus, surface tension remains constant with increasing surfactant concentration as HMP-surfactant complexes form in solution. This plateau ends at a higher surfactant concentration, where the HMP has adsorbed a quantity of surfactant large enough such that polymer-surface competition (PSC) ensues. At this point, adsorption of the surfactant at the air-water interface becomes competitive with further adsorption onto the HMP. Therefore, increasing concentrations of surfactant will resume populating the air-water interface and surface tension will be lowered further. At the point CMC_P, the chemical potential of the surface becomes equal to the chemical potential required for free micelle formation in the presence of the HMP. Any excess surfactant added to the HMP-surfactant solution above CMC_P, will form micelles and the surface tension will remain constant.

For a given HMP-surfactant combination, the difference between the values of CMC in the presence (CMC_P) and absence (CMC) of the HMP, referred to as ΔCMC, is a measure of HMP surfactant binding efficiency (Figure 5). ΔCMC corresponds to the concentration of surfactant that would otherwise be present as free micelles in the absence of the HMP. Conceptually, by associating surfactant, the HMP acts to reduce the number of free micelles in a surfactant system above its CMC (Figure 6). By lowering the apparent concentration of free micellar species that can penetrate into living tissue, the HMP effectively lowers the irritation potential of the surfactant system.

Figure 7 shows surface tension profiles used to determine the ΔCMC for the association of the anionic surfactant Sodium Trideceth Sulfate (TDES) with a commercially-available HMP (International Nomenclature of Cosmetic Ingredients (INCI) Name: Acrylates Copolymer; a crosslinked alkali-swellable emulsion copolymer of methacrylic acid (MAA) and ethyl acrylate (EA) sold under the trade name Carbopol® AQUA SF-1 by Lubrizol, Inc.). Curvature in the profiles near the CMC indicates deviation from ideality due to trace impurities in the technical grade surfactant; however, ΔCMC calculations are possible via appropriate interpolation.

ΔCMC and Irritation Reduction

We have learned that by combining surfactants with HMPs exhibiting large ΔCMC values (i.e. high surfactant binding efficiency), it is possible to reduce the effective concentration of free micelles in a manner that is practical for the formulation of personal care products. As a result, surfactant-tissue interaction is dramatically reduced, leading to reduced irritation potential (*23*, *25–29*).

Downloaded by PENNSYLVANIA STATE UNIV on June 23, 2012 | http://pubs.acs.org
Publication Date (Web): November 17, 2010 | doi: 10.1021/bk-2010-1053.ch012

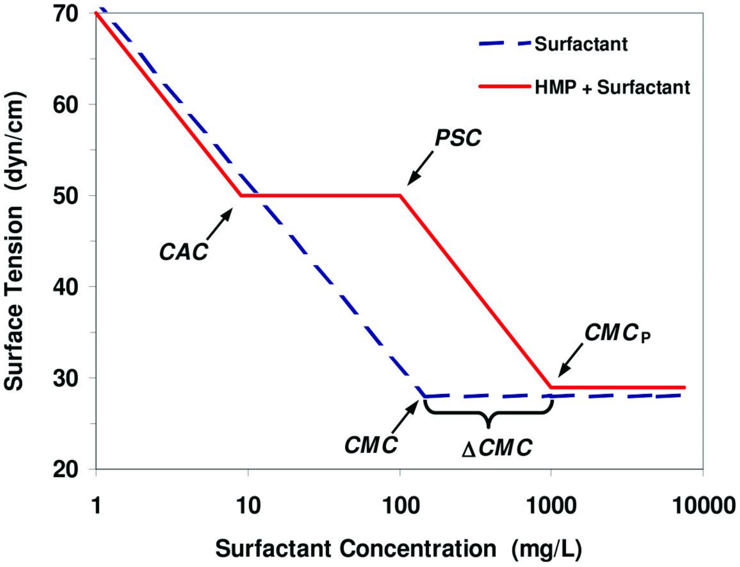

Figure 5. Idealized plot of equilibrium surface tension as a function of surfactant concentration for titrations of surfactant into water (dashed blue line) and surfactant into a HMP solution (solid red line). CAC = critical aggregation concentration, CMC = critical micelle conentration, PSC = point of polymer-surface competition,CMC_P = CMC in presence of HMP, ΔCMC = CMC_P – CMC. (see color insert)

The data in Table II demonstrate the relationship between ΔCMC and irritation reduction when using a HMP (Acrylates Copolymer, Carbopol® AQUA SF-1) to improve the mildness of a cleanser formulated with a high TDES loading. In this case, a reverse titration tensiometry method (i.e. surface tension is measured as a function of formula dilution) was employed to measure CMC, CMC_P, and ΔCMC values as a function of increasing HMP concentration (*23*). As the level of HMP in the formula is initially increased from zero to 1.2 wt%, the value of ΔCMC also increases, corresponding to a reduction in free micelle concentration. Beyond 1.2 wt% HMP, ΔCMC reaches a plateau value of 334 ± 15 mg/mL with increasing HMP concentration. This plateau is due to a loss of surfactant association efficiency above polymer loadings of 1.2 wt% (*28*). The loss of efficiency at higher polymer loadings is attributed to intermolecular repulsions between HMP-surfactant complexes that prevent the HMP coils from further expanding to present more binding sites for surfactant association.

Addition of the HMP to this formula leads to a marked increase in the mildness of the formula as measured by the TEP assay (Table II). A step-change improvement in the EC_{50} value of the formula is observed upon initial addition of the HMP, and further improvments in mildness are realized as the concentration of HMP is increased. The increases in ΔCMC values with increasing HMP concentration are generally accompanied by increases in ΔTEP EC_{50} values (where ΔTEP = [EC_{50} in presence of HMP] – [EC_{50} in absence of HMP]), suggesting that the irritation

Downloaded by PENNSYLVANIA STATE UNIV on June 23, 2012 | http://pubs.acs.org
Publication Date (Web): November 17, 2010 | doi: 10.1021/bk-2010-1053.ch012

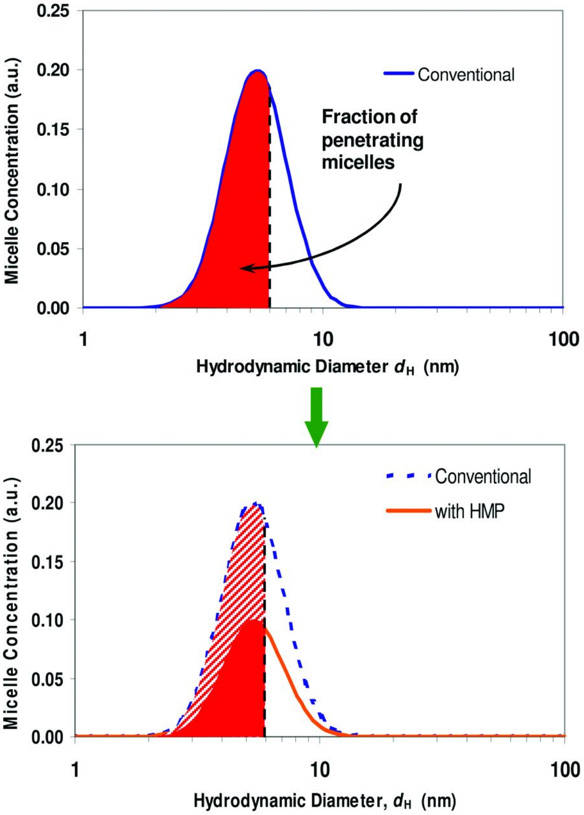

Figure 6. Conceptual diagram of free micelle concentration as a function of d_H for a conventional surfactant system (top) and a surfactant system containing a HMP (bottom). The dashed lines at d_H = 6 nm represent the upper size limit of aqueous pore radii in the SC as measured by Moore et al. (13). (see color insert)

potential of the formula decreases with increasing HMP concentration. It should be noted that the error associated with the TEP EC_{50} values is expected due to the inherently high variability associated with in vitro biological assays based on living cells. This variability leads to difficulty in establishing precise correlations of TEP data with sensitive instrumental techniques, such as ΔCMC determination. Nevertheless, a positive correlation between ΔTEP and ΔCMC ($R^2 = 0.97$) is observed when the appropriate statistical analysis is applied, noting that one data point (HMP = 1.2 wt%) is excluded as an outlier.

In summary, the ΔCMC value is a critical parameter for the proper application of HMPs to reduce irritation. Not only does the ΔCMC concept enable formulators to select the proper HMP and correct usage levels for a given surfactant blend, it also provides a clear design criterion for the development of HMPs as irritation mitigants.

Downloaded by PENNSYLVANIA STATE UNIV on June 23, 2012 | http://pubs.acs.org
Publication Date (Web): November 17, 2010 | doi: 10.1021/bk-2010-1053.ch012

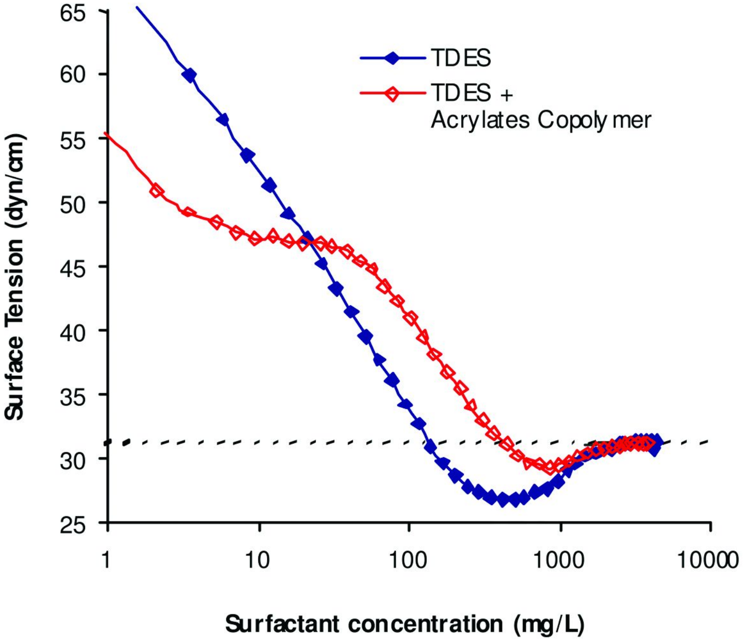

Figure 7. Surface tension profiles for ΔCMC determination of TDES in the presence of a MAA-EA copolymer, INCI Name: Acrylates Copolymer, Carbopol® AQUA SF-1 (23). Horizontal dotted line indicates ultimate equilibrium surface tension. (see color insert)

Table II. Surface Tensiometry and TEP Assay Data for a Surfactant-Based Cleanser Incorporating a HMP (*23*)

HMP Conc. (wt% active)	*CMC or CMC_P (mg/L)*	*ΔCMC (mg/L)*	*TEP EC_{50} (% formula)*	*ΔTEP EC_{50} (% formula)*
0.0	48	–	1.46 ± 0.26	–
0.3	65	17	2.68 ± 0.28	1.22
0.9	136	88	2.85 ± 0.51	1.39
1.2	377	329	2.74 ± 0.18	1.28
1.5	370	322	3.34 ± 0.83	1.88
1.8	398	350	3.26 ± 0.39	1.80

Representative HMP Chemistries

Many synthetic routes exist for the preparation of HMPs, ranging from free-radical copolymerization of hydrophilic and hydrophobic ethylenically-unsaturated monomers to post-polymerization modification of hydrophilic polymers to include hydrophobic moieties (*31–34*). As a result, a wide array of HMP compositions and architectures are easily accessible for application as irritation mitigants. The polymer structures shown in Figure 8 represent three

Downloaded by PENNSYLVANIA STATE UNIV on June 23, 2012 | http://pubs.acs.org
Publication Date (Web): November 17, 2010 | doi: 10.1021/bk-2010-1053.ch012

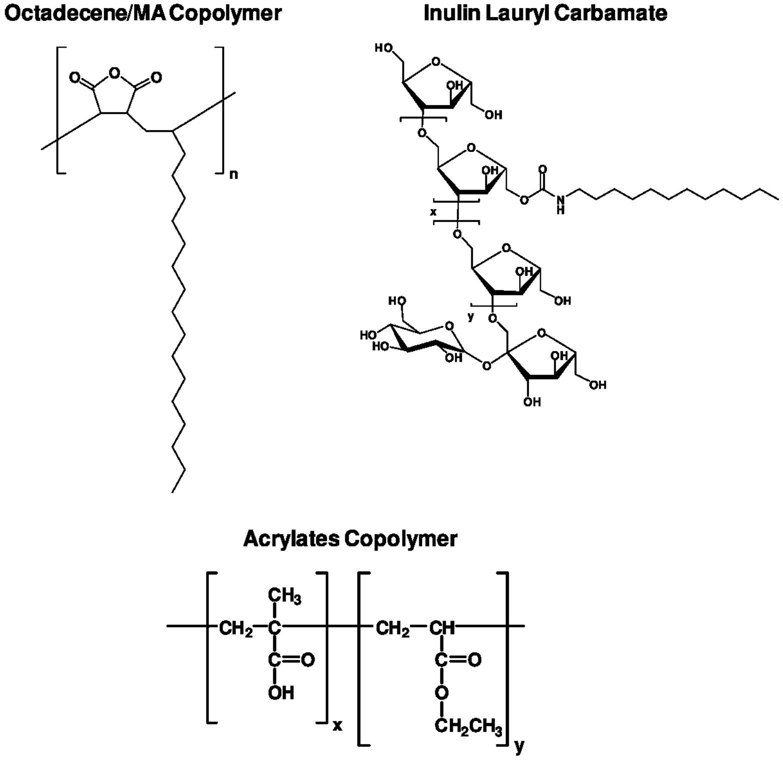
Octadecene/MA Copolymer

Inulin Lauryl Carbamate

Acrylates Copolymer

Figure 8. INCI Names and chemical structures of irritation mitigating HMPs.

general classes of HMPs that demonstrate high surfactant binding efficiency and the ability to reduce irritation potential in personal cleansers. These HMP classes include water-soluble polysaccharides that have been functionalized with hydrophobic alkyl chains (e.g. Inulin Lauryl Carbamate, sold as Inutec SP-1 by BENEO-Orafti, Inc.), one-to-one alternating copolymers of long chain α-olefins with maleic anhydride that can be hydrolyzed in situ to yield water-soluble derivatives (e.g. Octadecene/MA Copolymer, sold as PA-18 by Chevron Philips Chemical Co.), and alkali-swellable emulsion (ASE) copolymers of MAA and EA which may be optionally crosslinked (e.g. Acrylates Copolymer, sold as Carbopol® AQUA SF-1 by Lubrizol, Inc.).

The ASE copolymers of MAA and EA are unique in that they do not derive their hydrophobicity from the inclusion of long chain alkyl groups; indeed, the C_2 side chain of the EA monomer renders it only marginally hydrophobic. However, the emulsion copolymerization process and reactivity ratios of MAA and EA lead to blocky incorporation of the EA monomer into the ASE copolymer (*35*). Therefore, the Acrylates Copolymer shown in Figure 8 is able to absorb large quantities of surfactant on hydrophobic domains comprised of long, blocky runs of EA in the copolymer backbone (Figure 9).

Downloaded by PENNSYLVANIA STATE UNIV on June 23, 2012 | http://pubs.acs.org
Publication Date (Web): November 17, 2010 | doi: 10.1021/bk-2010-1053.ch012

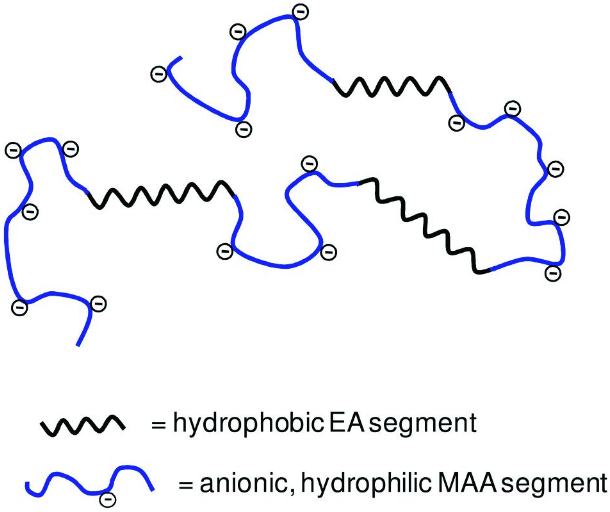

Figure 9. Schematic diagram showing blocky incorporation of EA hydrophobic monomer in MAA-EA ASE copolymers. (see color insert)

ΔCMC for pH-Responsive Copolymers

HMPs that contain pH-responsive ionizable moieties, such as carboxylic acids or tertiary amines, exhibit pH-dependent surfactant binding affinity, especially for ionic surfactants. For example, the ASE copolymers of MAA and EA discussed above bear carboxylic acid groups and exhibit apparent pK_a values ranging from 5 to 7, depending on exact copolymer composition and architecture. Figure 10 shows values of ΔCMC and solution pH as a function of degree of neutralization (α) for the anionic surfactant Sodium Laureth-2 Sulfate and the HMP Acrylates Copolymer (Carbopol® AQUA SF-1) (*36*). ΔCMC is observed to increase with decreasing values of α, indicating greater surfactant binding as the anionic charge density on the copolymer is decreased (i.e. by lowering solution pH). This effect is attributed to decreased electrostatic repulsion between the copolymer and the anionic surfactant and the increasingly hydrophobic character of the copolymer with decreasing solution pH.

The pH-responsive nature of ionizable HMPs allows formulators to further enhance irritation mitigation by simply adjusting the formula pH to elicit greater HMP-surfactant association. This method of increasing HMP-surfactant association via pH adjustment has also been exploited for the purpose of rheology modification: the so-called *back-acid thickening* mechanism is used to increase association of surfactants to crosslinked ASE copolymers to build viscosity and yield value in surfactant-based cleansing formulations (*37*).

Low Molecular Weight HMPs for Improved Performance

Most commercially-available HMPs have been developed for the purpose of rheology modification. The compositions, architectures, and molecular weights

Downloaded by PENNSYLVANIA STATE UNIV on June 23, 2012 | http://pubs.acs.org
Publication Date (Web): November 17, 2010 | doi: 10.1021/bk-2010-1053.ch012

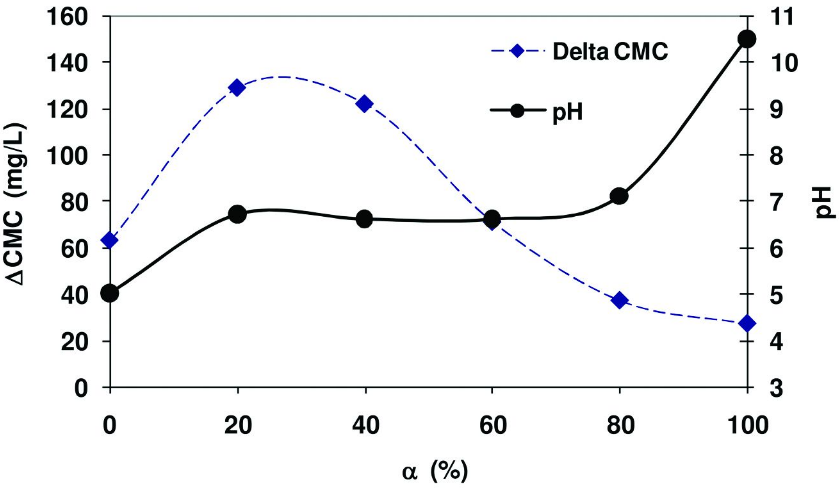

Figure 10. ΔCMC and solution pH as a function of α for the combination of Acrylates Copolymer (Carbopol® AQUA SF-1) and Sodium Laureth-2 Sulfate (36). (see color insert)

of these HMPs have been optimized to promote intermolecular hydrophobic associations and chain entanglement at very low concentrations in aqueous solution, thereby enabling maximum thickening efficiency and high yield value at relatively low use levels. For example, rheological performance in ASE rheology modifiers has been improved by crosslinking the copolymers to yield extremely high molecular weight (MW) *microgel* polymers, and/or by incorporating associative macromonomers to increase intermolecular associations (*38*).

When incorporated into surfactant-based cleansers at low levels (e.g. ≤ 1.0 wt% active solids), these HMPs provide ample viscosification without negatively impacting other formula attributes, such as clarity, dispensability, spreading, or lathering. However, when rheology modifying HMPs are employed at higher concentrations to achieve adequate irritation mitigation, product formulations often become so viscous that aesthetics and performance are negatively impacted.

We have discovered that low MW HMPs are preferred for irritation mitigation in surfactant-based cleansers. Preferred HMPs have linear architectures and MW values ranging from 3,500 – 60,000 g/mol, though the optimum MW for a given HMP will depend on the particular polymer chemistry and its solution properties. Low MW HMPs have equal (and in some cases, greater) surfactant binding capacity compared to their high MW analogs, yet they are not capable of building high viscosity or yield value (*28*, *29*, *39*). Therefore, low MW HMPs may be used at high concentrations for effective irritation mitigation without negative rheological consequences. Also, surfactant systems containing low MW HMPs usually do not exhibit the turbidity associated with incorporation of high MW HMPs; thus, low MW HMPs are ideal for irritation mitigation in clear cleanser formulations.

Downloaded by PENNSYLVANIA STATE UNIV on June 23, 2012 | http://pubs.acs.org
Publication Date (Web): November 17, 2010 | doi: 10.1021/bk-2010-1053.ch012

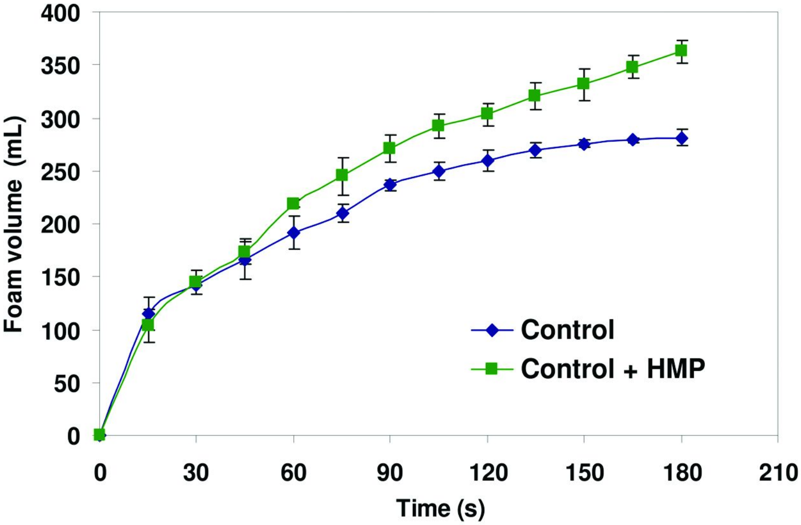

Figure 11. Foam generation profiles as a function of agitation time for a mild surfactant blend in the absence and presence of a HMP (48). (see color insert)

Effect of HMPs on Foam Performance

In addition to providing the benefit of enhanced mildness, HMPs can also improve the lathering and foam quality of personal cleansing products, thereby improving consumer perception of the products. Water-soluble polymers are well-known as additives for enhancing the foaming properties of surfactant systems (*24*, *40–43*). The idea that a surfactant-binding HMP will improve foam performance may seem counterintuitive at first to some, since polymer-surfactant association would seemingly decrease the availability of free surfactant for foam generation and stabilization. However, both HMPs and HMP-surfactant complexes exhibit surface activity and the ability to stabilize newly formed air-water interfaces . HMPs and HMP-surfactant complexes are also capable of increasing the thickness and viscosity of foam bubble lamella and inhibiting drainage at the plateau borders of the foam bubbles (*44–47*). Collectively, these phenomena lead to thicker, denser (i.e. creamier), longer-lasting foams in surfactant-based cleansers that incorporate HMPs.

Figure 11 demonstrates the ability of a HMP to improve foam performance in a mild cleansing system. In this case, the control formula was a mild surfactant blend comprising PEG-80 Sorbitan Laurate, Cocamidopropyl Betaine, Decyl Glucoside and Disodium Lauroamphodiacetate at ca. 12 wt% active solids. To this control formula was added ca. 1 wt% active of a HMP (INCI Name: Potassium Acrylates Copolymer). Diluted solutions (0.05 wt% formula in hard water containing 130 ppm Ca^{2+}) of each formula were analyzed for foam generation using a SITA R-2000 Foam Tester (SITA Messtechnik GmbH) operating at 30 °C and 1200 rpm. The foam generation profiles in Figure 11 suggest that addition of the HMP to this surfactant blend can significantly increase its foaming ability, in some cases increasing the volume of foam produced by up to 35%.

Downloaded by PENNSYLVANIA STATE UNIV on June 23, 2012 | http://pubs.acs.org
Publication Date (Web): November 17, 2010 | doi: 10.1021/bk-2010-1053.ch012

Conclusions

Recent advances in the understanding of surfactant-tissue interaction, in particular the proposal of the micelle penetration model for surfactant skin penetration, have provided new technical insights leading to the development of novel approaches for designing mild personal cleansing products. By adding HMPs to surfactant-based cleansers, one can effectively manage the concentration of free micelles that are potential skin penetrants and dramatically reduce irritation potential. The principle benefits of HMP technology for irritation mitigation are two-fold: 1) HMPs allow for the use of higher surfactant loads for increased foam performance without concomitant increase in irritation potential, and 2) HMPs enable previously unattainable levels of mildness in sensitive skin products for improved health and beauty. Proper polymer design is critical for successful application of HMPs as irritation mitigants in cleanser formulations: Ideal HMPs should exhibit large values of ΔCMC for maximum surfactant binding efficiency and low MWs for preferred product aesthetics and performance.

References

1. Holmberg, K.; Jönsson, B.; Kronberg, B.; Lindman, B. *Surfactants And Polymers In Aqueous Solution*, 2nd ed.; John Wiley & Sons: New York, 2002.
2. Ananthapadmanabhan, K. P.; Moore David, J.; Subramanyan, K.; Misra, M.; Meyer, F. *Dermatol. Ther.* **2004**, *17* (1), 16–25.
3. von Rybinski, W. In *Handbook of Applied Surface and Colloid Chemistry*; Holmberg, K.,, Ed.; John Wiley & Sons, Ltd.: New York, 2002; Vol. 1, pp 53−72.
4. O'Lenick, A. J., Jr. *Surfactants: Strategic Personal Care Ingredients*; Allured Publishing Corp.: Carol Stream, IL, 2005.
5. Rieger, M. M. *Cosmet. Toiletries* **1995**, *110* (4), 31–50.
6. Curren, R. D.; Harbell, J. W. *Environ. Health Perspect.* **1998**, *106* (Suppl. 2), 485–492.
7. Moore, P. N.; Puvvada, S.; Blankschtein, D. *Langmuir* **2003**, *19* (4), 1009–1016.
8. Shaw, A. J.; Balls, M.; Clothier, R. H.; Bateman, N. D. *Toxicol. in Vitro* **1991**, *5* (5-6), 569–571.
9. Gautheron, P.; Duprat, P.; Hollander, C. F. *Toxicol. in Vitro* **1994**, *7* (1), 33–43.
10. Cottin, M.; Zanvit, A. *Toxicol. in Vitro* **1997**, *11* (4), 399–405.
11. Clothier, R.; Starzec, G.; Stipho, S.; Kwong, Y. C. *Toxicol. in Vitro* **1999**, *13* (4/5), 713–717.
12. Walters, R. M.; Fevola, M. J.; LiBrizzi, J. J.; Martin, K. *Cosmet. Toiletries* **2008**, *123* (12), 53–60.
13. Moore, P. N.; Puvvada, S.; Blankschtein, D. *J. Cosmet. Sci.* **2003**, *54* (1), 29–46.
14. Rhein, L. D. *J. Soc. Cosmet. Chem.* **1997**, *48* (5), 253–274.

15. Moore, P. N.; Shiloach, A.; Puvvada, S.; Blankschtein, D. *J. Cosmet. Sci.* **2003**, *54* (2), 143–159.
16. Ghosh, S.; Blankschtein, D. *J. Cosmet. Sci.* **2007**, *58* (3), 229–244.
17. Zana, R. In *Dynamics of Surfactant Self-Assemblies, Surfactant Science Series*, Zana, R., Ed.; CRC Press: Boca Raton, FL, 2005; pp 75−160.
18. Ghosh, S.; Blankschtein, D. *J. Cosmet. Sci.* **2007**, *58* (2), 109–133.
19. Ghosh, S.; Hornby, S.; Grove, G.; Zerwick, C.; Appa, Y.; Blankschtein, D. *J. Cosmet. Sci.* **2007**, *58* (6), 599–620.
20. Ghosh, S.; Kim, D.; So, P.; Blankschtein, D. *J. Cosmet. Sci.* **2008**, *59* (4), 263–289.
21. Holmberg, K.; Jönsson, B.; Kronberg, B.; Lindman, B. In *Surfactants and Polymers in Aqueous Solution*, 2nd ed.; John Wiley & Sons, Ltd.: Hoboken, NJ, 2003; pp 277−303.
22. Lindman, B. In *Handbook of Applied Surface and Colloid Chemistry*; Holmberg, K., Ed.; John Wiley & Sons, Ltd.: New York, 2002; Vol. 1, pp 445−463.
23. LiBrizzi, J.; Protz, A.; Ganopolsky, I.; Walters, R. U.S. Pat. 7,157,414, 2007.
24. Goddard, E. D. In *Principles of Polymer Science and Technology in Cosmetics and Personal Care*; Goddard, E. D., Gruber, J. V., Eds.; Marcel Dekker, Inc.: New York, 1999; pp 181−215.
25. Martin, A.; LiBrizzi, J.; Ganopolsky, I.; Lukenbach, E. R.; Eknoian, M. W. U.S. Pat. 7,084,104, 2006.
26. LiBrizzi, J.; Martin, A.; Ganopolsky, I.; Lukenbach, E. R.; Eknoian, M. W. U.S. Pat. 7,119,059, 2006.
27. Ganopolsky, I.; LiBrizzi, J.; Martin, A.; Lukenbach, E. R.; Eknoian, M. W. U.S. Pat. 7,098,180, 2006.
28. Walters, R.; Fevola, M.; LiBrizzi, J. U.S. Pat. Appl. 20070111910 A1, 2007.
29. Walters, R.; Fevola, M.; LiBrizzi, J. U.S. Pat. Appl. 20060257348 A1, 2006.
30. Johnson, K. M.; Fevola, M. J.; Lochhead, R. Y.; McCormick, C. L. *J. Appl. Polym. Sci.* **2004**, *92* (1), 658–671.
31. Glass, J. E. *Polymers in Aqueous Media: Performance Through Association*; Advances in Chemistry Series; American Chemical Society: Washington, DC, 1989; Vol. 223.
32. Glass, J. E. *Associative Polymers in Aqueous Media*; ACS Symposium Series; American Chemical Society: Washington, DC, 2000; Vol. 765.
33. Schulz, D. N.; Bock, J.; Valint, P. L., Jr. In *Macromolecular Complexes in Chemistry and Biology*; Dubin, P., Bock, J., Davis, R. M., Schulz, D. N., Thies, C., Eds.; Springer-Verlag: New York, 1994; pp 3−13.
34. Landoll, L. M. *J. Polym. Sci., Polym. Chem. Ed.* **1982**, *20* (2), 443–455.
35. Dai, S.; Tam, K. C.; Jenkins, R. D. *Eur. Polym. J.* **2000**, *36* (12), 2671–2677.
36. Tamareselvy, K.; Masler, W. F.; Filla, D. S.; Gray, G. U.S. Pat. Appl. 2008113895A1, 2008.
37. Schmucker-Castner, J. F.; Ambuter, H.; Snyder, M.; Weaver, A. A.; Kotian, S. V. U.S. Pat. 6,635,702, 2003.
38. Gruber, J. V. In *Principles of Polymer Science and Technology in Cosmetics and Personal Care*; Goddard, E. D., Gruber, J. V., Eds.; Marcel Dekker, Inc.: New York, 1999; pp 217−274.

Downloaded by PENNSYLVANIA STATE UNIV on June 23, 2012 | http://pubs.acs.org
Publication Date (Web): November 17, 2010 | doi: 10.1021/bk-2010-1053.ch012

39. LiBrizzi, J. J.; Walters, R. M.; Fevola, M.; Tamareselvy, K. U.S. Pat. Appl. 20080112913A1, 2008.
40. Goddard, E. D.; Hannan, R. B. *J. Colloid Interface Sci.* **1976**, *55* (1), 73–79.
41. Regismond, S. T. A.; Winnik, F. M.; Goddard, E. D. *Colloids Surf., A* **1998**, *141* (2), 165–171.
42. Folmer, B. M.; Kronberg, B. *Langmuir* **2000**, *16* (14), 5987–5992.
43. Djuve, J.; Pugh, R. J.; Sjoblom, J. *Colloids Surf., A* **2001**, *186* (3), 189–202.
44. Goddard, E. D.; Braun, D. B. *Cosmet. Toiletries* **1985**, *100* (7), 41–47.
45. Ananthapadmanabhan, K. P.; Leung, P. S.; Goddard, E. D. In *Polymer Association Structures*; ACS Symposium Series; American Chemical Society: Washington, DC, 1989; Vol. 384, pp 297−309.
46. Dong, X.; Sun, D.; Liu, G.; Cao, C.; Jiang, X. *Colloids Surf., A* **2009**, *345* (1−3), 58–64.
47. Jean, B.; Lee, L.-T.; Cabane, B.; Bergeron, V. *Langmuir* **2009**, *25* (7), 3966–3971.
48. Walters, R. M.; Bussey, D.; Tierney, N.; Martin, K. Unpublished results.

Downloaded by PENNSYLVANIA STATE UNIV on June 23, 2012 | http://pubs.acs.org
Publication Date (Web): November 17, 2010 | doi: 10.1021/bk-2010-1053.ch012

Downloaded by CORNELL UNIV on June 23, 2012 | http://pubs.acs.org
Publication Date (Web): November 17, 2010 | doi: 10.1021/bk-2010-1053.ch013

Chapter 13

Silicone Polyethers as Stabilizers of Water-in-Oil Emulsions

Tatiana D. Dimitrova,[1,*] Laurie Saulnier,[1] Véronique Verhelst,[1] and Isabelle Van Reeth[2]

[1]Dow Corning S.A, Parc Industriel Zone C, B-7180 Seneffe, Belgium
[2]Dow Corning (Shanghai) Co, 448 East Rong Le Road, Songjiang Industrial Zone Shanghai 201613, People's Republic of China
[*]t.dimitrova@dowcorning.com

The emulsifying properties of silicone–polyether block copolymers (SPE) have been studied. Linear SPEs produce water-in-oil droplets of practically the same mean size regardless the hydrodynamic conditions of mixing. On the contrary, rake SPEs produce droplets of 1-2 microns under conditions of turbulent inertial emulsification and much larger droplets under turbulent viscous regime. All studied emulsions are flocculated, but the physical origins of the phenomenon are different for the different polymer morphologies. The amount of polymer adsorbed on the water droplets has been determined and it has been demonstrated that the SPEs adsorb on the droplets' surface via the formation of multilayers. The dilatational elasticity of the adsorbed layers decreases with the increase of the concentration. This effect suggests in-surface configurational relaxation upon deformation.

Introduction

Emulsions are thermodynamically unstable and therefore do not form spontaneously. The necessary energy is provided through shaking, stirring, high pressure homogenization, etc. and the hydrodynamic conditions typical for each emulsification method differ considerably. The kinetic stability is achieved by adding a surface active material (emulsifier) - a single chemical component, or mixture of components, having the capacity of promoting emulsion formation

In Polymeric Delivery of Therapeutics; Morgan, S., et al.;
ACS Symposium Series; American Chemical Society: Washington, DC, 2010.

Downloaded by CORNELL UNIV on June 23, 2012 | http://pubs.acs.org
Publication Date (Web): November 17, 2010 | doi: 10.1021/bk-2010-1053.ch013

and stabilization by interfacial action. According to the empirical Bancroft's rule the emulsifiers tend to promote the dispersion of the phase in which they do not dissolve well. In practice, for leave-on cosmetics, as well as for pharmaceutical and cosmeceutical applications, the low molecular weight emulsifiers can not be always endorsed because many of these molecules have poor toxicological and/or environmental profile. A possible way to overcome this problem is the use polymers instead of low molecular weight emulsifiers. Employing particles is another possibility, but the emulsions generated this way (i.e. Pickering emulsions) are of limited commercial interest, due to the fact that the three-phase contact angle of the stabilizing particles is easily influenced by the presence of small molecular weight amphiphiles (*1*). In other words, a destabilization is frequently observed when Pickering emulsions are incorporated in more complex formulations.

Water-in-oil (W/O; sometimes referred to as "inverted") emulsions have multiple applications in personal care and cosmetic formulations (*2–4*), particularly in sunscreens, foundations and antiperspirant gels. Benefits of W/O systems include wash-off resistance, improved barrier properties, emolliency, moisturization and, in some cases, an influence on the penetration of actives. It is known that inverted emulsions are trickier to stabilize than their oil-in-water counterparts because the electrostatic repulsion is by far less involved.

Polymer emulsifiers are popular stabilizers for W/O emulsions. Although silicone polyethers have been used in personal care and beauty care industries since a long time, relatively little systematic information on their function and properties has been gathered. The emulsification power and the interfacial properties of a wide range of silicone–polyether copolymers (SPE) have been examined in the present work. The main goal of the research has been to determine the influence of the main structural parameters (as, for example, molecular weight, branching structure, length and number of the polyether chains) on the properties of corresponding W/O emulsions. The materials used in this report are large block copolymers of various morphologies, comprising hydrophilic (polyether) and hydrophobic (polydimethylsiloxane, PDMS) blocks. The different polarity of the blocks makes the adsorption on oil-water interfaces energetically favorable and therefore promotes the stabilization of disperse systems. The goals of the resent work are a better understanding of the interfacial activity of these molecules and the establishment of a basic function-properties relationship. The latter could be useful in the development of new SPE materials, tailored to specific applications and in the optimization of formulations in cosmetic, healthcare and household industries.

Experimental

Substances

The silicone polyethers employed in this study have been synthesized by hydrosilylation and characterized by Gel Permeation Chromatography and NMR (*5*). Figure 1 shows the chemical structures, the molecular details are summarized in Table I. The name is constructed as X-YZ where X denotes the morphology i.e.

Downloaded by CORNELL UNIV on June 23, 2012 | http://pubs.acs.org
Publication Date (Web): November 17, 2010 | doi: 10.1021/bk-2010-1053.ch013

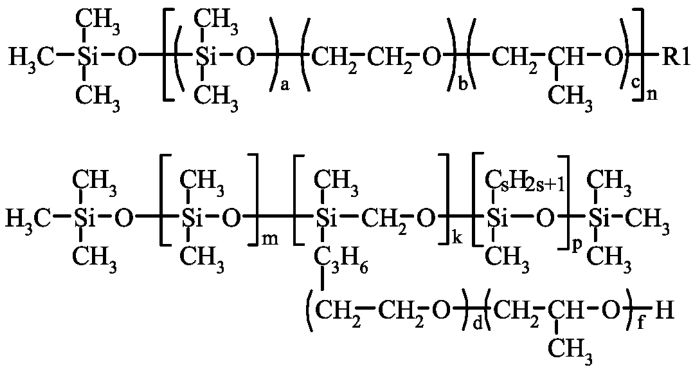

Figure 1. Structure of the SPEs Used in the Study. Top: ABn type, Bottom: rakes. For the R type p=0

Table I. SPEs Employed in the Study[a]

	R-MM	*R-MH*	*R-LL*	*R-HL*	*AB-15M*	*AB-107M*	*AB-15H*	*DR-L*
Morphology	Rake	Rake	Rake	Rake X-link	ABn	ABn	ABn	Double Rake
Functionalities	PEG/ PPG 19/19	PEG/ PPG 18/18	PEG9	PEG12	PEG15	PEG/ PPG 10/7	PEG15	PEG8/ C12
MW (kDa)	30-60	30-60	4-15	300-1000	30-60	30-60	300-1000	4-15

[a] NOTE: PEG = polyethylene glycol, PPG = polypropylene glycol

ABn, **R**ake and **D**ouble_**R**ake. For the R and DR types Y denotes the molecular weight (i.e. **L**ow, **M**edium or **H**igh). For the AB type Y is numeric and denotes the type of the polyglycol fragment. In the case of R type Z denotes the average length (i.e. **L**ow, **M**edium or **H**igh) of the PDMS chain between two polyglycol grafts, while for the AB type Z signifies the molecular weight.

Emulsification

Model emulsions containing 62% water phase and 38% oil have been used. This volume fraction is typical for cosmetic formulations. Unless stated otherwise, 1.1% NaCl and 6.65% glycerol (by weight, calculated over the entire composition) have been added to the aqueous phase. These two are often present in the cosmetic formulations, but this is not the only reason of using them. In fact, both increase the osmotic pressure in the aqueous phase thus suppressing the instability provoked by the Ostwald ripening. (Ostwald ripening is a process of disappearance of the smaller droplets in favor of the bigger ones. It is driven by the difference between the capillary pressures in droplets of different size and is greatly facilitated by even very limited solubility of the dispersed phase in the continuous one.) Notably both NaCl and glycerol influence the quality of the solvent with respect to the poly(PEG/PPG) blocks.

Downloaded by CORNELL UNIV on June 23, 2012 | http://pubs.acs.org
Publication Date (Web): November 17, 2010 | doi: 10.1021/bk-2010-1053.ch013

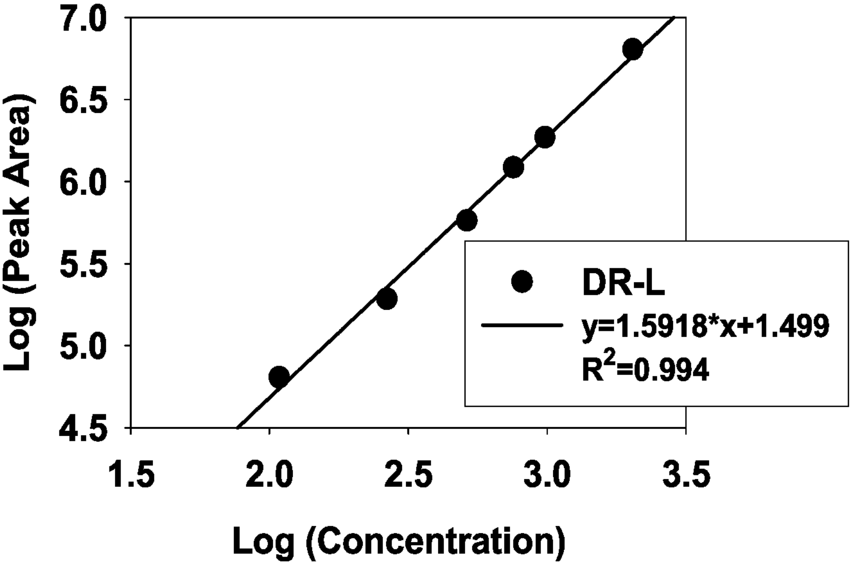

Figure 2. Example Calibration Curve

The polymeric emulsifier was dissolved in the oil, typically PDMS, (5 cSt. Dow Corning ® 200 fluid) by stirring overnight at concentrations of 1, 2 or 4.6% (with respect to the oil phase). The mineral oil used in some of the experiments was Klearol® from Sonneborn. The water phase was added drop-wise to the continuous oil phase. This process affords crude W/O emulsions, which have been consecutively "refined" by a second emulsification step consisting either in high-turbulent shear (Ultra Turrax, 1 min at 16000 RPM) or in high shear in pseudo-laminar conditions (Hauschield DAC FV 605 Speed Mixer®). These two devices are believed to operate in different regimes (*6*, *7*) (see results section).

Drop Size Distributions

The droplet size distribution of the studied emulsions was determined optically. Because the continuous phase is oil, the use of commercial static light scattering equipment is technically challenging, as this would imply filling the circulation system of the instrument with silicone oil. Furthermore, as discussed later, the majority of the emulsions are strongly flocculated even following a serious dilution, therefore employing a laser scattering technique would have resulted in the average size of flocks, rather than the in size of individual droplets.

Each emulsion was carefully diluted in pure PDMS to 2% volume fraction and observed in transmitted illumination on a Zeiss Axioplan microscope equipped with a 100x objective. Series of photographs were taken for each diluted emulsion at randomly chosen, non-overlapping spots. Droplets visible on each picture were counted employing a home-developed routines based on Visilog 6.2 image analysis software. The counting consisted of the determination of the area of the individual circular objects (droplets) detected on each picture by the image analysis routine. The outcome of this routine was converted in size (diameter)

Downloaded by CORNELL UNIV on June 23, 2012 | http://pubs.acs.org
Publication Date (Web): November 17, 2010 | doi: 10.1021/bk-2010-1053.ch013

and the emulsion's droplet size distribution was obtained on the basis of ca. 1000 counted drops. Hereafter the mean diameter used is D_{32}, the so called volume weighted surface mean, or Sauter mean. The formal definition of this mean reads:

$$D_{32} = \frac{\sum_i N_i D_i^3}{\sum_i N_i D_i^2} \qquad (1)$$

where N_i and D_i denote respectively the number and the diameter of the elements in the i^th^ bin of the histogram. The interest of using D_{32} is that it mathematically represents the diameter of an equivalent, perfectly monosdiperse emulsion which has the same surface area as the real one.

Amount of Adsorbed Polymer

The emulsions were centrifuged at 12000×g for 15 minutes. Because the water droplets are heavier than the surrounding oil, this process results in their sedimentation. The supernatant above the droplets was taken and analyzed by High Performance Liquid Chromatography (HPLC, see next section) to determine the residual concentration of SPE with the help of a calibration curve. This permits the calculation of the amount of the polymer adsorbed on the droplets' phase as:

$$\Gamma = R_{32}\frac{(C_{INI} - C_{HPLC})(1-\phi)}{3\phi} \qquad (2)$$

where Γ is the adsorbed amount expressed in mg/m^2, ϕ is the water volume fraction (dimensionless), C_{INI} and C_{HPLC} are the concentrations of the polymer initially and in the supernatant (expressed in mg/L) respectively. R_{32} is the volume weighted surface mean (Sauter mean) radius, calculated from the size distributions. Equation (2) implicitly supposes that:

(a) The droplet size distribution does not change during the centrifugation. Employing image analysis (see above) we have confirmed that this is the case.
(b) The supernatant is homogeneous. This point has been checked by HPLC.

High Performance Liquid Chromatography

The instrument used was Water Alliance 2960 HPLC system, coupled to a Sedere SEDEX 85 low temperature evaporative light scattering detector (ELSD). The quantification of non-adsorbed SPE in the continuous phase has been achieved by gradient elution HPLC combining precipitation and adsorption retention. In such chromatographic conditions, the SPE solution is injected in a mobile phase where the SPE is insoluble, causing the copolymer to precipitate at the top of the column. The SPE is then dissolved during gradient elution at an eluent composition characteristic for its molecular weight and chemical properties. Typically, C18 stationary phases of different pore sizes, and mobile phases

Downloaded by CORNELL UNIV on June 23, 2012 | http://pubs.acs.org
Publication Date (Web): November 17, 2010 | doi: 10.1021/bk-2010-1053.ch013

consisting of tetrahydrofuran as strong solvent combined with non-solvents, like methanol and water are used.

Because SPEs do not contain UV-absorbing groups, they can only be detected by “universal” detector (like refractive index, RI, evaporative detectors) instead of selective detector (like photometric detectors). In order to avoid any mobile phase influence on the detector signal ELSD detector was used (*8*). One of its main advantages (versus RI detector) is the possibility of using complex gradient elution, as chromatographic solvents are nebulized and evaporated and only non-volatile analytes are detected. The response of ELSD depends on the number and size of non-volatile analyte particles and is not linear. It, rather, follows the equation: $A_P = a\ C^B$ where A is the peak area, C is the analyte concentration. B and a are coefficients dependent upon the ELSD instrument settings and the mobile phase. As a result, double logarithmic coordinates are necessary to obtain a linear calibration curve, as shown in Figure 2.

Model Interfacial Experiments

General

The interfacial tension and the surface dilatational elasticity were measured employing a Tracker instrument from IT Concept. The measurement is based on the reconstruction of the profile of a pendant droplet (also known as Axi-symmetric Drop Shape Analysis) and fitting a Laplace profile to it. The calculation supposes a droplet of constant volume and requires the density difference between the two phases. Typically, the density difference between silicone oil and water is very small (ca. 0.08 g/cm^3), therefore the density of each solution was determined as an average of 5 measurements preformed using a DMA 38 densitometer operating on acoustic principle.

Two types of experiments were performed. First, we have determined the kinetics of adsorption by following the interfacial tension, and second, we have measured the dilatational elasticity of the layers by performing the oscillation measurements at different frequencies. A plateau in the dynamic interfacial tension has never been reached and therefore the equilibrium interfacial tension was obtained via extrapolation of the interfacial tension at infinite time assuming diffusion controlled adsorption as considered by Ward and Torday (*9*). Their analysis includes the back-diffusion and yields the following kinetic relation for the adsorption, Γ:

$$\Gamma = 2c\left(\frac{Dt}{\pi}\right)^{0.5} - 2\left(\frac{D}{\pi}\right)^{0.5}\int_0^{\sqrt{t}} c_S(t-\tau)\,d\tau^{0.5} \qquad (3)$$

where c and c_S stand for the surfactant bulk and sub-surface concentration respectively, D is the diffusion coefficient and τ is an integration variable.

For the long times (if the bulk-to-surface transport remains diffusion-controlled) one has:

$$\gamma(t)=\gamma_{EQ}+\frac{RT\Gamma_{EQ}^{2}}{c}\sqrt{\frac{\pi}{D}}\frac{1}{\sqrt{t}} \quad at \quad t\to\infty \tag{4}$$

where R is the universal gas constant, γ_{EQ} is the equilibrium surface tension, and Γ_{EQ} is the equilibrium adsorption. Plotting the interfacial tension decay against the inverse square root of time allows the determination of γ_{EQ}.

Interfacial Dilatational Elasticity

The Gibbs surface elasticity is a derivative of the interfacial tension. The definition reads:

$$E_0=\frac{d\gamma}{d\ln A} \tag{5}$$

where A is the surface area. This definition implies that the surface is purely elastic, excluding the time-dependent responses (as for example Marangoni elasticity which is connected to the surface viscosity). This deficiency is circumvented by introducing the complex surface elasticity, E*, defined as:

$$E^{*}=E'+iE'' \tag{6}$$

where E' is the elastic (storage) modulus, and E" is the loss modulus.

To determine these two quantities, the surface area is varied in time, *t*, by pulsating the drop in sinusoidal manner as:

$$\Delta\ln A\sim\exp(i\omega t) \tag{7}$$

where ω is the angular rate. The response of the surface tension is then:

$$\Delta\gamma=\gamma_A\sin(\omega t+\delta) \tag{8}$$

where γ_A is the measured amplitude, and δ is the phase lag. The process described in eqs. 7 and 8 is automatically performed by the instrument and the values for E*, E' and E" are extracted by fitting a sine to the response of the interfacial tension.

Analytical Centrifugation

Analytical centrifugation experiments were performed using Lumisizer® 611 from LUM GmbH. In this instrument plastic centrifugation cells containing the emulsion samples are fixed horizontally to the rotor. While being centrifuged the samples are transversally illuminated by a near infrared light. A detector placed below the rotor captures the light transmitted through the samples. The transmission is spatially resolved which allows the quantification of the sedimentation phenomena in each sample as a function of the centrifugation time.

Downloaded by CORNELL UNIV on June 23, 2012 | http://pubs.acs.org
Publication Date (Web): November 17, 2010 | doi: 10.1021/bk-2010-1053.ch013

Downloaded by CORNELL UNIV on June 23, 2012 | http://pubs.acs.org
Publication Date (Web): November 17, 2010 | doi: 10.1021/bk-2010-1053.ch013

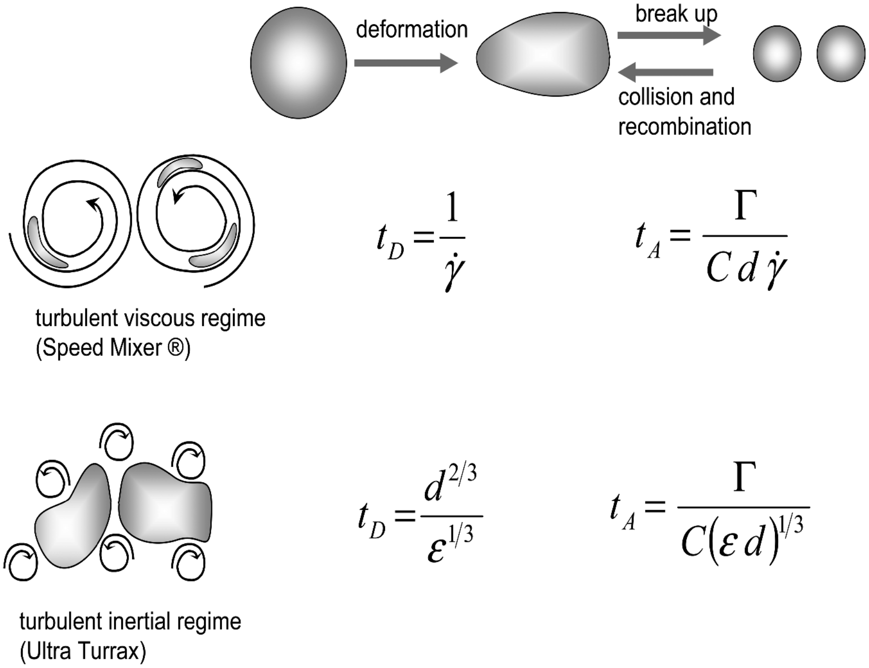
deformation
break up
collision and recombination
turbulent viscous regime (Speed Mixer ®)
$t_D = \frac{1}{\dot{\gamma}}$
$t_A = \frac{\Gamma}{C d \dot{\gamma}}$
turbulent inertial regime (Ultra Turrax)
$t_D = \frac{d^{2/3}}{\varepsilon^{1/3}}$
$t_A = \frac{\Gamma}{C(\varepsilon d)^{1/3}}$

Figure 3. Characteristic Times for Droplet Deformation and Coalescence

Results and Discussion

Droplet Size Distributions

To refine the crude emulsions two different instruments, namely an Ultra Turrax (UT) and a Hauschield Speed Mixer®, were used. The principle of drop rupturing for each of them is schematized in Figure 3. By using the UT one disrupts the droplets, because the small turbulent eddies are "eating" the large droplets little by little. On the contrary, the Hausschield mixer creates larger eddies which entrap the droplets and shear them. In this case the droplets experience laminar flow. Basically, the process of droplet break-up could be considered as a two-way process involving a droplet deformation and then break-up into smaller particles on one side, and collision and recombination (coalescence) on the other. The creation of new interface is an energetically unfavorable process; therefore the newly formed droplets will have the tendency to coalesce. To protect the new drops against coalescence one needs to cover the freshly created surface by adsorbing surface active molecules. Each of these individual processes has a characteristic time, which depends on the parameters of the system. Figure 3 provides a simplified summary for the case of low viscosity of the internal (droplet) phase. In Figure 3 t_A denotes the adsorption time, t_D - the deformation time, ε -the energy dissipation, C- the emulsifier concentration, Γ - the adsorption, $\dot{\gamma}$ - the shear rate and d - the diameter of the mother droplet. The equations listed on the figure hold for Newtonian oil and aqueous phases of similar viscosities. These assumptions are true for the fluids used in the present study. It becomes clear that the emulsifier could influence the outcome of the emulsification mainly via the

Downloaded by CORNELL UNIV on June 23, 2012 | http://pubs.acs.org
Publication Date (Web): November 17, 2010 | doi: 10.1021/bk-2010-1053.ch013

concentration and the adsorption. The direct result/success of the emulsification is measured via the droplet size distributions (DSD). Because the energy applied in the different cases, as well as the size/shape of the container was kept the same, any difference of the DSD could be associated to the intrinsic properties of the emulsifier.

Figure 4 compares the mean sizes (D_{32}) of the emulsions obtained using the Ultra Turrax and the Speed Mixer®. Except for one case (1% AB-15M) the diameters obtained for the AB type under different shear conditions are comparable. This means that for the ABn type SPE the emulsions are independent on the process of emulsification, which is very interesting from application point of view. Indeed, it would be reassuring for a formulator to know that the outcome of emulsification is the same regardless the shearing device.

From Figure 4 it is concluded that the higher molecular weight ABn polymers produce larger droplets. Although some decrease of D_{32} with the concentration is observed, the influence of SPE concentration on the final size is relatively weak for the AB type having 15 PEG units. The situation is considerably different for more hydrophobic polyglycol fragments (AB-107M). In this case, the influence of the concentration on the final particle size is substantial and this is definitely a parameter to be used for fine tuning of the particle size of the final product.

Contrary to the linear molecules, the rake type exhibits a dependence of the mean size on the process; the droplets generated with the Speed Mixer® (turbulent viscous regime) being almost always larger than the ones produced using the Ultra Turrax. This is explained by the fact that these emulsifiers are fairly large, spatially hindered molecules and would need transport to migrate and to position them at the interface. For the smaller molecules, the impact of the process seems to be less important. Practically equivalent particle sizes for the two emulsification methods have been measured for R-LL rake polymer. It is worth remembering that this is a substantially smaller molecule (Mw of below 15000 in contrast to at least 35000 for the other rakes). For the larger rakes, the outcome of the Speed Mixer® process seems to be coupled to the concentration of the SPE in the continuous phase: the higher concentration the smaller the droplets. This effect has not been observed for the turbulent inertial regime of emulsification (Ultra Turrax), where the droplet size is essentially independent on the concentration. The comparison between R-MH and R-MM reveals the influence of the grafting density: slightly smaller droplets are obtained in turbulent inertial regime for the SPE having a larger distance between the polyglycol pendant chains.

The molecule DR-L is not really comparable to the other rakes, as it has two types of grafts i.e. polyglycol and hydrocarbon pending chains. The latter make the material compatible with a large number of organic oils. The biggest difference in the mean droplet size with respect to the hydrodynamic conditions of emulsification has been observed for this molecule. While the Ultra Turrax produces 1-2 micron particles at all concentration studied, the Speed Mixer® is unable to efficiently disrupt the droplets of the crude emulsion.

Downloaded by CORNELL UNIV on June 23, 2012 | http://pubs.acs.org
Publication Date (Web): November 17, 2010 | doi: 10.1021/bk-2010-1053.ch013

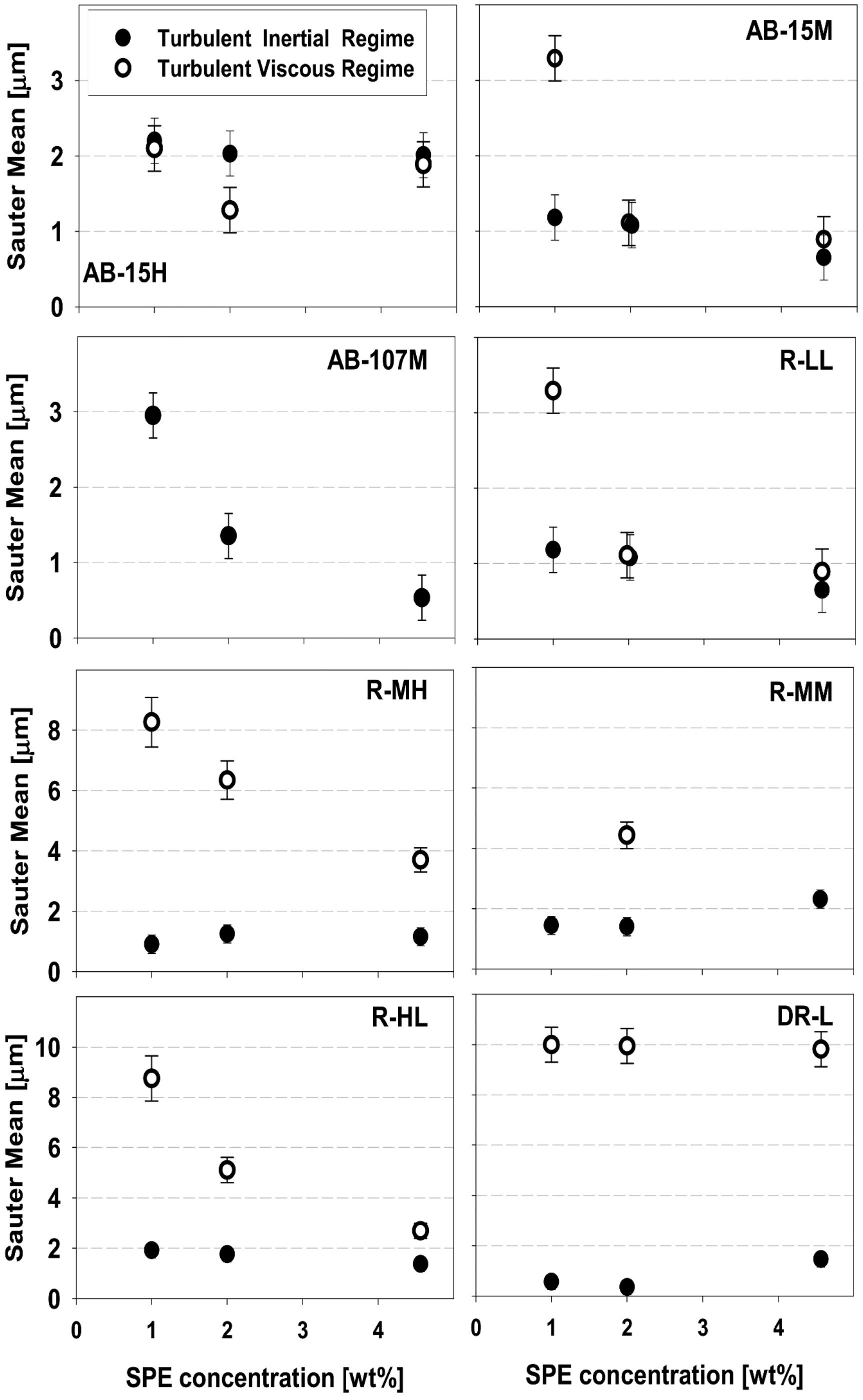

Figure 4. Influence of the Process on the Mean Drop Size of Emulsions Stabilized by SPEs

The polysispersity, $\widetilde{P}$, of the emulsions has been defined as $\widetilde{P} = \left(D_V^{90} - D_V^{10}\right) / D_V^{50}$, where D_V^i is the i-th percentile of the cumulative distribution (by volume). Regardless the process and the molecular structure the distribution have been monomodal with $\widetilde{P}$ in the range 0.7-1.4.

Flocculation

As illustrated on Figure 5, for practically all studied emulsions, a very strong flocculation of the droplets has been observed. Flocculation is an aggregation of the droplets of preserved integrity. Physically this means that an attractive force, causing droplets to "stay together" exists.

There are several possible mechanisms for flocculation; some of them are illustrated on the cartoons in Figure 6. For the sake of clarity the different physical principles are presented separately, but it is well possible to observe more than one effect in a time.

(A) Bridging flocculation is a phenomenon frequently observed in emulsions stabilized by polymers. It is caused by the adsorption of one (or more) molecules on more than one droplet, forming a "bridge". This phenomenon is impossible in the case of surfactant-stabilized particles. Dilution of an emulsion sample affected by bridging flocculation does not de-flocculate it. The dilution is not by itself capable of changing anything with respect to molecular adsorption. It is useful to remind that polymers adsorb on a multitude of adsorption sites, which means that the energy of de-sorption is significant.

(B) Depletion effect. In this case the flocculation is caused by the osmotic pressure of non-adsorbed polymer molecules, and it is relatively easy to deflocculate the system by severe dilution, as this reduces the concentration of the free polymer in the continuous phase. The depletion effect can be influenced by the quality of the solvent with respect to the depleting polymer. Indeed in theta - solvent the radius of gyration, Rg, of the polymer varies as $N^{0.5}$ (N being the number of segments), while in good solvent $Rg \sim N^{0.6}$.

(C) The solvent quality is a third possible reason for flocculation. The continuous phase (PDMS) is (supposedly) a theta solvent for the silicone moieties of the SPE, but it is a bad solvent of the PEG/PPG and hydrocarbon chains (when present). "Bad solvent" means that the attraction force existing between the segments of a polymer chain is greater that the attraction between the segment and the molecules of the solvent. Therefore, if sufficiently flexible, the chain creates self-associative structures which allow the attracting segments to stay together. Self-association phenomena have been reported for numerous block copolymers, including silicone polyethers (*10*). As in the case of bridging flocculation, this phenomenon will not be affected by any dilution of the emulsion because the quality of the solvent will not change. However, if a change of the continuous phase (i.e. solvent of a different quality) induces a change of the flocculation state, this undoubtedly means that the quality of the solvent is the main cause of flocculation.

Downloaded by CORNELL UNIV on June 23, 2012 | http://pubs.acs.org
Publication Date (Web): November 17, 2010 | doi: 10.1021/bk-2010-1053.ch013

Downloaded by CORNELL UNIV on June 23, 2012 | http://pubs.acs.org
Publication Date (Web): November 17, 2010 | doi: 10.1021/bk-2010-1053.ch013

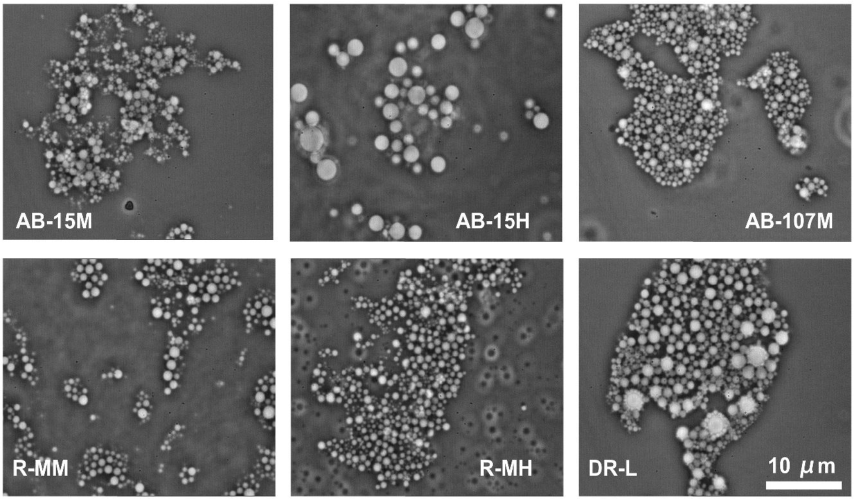

Figure 5. Examples of Flocks in Emulsions Stabilized by Different SPEs. The scale bar is the same for all images.

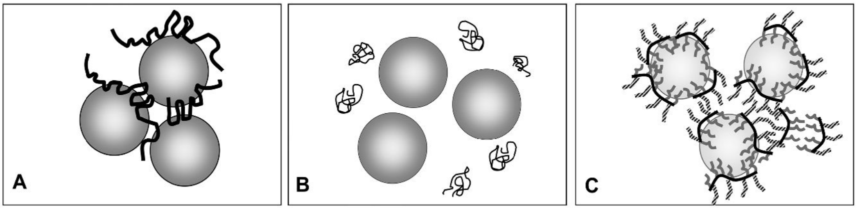

Figure 6. Most Common Flocculation Mechanisms in the Presence of Polymers (not to scale) (A): Bridging, (B): Depletion (C): Solvent quality

Diluting the ABn-stabilized emulsions in different solvents (mineral oil, PDMS, cyclic siloxane) was not able to diminish the flocculation. Therefore the flocculation in the case of ABn polymers is probably of bridging type.

Severe dilution of the emulsions stabilized by the rakes was able to suppress the flocks. Therefore for this type of structure the flocculation is mainly caused by the excess polymer in the continuous phase. Because molecular flexibility of the rake structure is much lower, the bridging phenomenon is less likely.

In the case of DR-L, equivalent emulsions using mineral oil instead of PDMS were prepared. Salt-free water was used in some experiments as well. The idea was to change the quality of the solvent for the pendant hydrocarbon and PEG fragments respectively. Representative images of these emulsions are presented in Figure 7. There is no flocculation in the emulsions having mineral oil as continuous phase. This means that the reason for the flocculation observed for PDMS oil is clearly a solvent-induced aggregation of the polymer, as schematized in Figure 6 C. The influence of the NaCl is not that visual, but interfacial tension experiments have shown that the kinetics of adsorption changes in presence of NaCl.

Identifying the origin of the flocculation is important for the control of the macroscopic properties, because the flocculation determines the appearance and

Downloaded by CORNELL UNIV on June 23, 2012 | http://pubs.acs.org
Publication Date (Web): November 17, 2010 | doi: 10.1021/bk-2010-1053.ch013

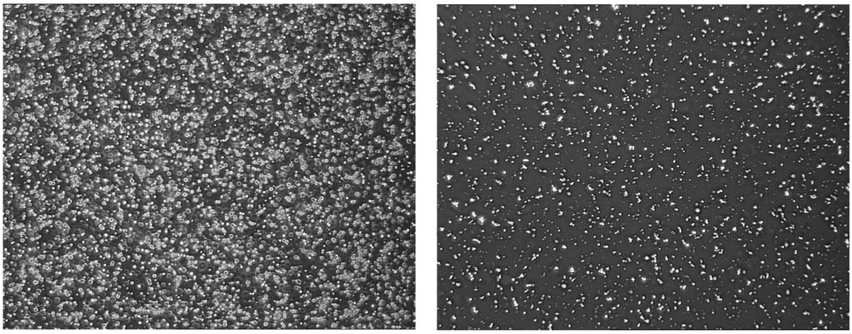

Mineral Oil (NaCl) **Mineral Oil (no NaCl)**

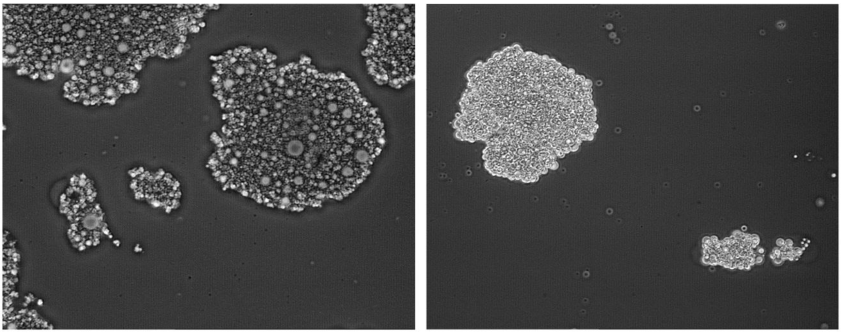

PDMS (NaCl) **PDMS (no NaCl)**

Figure 7. Flocculation in Water-in-Oil Emulsions Stabilized by 2% DR-L

the rheology of the emulsions. This is illustrated in Figure 8 which compares the flow curves of two otherwise identical emulsions having either PDMS or mineral oil as continuous phase. The flow curves have been fitted with the Herschel-Bulkley equation. According to this model the shear stress (τ, the measured value) depends on the shear rate $\dot{\gamma}$ as:

$$\tau = \tau_0 + K\dot{\gamma}^n \tag{9}$$

where τ_0 is the yield stress, K is the consistency and n is the thinning (or decay) rate. The viscosity, η, is defined as the ratio between τ and $\dot{\gamma}$ as:

$$\eta = \frac{\tau}{\dot{\gamma}} \qquad or \qquad \eta = \frac{\tau_0}{\dot{\gamma}} + K\dot{\gamma}^{n-1} \tag{10}$$

The fits are shown as straight lines in Figure 8 and the numerical parameters are listed in Table II. The flocculated emulsion has a creamy appearance, while the non-flocculated one (continuous phase mineral oil) is much more liquid lotion-like.

Downloaded by CORNELL UNIV on June 23, 2012 | http://pubs.acs.org
Publication Date (Web): November 17, 2010 | doi: 10.1021/bk-2010-1053.ch013

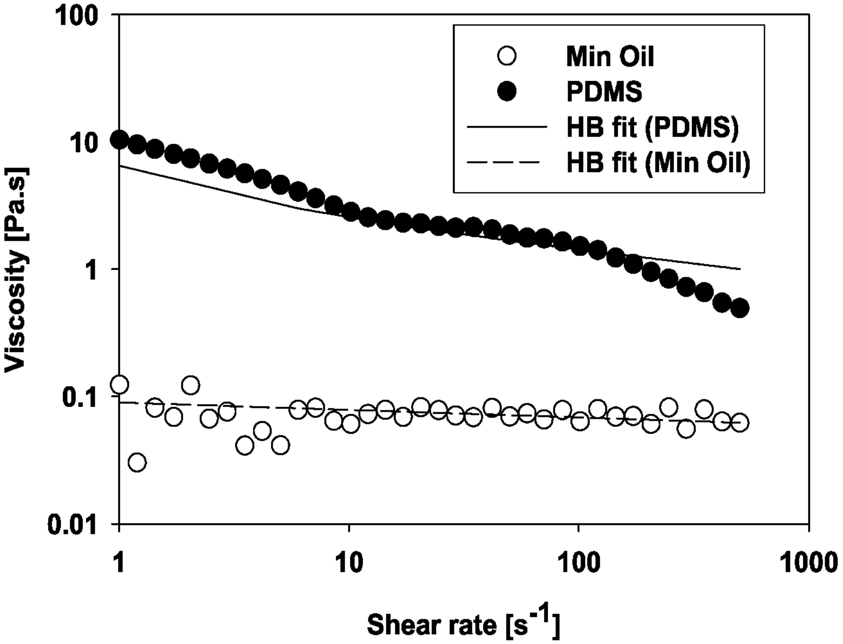

Figure 8. Flow Curves of Water-in-Oil Emulsions Stabilized by 2% DR-L

Adsorbed Amount

For the linear SPE the amount of the polymer adsorbed on the droplets has been determined using a combination of optical microscopy and HPLC. It is worth mentioning that for complex molecules, which occupy a multitude of adsorption sites on the interface, one can not use the Gibbs equation of the interfacial tension to estimate the adsorbed amount. Instead, a measurement of the non-adsorbed amount and a calculation (eq 2) is recommended.

Figure 9 shows the mean diameter plotted against the adsorbed amount. For emulsions produced using Ultra Turrax (turbulent inertial regime) different adsorbed amounts has been measured at one and the same radius. The only possibility to accommodate the “extra” polymer on the interfaces is the formation of multilayers. An interesting effect is observed for AB-107M which has more hydrophobic structure than AB-15M at comparable molecular weight. For this molecule the adsorption increases with the increase of the radius, that is with the decrease of the interfacial area. It is hypothesized that multi-layers are formed in this case as well, but that their structure and density seem to depend on the SPE concentration. Similar conclusions can be drawn for AB-15M for the case of turbulent viscous emulsification.

The data from Figure 9 could be plotted in a different manner, showing the influence of the processing on the adsorbed amount (Figure 10). Indeed, in turbulent inertial regime the absorbed amount is more or less the same for both low and high molecular weight polymers. In turbulent viscous regimes, where the droplet “sees” laminar flow, the difference in adsorption is dramatic. The

Downloaded by CORNELL UNIV on June 23, 2012 | http://pubs.acs.org
Publication Date (Web): November 17, 2010 | doi: 10.1021/bk-2010-1053.ch013

Table II. Fit Parameters According to Herschel-Bulkley Model

Herschel-Bulkley	*PDMS*	*Min Oil*
τ_0 (yield), [Pa]	2.783	0.0
K (consistency)	3.727	0.0897
n (decay rate)	0.788	0.9414
D_{32} [um]	2.030	1.760

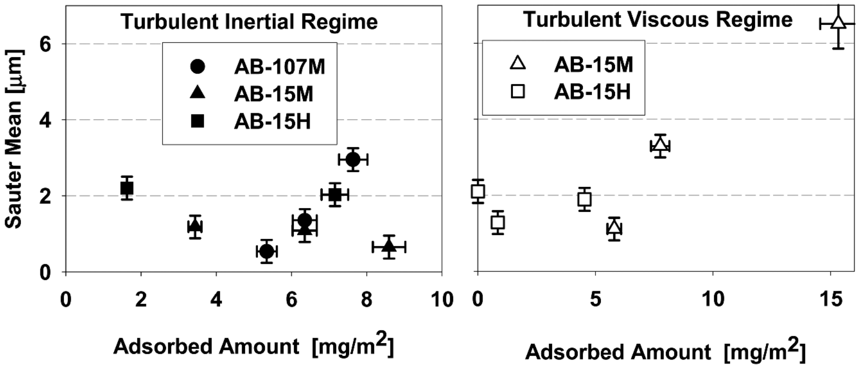

Figure 9. Mean Diameter as a Function of Adsorbed Amount of Linear SPEs

high molecular weight polymer exhibits very low adsorption. However, even these small adsorbed amounts are sufficient to obtain stable emulsions which do not coalesce upon 12 months of storage. It is worth to remind that the effects described in this part are unlikely for low molecular weight surfactants, which are characterized by a specific area per molecule.

Formation of multilayers could also be concluded for the double-rake material (DR-L), as in this case we have also measured increasing adsorption amounts at practically equivalent or increasing radii. Figure 11 shows the dependence of the mean radius on the adsorbed amount for turbulent inertial regime.

Centrifugation Stability

The osmotic resistance of emulsions stabilized by linear SPE containing 15 PEG fragments and produced using the Ultra Turrax was checked employing analytical centrifugation. The linear SPEs have been selected for two reasons. First, the morphological comparison between these two molecules is straightforward. Second, the adsorbed amount of polymer is practically the same (see previous section). The centrifugation itself is equivalent to the application of an osmotic pressure, the faster the centrifugation the higher the pressure. Indeed, neglecting the spatial gradient in the acceleration, the osmotic pressure, Π, applied when centrifuging can be expressed as:

$$\Pi = l \Delta \rho \varpi^2 \phi_I d_\perp \qquad (11)$$

Downloaded by CORNELL UNIV on June 23, 2012 | http://pubs.acs.org
Publication Date (Web): November 17, 2010 | doi: 10.1021/bk-2010-1053.ch013

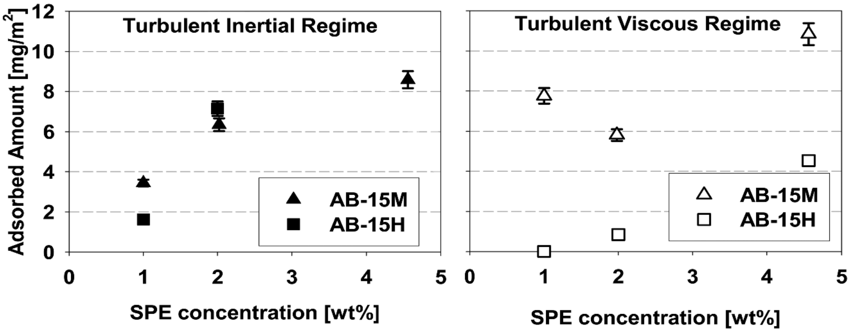

Figure 10. Influence of the Emulsification Conditions on the Adsorption of Linear SPEs

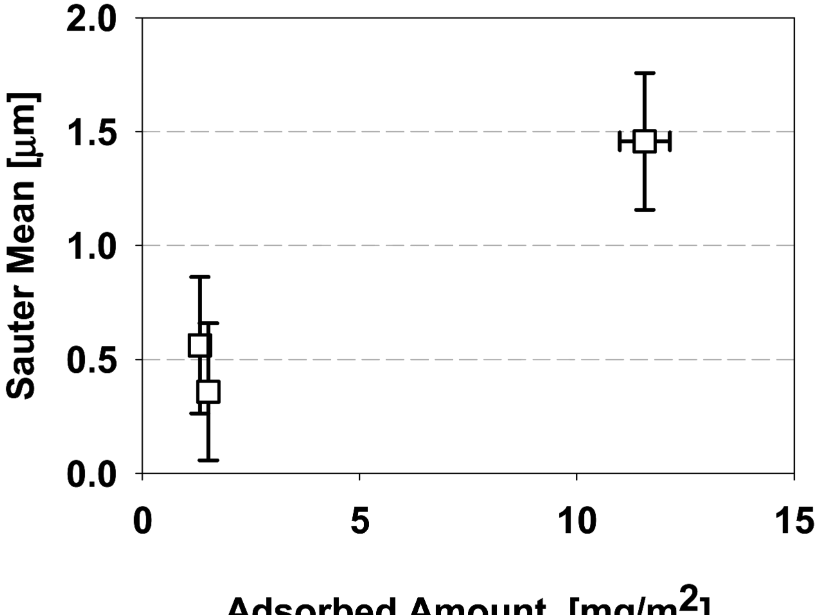

Figure 11. Mean Size vs. Adsorbed Amount for DR-L

where l is the total liquid height in the centrifuge tube, ϕ_I is the initial volume fraction (before centrifugation), $\Delta\rho$ is the density difference, $d_\wedge$ is the length of the lever arm, and ϖ is the rotation speed of the centrifuge.

The Lumisizer® 611 records the position of the phase boundary between the concentrated emulsion and the clear continuous phase as a function of time. From the initial volume fraction and the position of the boundary concentrated emulsion - continuous phase one calculates the effective volume fraction corresponding to the specific osmotic pressure. Therefore by varying the centrifugal speed one could measure the critical osmotic pressure for each volume fraction (*11*). An example profile is shown in Figure 12. The stabilizing polymer in this example is 2% AB-15H.

Downloaded by CORNELL UNIV on June 23, 2012 | http://pubs.acs.org
Publication Date (Web): November 17, 2010 | doi: 10.1021/bk-2010-1053.ch013

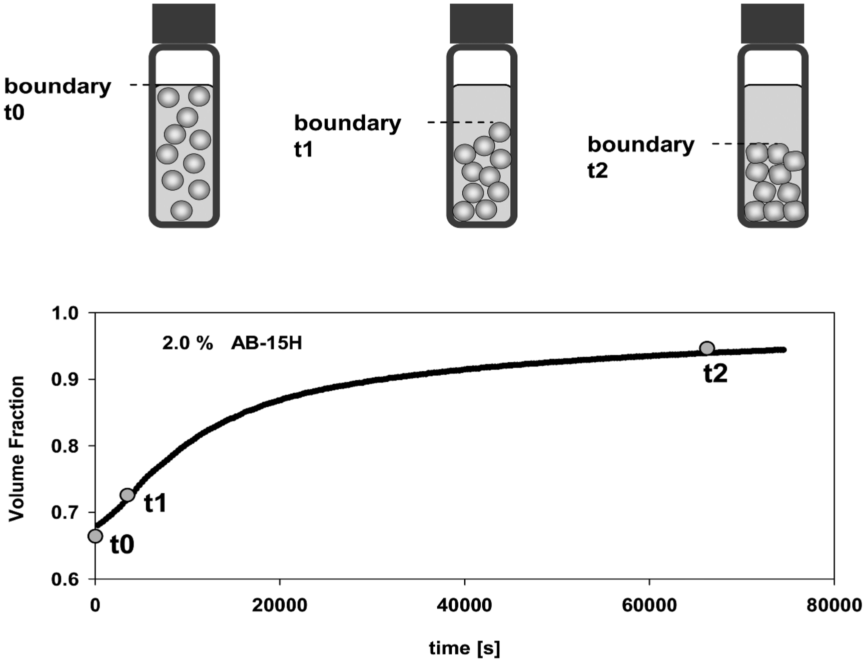

Figure 12. Volume Fraction of the Concentrated Emulsion, Calculated from the Position of the Boundary between the Clear Supernatant and Concentrated Emulsion Phase

In the beginning of the centrifugation (t=t0 on the cartoon in Figure 12) the experiment starts and the volume fraction is the one of the original emulsion. During the centrifugation the droplets are first concentrated at the bottom of the cuvette to a volume fraction of ca. 64-70%, which corresponds to the random close packing of equivalent hard spheres. The random close packing is about 64% for perfectly monodisperse spheres and increases with polydispersity. At some point (t=t1 in Figure 12) the sediment is above the random close packing and the concentration of the emulsion is accompanied by the deformation of the droplets into polyhedrons. The total interface in the emulsion is thus increased. This energetically unfavorable process is counterbalanced by the capillary pressure of the individual droplets. When the capillary pressure equals the applied osmotic stress (t>t2 in Figure 12) the maximum compression is attained and the droplets can not be compressed any further. Therefore the plateau in the volume fraction is interpreted as critical volume fraction of the concentrated phase at the given osmotic pressure (set by the centrifugal speed).

It is more convenient to scale the osmotic pressure by the capillary pressure of the droplets (that is γ/D_{32}). Thus samples of different particle sizes and interfacial tensions can be compared (Figure 13). Moreover, the scaled osmotic pressure plots should fall on a master curve (*12*). Below the random close packing non-yielding samples show very little osmotic pressure resistance (*11*, *12*). Indeed this is what we observe for the low concentrations of SPEs AB-15M and AB-15H (Figure 13A, B and D). Increasing the concentration of the polymer leads to a formation of

Downloaded by CORNELL UNIV on June 23, 2012 | http://pubs.acs.org
Publication Date (Web): November 17, 2010 | doi: 10.1021/bk-2010-1053.ch013

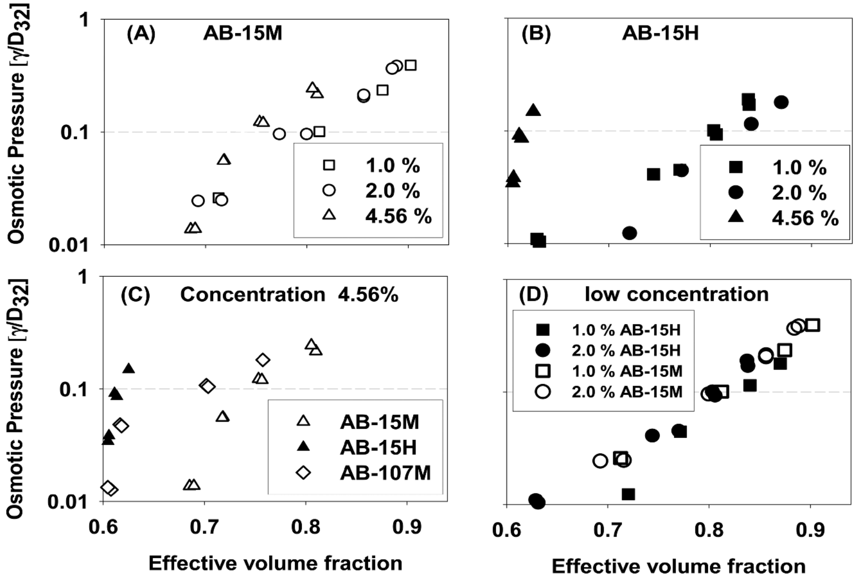

Figure 13. Osmotic Pressure for SPE-Stabilized Water-in-Oil Emulsions

thicker multilayers (see previous part) which, when brought in contact, provide an additional centrifugal resistance especially at low volume fraction of the dispersed phase. Indeed, bringing the droplets closer would require squeezing the continuous phase from the polymer film. What has been observed translates on a macroscopic scale as an additional repulsion between the droplets. Inter-droplet repulsion is beneficial for the emulsion stability as it delays the onset of creaming.

Fig. 13C compares the emulsions at the highest concentration of ABn SPEs. The results for AB-107M are provided for comparison. These data suggest that at equivalent volume fraction of the dispersed phase, the sample stabilized with AB-15H is much more resistant to compression. According to Isrealshvili (*13*) the steric repulsion in this case scales as 8Rg, where Rg is the radius of gyration of the polymer. Because the studied ABn have similar structure, it is reasonable to assume that the higher the molecular weight the higher the Rg. Therefore, equivalent emulsions stabilized with higher molecular weight ABn should be more stable in static conditions.

Interfacial Properties

Interfacial Tension (IFT)

Figure 14 shows the equilibrium interfacial tension (obtained as extrapolation to infinite time) of the investigated SPE. For large polymer molecules the concept of critical micellar concentration is not straightforward. Frequently the term "critical aggregation concentration" (CAC) is used, reflecting the associative behavior of the molecules in bulk solutions. For some of the SPEs in the study the CAC has been attained (see Figure 14) for concentrations in the interval 0.1-1

Downloaded by CORNELL UNIV on June 23, 2012 | http://pubs.acs.org
Publication Date (Web): November 17, 2010 | doi: 10.1021/bk-2010-1053.ch013

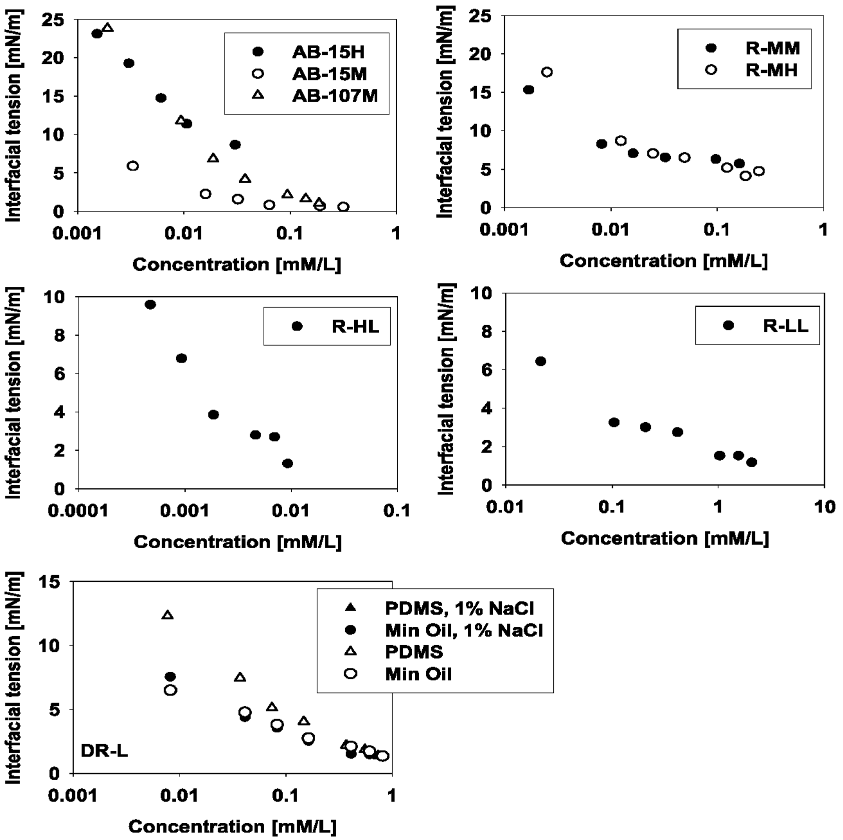

Figure 14. Equilibrium Interfacial Tension of the Studied SPEs

mM/L, while for others, as for example the R-HL and Ab-15H the equilibrium interfacial tension has never reached a real plateau.

The molecule DR-L has been studied to a greater extent. The PDMS was replaced with mineral oil. The influence of the composition of the aqueous phase, i.e. with or without of NaCl, has been examined as well because the water phase accommodates the PEG chains of the DR-L. Basically, the increase of the NaCl concentration decreases the hydration of the PEG units. Due to the intrinsic sterical hindrance of this molecule, the influence of the salt is much more complex. For instance, in the case of mineral oil, the influence of the salt is minimal, while in the case of PDMS the salt considerably diminishes the interfacial tension at equal concentration. Figure 14 also suggests that the affinity of DR-L to the interface is greater in the case of mineral oil (the interfacial tension is systematically lower for water/mineral oil interface).

Figure 14 illustrates an important point: The equilibrium interfacial tension can not be used for the prediction of the emulsification ability. Although the vast majority of hydrodynamic treatment of drop break-up considers the interfacial properties only through the reduction of the interfacial tension, the main function of surfactant is not to produce a low interfacial tension, but to impart surface

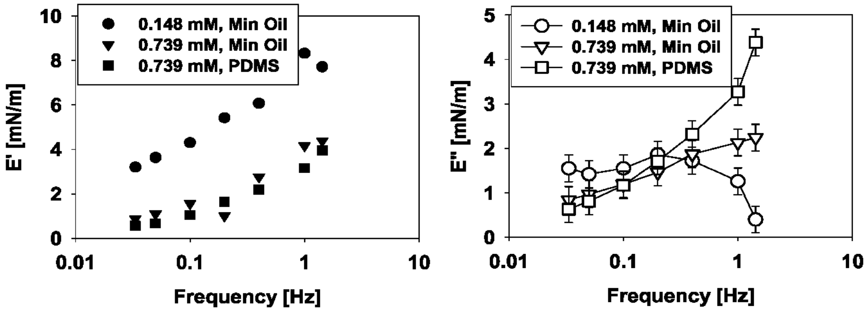

Figure 15. Surface Dilatational Moduli of DR-L

Downloaded by CORNELL UNIV on June 23, 2012 | http://pubs.acs.org
Publication Date (Web): November 17, 2010 | doi: 10.1021/bk-2010-1053.ch013

rheological properties, which enable the newly formed droplets to resist the tangential stress (e.g. coalescence) (*14–17*).

If the reduction of the surface pressure were the only function of emulsifiers one would expect linear variation between the size of the droplets and the interfacial tension (under equivalent emulsification conditions). This is obviously not the case. During emulsification, the interfacial tension of the droplets is neither constant nor uniform. The average value is most probably higher than equilibrium, because due to the overstretching of droplets' interface some regions might have much lower interfacial tension than others (*15*).

Dilatation Elasticity

The dilatational elasticity provides information about the relaxation and energy storage of the interfaces when these are subject to deformation. Note that drop deformation is an important step in the emulsification process. There are two main types of processes that are thought to be responsible for surface elasticity variations. One is in-surface processes (e.g. molecular rearrangements); the other is out-of-surface processes (e.g. transport across the surface as for example adsorption and/or desorption). Different processes dominate for different systems. For simple surfactants, the diffusion coefficients are high, the molecules are easily soluble. Therefore the relaxation effects are hard to measure unless for very low concentrations (far below CMC) or very high frequencies (hundreds of Hz).

To investigate whether the measured dilatational elasticity is due to pure diffusion exchange, the approach of Hansen (*16*, *17*) has been followed. In the case of diffusional relaxation E' should increase with the increase of the concentration.

Figure 15 shows the dependence of E' and E" on the deformation frequency for DR-L. In the whole frequency range lower E' was measured for the higher concentration. This result rules out the diffusion relaxation and suggests that the relaxation proceeds via configurational rearrangements in the surface layer. It is to be noted than a decrease of E' with the concentration is rarely observed.

Downloaded by CORNELL UNIV on June 23, 2012 | http://pubs.acs.org
Publication Date (Web): November 17, 2010 | doi: 10.1021/bk-2010-1053.ch013

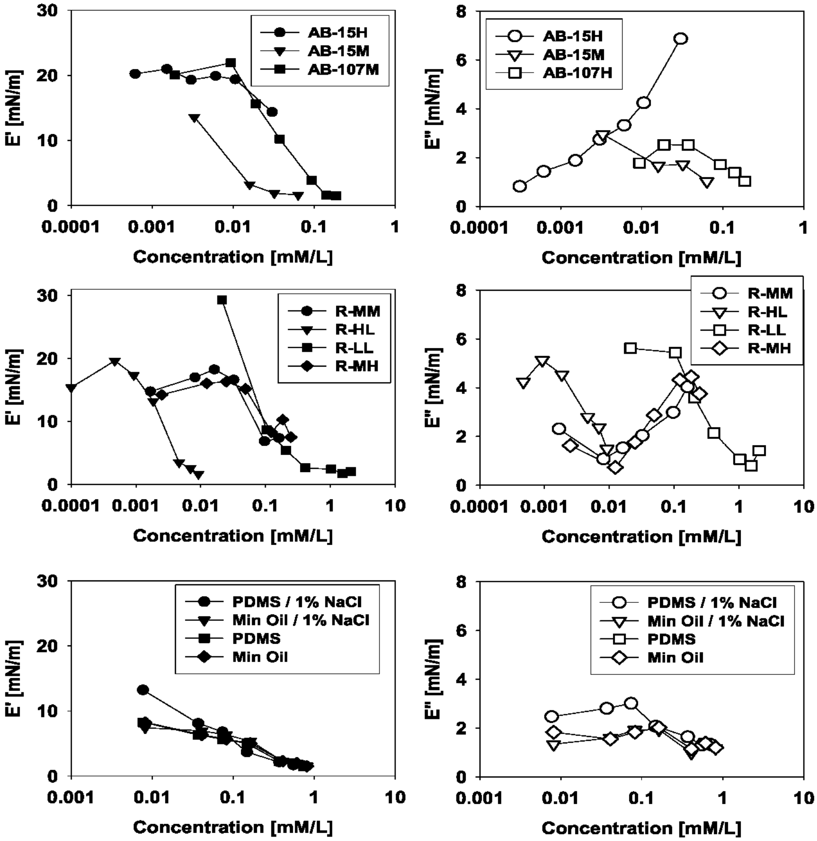

Figure 16. Surface Dilatational Moduli of SPEs

For 0.739 mM/L DR-L, regardless the oil type, E” increases with the frequency which means that E” is solely due to viscous friction in the layer. For the concentration of 0.148mM/L E” is mostly constant, but given large uncertainty of the E” data, no firm statement could be made.

Although measured at one single frequency, the data in Figure 16 allow for some interesting conclusions. Except for R-MH and R-MM the elastic modulus E’ decreases with the increase of the concentration, suggesting (for the studied concentration range) a relaxation proceeding predominantly via in-layer rearrangements. R-MH and R-MM exhibit a more complex dependence of E’. After a region of very slight increase (for lower concentrations) a decrease was observed, exactly as for the other SPEs. These two molecules differ solely in their grafting density, which apparently has no measurable influence on the interfacial elasticity. In the case of DR-L, for concentrations above 0.01 mM/L, the elasticity depends neither on the oil type nor on the presence of salt in the aqueous phase.

The data for the E” could be converted directly to interfacial dilatational viscosity, η_D , as

$$\eta_D = E''/\omega \qquad (12)$$

For low molecular weight surfactants the dependence of η_D on the concentration passes through a maximum at concentration of saturated adsorption (*18*). None of the curves in Figure 16 exhibits a well-defined maximum. It might well be that data in a wider concentration range is necessary to fully describe the concentration dependence. However, the maximal (saturated) adsorption in the case of low molecular weight surfactants is straightforward to define, while for slowly diffusing polymers, able to form complex and thick interfacial layers, the "maximal adsorption" state could be hard to achieve. Moreover kinetic curves for the interfacial tension (not shown here) suggest that plateau in the interfacial tension is almost never achieved, most probably due to multilayer formation as shown in the "adsorption" section.

Downloaded by CORNELL UNIV on June 23, 2012 | http://pubs.acs.org
Publication Date (Web): November 17, 2010 | doi: 10.1021/bk-2010-1053.ch013

Conclusions

Some fundamental understanding of the emulsification properties of SPEs for water-in-oil systems has been gained. The optimization and adaptation of a series of analytical methods has allowed us to better understand the behavior and properties of the SPE-based emulsifiers.

It has been demonstrated that linear SPE produce emulsions of practically the same mean particle size under different conditions of mixing. This versatility, which is a plus point for a formulator, has not been observed for the branched SPE studied with a minor exception of R-LL. The latter has a considerably lower molecular weight in comparison with the other molecules used in this study. Indeed, for the rake SPEs, the turbulent inertial regime (e.g. tools like Ultra Turrax, Silverson and the like) produces droplets of 1-2 micron in size regardless the SPE concentration, while the emulsification under turbulent viscous regime (e.g. Speed Mixer®) results in much larger droplets. Moreover in the latter case the higher the concentration the lower the particle size.

For all emulsions studied we have observed a substantial flocculation; that is a formation of tight clusters of intact droplets. The origins of this phenomenon have been analyzed. ABn- stabilized emulsions flocculate mainly due to a bridging mechanism, while the excess of simple rakes in the oil phase seem to cause a depletion effect. For the double rake DR-L the quality of the solvent with respect to the different fragments of the molecule plays a huge role. Water-in-PDMS emulsions are strongly flocculated most probably because of a clustering of the hydrocarbon pendant chains of DR-L. On the contrary, the water-in-mineral oil emulsions stabilized with the same emulsifier are not flocculated at all, as the hydrocarbon chains are well compatible with the external phase.

The combination of droplet size distribution measurements and HPLC has allowed us to determine the amount of polymer adsorbed on the water droplets. The main conclusion is that the adsorption of the SPEs on drop interface proceeds via the formation of mulilayers. These are able (especially in the case of large, linear SPE) to substantially increase the osmotic resistance of the emulsions. This fact could be used to design molecules able to impart not only anti-coalescence but anti-creaming resistance to the emulsion systems.

Lastly, we have performed model experiments focused on the interfacial properties of the SPE, using axi-symmetric drop shape analysis. Although some extra data might be required for completion, the following conclusions could be drawn: The adsorption kinetics of these molecules is slow, and plateau in the interfacial tension could not been reached for 15 min, even at the highest concentrations studied. The dilatational elastic moduli are in general at least twice higher than those for low-molecular surfactants and decrease with the increase of the concentration. This behavior is not standard and suggests a relaxation process driven by in-surface configurational relaxation rather than bulk-surface diffusion exchange.

Downloaded by CORNELL UNIV on June 23, 2012 | http://pubs.acs.org
Publication Date (Web): November 17, 2010 | doi: 10.1021/bk-2010-1053.ch013

Acknowledgments

The authors thank Stephane Van Oycke, Blondine Van Roy, Heidi VanDort, Mike Starch, Joanna Newton and Len Pettroff (all of Dow Corning) for their helpful comments. Blondine Van Roy is acknowledged for proofreading.

References

1. Binks, B. P. *Curr. Opin. Colloid Interface Sci.* **2002**, *7*, 21–41.
2. Kasprzak, K. A. *A Guide to Formulating Water-in-Silicone Emulsions with Dow Corning® 3225C Formulation Aid.* Dow Corning White Paper 25-713-95.
3. Dahms, G.; Zombeck, A. *Cosmet. Toiletries* **1995**, *110*, 91–100.
4. Van Reeth, I.; More, M.; Hickerson, R. *New Formulating Options with Silicone Emulsifiers*. Dow Corning White Paper 27-1082-01.
5. LeGrow, G.; Petroff, L. In *Silicone Surfactants*; Hill, R. M., Ed.; Surfactant Science Series 86; Marcel Dekker: New York, 1999.
6. Tcholakova, S.; Denkov, N. D; Danner, T. *Langmuir* **2004**, *20*, 7444–7458.
7. Tcholakova, S.; Denkov, N. D.; Ivanov, I. B.; Vulchev, V. D.; Danner, T. *J. Colloid Interface Sci.* **2007**, *312*, 363–380.
8. Vershelst, V.; Vandereecken, P. *J. Chromatogr., A* **2000**, *871*, 269–277.
9. Eastoe, J.; Dalton, J. S. *Adv. Colloid Interface Sci.* **2000**, *85*, 103–144.
10. Lin, Y.; Alexandridis, P. *J. Phys. Chem. B* **2002**, *106*, 10845–10853.
11. Mason, T. Ph.D. Thesis, Princeton University, Princeton, NJ, 1995.
12. Mason, T. G.; Lacassse, M.-D.; Grest, G. S.; Levine, D.; Bibettre, J.; Weitz, D. *Phys. Rev. E* **1997**, *56*, 3150–3166.
13. Israelashvili, J. *Intermolecular and Surface Forces*, 2nd ed.; Academic Press: New York, 1992.
14. Myrvold, R.; Hansen, K. *J. Colloid Interface Sci.* **1998**, *207*, 97–105.
15. Lucassen-Reynders, E.; Kuijpers, K. A. *Colloids Surf.* **1992**, *65*, 175–184.
16. Hansen, F. K. *Langmuir* **2008**, *24*, 189–197.
17. Frømyr, T.; Hansen, F. K.; Kotzev, A.; Laschewsky, A. *Langmuir* **2001**, *17*, 5256–5264.
18. Nakamura, M.; Takeuchi, S. *Bull. Chem. Soc. Jpn.* **1978**, *51*, 2776–2780.

Downloaded by STANFORD UNIV GREEN LIBR on June 23, 2012 | http://pubs.acs.org
Publication Date (Web): November 17, 2010 | doi: 10.1021/bk-2010-1053.ch014

Chapter 14

Recent Trends in the United States Patent Law

Joann M. Neth* **and Mukta Jhalani**

Finnegan, Henderson, Farabow, Garrett & Dunner, LLP
***joann.neth@finnegan.com**

Intellectual property continues to be one of the most important areas of the law in the United States. In recent years, the United States Supreme Court has heard several patent cases that have resulted in significant changes in patent law. These decisions embody the Supreme Court's recent trend of cutting back on protections granted to patent owners by the United States Court of Appeals for the Federal Circuit, the appellate court which reviews all patent disputes arising in the district courts across the country. This trend is especially apparent in the Supreme Court's decisions in four cases it reviewed in the last two years where it unanimously, or almost unanimously, reversed the Federal Circuit, finding it too favorable to patent owners.

Even at the Federal Circuit, patent law may change drastically depending on the court's decision in a recently-heard case, which might bring into question the validity of all business method patents (*1*). Congress may also make further changes to the United States patent laws with the passage of the Patent Reform Act of 2007.

eBay, Inc. v. MercExchange, L.L.C., 547 U.S. 388 (2006)

Decided in May of 2006, *eBay* was one of the first cases where the Supreme Court disagreed with the Federal Circuit and overruled a long series of Federal Circuit precedent holding that a prevailing patentee is automatically entitled to a permanent injunction. The Supreme Court held that patent owners who prevail in an infringement trial must satisfy the same four-part test as plaintiffs in non-patent cases before a court may grant a permanent injunction (*2*). Thus, a party in a patent suit seeking a permanent injunction must demonstrate that (1) it has suffered irreparable injury, (2) remedies available at law, such as monetary damages, are

In Polymeric Delivery of Therapeutics; Morgan, S., et al.;
ACS Symposium Series; American Chemical Society: Washington, DC, 2010.

not adequate to compensate for the injury, (3) injunction is warranted considering the balance of hardships between parties, and (4) public interest would not be disserved by an injunction (*3*).

Looking at the lower courts' opinions, the Supreme Court concluded that neither the trial court nor the Federal Circuit had fairly applied these traditional principles of equity in this case (*4*). It criticized the trial court for adopting an overly expansive view suggesting that plaintiffs who are willing to license their patents or who do not themselves practice the inventions commercially cannot establish the irreparable harm factor of the four-part test required for an injunction (*5*). Pointing to patent holders such as universities and self-made inventors, who may prefer to license their patents rather than commercially practicing them, the Court rejected the trial court's categorical rule denying patent holders the protection of an injunctive relief (*5*).

On the other hand, the Supreme Court found the Federal Circuit's approach to be too restrictive. Specifically, the Court rejected the Federal Circuit's "general rule" that "a permanent injunction will issue once infringement and validity have been adjudged" and will be denied "only in the *unusual* case, under *exceptional circumstances* and in *rare instances* … to protect the public interest (*6*)." In rejecting the Federal Circuit's "general rule," the Court repeatedly pointed to the language of the Patent Act, which states that a trial court "may" grant an injunction, not that it *must* grant an injunction in all patent cases (*7*).

Refusing to take a position on whether to grant a permanent injunction in this case, the Court remanded the case to the trial court to allow it to properly apply the above-stated four-part test to the facts of this case (*8*).

There is healthy debate about whether or not the *eBay* decision will have a profound impact on the availability of injunctions to prevailing patentees. Almost two years after the Supreme Court's ruling in *eBay*, in January 2008, the Federal Circuit applied the Supreme Court's *eBay* holding to a patent infringement suit and, after analyzing the *eBay* factors, vacated the trial court's grant of a permanent injunction to plaintiff in *Innogenetics, N.V. v. Abbott Labs.*, 512 F.3d 1363 (2008). The Federal Circuit denied a grant of permanent injunction because it did not find plaintiff to have suffered an irreparable harm (*9*). In particular, the Federal Circuit found that because the $7 million damages award included a market entry fee and an ongoing royalty payment in anticipation of Abbott's long-term license to sell its infringing products, plaintiff Innogenetics had not suffered an irreparable harm by Abbott's future sales of the infringing product (*9*). The court remanded the case to the trial court to delineate the terms of the compulsory license governing the royalty payments (*10*).

MedImmune, Inc. v. Genentech, Inc., 127 S. Ct. 764 (2007)

It did not take very long for the Supreme Court to review and disagree with another one of the Federal Circuit's decisions. In *MedImmune,* decided in January of last year, the Supreme Court reversed the decision of the Federal Circuit, requiring a licensee to breach its patent license agreement in order to have standing to sue for a declaration that the underlying patent was invalid (*11*).

Downloaded by STANFORD UNIV GREEN LIBR on June 23, 2012 | http://pubs.acs.org
Publication Date (Web): November 17, 2010 | doi: 10.1021/bk-2010-1053.ch014

The Supreme Court held that a party has the right to challenge the validity of a patent in court, even if it has already agreed to license the patented invention and is paying royalties to the patent owner (*12*).

The dispute in *MedImmune* grew out of a license agreement entered into in 1997 by MedImmune, allowing it to use, sell, and make Genentech's patented invention (*13*). In 2002, Genentech asserted that one of MedImmune's most lucrative drugs, marketed as Synagis in the United States, infringed one of its newly issued patents (*14*). Although MedImmune disputed infringement and believed Genentech's patent to be invalid, it did not challenge the validity of the patent due to the risk that it might be ordered to stop selling its drug or to pay triple damages for willfully infringing a patent (*14*). Instead, MedImmune, "under protest," agreed to pay royalties to Genentech, allowing MedImmune to continue selling Synagis, which then accounted for 80 percent of the company's revenues (*14*). MedImmune subsequently filed a lawsuit seeking a declaratory judgment that Genentech's patent was invalid (*14*).

A federal district court dismissed the complaint, siding with Genentech to hold that MedImmune had no standing to bring the case because, as a licensee in good standing, it was not at risk of being sued for infringement (*14*). The Federal Circuit affirmed (*14*). The Supreme Court, however, reversed and remanded the case back to the district court so that MedImmune's request for a declaratory judgment could be decided on its merits (*12*). The Court's majority opinion did not agree that a plaintiff must "bet the farm, or (as here) risk treble damages and the loss of 80 percent of its business, before seeking a declaration of its actively contested legal rights" (*15*). Justice Clarence Thomas dissented, finding MedImmune to lack "standing to obtain rulings on matters that remain hypothetical or conjectural" (*12*).

For universities and other patent holders who negotiate licenses to allow others to use their inventions, this decision could prove costly, as it will likely encourage licensees to challenge the validity of the patents that are subject to the license agreement. The ruling makes it easier and more attractive for a licensee to take actions to defeat a patent because the licensee will not have to put the license at risk to do it.

Downloaded by STANFORD UNIV GREEN LIBR on June 23, 2012 | http://pubs.acs.org
Publication Date (Web): November 17, 2010 | doi: 10.1021/bk-2010-1053.ch014

Microsoft Corp. v. AT&T Corp., 127 S. Ct. 1746 (2007)

In April 2007, the Supreme Court handed down two rulings significantly cutting back on the scope of patent protection in the United States. The first one of those was *Microsoft Corp. v. AT&T Corp.*, where the Supreme Court held that Microsoft is not liable for infringement under 35 U.S.C. § 271(f) of the Patent Act by supplying master versions of its Windows software that are copied and installed on computers outside the United States (*16*). It was not disputed that computers with Windows software would have infringed AT&T's patent if they had been made, used, sold, or offered for sale in the United States (*17*). AT&T holds a patent on an apparatus for digitally encoding and compressing recorded speech, and Microsoft's Windows software, when installed, allows a computer to perform functions in a manner claimed by AT&T's patent (*17*).

Downloaded by STANFORD UNIV GREEN LIBR on June 23, 2012 | http://pubs.acs.org
Publication Date (Web): November 17, 2010 | doi: 10.1021/bk-2010-1053.ch014

In addition to licensing Windows to computer manufacturers in the United States who install the software onto the computers they sell, Microsoft also sends a master version of Windows to computer manufacturers outside the United States, either on disk or via electronic transmission (*18*). From this master version, copies of Windows are made for installation on computers sold to users abroad. While Microsoft admitted domestic liability, Microsoft denied any liability for copies of Windows installed on foreign-manufactured computers that were replicated from the master version of Windows it sent outside the United States (*18*).

Although the general rule under United States patent law is that no infringement occurs when a patented product is made and sold in another country, 35 U.S.C § 271(f) is an exception (*19*). It imposes liability for patent infringement when a party supplies from the United States the components of a patented invention for combination abroad (*19*).

AT&T argued that by providing manufacturers outside the United States a master copy of Windows, Microsoft supplied “components” of AT&T’s patented apparatus for combination into computers sold abroad (*19*). Microsoft countered that intangible, unincorporated software cannot be a “component” of a patented invention as required by 35 U.S.C. § 271(f) (*19*). Both the district court and the Federal Circuit rejected Microsoft’s position and held Microsoft liable under 35 U.S.C. § 271(f) for supplying the master copy of Windows software that could be installed on computers, infringing AT&T’s patent (*19*).

The Supreme Court disagreed and concluded that 35 U.S.C. § 271(f) applies only to “components” that can be “combined” to form the patented invention (*20*). It reasoned that software in the abstract, without a physical embodiment, is not combinable and thus, does not constitute a “component” of a patented apparatus (*20*). Next, the Court concluded that Microsoft’s liability did not extend to computers made in foreign countries when loaded with Windows from the United States because *copies* of Windows actually installed on foreign computers were not themselves “supplied from the United States” (*21*). A copy made entirely abroad does not fit 35 U.S.C. § 271(f) without stretching the statute beyond its plain meaning, and the Court refused to make this stretch (*22*).

The Supreme Court also relied on the presumption against extraterritoriality of United States patent laws and emphasized that foreign law alone, not United States law, currently governs the manufacture and sale of components of patented inventions in foreign countries (*23*). To the extent that its holding can be seen as a “loophole” for software makers to avoid infringement of a United States patent by making copies abroad, the Supreme Court explained that Congress, not the Court, is responsible for addressing any such loophole (*23*).

In *Microsoft*, the Supreme Court expressed its reluctance to interpret 35 U.S.C. § 271(f) to address advances in technology, particularly the software industry, and to expand the extraterritorial effect of the United States patent laws. This opinion is instructive on the application of 35 U.S.C. § 271(f) in other industries as well, for instance in the context of biotechnology where biological materials, such as genes or cell lines, can be manufactured in the United States and sent abroad for replication and incorporation into organisms in an infringing manner. The impact of the Court’s decision in *Microsoft* is clear—unless the United States Congress acts, manufacturers of software and other products may continue to develop infringing technology in the United States and supply it for use outside the country without being subject to patent liability in the United States.

KSR Int'l Co. v. Teleflex, Inc., 127 S. Ct. 1727 (2007)

On the same day that the Supreme Court decided *Microsoft*, it decided another patent case, *KSR Int'l Co. v. Teleflex, Inc.*, addressing the burden required to prove the obviousness of an invention.

The *KSR* case began when Teleflex, a Pennsylvania-based auto parts manufacturer, sued rival KSR, alleging that the Canada-based firm was selling infringing gas pedals in the United States (*24*). KSR sought to dismiss the suit on a summary judgment motion, alleging that Teleflex's invention was too obvious to be patented (*24*).

The patent at issue covers a gas pedal that is adjustable and that controls the engine by means of an electronic sensor. Long before the invention date of this patent, companies had been making and selling adjustable gas pedals, as well as pedals that had electronic sensors (*25*). According to KSR, the Teleflex patent was an obvious combination of these two well-known designs, and thus, it was unpatentable.

The trial court agreed with KSR and granted its summary judgment motion (*26*). But the Federal Circuit reversed, holding that a combination of existing elements can be considered obvious only if one can prove that, prior to the date of the invention, there was an explicit "teaching, suggestion, or motivation" to combine the existing elements (for instance, a technical manual or scientific journal that discussed the advantages of putting a sensor on an adjustable pedal) (*27*).

The Supreme Court unanimously rejected the Federal Circuit's "rigid" approach to the obviousness inquiry and ruled in favor of KSR. The Court refused to confine the obviousness analysis by "a formalistic conception of the words *teaching*, *suggestion*, and *motivation*, or by overemphasis on the importance of published articles and the explicit content of issued patents" because in certain fields there may be little discussion of obvious techniques or combinations, or it may be market demand, rather than scientific literature, driving design trends (*28*).

The Court called for a more open-ended approach to determine obviousness, one in which teaching, suggestion, and motivation should be viewed in broader terms, and where other factors should also be considered. One of the factors recognized by the Court is that people regularly combine existing items for new purposes. If such combinations are only mildly creative, they are too obvious to be patentable (*29*).

As for the Federal Circuit's specific analytical errors, the Supreme Court found that the Federal Circuit first erred in holding that courts and patent examiners should look only to the problem the patentee was trying to solve (*30*). Under the Supreme Court's analysis, any problem known in the field of invention of the patent can provide a reason for combining the elements in the manner claimed (*30*).

Downloaded by STANFORD UNIV GREEN LIBR on June 23, 2012 | http://pubs.acs.org
Publication Date (Web): November 17, 2010 | doi: 10.1021/bk-2010-1053.ch014

Second, the Federal Circuit erred in assuming that "a person of ordinary skill [in the art] attempting to solve a problem will be led only to those prior art elements designed to solve the same problem" (*30*). The appellate court did not consider that a person of ordinary skill may use familiar items for obvious uses that are beyond their primary purposes (*30*).

Third, the Federal Circuit was wrong in concluding that a patent claim cannot be proved obvious merely by showing that the combination of elements was "obvious to try" (*30*). The Supreme Court stated that "when there is a design need or market pressure to solve a problem and there are a finite number of *identified, predictable solutions*, a person of ordinary skill in the art has good reason to pursue the known options within his or her technical grasp"; if the "anticipated success" results, it is likely the product of ordinary skill and common sense, not innovation (*31*).

The *KSR* ruling will make it easier for the Patent Office to reject applications on the grounds of obviousness, thus raising the bar of patentability. Similarly, it will be easier for accused infringers to argue obviousness in court to challenge the validity of patents.

Downloaded by STANFORD UNIV GREEN LIBR on June 23, 2012 | http://pubs.acs.org
Publication Date (Web): November 17, 2010 | doi: 10.1021/bk-2010-1053.ch014

In re Bilski, Case Number 2007-1130

On May 8, 2008, the Federal Circuit heard oral arguments in the case of *In re Bilski* (*32*). The en banc hearing addressed five questions, perhaps the most important being the standard that should govern the determination of whether a process is patentable subject matter under 35 U.S.C. § 101 (*32*). The invention in *Bilski* related to a method of managing the consumption risk costs associated with a commodity sold at a fixed price for a given period of time (*33*).

The patent Examiner had rejected the claims of Bilski's patent application in March 2000 on the grounds that the invention was not implemented by a machine, that it manipulated an abstract idea, and that the invention did not have a practical application (*33*). In 2006, the Board of Patent Appeals and Interferences affirmed the rejection on the basis that the subject matter of Claim 1 was directed to an "abstract idea" (*33*).

Expected no earlier than late August 2008, the Federal Circuit's opinion may change the standard of patentability for all method and process claims, thus calling into question the validity of many business method patents.

The Patent Reform Act of 2007

The United States patent statutes have remained essentially the same since 1952. However, that may soon change. The Patent Reform Act of 2007 introduced in Congress on April 18, 2007, proposes extensive changes that would reform the law governing how patents are obtained and enforced (*34*).

While patent reforms introduced in recent years have languished in Congress, the Patent Reform Act of 2007 has the backing of the House of Representatives and the Senate, and both the Democratic and Republican parties. These bills also have the backing of numerous corporations and industry groups who believe many invalid patents are being granted and that patent litigation in the United States is out of control. It remains to be seen whether, and which version of, the Patent Reform Act of 2007 will pass Congress.

References

1. *See generally In re Bilski*, 264 Fed. Appx. 896 (Fed. Cir. en banc hearing granted Feb. 15, 2008).
2. *eBay, Inc. v. MercExchange, L.L.C.*, 547 U.S. 388 (2006).
3. *eBay, Inc. v. MercExchange, L.L.C.*, 547 U.S 391 (2006).
4. *eBay, Inc. v. MercExchange, L.L.C.*, 547 U.S 393 (2006). At the trial level, the jury had found that eBay's web feature infringed MercExchange's patent covering a method of selling goods over the Internet. *MercExchange, L.L.C. v. eBay, Inc.*, 275 F. Supp. 2d 695, 698 (E.D. Va. 2003). The jury also found that the patent was valid and awarded $35 million in damages. *Id.* The judge, however, refused to enter a permanent injunction against eBay, based partly on the fact that MercExchange was not actually practicing its patent, and because of his general concerns over business method patents. *See id.* at 711-15.
5. *eBay*, 547 U.S. at 393.
6. *eBay*, 547 U.S. at 393-94 (internal quotations omitted and emphasis added).
7. *eBay*, 547 U.S. at 392 (citing 35 U.S.C. § 283).
8. *eBay*, 547 U.S. at 394.
9. *Innogenetics, N.V. v. Abbott Labs.*, 512 F.3d 1363, 1380 (Fed. Cir. 2008).
10. *Innogenetics, N.V. v. Abbott Labs.*, 512 F.3d 1381 (Fed. Cir. 2008).
11. *MedImmune, Inc. v. Genentech, Inc.*, 127 S. Ct. 764, 768 (2007).
12. *MedImmune, Inc. v. Genentech, Inc.*, 127 S. Ct. at 777 (2007).
13. *MedImmune, Inc. v. Genentech, Inc.*, 127 S. Ct. at 767-68 (2007).
14. *MedImmune, Inc. v. Genentech, Inc.*, 127 S. Ct. at 768 (2007).
15. *MedImmune, Inc. v. Genentech, Inc.*, 127 S. Ct. at 775 (2007).
16. *Microsoft Corp. v. AT&T Corp.*, 127 S. Ct. 1746, 1750-51 (2007).
17. *Microsoft Corp. v. AT&T Corp.*, 127 S. Ct. at 1750 (2007).
18. *Microsoft Corp. v. AT&T Corp.*, 127 S. Ct. at 1753 (2007).
19. *Microsoft Corp. v. AT&T Corp.*, 127 S. Ct. at 1750 (citing 35 U.S.C. § 271(f)).
20. *Microsoft Corp. v. AT&T Corp.*, 127 S. Ct. at 1755.
21. *Microsoft Corp. v. AT&T Corp.*, 127 S. Ct. at 1756 (emphasis added).
22. *Microsoft Corp. v. AT&T Corp.*, 127 S. Ct. at 1757.
23. *Microsoft Corp. v. AT&T Corp.*, 127 S. Ct. at 1759.
24. *KSR Int'l Co. v. Teleflex, Inc.*, 127 S. Ct. 1727, 1734 (2007).
25. *KSR Int'l Co. v. Teleflex, Inc.*, 127 S. Ct. at 1735 (2007).
26. *KSR Int'l Co. v. Teleflex, Inc.*, 127 S. Ct. at 1737 (2007).
27. *KSR Int'l Co. v. Teleflex, Inc.*, 127 S. Ct. at 1738 (2007).
28. *KSR Int'l Co. v. Teleflex, Inc.*, 127 S. Ct. at 1741 (2007) (emphasis added).
29. *KSR Int'l Co. v. Teleflex, Inc.*, 127 S. Ct at 1739-41 (2007).
30. *KSR Int'l Co. v. Teleflex, Inc.*, 127 S. Ct. at 1742 (2007).

Downloaded by STANFORD UNIV GREEN LIBR on June 23, 2012 | http://pubs.acs.org
Publication Date (Web): November 17, 2010 | doi: 10.1021/bk-2010-1053.ch014

31. *KSR Int'l Co. v. Teleflex, Inc.*, 127 S. Ct. at 1742 (2007) (emphasis added).
32. *In re Bilski*, 264 Fed. Appx. 896 (Fed. Cir. 2008).
33. *In re Bilski*, 2006 WL 4080055 (B.P.A.I. 2006).
34. H.R. 1908, 110th Cong. (2007); S. 1145, 110th Cong. (2008).

Downloaded by STANFORD UNIV GREEN LIBR on June 23, 2012 | http://pubs.acs.org
Publication Date (Web): November 17, 2010 | doi: 10.1021/bk-2010-1053.ch014

Subject Index

A

(A/A70f)PA microcapsule, 151*f*
(A/A100f)PA microcapsule, 145, 149*f*, 150*f*
(A/A70)PLLr composite capsules, 151*f*
AC70A70 microcapsule
  C_2C_{12} cells, 142*f*
  OM image, 141*f*, 146*f*
AC70A70PA microcapsules, 4-layer, 144*f*
AC70A100PA microcapsule, 144*f*
Acrylates Copolymer, 238*f*
2-Acryloyltetrahydro-1,2-oxazine
  polymerization, 169*s*
  synthesis, 167*s*
AEMA. *See* 2-Aminoethyl methacrylate
Alginate microapsules and polycations, 143
Alginate/poly-L-lysine/alginate
  BSA-FITC exposure, 144*f*
  C_2C_{12} cells, 142*f*
  mechanical stability, 153, 154*f*
  MW cut-off, 154, 155*f*
Alkyl azide-functionalized silicon wafer, 119, 121, 123*f*, 124*s*
Alkyl bromide-functionalized silicon wafer, 123*f*
α-Alkynyl-functionalized poly(2-aminoethyl methacrylate), 113
  alkyl azide-functionalized silicon wafer, 121, 124*s*
  DMSO, 122*f*
  ^{1}H NMR spectrum, 122*f*
  preparation, 118, 120*s*, 120*t*
  RAFT polymerization, 120*s*
Amine-functionalized silicon surfaces, 113
2-Aminoethyl methacrylate, 113
APA. *See* Alginate/poly-L-lysine/alginate
APA70PA microcapsule, 144*f*
APA100PA microcapsule, 144*f*
A-PAPM-A70 capsules shell, 146*f*
Azide-modified silicon wafer
  poly(2-aminoethyl methacrylate), 117
  synthesis, 122*s*

B

BAB triblock micellar network, 52*f*
Biopolymers
  design, 49
  RAFT polymerization, 49
3-Bromopropyltrichlorosilane and silicon wafers, 117

C

C70/A70 polyelectrolyte complex, 140*f*
Ca(A/A70f) composite capsule, 149*f*, 151*f*
CaAlg beads, 136*s*, 141*s*, 147*f*
Ca(Alg/A70f) composite beads, 147*f*
Cancer treatment and nanoparticle agents, 65
Carboplatin, 162
Catecholato(1,2-diaminocyclohexane)platinum (II) compounds, 166*t*
C_2C_{12} cells
  encapsulation
    (A/A70)PA capsules, 153*f*
    AC70A70 capsule, 142*f*
    A-C70-A70-PLL-Alg, 146*f*
    APA, 142*f*, 146*f*, 153*f*
    in vitro cell viability, 153*f*
Cell encapsulation and synthetic reactive polyelectrolytes, 131
Cisplatin, 162
Cleansers formulation, 221
Click chemistry, 113
CMC. *See* Critical micelle conentration
Complex coacervation and encapsulation for delivery, 14
Composite cross linked capsules, 154, 155*f*
Composite microcapsules, 144, 147*f*
Core-cross linked (A/A70)PA microcapsules, 148
  in-vitro cell viability, 152
  mechanical stability, 153, 154*f*
  MW cut-off, 154
Cosmetic and polymeric delivery of attributes, 3
Critical micelle conentration
  acrylates copolymer, 238*f*
  HMP, 231
  pH-responsive copolymers, 237
  sodium laureth-2 sulfate, 238*f*
  surface tension, 233*f*
  TDES, 235*f*
CTP. *See* 4-Cyanopentanoic acid dithiobenzoate
Cu-MOF nanocrystals
  PLA composite fibers, 188*f*

In Polymeric Delivery of Therapeutics; Morgan, S., et al.;
ACS Symposium Series; American Chemical Society: Washington, DC, 2010.

Downloaded by 89.163.34.136 on June 23, 2012 | http://pubs.acs.org
Publication Date (Web): November 17, 2010 | doi: 10.1021/bk-2010-1053.ix002

Downloaded by 89.163.34.136 on June 23, 2012 | http://pubs.acs.org
Publication Date (Web): November 17, 2010 | doi: 10.1021/bk-2010-1053.ix002

- structure, 185*f*, 186*f*
- synthesis, 183

4-Cyanopentanoic acid dithiobenzoate
- alkynyl-functionalized
  - ^{1}H NMR spectrum, 120*f*
  - preparation, 119*s*

Cyclodextrins, 15

D

DDMAA. *See* (2,2-Dimethyl-1,3-dioxolane) methyl acrylamide
Delivery system polymer technology, 195
Dendrimers, 36, 37*f*
- iontophoresis, 17
- organoplatinum antitumor agents, 161, 176
- PAMAM, 166
- polymer gels, 17

Desferrioxamine ligand, 105*f*
- hemoglobin oxidation inhibitory effect, 109*f*
- and HUVEC cells, 110*f*
- synthesis, 109*f*

Dextran-based iron chelators, 105
DFO. *See* Desferrioxamine ligand
(2,2-Dimethyl-1,3-dioxolane) methyl acrylamide, 107*f*
Dimethylsulfoxide, 122*f*
DLS. *See* Dynamic light scattering
DMSO. *See* Dimethylsulfoxide
DR-L
- flocculation, 255*f*
- mean size vs. adsorbed, 258*f*

Drug
- circulation, 28*f*
- physical gels, 58

Dynamic light scattering, 228*t*

E

EA hydrophobic monomer, 237*f*
eBay, Inc. v. MercExchange, L.L.C., 269
Emulsions, 243, 259*f*
Encapsulation, 16

F

Flash NanoPrecipitation process, 33*f*, 35*f*
Flocculation
- bridging, 253, 254*f*
- depletion effect, 253, 254*f*
- DR-L, 255*f*
- emulsions, 253
- polymers, 254*f*
- silicone-polyether, 254*f*
- solvent quality, 253, 254*f*
- water-in-oil emulsions, 255*f*

Fluorescein dye leakage assay, 223, 224*f*
Foam performance and HMP, 239, 239*f*
Four-layer (A-C70-A70-PLL-Alg) microcapsules, 142

G

Gadolinium metal-organic framework nanoparticle
- hydrophilic RAFT polymers, 79
- modification, 70*s*, 73, 80
- MRI contrast agents, 89*t*
- multifunctional copolymers, 85*s*
- multifunctional RAFT copolymers, 80
- nanomedicines, 72
- PNIPAM homopolymer, 75*f*
- PNIPAM-co-PNAOS-co-PFMA, 85*f*
- polymer
  - coating thickness, 81
  - grafting density, 81, 82
  - surface modification technique, 79
- polystyrene, 80
- RAFT
  - homopolymer and copolymers, 71
  - polymerization, 74*f*, 84
- stability study, 84
- surface modification, 71, 80, 83
- synthesis, 71
- thiolate polymer chain ends, 86*s*

Gd MOF nanoparticle. *See* Gadolinium metal-organic framework nanoparticle
GRGDS-NH_2. *See* H-glycine-arginine-glycine-aspartate-serine-NH_2

H

Hair conditioning polymers, 13
Hair fixatives, 11
HASE. *See* Hydrophobically-modified alkali-soluble emulsion polymers
HEAT. *See* Hydrophobically-modified aminoplast technology copolymers
Hemoglobin oxidation inhibitory effect and DFO, 109*f*
Herschel-Bulkley model, 257*t*

Downloaded by 89.163.34.136 on June 23, 2012 | http://pubs.acs.org
Publication Date (Web): November 17, 2010 | doi: 10.1021/bk-2010-1053.ix002

HEURH. *See* Hydrophobically-modified ethoxylated urethanes
H-glycine-arginine-glycine-aspartate-serine-NH_2, 71
HMHEC. *See* Hydrophobically-modified hydroxyethyl cellulose
HMP. *See* Hydrophobically-modified polymers
HUVEC cells and DFO, 110*f*
Hydrogels, 51
Hydrophilic RAFT polymers and Gd MOF surface modification, 79, 87
Hydrophobic RAFT homopolymer and Gd MOF nanoparticles, 88
Hydrophobically-modified alkali-soluble emulsion polymers, 7
Hydrophobically-modified aminoplast technology copolymers, 7
Hydrophobically-modified ethoxylated urethanes, 7
Hydrophobically-modified hydroxyethyl cellulose, 7
Hydrophobically-modified polymers, 221
  chemistries, 235
  ΔCMC concept, 231, 232, 233*f*
  foam performance, 239, 239*f*
  free micelle concentration, 234*f*
  irritation mitigation, 231
    INCI names and chemical structures, 236*f*
  low molecular weight, 237
  polymer-surfactant association, 230*f*
  surfactant-based cleanser
    surface tensiometry, 235*t*
    TEP assay data, 235*t*

I

IBMA. *See* Isobornylmethacrylate
IFT. *See* Interfacial tension
Imaging properties of RAFT polymers, 86
In re Bilski, 274
Interfacial tension and silicone-polyether, 260
Intravascular iron chelation therapy, 103
Iontophoresis, 17
Iron chelating macromolecules, 103
Iron chelators
  dextran, 105
  PEG, 106
  starch, 105
Iron-chelating polymer therapeutic, 106*f*
Irritation reduction and polymer-surfactant association, 229
Isobornylmethacrylate, 199

K

KSR Int'l Co. v. Teleflex, Inc., 273

L

Laurylmethacryate, 199
Limonene, 204*f*
LMA. *See* Laurylmethacryate

M

MAA-EA ASE copolymers, 235*f*, 237*f*
Magnevist®, 89*t*
MedImmune, Inc. v. Genentech, Inc., 270
Metal-ligand absorption bands
  catecholato(1,2-diaminocyclohexane)platinum (II) compounds, 166*t*
  salicylato(1,2-diaminocyclohexane)platinum(II) compounds, 167*t*
Methotrexate, 71, 78*s*
Micelle penetration model, 226, 227
Micelles, 31
  reversible shell cross-linking, 59*s*
Microcapsules properties, 136
Microsoft Corp. v. AT&T Corp., 271
Milling, 28
Molecular sieve composite fibers
  application, 187
  electrospinning, 183
  NO release, 181, 187*f*, 188*f*
  rat hearts, 187, 188*f*
Monomer penetration model and surfactant skin penetration, 224
MRI
  agents and Gd MOF nanoparticles, 89*t*
  and nanoparticle, 67
MTX. *See* Methotrexate
Multifunctional nanoparticle formation reagents, cell growth inhibition, 91*f*
Multifunctional polymers and RAFT polymerization, 73
Multifunctional RAFT copolymers and Gd MOF nanoparticles, 80, 90, 92
Multihance®, 89*t*

Downloaded by 89.163.34.136 on June 23, 2012 | http://pubs.acs.org
Publication Date (Web): November 17, 2010 | doi: 10.1021/bk-2010-1053.ix002

N

Nanomedicines and Gd MOF nanoparticles, 72
Nanoparticles
  MRI, imaging agents, 67
  RAFT polymers, 68
  surface modification, 68
Nano pharmaceutical materials and polymers, 25
  bottom-up approaches
    dendrimers, 36
    micelles, 31
    rapid precipitation and directed-assembly, 34
    spray drying, 39
    supercritical fluid methods, 37
  top-down approaches
    milling, 28
    solid solutions, 29
Nanoscale theragnostic devices, 66
Nanozeolite A/PLA composite fibers, 188*f*
Naproxen crystals, 29*f*
Neat silicon wafer, 123*f*, 124*f*, 126*f*
Nitric oxide
  bandage and rat hearts, 188*f*
  molecular sieve composite fibers, 181, 187*f*
NO. *See* Nitric oxide
Non-viral polymer based carriers, 50

O

Octylmethoxycinnamate, 203*f*
Oil absorption and skin and hair care, 195
Oil imbibing copolymers, sebum, absorption, 200*f*
OMC. *See* Octylmethoxycinnamate
Organoplatinum antitumor agents
  dendrimer supported, 161
  PAMAM dendrimers supported, 166
  polymer supported, 161, 163

P

PAMAM dendrimer. *See* Poly(amidoamine) dendrimers
P210 and P277, storage modulus, 61*f*
Patent Reform Act of 2007, 274
PDMS. *See* Polydimethylsiloxane
PEC. *See* Polyelectrolyte complexes
PEG. *See* Poly(ethylene glycol)
PEGMA. *See* Poly(ethylene glycol) methyl ether methacrylate
Personal care products and polymeric delivery of attributes, 3
Personal cleansing products
  surfactants, 221
  TEP assay, 225*f*
PFMA. *See* Poly(fluorescein O-methacrylate)
P(HPMA-stat-APMA)-b- DMAPMA, 56*f*
pH-responsive triblock copolymer gels, 59
Physical gels for drug delivery, 58
  triblock copolymer gels
    pH-responsive, 59
    temperature-responsive, 60, 60*f*
PLL. *See* Poly-L-lysine
PNAOS. *See* Poly(N-acryloxysuccinimide)
PNIPAM. *See* Poly(N-isopropylacrylamide)
PNIPAM-co-PNAOS-co-PFMA
  copolymer, 71, 85*f*
  functional biocompatible polymers, 75
  Gd MOF nanoparticles, 85*f*
  GRGDS-NH_2, 78*s*
  methotrexate, 78*s*
  modification, 78*s*
  RAFT polymerization, 74*f*, 75
Poly(AEMA). *See* Poly(2-aminoethyl methacrylate)
Poly(amidoamine) dendrimers
  supported organoplatinum antitumor species, 166
    [(DACH)Pt], 173
    PAMAM(G3.5)-cisplatin, 166
    PAMAM(G4.5)-[(DACH)Pt], 168, 171*f*, 171*s*, 173*f*, 173*t*, 174*f*, 175*f*
Poly(2-aminoethyl methacrylate)
  azide-modified silicon wafers, 117
  silicon wafer modification, 123*f*, 124*f*, 126*f*
Polycations and alginate microcapsules, 143
Polydimethylsiloxane, 209*f*, 255*f*
Polyelectrolyte complexes, 54, 138, 140*f*
Polyelectrolytes
  cell encapsulation, 131
  natural and synthetic, 139*s*
  properties, 140*t*
Poly(ethylene glycol)
  iron chelators
    design, 106
    iron-binding properties, 108
    polymer degradation pathway, 108
    synthesis, 107
    in vitro cell toxicity and blood compatibility, 110

Poly(ethylene glycol) methyl ether methacrylate, 107*f*
Poly(fluorescein O-methacrylate), 74*f*
Poly[3-(4-hydroxybutylamino)propylene]
  formation, 170*s*
  tetrachloroplatinate, interaction, 170*s*
Poly-L-lysine, 149*f*
  (A/A70)PA capsules, 149*f*
  Ca(A/A70f) composite capsule, 149*f*
  CaAlg capsule, 136*s*
  C_2C_{12} cells, 142*f*
Polymer
  hair fixatives, 11, 13
  IBMA: LMA
    Glucam P10, 202*f*
    limonene, 202*f*
    octylmethoxycinnamate, 203*f*
    oil based active ingredients, absorption, 202*f*
    sebum, 201*f*, 204*f*
    vitamin E, 203*f*
  isobornylmethacrylate, 199*f*
  laurylmethacryate, 199*f*
  nano pharmaceutical materials, 25
  oil absorption and delivery system, 195
  supported organoplatinum drugs, 161
  surface characterization, 117
Polymeric antimicrobials and bacteriostats, 18
Polymeric carrier, 51*f*
Polymeric delivery
  cosmetic, 3
  personal care products, 3
  vehicles, 52
    polyelectrolyte complexes, 54
    polymer backbone conjugation, 53
    polymer end-group conjugation, 53
    stimuli-responsive shell cross-linked micelles and vesicles, 56
Polymeric micelle formation, 33*f*
Polymer modified Gd MOF nanoparticles
  cell growth inhibition, 93
  Gd^{3+} leached, 87*t*
Polymer modified nanoparticle, 67*f*
Polymer-supported organoplatinum antitumor agents
  poly(N-vinylpyrollidone), 163
  potential, 176
  tetrahydro-1,2-oxazine, 165
Polymer surface modification technique and Gd MOF nanoparticles, 79
Polymer-surfactant association
  HMP, 230*f*
  irritation reduction, 229
Poly(N-acryloxysuccinimide), 74*f*
Poly(N-isopropylacrylamide)
  Gd MOF nanoparticles, 75*f*
  homopolymer, 75*f*
  RAFT polymerization, 74*f*, 75*f*
Poly(N-vinylpyrrolidone), 163
Polystyrene and Gd MOF nanoparticles modification, 80
Poly[3-(2-tetrahydro-1,2-oxazyl)propylene
  formation, 169*s*
  platinum species, interaction, 169*s*
Positive contrast nanoparticle agents
  cancer treatment, 65
  RAFT polymers, 65
  targeted imaging, 65
Primary amine-functionalized silicon surfaces, 113

R

RAFT. *See* Reversible addition fragmentation chain transfer
Rapid precipitation and directed-assembly, 34
Rat hearts
  molecular sieve composites fibers, 187
  NO releasing bandage, 188*f*
  testing of bandage, 184
Reverse microemulsion system, 86*s*
Reversible addition fragmentation chain transfer, 49
  copolymers, 71, 73, 77, 78*t*
  Gd MOF nanoparticle, 84
  homopolymers, 71, 73, 76*t*, 85*s*
  polymerization
    α-alkynyl-functionalized poly(2-aminoethyl methacrylate), 120*s*
    biopolymers, 49
    (2,2-dimethyl-1,3-dioxolane) methyl acrylamide, 107*f*
    functional biocompatible polymers, 75
    Gd MOF nanoparticles, 70*s*, 74*f*
    PNIPAM, 74*f*
    PNIPAM homopolymer, 75*f*
    PNIPAM-co-PNAOS-co-PFMA, 70, 71, 74*f*
    poly(ethylene glycol) methyl ether methacrylate, 107*f*
  polymers, 65
    formation and modification, 69
    imaging properties, 86, 88
    nanoparticles modification, 68
    positive contrast nanoparticle agents, 65

Downloaded by 89.163.34.136 on June 23, 2012 | http://pubs.acs.org
Publication Date (Web): November 17, 2010 | doi: 10.1021/bk-2010-1053.ix002

Downloaded by 89.163.34.136 on June 23, 2012 | http://pubs.acs.org
Publication Date (Web): November 17, 2010 | doi: 10.1021/bk-2010-1053.ix002

- therapeutic and molecular targeting agent, 77
- Rheology modifier, 6

S

- Salicylato(1,2-diaminocyclohexane)platinum(II) compounds, 167*t*
- Sebum
  - hair tresses, control, 201*f*
  - limonene, 204*f*
  - meter reading, 200*f*, 201*f*
  - oil imbibing copolymers, 200*f*
  - personal care formulations, 201
  - polymer, 201*f*
  - polymer A and OMC, 204*f*
  - silicone elastomeric particles, 216*f*
  - VITRO skin, 200*f*
- SEDS process. *See* Solution enhanced dispersion by supercritical fluids process
- SF. *See* Supercritical fluid method
- Shampoos, adult and baby
  - DLS, 228*t*
  - TEP data, 228*t*
- Shell-cross linked (A/A70)PA microcapsules, 145
- Silicone elastomeric particles, 209*f*
  - actives, delivery, 217
  - Al_2O_3 nanoparticles, 212*f*
  - aqueous dispersions, 215
  - dynamic shear modulus, 214*f*
  - inorganic oxides, 214
  - liquids absorption, 216*t*, 217
  - optical properties, 218
  - particle size distribution, 213*f*
  - preparation, 210*f*
  - sebum, 216*f*, 218
  - sensory feel, 217
  - skin care, applications, 207, 215
  - wrinkles, 217*f*, 218
- Silicone-polyether, 245*t*
  - dilatation elasticity, 262, 263*f*
  - interfacial tension, 260, 261*f*
  - water-in-oil emulsions, stabilizers, 243
    - adsorption, 256*f*, 257*f*, 258*f*
    - calibration curve, 246*f*
    - drop size distributions, 246, 250
    - droplet deformation and coalescence, 250*f*
    - emulsification, 245
    - flocculation, 253, 254*f*
    - high performance liquid chromatography, 247
    - mean drop size, 252*f*
    - osmotic pressure, 260*f*
    - structure, 245*f*
- Silicon wafers
  - alkyl azide-functionalized, 119, 123*f*
  - alkyl bromide-functionalized, 123*f*
  - azide-modified, 117
  - 3-bromopropyltrichlorosilane, deposition, 117
  - modified, 123*t*
  - neat, 123*f*
  - poly(AEMA)-modified, 123*f*
  - surface preparation, 116
- Siloxane polymers, 209
- SiRNA, degradation, 56*f*
- Skin and hair care
  - delivery system polymer technology, 195
  - oil absorption, 195
  - silicone elastomeric particles, 207, 215
- Smart polymers, 51
- Sodium laureth-2 sulfate, 238*f*
- Solid solutions and nano pharmaceutical materials, 29, 31*f*
- Solution enhanced dispersion by supercritical fluids process, 39*f*
- SPE. *See* Silicone-polyether
- Spray drying, 39
- Starch
  - DFO conjugate, 105*f*
  - iron chelators, 105
- Supercritical fluid method, 37
- Surface area and nano pharmaceutical materials, 27*f*
- Surface modification mechanism and Gd MOF nanoparticles, 83
- Surfactants
  - personal cleansing products, 221
    - fluorescein leakage assay, 223
    - irritation potential, 222
    - skin interaction, 222
    - TEP assay, 223
  - skin penetration
    - micelle penetration model, 226
    - monomer penetration model, 224
- Synthetic reactive polyelectrolytes and cell encapsulation, 131

T

- Temperature-responsive triblock copolymer gels, 60*f*
- TEP. *See* Transepithelial permeability assay
- Tetrachloroplatinate, 170*s*

Therapeutic and molecular targeting agent, 77
Transepithelial permeability assay, 223, 224*f*
  adult and baby shampoos, 228*t*
  personal cleansing products, 225*f*
Transfer-resistant color cosmetics, 6
Two-layer (A-C70-A70) microcapsules, 138

U

United States Patent Law
  eBay, Inc. v. MercExchange, L.L.C., 269
  KSR Int'l Co. v. Teleflex, Inc., 273
  MedImmune, Inc. v. Genentech, Inc., 270
  Microsoft Corp. v. AT&T Corp., 271
  In re Bilski, 274

V

Vinyl siloxane polymer, 210*f*
VITRO skin, 196, 200*f*

W

Water-in-oil emulsions
  flocculation, 255*f*
  silicone polyether, 243

Z

Zeolite, 186*f*

Downloaded by 89.163.34.136 on June 23, 2012 | http://pubs.acs.org
Publication Date (Web): November 17, 2010 | doi: 10.1021/bk-2010-1053.ix002